

Copyright

by

James Christopher Taylor

2007

This Dissertation Committee for James Christopher Taylor certifies that this is the approved version of the following dissertation:

Advanced Lithographic Patterning Technologies: Materials and Processes

Committee:

C. Grant Willson, Supervisor

Roger T. Bonnecaze

Thomas M. Truskett

Chris A. Mack

Alfred H. Stiller

**Advanced Lithographic Patterning Technologies: Materials and
Processes**

by

James Christopher Taylor, B.S. Ch.E.

Dissertation

Presented to the Faculty of the Graduate School of

The University of Texas at Austin

in Partial Fulfillment

of the Requirements

for the Degree of

Doctor of Philosophy

The University of Texas at Austin

May, 2007

Dedication

To My Family, Past, Present and Future

Acknowledgements

An endeavor of this magnitude could not be completed by one person alone. The full list of everyone who deserves credit for helping me get to this point would likely require another volume, so to all I say thank you. To start at the beginning, I must thank my parents. Their unending love and support have seen me through all stages of life, and this is as much a compilation of their work as it is mine. I also thank my sister, Katy, who has brought me joy and inspiration in my role as her big brother. My wife Brandi has provided me with unconditional love and care over the years of my graduate study. To her I am forever indebted.

I have had the good fortune to enjoy the friendship of several people throughout my life. Jarod McCormick, Chad Kanick, Raymond Chafin and Matt Cooper shared the experience of our education through undergraduate and into graduate school. It would never have been quite the same without them, even long distance. Jason Morehouse and Jason Cheung shared life, classes and quals here in Austin, among many others. I thank them as well for their continued friendship.

My education here at the University of Texas at Austin has been made successful thanks to the input of many people. I thank the entire Willson Research Group for serving as a family away from home. Sean Burns and Michael Stewart took me under their wings as my first year mentors, and what I learned from them has served as the fountain for my work. Charles Chambers, Bob LeSuer, Elizabeth Costner and Kane Jen contributed directly to this work, and I thank them deeply. A very special thank you goes to Kathleen Sparks, who has given more to our group than she will ever know. My work

was funded by SEMATECH and Hewlett-Packard. Thanks to Will Conley, for his advocacy of our research and many pizza lunches. Thanks to Bill Wojtczak, Dean Dewulf and Mark Stasney of SACHEM, Inc. for providing materials to support the high index fluids project. At Hewlett-Packard I would like to thank my-three-managers Sue Richards, Cathy Peltier and Laura King, as well as Tim Hostetler, Jim Ellenson, Ken Vandenberghe, Pavel Kornilovich, Bob Bicknell and Len Seals. Thanks to them for a great internship, assistance with experimentation and support for my final year.

I have been educated by many great teachers, from my first days in school to the present, and to all I am grateful. I would especially like to thank all of my committee members for helping to make this dissertation the best it can be, Dr. Bonneau, Dr. Truskett, Dr. Mack, Dr. Stiller and Dr. Willson. All have provided me with insightful discussions regarding research as well as my future. To Dr. Stiller, thanks for coming all the way from West Virginia and mentoring me while I was there. To Dr. Willson, thanks for taking a chance on an eager and bright-eyed kid from the Mountain State and introducing me to the field of microlithography. I have greatly appreciated all you have done for me over the past five years. The lessons learned here will certainly guide me through a positive and productive career. I hope to make you all proud.

Advanced Lithographic Patterning Technologies: Materials and Processes

Publication No. _____

James Christopher Taylor, Ph.D.

The University of Texas at Austin, 2007

Supervisor: C. Grant Willson

Immersion lithography has emerged as the next technology to achieve the resolution improvement needed to produce smaller and faster microelectronic devices. It involves filling the air gap between the lens and photoresist-coated silicon wafer in a lithographic exposure tool with a higher refractive index medium. This improves the coupling of light into the resist and allows for better resolution. At the current exposure wavelength of 193 nm, water has been identified as the most promising immersion medium. Several potential issues had to be resolved before the process would be adopted. One was the unknown consequence of intimate contact between water and a photoresist. Any extraction of small molecule photoresist components by water could lead to a degradation of imaging performance and/or contamination. To address this, the possible extraction of several examples of these components from model 193 nm

photoresists was studied by multiple experimental techniques including liquid chromatography/mass spectroscopy, scanning electrochemical microscopy and radiochemical analysis. It was found that both a photoacid generator and a base additive were extracted in small quantities.

A study of the optical properties of water-based solutions with ionic additives was then undertaken. This study was intended to identify fluids with a higher index than water for greater resolution improvement. The solutions had higher index values, though typically with prohibitively high absorbance. The survey did lead to a series of methylsulfonate salts with some of the highest index values paired with low absorbance found for these materials. However, none of the target fluid properties were reached, so a theoretical approach was then used to model the properties of an ideal additive. This model served as a guide to identify a new type of additive with both a high index and low absorbance.

The principles used for a high index/low absorbance additive were then applied to fabricate a polymer photonic device. A photonic crystal structure was designed for a polymer with an additive. A process for fabricating it was then developed using step and flash imprint lithography. The process development included a demonstration of a template created with a negative tone electron beam lithography process.

Table of Contents

List of Figures	xiv
List of Tables	xxiv
CHAPTER 1: INTRODUCTION TO SEMICONDUCTOR MICROLITHOGRAPHY..	1
1.1 OPTICAL LITHOGRAPHY IN SEMICONDUCTOR DEVICE FABRICATION.....	1
1.2 NEXT GENERATION LITHOGRAPHIC TECHNOLOGIES	8
1.3 193 NM AND IMMERSION LITHOGRAPHY	13
1.4 STEP AND FLASH IMPRINT LITHOGRAPHY	18
1.5 PHOTORESIST-WATER INTERACTIONS AND HIGH INDEX MATERIALS.....	21
1.6 REFERENCES	22
CHAPTER 2: IMMERSION LITHOGRAPHY AS A VIABLE TECHNOLOGY	31
2.1 PRINCIPLES OF IMMERSION LITHOGRAPHY.....	31
2.2 CHALLENGES IN IMMERSION LITHOGRAPHY.....	38
2.3 PHOTORESIST-WATER INTERACTIONS	42
2.4 SUMMARY.....	47
2.5 REFERENCES	48
CHAPTER 3: DETECTION OF PHOTORESIST COMPONENT EXTRACTION DURING IMMERSION	53
3.1 TECHNIQUES FOR EXTRACTION MEASUREMENTS	53
3.1.1 LIQUID CHROMATOGRAPHY/MASS SPECTROSCOPY	53

3.1.2	SCANNING ELECTROCHEMICAL MICROSCOPY	54
3.1.3	LIQUID SCINTILLATION COUNTING.....	54
3.2	MATERIALS: PHOTORESIST FORMULATIONS AND FILM PREPARATION	56
3.3	EXPERIMENTAL PROCEDURES FOR EXTRACTION MEASUREMENTS.	59
3.4	COMPONENT EXTRACTION FROM MODEL 193 NM PHOTORESIST FILMS BY WATER.....	61
3.4.1	LIQUID CHROMATOGRAPHY/MASS SPECTROSCOPY RESULTS...	62
3.4.2	SCANNING ELECTROCHEMICAL MICROSCOPY RESULTS.....	63
3.4.3	LIQUID SCINTILLATION COUNTING RESULTS	70
3.5	DISCUSSION OF PHOTORESIST COMPONENT EXTRACTION.....	80
3.6	SUMMARY.....	84
3.7	REFERENCES	85
CHAPTER 4: SECOND GENERATION FLUIDS FOR IMMERSION LITHOGRAPHY		89
4.1	INTRODUCTION TO SECOND GENERATION IMMERSION LITHOGRAPHY	89
4.2	CHARACTERIZATION OF OPTICAL AND PHYSICAL PROPERTIES OF FLUIDS.....	91
4.3	SURVEY OF IONIC ADDITIVES	102

4.3	DEVELOPMENT OF ADDITIVE FOR AQUEOUS 2 ND GENERATION IMMERSION FLUID	119
4.5	SUMMARY	133
4.6	REFERENCES	134
CHAPTER 5: THEORETICAL CONSIDERATIONS FOR HIGH REFRACTIVE INDICES AND LOW ABSORPTION COEFFICIENTS		139
5.1	INTRODUCTION	139
5.2	THE COMPLEX INDEX OF REFRACTION	140
5.3	THE KRAMERS-KRONIG RELATION.....	145
5.4	MODELS FOR OPTICAL PROPERTIES	147
5.5	CALCULATIONS OF DISPERSION CURVES FOR HIGH INDEX/LOW ABSORBANCE ADDITIVE.....	155
5.6	NEW ADDITIVE STRUCTURES.....	172
5.7	SUMMARY	176
5.8	REFERENCES	178
CHAPTER 6: FABRICATION OF POLYMER-BASED PHOTONIC CRYSTALS BY STEP AND FLASH IMPRINT LITHOGRAPHY		184
6.1	INTRODUCTION TO PHOTONIC CRYSTALS	184
6.2	FABRICATION OF 2D PHOTONIC CRYSTALS WITH STEP AND FLASH IMPRINT LITHOGRAPHY	186
6.3	SFIL TEMPLATE FOR 2D PHOTONIC CRYSTAL	188
6.3.1	DESIGN OF PHOTONIC CRYSTAL STRUCTURE	188

6.3.2	PREPARATION OF TEMPLATE BLANK	197
6.3.3	ELECTRON BEAM LITHOGRAPHY PATTERNING.....	198
6.3.4	DRY ETCH PATTERN TRANSFER	203
6.3.5	PATTERN VERIFICATION.....	203
6.4	FABRICATION OF POLYMER PHOTONIC CRYSTAL	206
6.4.1	MATERIALS.....	207
6.4.2	SFIL PROCESS	211
6.4.3	BREAKTHROUGH AND TRANSFER ETCHES	213
6.5	SUMMARY.....	216
6.6	REFERENCES	217
CHAPTER 7: CONCLUSIONS AND FUTURE WORK.....		222
7.1	PHOTORESIST COMPONENT EXTRACTION DURING IMMERSION ..	222
7.2	HIGH INDEX MATERIALS FOR IMMERSION LITHOGRAPHY	224
7.3	POLYMER-BASED PHOTONIC CRYSTALS FROM SFIL.....	227
7.4	REFERENCES	228
APPENDIX A: SYNTHESIS OF RADIOLABELED PHOTOACID GENERATOR AND BASE ADDITIVE.....		230
A.1	¹⁴ C-TRIPHENYLSULFONIUM PERFLUORO-1-BUTANESULFONATE.	230
A.2	¹⁴ C-TRIPENTYLAMINE	232
A.3	REFERENCES	233
APPENDIX B: CAUCHY COEFFICIENTS, MEAN SQUARED ERROR AND 90% CONFIDENCE LIMITS FOR ELLIPSOMETRY MEASUREMENTS		234

APPENDIX C: HIGH REFRACTIVE INDEX POLYMER STUDY	239
C.1 INTRODUCTION	239
C.2 MATERIALS AND SAMPLE PREPARATION.....	239
C.3 RESULTS	241
Bibliography	244
Vita.....	270

List of Figures

Figure 1.1	Schematic of the semiconductor microlithography process.	3
Figure 1.2	Components of cyclized rubber negative tone photoresists.....	5
Figure 1.3	Components of DNQ/novolak resists.	6
Figure 1.4	Decomposition of <i>t</i> -BOC into PHOST and side products in the presence of acid and heat.	8
Figure 1.5	Assist features are added to a mask pattern so that aerial image matches the desired pattern even though the mask does not.....	11
Figure 1.6	Effect of 180° phase shifter on aerial image intensity.	12
Figure 1.7	IBM and UT polymers used for 193 nm photoresists.....	14
Figure 1.8	Schematic of the step and flash imprint lithography process.	19
Figure 2.1	Snell's Law through a film stack	32
Figure 2.2	Intensity distribution of light transmitted through a screen with a) a single aperture and b) with multiple apertures	34
Figure 2.3	Illustration of an imaging system in a lithographic exposure tool.....	36
Figure 2.4	Structure of acrylic polymer from TOK	44
Figure 2.5	Structures of tert-butylphenyliodonium perfluorooctanesulfonate (TBI-PFOS) and triphenylsulfonium perfluorobutanesulfonate (TPS-PFBS) PAGs studied in photoresist extraction experiments	44
Figure 2.6	Film thickness vs. time of TOK resist during water immersion.....	46
Figure 2.7	Refractive index vs. time of TOK resist during water immersion.....	47
Figure 3.1	Model 193 nm photoresist polymers from TOK and AZ	57

Figure 3.2	Structures of radiolabeled photoresist components	58
Figure 3.3	Concentration of nonaflate anion from extracted PAG/photoacid in immersion water vs. contact time	62
Figure 3.4	pH measurements of liquid layer above a film of TOK-ILP01	64
Figure 3.5	Square wave voltammograms at a Hg hemisphere microelectrode above a film of TOK-ILP01, the distance between the electrode and the film is noted in the legend	66
Figure 3.6	Conductivity approach curves of 4 wt% PAG loaded T-518 immersed in 18 M Ω water	68
Figure 3.7	Change in conductivity of immersion water over various resist formulations and quartz. Inset is plot of the slopes of the conductivity versus time plot.....	70
Figure 3.8	Radioactivity expressed as total counts in 20 min from background and from water samples that immersed resist films with ¹⁴ C-labeled RCS for various times	72
Figure 3.9	Radioactivity in <i>CPM</i> of immersion water containing extracted ¹⁴ C-PAG vs. immersion time.....	74
Figure 3.10	Radioactivity in <i>CPM</i> of immersion water containing extracted ¹⁴ C-PAG from AZ T-518 vs. immersion time.....	74
Figure 3.11	Radioactivity in <i>CPM</i> of immersion water containing extracted ¹⁴ C-PAG from unexposed and exposed films of TOK-ILP01 vs. immersion time..	76

Figure 3.12	Radioactivity in <i>CPM</i> of 30 s pre-rinse and immersion water containing extracted ^{14}C -PAG from films of TOK-ILP01 vs. immersion time.....	76
Figure 3.13	Radioactivity in <i>CPM</i> of immersion water containing extracted ^{14}C -PAG from films of TOK-ILP04 vs. film thickness.....	77
Figure 3.14	Radioactivity in <i>CPM</i> of immersion water containing extracted ^{14}C -base vs. immersion time.....	78
Figure 3.15	Radioactivity in <i>CPM</i> of 30 s pre-rinse and immersion water containing extracted ^{14}C -base from films of TOK-ILP01 vs. immersion time	79
Figure 3.16	Radioactivity in <i>CPM</i> of immersion water containing extracted ^{14}C -base from films of TOK-ILP04 vs. film thickness.....	80
Figure 3.17	XPS analysis of fluorine content in wafers coated with AZ T-518 both washed (\blacklozenge) and unwashed (\blacksquare).....	83
Figure 4.1	Possible polarizations for an electric field vector	92
Figure 4.2	The electric field vectors of the <i>p</i> - and <i>s</i> -waves relative to the plane of incidence	93
Figure 4.3	Index of refraction of water vs. wavelength determined by direct ellipsometric measurement and by prism deviation methods used by NIST and with the Woollam VUV-VASE®	97
Figure 4.4	Interfaces in quartz cuvettes contributing to transmission losses	100
Figure 4.5	Transmittance of empty quartz cuvette vs. wavelength, both measured and corrected for interfacial reflections.....	101
Figure 4.6	Absorption coefficient of water vs. wavelength	101

Figure 4.7	Refractive index dispersion curves for sodium chloride solutions of difference concentrations	103
Figure 4.8	Dispersion curves for refractive indices of 2 M chloride salt solutions .	105
Figure 4.9	Dispersion curves for refractive indices of 2 M bromide salt solutions .	106
Figure 4.10	Dispersion curves for refractive indices of 2 M acetate salt solutions ...	106
Figure 4.11	Refractive index values of 2 M chloride, bromide and acetate salt solutions vs. cation at 193 nm	107
Figure 4.12	Dispersion curves for refractive indices of 2 M acid solutions	108
Figure 4.13	Dispersion curves for refractive indices of 2 M sodium salt solutions...	109
Figure 4.14	Refractive index values of 2 M acid solutions vs. anion at 193 nm	109
Figure 4.15	Refractive index values of 2 M sodium salt solutions vs. anion at 193 nm	110
Figure 4.16	Absorption spectra of sodium chloride solutions of different concentration vs. wavelength.....	111
Figure 4.17	Absorption spectra of 1 mM chloride salt solutions	112
Figure 4.18	Absorption spectra of 0.1 mM bromide salt solutions.....	113
Figure 4.19	Absorption spectra of 1 mM acetate salt solutions	113
Figure 4.20	Absorption coefficients of 1 mM chloride, 0.1 mM bromide and 1 mM acetate salt solutions at 193 nm vs. cation	114
Figure 4.21	Absorption spectra of 0.1 mM acid solutions	115
Figure 4.22	Absorption spectra of 0.1 mM sodium solutions	116
Figure 4.23	Absorption coefficients of 0.1 mM acid solutions at 193 nm vs. anion .	116

Figure 4.24	Absorption coefficients of 0.1 mM sodium salt solutions at 193 nm vs. anion.....	117
Figure 4.25	Dispersion curves for refractive indices of 5 mol% quaternary ammonium acetate salt solutions	120
Figure 4.26	Index values of 5 mol% quaternary ammonium acetate salt solutions at 193 nm vs. cation	121
Figure 4.27	Absorption spectra of 1 mM quaternary ammonium acetate salt solutions	121
Figure 4.28	Absorption coefficient values of 1 mM quaternary ammonium acetate salt solutions at 193 nm vs. cation.....	122
Figure 4.29	Dispersion curves for refractive indices of additional 5 mol% quaternary ammonium salt solutions	123
Figure 4.30	Index values of 5 mol% quaternary ammonium salt solutions at 193 nm	124
Figure 4.31	Refractive index dispersion curves for 2 M methylsulfonate salt solutions	126
Figure 4.32	Index values of 2 M methylsulfonate salt solutions at 193 nm vs. cation	127
Figure 4.33	Absorption spectra for 2 M methylsulfonate salt solutions	127
Figure 4.34	Absorption coefficients of 2 M methylsulfonate salt solutions at 193 nm vs. cation	128

Figure 4.35	Refractive index dispersion curves for saturated quaternary ammonium methylsulfonate salt solutions, where R = H or alkyl chain	129
Figure 4.36	Index values of saturated quaternary ammonium methylsulfonate salt solutions at 193 nm, where R = H or alkyl chain	130
Figure 4.37	Absorption spectra for saturated quaternary ammonium methylsulfonate salt solutions, where R = H or alkyl chain	130
Figure 4.38	Absorption coefficients of saturated quaternary ammonium methylsulfonate salt solutions at 193 nm, where R = H or alkyl chain ..	131
Figure 4.39	Scanning electron micrographs (SEM) of 65 nm half-pitch lines and spaces imaged with methylsulfonate solutions.	132
Figure 4.40	SEM micrographs of line and space patterns imaged with saturated lanthanum methylsulfonate solution	132
Figure 4.41	SEM micrograph of 34.5 nm half-pitch line and space pattern imaged with NR ₄ O ₃ SCH ₃ (c).....	133
Figure 5.1	Dispersion curves calculated from Equations 5.37 and 5.38 for ϵ_1 and ϵ_2 versus wavelength.....	152
Figure 5.2	Dispersion curves calculated from Equations 5.37 and 5.38 for n and k versus wavelength.....	153
Figure 5.3	Index offset at higher wavelengths increases as amplitude of absorption peak at lower wavelengths increases, indicating benefit of additional absorption in immersion additives	156

Figure 5.4	Refractive index and extinction coefficient values for water from the <i>Handbook of Optical Constants</i>	159
Figure 5.5	Absorption peak shoulders at 125 nm, 70 nm and 50 nm.....	159
Figure 5.6	Dispersion of the refractive index of water calculated from two-oscillator Lorentz model compared to reported values from the <i>Handbook of Optical Constants</i>	161
Figure 5.7	Dispersion of the extinction coefficient of water calculated from two-oscillator Lorentz model compared to reported values from the <i>Handbook of Optical Constants</i>	162
Figure 5.8	Dispersion of the refractive index of water calculated from three-oscillator Lorentz model compared to reported values from the <i>Handbook of Optical Constants</i>	163
Figure 5.9	Dispersion of the extinction coefficient of water calculated from three-oscillator Lorentz model compared to reported values from the <i>Handbook of Optical Constants</i>	163
Figure 5.10	Refractive index at 193 nm of modeled solution versus amplitude of first absorption peak for different broadening values	167
Figure 5.11	Extinction coefficient at 193 nm of modeled solution versus amplitude of first absorption peak for different broadening values.....	168
Figure 5.12	Dispersion curves for additive with one absorption peak at $E_0 = 6.85$ eV, $A = 21.5$ and $\Gamma = 1$	168

Figure 5.13	Dispersion curves for Lorentz model of additive calculated from parameters in Table 5.3.....	170
Figure 5.14	Dispersion curves for Lorentz model of additive calculated from parameters in Table 5.4.....	171
Figure 5.15	Dispersion curves for model solution of the additive and water, with $n = 1.65$ and $k = 0.087$	171
Figure 5.16	Refractive index dispersion curves for hexane, cyclohexane and decalin	174
Figure 5.17	Absorption coefficients of hexane, cyclohexane and decalin.....	175
Figure 5.18	Refractive index dispersion of solutions of sodium cyclohexanesulfonate and sodium decalinsulfonate compared to that of water.....	175
Figure 5.19	Absorbance of sodium cyclohexanesulfonate and sodium decalinsulfonate referenced to water.....	176
Figure 6.1	Possible configurations for photonic crystals with one-, two- and three-dimensional dielectric periodicity.....	186
Figure 6.2	Two-dimensional photonic crystal with triangular lattice of air holes in a dielectric slab. The unit cell of the lattice is shown in orange and the first Brillouin zone is shown in the right inset	191
Figure 6.3	Photonic crystal band structure for 2D triangular lattice of air holes in PMMA slab of $n = 1.5$	191
Figure 6.4	Close-up of initial band structure showing no complete band gap exists since adjacent bands either intersect or overlap.....	193

Figure 6.5	Direction dependent band gaps following $\Gamma - M$ path along Brillouin zone	193
Figure 6.6	Gap map for triangular lattice of air holes in PMMA slab	194
Figure 6.7	Layout of structures for photonic crystal template	196
Figure 6.8	Scanning electron micrograph of photonic crystal structure exposed at 10 $\mu\text{C}/\text{cm}^2$ with 150 nm nominal feature sizes	200
Figure 6.9	Feature diameter vs. e-beam exposure dose for 150 nm and 175 nm posts	200
Figure 6.10	SEMs of nominally 150 nm and 175 nm posts exposed at $7.3 \mu\text{C}/\text{cm}^2$..	201
Figure 6.11	SEM of test imprint from first template showing no photonic crystal structure and oversized ridges almost merged together	202
Figure 6.12	SEM micrographs of photonic crystal structures on SFIL template.....	204
Figure 6.13	Micrograph of photonic crystal structure in test imprint	205
Figure 6.14	Micrographs of a) 150 nm nominal photonic crystal features and b) 175 nm nominal features.....	206
Figure 6.15	Cross-section micrograph of guide ridges showing 200 nm imprint depth	206
Figure 6.16	Structures of coumarin 6 and generic Clariant benzoxazine dye.....	208
Figure 6.17	Absorption spectrum of coumarin 6	209
Figure 6.18	Absorption spectra for two Clariant benzoxazine dyes	209
Figure 6.19	Refractive index dispersion curves for PMMA and dye composite films	210

Figure 6.20	Extinction coefficient dispersion curves for PMMA and dye composite films	210
Figure 6.21	Gap map for triangular lattice in PMMA/coumarin 6 composite	211
Figure 6.22	SEM micrographs of imprinted photonic crystal structures showing defect-free and defect-containing fields after over one hundred imprints	212
Figure 6.23	SEM micrographs showing feature measurements of a) 150 nm nominal features and b) 175 nm nominal features	213
Figure 6.24	SEM micrographs of structures with undercut defects	215
Figure 6.25	SEM micrographs of defect-free structure after etch and cross-section view of guide ridges confirming complete etch transfer into polymer film	215
Figure 6.26	Micrograph showing feature measurements of 175 nm nominal features	216
Figure C.1	Structures of dissolution inhibitors used in PNBHFA	241
Figure C.2	Index of refraction vs. wavelength of polystyrene and derivatives	242
Figure C.3	Index of refraction vs. wavelength of PNBHFA and PNBHFA-SO ₂	243
Figure C.4	Index of refraction PNBHFA with 5 wt% loading of dissolution inhibitors	243

List of Tables

Table 4.1	Kinematic viscosities of 2 M ionic solutions.....	118
Table 4.2	Contact angles of 2 M ionic solutions.....	118
Table 4.3	Kinematic viscosities of quaternary ammonium salt solutions.....	124
Table 4.4	Contact angles of quaternary ammonium salt solutions	124
Table 4.5	Surface tension and viscosity of methylsulfonate solutions	128
Table 4.6	Surface tension and viscosity of methylsulfonate solutions	131
Table 5.1	Parameters for two-oscillator Lorentz model of water	161
Table 5.2	Parameters for three-oscillator Lorentz model of water	162
Table 5.3	Initial parameters for Lorentz model of additive	169
Table 5.4	Parameters for Lorentz model of additive found by Excel Solver.....	170
Table 6.1	Template fabrication procedure for NEB 31A3 resist	202
Table 6.2	Process conditions for etch transfer into template	203
Table 6.3	Etch recipes for photonic crystal pattern transfer into PMMA.....	214

CHAPTER 1: INTRODUCTION TO SEMICONDUCTOR MICROLITHOGRAPHY

1.1 OPTICAL LITHOGRAPHY IN SEMICONDUCTOR DEVICE FABRICATION

In 1947, researchers at Bell Laboratories built the first functioning transistor with the hope of replacing vacuum tubes in electronic devices with faster-switching solid state components. The transistor, a device made by creating two junctions between *p*- and *n*-type semiconductors, had such an immediate and profound impact on the electronics industry that its inventors, William Shockley, John Bardeen and Walter Brattain, were awarded the Nobel Prize in 1956.¹⁻³ Just three years later, in 1959, the transistor was involved in another innovation which would have even farther-reaching consequences. Jack Kilby of Texas Instruments and Robert Noyce of Fairchild Semiconductor (and a former employee of Shockley) independently demonstrated devices in which all of the components of an electrical circuit – transistors, resistors, capacitors, interconnections, etc. – were built out of a common substrate.⁴ By allowing all of these components to be placed and connected so close together, the integrated circuit (IC) enabled devices of significantly smaller size and much greater computing power to be created. The resulting technological revolution has put telephones in people's pockets, computers in their hands and connected almost all parts the world. There is even further promise of new technologies, greater computing power and even a deeper understanding of our world that relies on continuing to improve the performance of integrated circuits.

The key to improved device performance and reduced cost has been fabricating circuits with smaller and more closely packed components. Indeed, since 1965 it has been observed that the number of components per chip has doubled every one to two years.⁵ This trend – now commonly known as Moore’s Law, after Gordon Moore, a colleague of Noyce at Fairchild and later co-founder of Intel, who first noted it – has driven the semiconductor industry’s technology roadmap for the past forty years, and will continue to do so.⁶ The devices in an IC are built up layer by layer through a process known as semiconductor microlithography.⁷⁻⁹ In the basic process flow, a semiconductor substrate, typically a silicon wafer, is spin coated with a photosensitive polymeric film, which is selectively exposed to ultraviolet radiation through a chromium plated quartz photomask. The chromium is arranged in a pattern that corresponds to a particular layer design. The exposure and a subsequent bake step initiate a solubility switching reaction in the polymer, after which the soluble portion is removed and the underlying substrate is revealed. Etch or implant and strip processes then transfer the resulting pattern into the substrate and remove the polymer. The process is shown schematically in Figure 1.1.

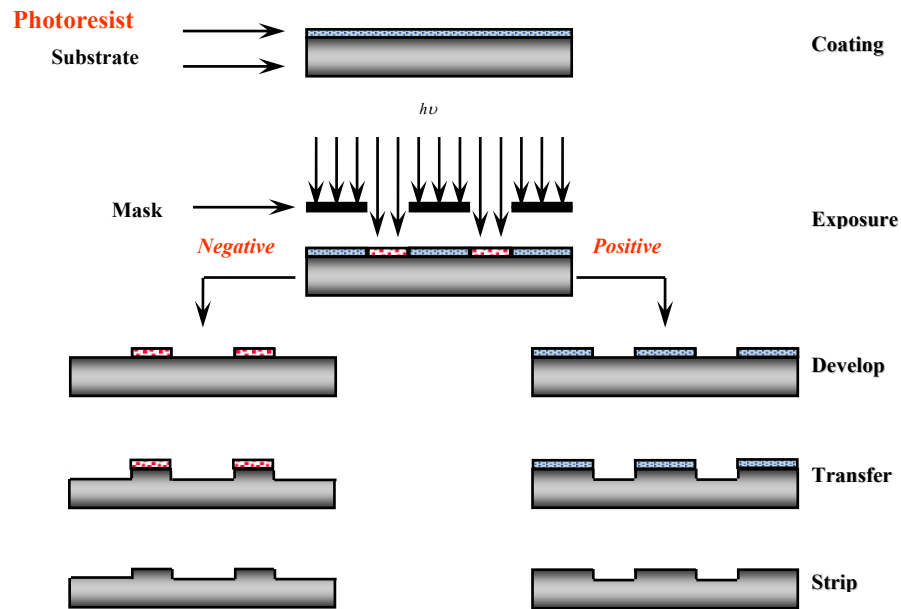


Figure 1.1 Schematic of the semiconductor microlithography process.

The size of the device features is determined by the exposure step. Early lithographic technology brought the photomask into contact with the polymer-coated wafer, which was then flood exposed by a UV light source. The features drawn in chromium on the masks were the same size as those printed on the wafer. While this technique was relatively inexpensive and had high resolution, it also created an increasing number of defects each time a mask touched a wafer, leading to decreasing device yields.^{7,8} This issue was reduced by introducing a gap between the mask and the wafer in what was called proximity printing. However, the resolution was markedly decreased due to diffraction of light at the edges of mask features.⁹ In order to improve resolution and reduce defects, projection printing techniques were adopted in the mid-1970s. Projection lithography involves the use of a lens system to focus the diffraction

pattern created by a photomask onto the wafer. The first projection systems used a 1:1 imaging scheme before being replaced with reduction optics. With this type of lens system, devices with feature sizes four to five times smaller than those on the mask (now called a reticle) could be fabricated. The minimum resolution of these systems is given by the Rayleigh criterion,

$$R = k_1 \frac{\lambda}{n \sin \theta} = k_1 \frac{\lambda}{NA} \quad (1.1)$$

where R is the minimum resolvable feature size, k_1 is a process dependent parameter, λ is the vacuum wavelength of the exposure radiation, n is the index of refraction of the medium into which the image is being projected (typically air) and θ is the half angle aperture of the lens. The product of n and $\sin \theta$ is called the numerical aperture (NA) of the lens.¹⁰ According to Equation 1.1, feature sizes can be reduced by lowering k_1 , lowering λ or increasing NA . Improvements in the imaging system to lower k_1 , and the use of larger lenses with larger NA s have lead to incremental improvements in resolution, but the biggest changes have occurred with new exposure sources producing smaller wavelengths of light. The flood exposure sources of the first systems were replaced with mercury arc lamps filtered to produce 436 nm and then 365 nm light for projection lithography. These were eventually replaced with excimer lasers producing deep ultraviolet (DUV) radiation, first at 248 nm with krypton-fluorine (KrF) lasers and now at 193 nm with argon-fluorine (ArF) lasers. These improvements and process changes have reduced device feature sizes from tens of microns in the mid-1970s to sub-100 nm today.

Each step down in exposure wavelength involved more than just a change in the radiation source. New optical systems had to be developed, and new materials were needed. The most crucial material was the polymer used in the imaging step. The polymer involved in the lithographic process is known as a photoresist; “photo” indicates that it is chemically sensitive to light, and “resist” refers to its ability to act as a barrier to the etch transfer or other post exposure process.^{7, 8} The first photoresists were cyclized 1,4-poly(*cis*-isoprene) rubbers sensitized with a photoactive *bis*-aryldiazide, Figure 1.2.^{7, 8, 11} Upon exposure to 300 – 400 nm radiation, the sensitizer decomposes into a highly reactive cross-linking agent, which attaches polymer chains together, effectively increasing the polymer’s molecular weight in the exposed region and reducing its solubility in an organic solvent. The solvent used to dissolve the unexposed regions of the resist (known as developing the resist) leaves a negative tone image of the pattern on the photomask (as seen in Figure 1.1). These resists were used until the mid-1970s, when their ability to resolve micron size features reached its limit, partially due to swelling caused by the organic developers.

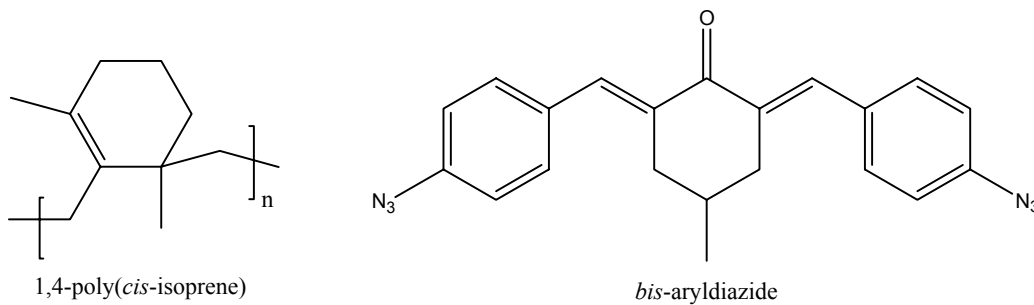


Figure 1.2 Components of cyclized rubber negative tone photoresists.

The next major resist platform to be used was a positive tone resist, where the exposed portions are rendered soluble in a developer. This system used a novolak polymer with a diazonaphthoquinone (DNQ) sensitizer and was exposed with mercury arc lamps, producing either 436 nm or 365 nm radiation, Figure 1.3.^{8, 12} Novolak provided good etch resistance, and when immersed in an aqueous base, the DNQ acted as a dissolution inhibitor to the slightly acidic polymer. The aqueous solution was used to limit swelling. During exposure, the DNQ, generically referred to as a photoactive compound (PAC), undergoes a photo-induced reaction to form a more transparent product and that accelerates dissolution in the base developer, typically 0.26 N tetramethylammonium hydroxide (TMAH). The bleaching of the PAC was facilitated by novolak's transparency to UV radiation through 365 nm. Photosensitivity, transparency, etch resistance and solubility in TMAH all became major requirements for new photoresist materials. DNQ/novolak resists were so successful that they were used to fabricate the bulk of semiconductor devices from the mid-1970s through the late 1990s, and they are still used today.¹³

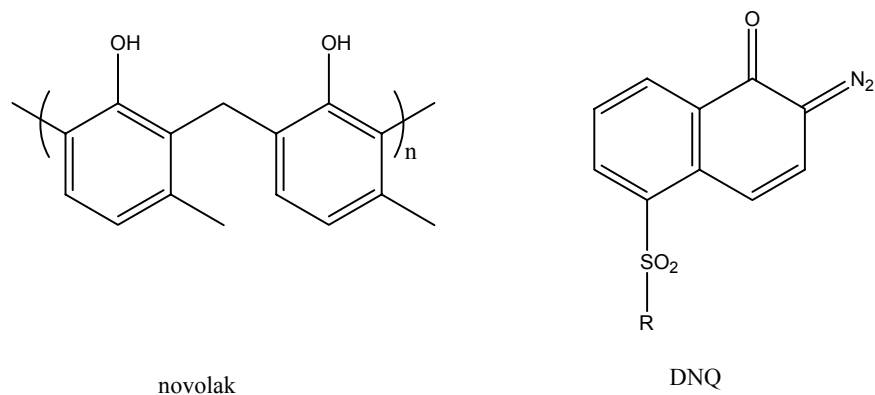


Figure 1.3 Components of DNQ/novolak resists.

The switch to 248 nm excimer lasers required a new type of photoresist platform. The novolak polymers were found to be too opaque in the DUV region to be used effectively. A similar polymer, polyhydroxystyrene (PHOST), was found to be transparent at 248 nm; however, the dissolution inhibition behavior of the DNQ/novolak systems was never observed when typical PACs were added to PHOST. This difficulty was compounded by the fact that early DUV sources produced lower intensity radiation than the higher wavelength sources, so the sensitivity of resists was also in need of improvement. These issues were addressed with a new approach to photo-induced solubility switching reactions. Instead of relying on one photon to initiate one reaction, *e.g.*, activating one cross-linking agent or decomposing one DNQ molecule, it was found that the PAC could become a catalyst for several reactions through a process known as chemical amplification.¹⁴⁻¹⁶ After exposure, a post exposure bake step (PEB) would initiate a reaction in which the catalyst reacts with groups pendant from the polymer backbone changing the solubility properties of individual monomer units, and thus minimizing the exposure dose, the energy deposited per unit area, needed for the imaging process. A common example of a chemically amplified resist is poly(*p*-*t*-butyloxycarbonyloxystyrene) (*t*-BOC), which in the presence of an acid catalyst and heat undergoes a deprotection reaction that forms PHOST, carbon dioxide and isobutylene as side products, Figure 1.4. The deprotection therefore increases the solubility in the exposed regions. The most common PACs for chemically amplified resists form acid catalysts and are called photoacid generators (PAGs). Chemically amplified resists have been successfully used for lithography at 248 nm, 193 nm (with acrylic based polymers)

and even at 157 nm (with fluorinated alicyclic polymers) and are the most prominent resist platform today.¹⁷

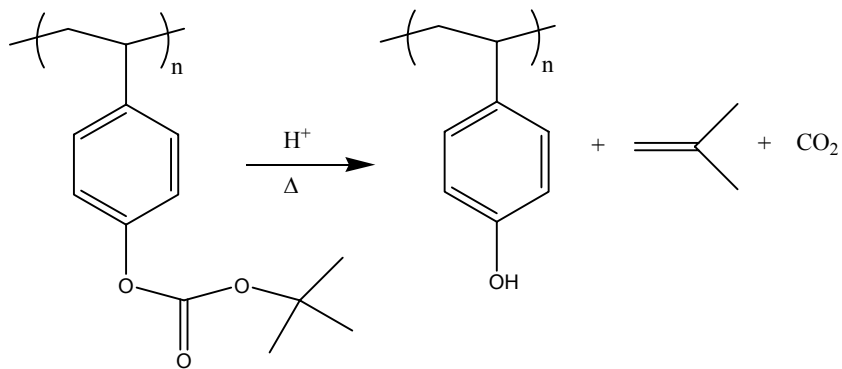


Figure 1.4 Decomposition of *t*-BOC into PHOST and side products in the presence of acid and heat.

1.2 NEXT GENERATION LITHOGRAPHIC TECHNOLOGIES

Even though lithography using the optical techniques previously described has been the mainstay of the semiconductor industry for over thirty years, its demise has been predicted many times.¹¹ An array of alternative lithographic technologies collectively known as next-generation lithography (NGL) has been proposed for that time, but none have yet to supplant optical lithography. The most drastically different techniques involve particle beams as the exposure sources. Electron-beam lithography (e-beam) focuses a stream of electrons onto a resist coated wafer.¹⁸ The electrons cause a reaction in the polymer in the exposed regions which changes its solubility properties.¹⁹ Because of the extremely small wavelength associated with electrons, e-beam is not limited by diffraction so it can achieve very small resolution. However, it is a direct write process,

i.e., the electron beam writes features one at a time directly into the resist instead of passing through a reticle, so the exposure time is long compared to optical lithography. Low throughput has prohibited e-beam from being adopted in high volume manufacturing. A similar process is called ion-beam lithography, where the stream of electrons is replaced with one of ions.¹⁹ Ion-beam offers improved resolution over e-beam because of the lower scattering of ions as well as the potential for large-area projection, but technical challenges such as insufficient sources have precluded its adoption as well.⁸

Another more evolutionary NGL is extreme ultraviolet lithography (EUV), which was first proposed in 1988.^{13, 20} EUV uses exposure radiation that is in a much lower wavelength range than DUV sources, typically 13 nm. In this range, essentially all material is opaque, so refractive optical systems and transparent photoresists are not feasible. All of the optics in EUV systems are reflective, including the masks. These mirrors are fabricated with multilayer dielectrics, such as alternating layers of molybdenum and silicon, and can only tolerate a few defects 1 nm in size or less.²¹ Since the photoresists are also absorbing, a different imaging scheme such as top-surface imaging or a bilayer system is also necessary. Currently, the biggest challenge for adoption of EUV is the lack of an efficient exposure source that produces adequate energy. EUV sources have included synchrotrons, free-electron lasers and hot plasmas, with efficiencies for the latter reported to be approximately 2%.^{22, 23} Despite the difficulties, EUV is the favored NGL to eventually replace optical lithography.

The least extreme NGL has already found some application in semiconductor fabrication. Resolution enhancement techniques (RET) do not involve major changes to the exposure systems like the previously discussed NGLs. Instead, they modify current optical systems based on an advanced understanding of how actual images of the features are formed during exposure.²⁴⁻²⁶ This approach focuses on lowering the k_1 parameter in the Rayleigh criterion, Equation 1.1. Three common RETs are optical proximity correction (OPC), off-axis illumination (OAI) and phase-shift masking (PSM). OPC involves adding assist features to a mask pattern so that the aerial image formed during exposure will more closely resemble the target pattern. This image correction becomes necessary when an exposure tool is pushed toward its resolution limit. At that condition, adjacent features affect how each other are imaged. This effect is manifested by line shortening, corner rounding and iso-dense bias, where isolated features are printed differently than densely packed features. Figure 3 illustrates how OPC would be used to obtain a 90° bend feature.

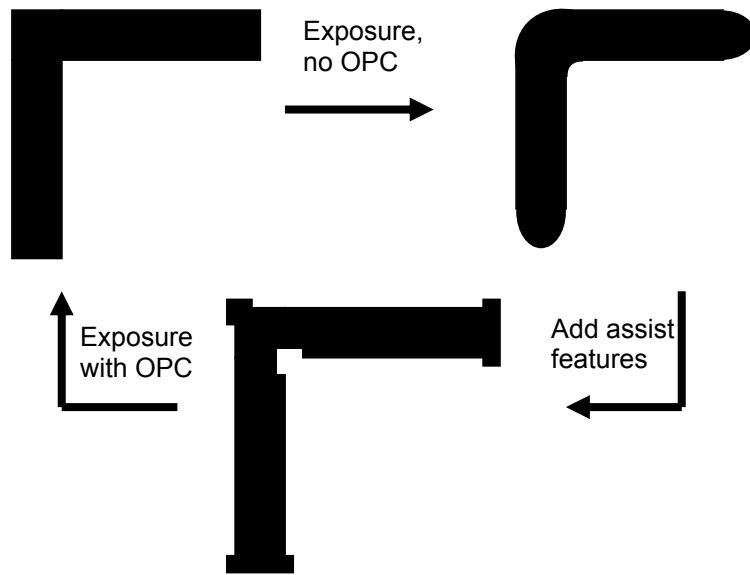


Figure 1.5 Assist features are added to a mask pattern so that aerial image matches the desired pattern even though the mask does not.

OAI uses pupil filters to shape the illumination from an exposure source. Conventional illumination is circular, whereas OAI typically uses an annular, dipole or quadrupole (two or four symmetric openings) shape. These shapes prevent on-axis diffraction orders from being collected by the lens and imaged. This increases the contrast of aerial images of small, densely packed features. However, OAI can only be optimized for one pattern configuration and pitch at a time, so it's often used with other RETs, such as OPC and PSM.^{13, 27} PSM takes advantage of the relationship between the amplitude and intensity of light. When light passes through a reticle with a line and space pattern, the amplitude at the center of the spaces is equal in magnitude and direction and non-zero at the center of the lines. The intensity, which is the square of the amplitude, of the light in the region of the line can become so high that the two spaces

become blurred together. By introducing a 180° phase shift through an additional length of quartz at every other space, the amplitude and therefore the intensity drops to zero between each, allowing for a distinct image of each line to be formed, Figure 1.6.

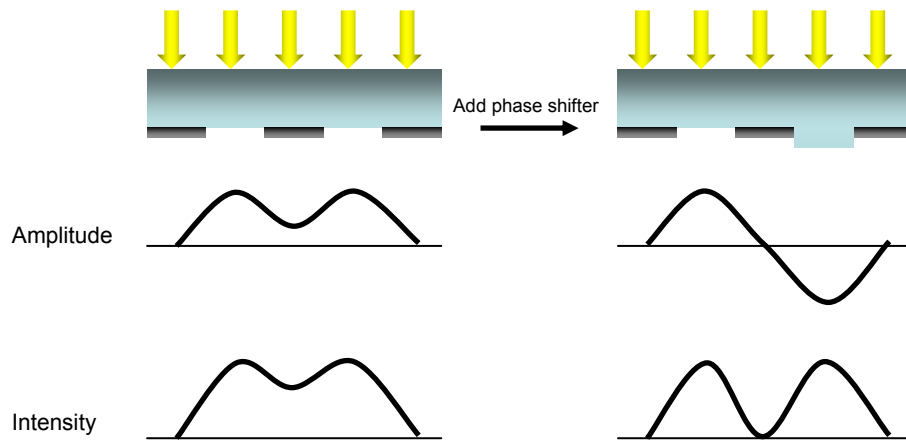


Figure 1.6 Effect of 180° phase shifter on aerial image intensity.

While these three RETs are being used for leading edge lithography, there are still others yet to be adopted in mainstream semiconductor fabrication. Maskless interferometric lithography is perhaps the ultimate RET. In this approach, two beams of coherent light interfere with each other to produce a periodic pattern whose minimum achievable pitch is determined only by the wavelength of light and the angle at which the two beams intersect. However, it has not yet been shown to create the array of arbitrary shapes that optical lithography can. Another technique which could be seen as an extreme form of PSM is called double patterning. Instead of placing an additional amount of quartz on every other line as shown in Figure 1.6, those lines are actually removed from one reticle and placed on another. The full pattern is created by exposing

and etching a wafer to one of the masks first, and then to the other. This process would likely result in reduced throughput as well as introduce the technical challenge of ensuring accurate overlay of the two exposures, but it has been attracting serious consideration from the semiconductor industry.

1.3 193 NM AND IMMERSION LITHOGRAPHY

Despite the availability of NGLs, optical lithography has remained the preferred patterning technology of the semiconductor industry. In the past several years, 248 nm lithography has given way to 193 nm lithography as the state of the art. The switch required the development of new photoresists since the aromatic polymers used at 248 nm were not transparent at 193 nm. Initial development at IBM focused on acrylic-based polymers which had the necessary transparency and could be imaged with chemical amplification.^{28, 29} These polymers lacked the etch resistance needed for use as photoresists, so alicyclic pendant groups were added to the polymer, Figure 1.7.³⁰ A steroid-based additive was also added to the resist formulation to improve both dissolution characteristics and etch resistance. Here at The University of Texas at Austin, polymers of cycloolefins were developed to further improve etch resistance. A resist formulation with a copolymer of *tert*-Butyl tetracyclo[4.4.0.1.1]dodec-3-ene-5-carboxylate and maleic anhydride (DBNC-*alt*-MA), Figure 1.7, a photoacid generator, a dissolution inhibitor and a base additive successfully imaged 110 nm features with a conventional reticle and imaged 80 nm features with PSM.³¹ Further refinements to the acrylic and DBNC-*alt*-MA resist formulations have resulted in successful, but complex,

systems that have become the basis for commercial photoresists.³²⁻³⁶ Once expected to reach a minimum feature size of 130 nm, 193 nm lithography with RET has pushed through the 90 nm node and is being ramped up to produce devices with 65 nm features. Intel has also recently announced plans to use 193 nm technology for its 45 nm process.

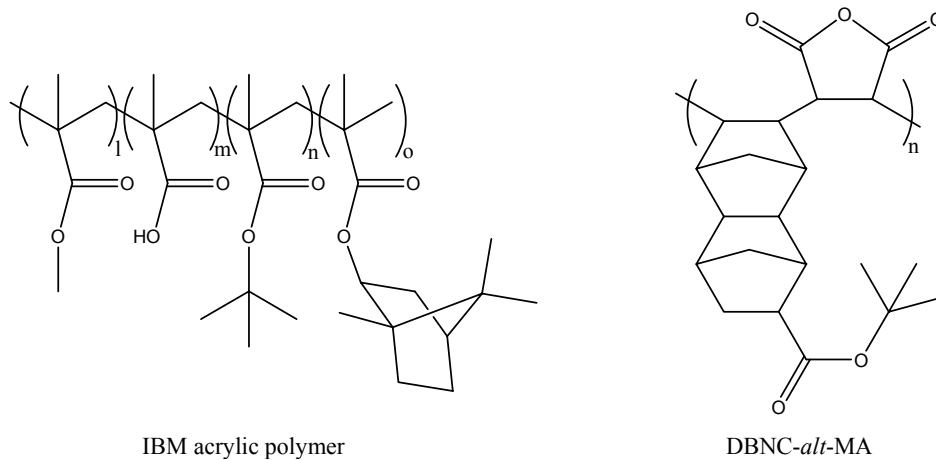


Figure 1.7 IBM and UT polymers used for 193 nm photoresists.

Until the early 2000s, 193 nm lithography was expected to be replaced with optical lithography using 157 nm light until an NGL such as EUV became production ready.¹⁷ While the move to 157 nm would have maintained the spirit of optical lithography, it faced major technical challenges. At 157 nm, more than just the current photoresists became opaque. Conventional silica-based optical elements would have had to be replaced with calcium fluoride lens elements. The reticle substrate would also need to be changed. A particular challenge was developing a new pellicle, which is a thin, transparent film placed just above the reticle surface to protect against particle

contamination. These difficulties were further compounded by the need to purge the exposure tool with nitrogen since most of the other components of air are also strongly absorbing.³⁷

The relatively small resolution improvement in the switch to 157 nm compared to the earlier wavelength reductions was an additional concern. In 2001, researchers at Massachusetts Institute of Technology's Lincoln Laboratory demonstrated the use of an unconventional RET with 157 nm lithography which resulted in a resolution enhancement comparable to that obtained by switching from 248 nm light to 193 nm.³⁸ This technique, called immersion lithography, was first proposed in the 1980s and studied theoretically as a means of achieving improved resolution as well as depth of focus.³⁹⁻⁴² Depth of focus (DOF) is a process parameter that defines the required range of focus for a pattern to be accurately printed.¹⁰ For low NA lenses, it is conventionally given by

$$DOF = k_2 \frac{\lambda}{NA^2} \quad (1.2)$$

where the parameters are defined as in Equation 1.1; note that k_2 is not the same as k_1 . Immersion lithography is an adaptation of oil immersion microscopy where the gap between the final lens element of an exposure tool and photoresist is filled with a fluid with an index of refraction greater than that of air. Resolution enhancement from immersion had been previously demonstrated with interferometric lithography, where the periodicity (P) is given by

$$P = \frac{\lambda}{2n \sin \theta} \quad (1.3)$$

where λ is the wavelength of the interfering light, n is the index of refraction of the medium in which the interference takes place and θ is the angle of incidence of the beams.⁴³ In a projection system immersion was predicted to result in an improvement in resolution by a factor of $1/n$, according to Equation 1.1, by permitting lenses with NAs greater than one to be fabricated. Alternatively, if resolution was kept constant, it would result in an improvement in DOF by a factor of approximately n by redefining the expression for DOF as

$$DOF = k_3 \frac{\lambda}{n} \frac{1}{\sin^2 \left[\frac{1}{2} \sin^{-1} \left(\frac{1}{n} \sin \theta_0 \right) \right]} \quad (1.4)$$

where $\sin \theta_0 = n \sin \theta$.⁴⁴ While immersion was initially being proposed for use at 157 nm, it was noted in early 2002 that the desired properties of a high index of refraction and a low absorbance from an immersion fluid would be more easily obtained at the 193 nm wavelength. It was also noted that at that wavelength, water was the most transparent liquid tested with an absorption coefficient of $\alpha = 0.036 \text{ cm}^{-1}$ base 10 and an index previously measured of $n = 1.47$.⁴⁵

The unresolved technical issues associated with 157 nm lithography and the high costs of manufacturing exposure tools with all calcium fluoride lens elements had been raising doubts about the feasibility of its implementation in high volume manufacturing. The identification of water as a potential immersion fluid at 193 nm and the subsequent recognition that immersion at 193 nm could offer greater resolution enhancement than that offered by the switch to 157 nm resulted in a movement away from 157 nm as the next lithographic technology.⁴⁶⁻⁵¹ In 2002, SEMATECH, an international consortium of

semiconductor companies began leading a collaborative effort to fully investigate 193 nm immersion lithography as a potential candidate for device fabrication. Of the major issues identified in this effort, interactions between the photoresist and immersion fluid were of chief concern. Degradation of image quality, creation of defects and/or contamination as a result of these interactions could have been showstoppers for immersion. A thorough understanding of these interactions was needed to move forward with the development of the process. However, photoresists had become multi-component materials with many potentially water soluble small molecule additives. Sensitive measurement techniques would be needed to detect extraction of any of these components by water during immersion. Also, water absorption by the photoresist needed to be quantified to ensure that it did not pose a problem. To create a clear picture of photoresist-water interactions, multiple experimental techniques were used. Water absorption was measured by quartz crystal microbalance, reflectance spectroscopy, secondary ion mass spectroscopy, spectroscopic ellipsometry, and neutron and x-ray reflectivity.⁵²⁻⁵⁴ Photoresist component extraction was examined by near-edge x-ray absorption fine structure spectroscopy, gas chromatography/mass spectrometry, liquid chromatography/mass spectrometry, radiochemical analysis with liquid scintillation counting, and three types of scanning electrochemical microscopy.^{52, 53, 55}

This combined body of work made it clear that some of the small molecule components did indeed get extracted by the water and that a small amount of water was absorbed during immersion. Several schemes such as resist top-coats or pre-rinses were proposed to avoid contamination issues, but the overall impact on imaging performance

did not create any major difficulties for the process. In fact, none of the major concerns first associated with immersion have prevented it from moving forward. It has been placed on the International Technology Roadmap for Semiconductors, and the first functioning devices made with immersion technology have already been announced.^{6, 56} Yet while those issues were beginning to be addressed, questions were posed about the feasibility of pushing immersion past the resolution potential of water.⁵⁷ Calculations show even greater gains in resolution and DOF if water is replaced by a fluid with a higher index. Research efforts began to shift toward the development of high index materials for use with immersion in the hopes of extending optical lithography toward not just the limits of the optical systems, but the imaging limits of the entire lithographic process. If these efforts are successful, then the NGLs currently in development may ultimately be inadequate in the push to follow Moore's Law. In this case, a new type of patterning technology may be needed.

1.4 STEP AND FLASH IMPRINT LITHOGRAPHY

Step and flash imprint lithography (SFIL) is a high resolution, low pressure, room temperature patterning technique developed at The University of Texas at Austin as an alternative to current NGLs.^{58, 59} In SFIL, a device pattern is defined by features etched into a quartz template, instead of outlined on a reticle. The template is patterned with both laser mask writing or electron beam lithography and conventional etching processes. The resolution of SFIL is therefore set by the resolution of the template writing process. In typical SFIL processing, a low viscosity, monomeric liquid is dispensed onto an

organic transfer layer coated substrate. The liquid is a multicomponent formulation comprised of a silicon-containing monomer, a cross-linking agent, a reactive diluent and a photoinitiator, which upon exposure to UV radiation polymerizes to create a solid hard mask, or etch barrier. Once the etch barrier material is dispensed, the template is brought into contact with it and is filled through capillary forces. The etch barrier is then UV-cured, and the template is pulled off. A breakthrough-etch removes a residual layer left from the imprint and exposes the transfer layer. The etch barrier then acts as a hard mask as the pattern is transferred down to the substrate by anisotropic etching, resulting in high aspect ratio features. Typical post-lithography process steps can then be used to transfer the pattern into the substrate and build up the layers of a device. Figure 1.8 illustrates the SFIL process.

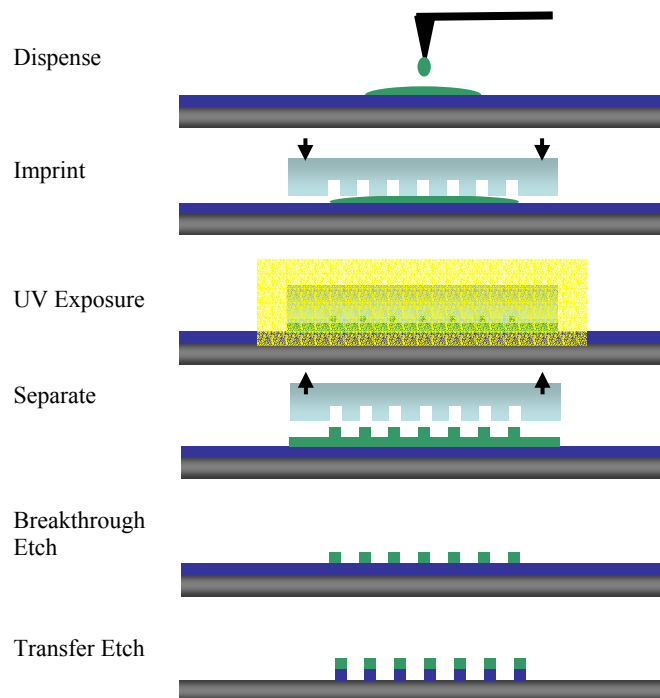


Figure 1.8 Schematic of the step and flash imprint lithography process.

The SFIL process has been shown to have the capabilities to pattern multi-layer, micron size features for back-end-of-line wiring levels as well as sub-50 nm features.^{60, 61} It has also been shown to be compatible with a variety of photopolymerizable materials.⁶²⁻⁶⁴ Current efforts are focused on developing an imprintable low dielectric constant material for dual damascene processing.⁶⁵⁻⁶⁷ This material would be patterned in the same manner as the etch barrier in Figure 1.8, but after the breakthrough etch it would remain as part of the device. Using this material with a multi-layer template could potentially reduce the number of process steps required for interconnection levels by one hundred steps per device and provide an insertion point for SFIL in the semiconductor fabrication process flow.

The versatility of the SFIL process, its lower cost compared to state of the art optical lithography and its faster throughput compared to direct write technologies are allowing to it find applications outside of semiconductor processing. It has the potential to be used for microelectromechanical devices, optoelectronics and photonics, microfluidics and even biological applications.⁶⁸⁻⁷⁰ Its ability to directly pattern novel materials with feature sizes in the range of 100 – 500 nm is particularly attractive for photonic applications that require those feature sizes in low loss materials.⁷¹ This provides an opportunity to combine the principles used to develop imprintable functional materials with the understanding of optical properties from the development of new materials for immersion lithography.

1.5 PHOTORESIST-WATER INTERACTIONS AND HIGH INDEX MATERIALS

The primary focus of this dissertation is the study of materials related to immersion lithography. Chapter 2 discusses the principles governing immersion lithography, the issues related to its implementation in semiconductor fabrication and the means by which these issues have been addressed. One of the main concerns with immersion was that water would have an adverse effect on the imaging performance of a photoresist and cause contamination as a result of water absorption and leaching of small molecule components from the resist film. Spectroscopic ellipsometry was used to take real time measurements of film thickness and refractive index as model photoresist films are immersed in water. An effective medium approximation was used to estimate the amount of water absorption from these measurements and the results were compared to those from other experimental techniques. In Chapter 3, the results of a radiochemical analysis of carbon-14 labeled photoresist components extracted from a resist film under immersion conditions are compared to the results of other measurement techniques. The observations of the radiochemical analysis are combined with those from scanning electrochemical microscopy and liquid chromatography/mass spectrometry to create a qualitative model of component extraction by water. In Chapter 4, the focus shifts from the initial issues facing immersion to ways to extend the technology. The use of high index fluids is discussed, and a systematic survey of the optical properties of ionic solutions is presented. The empirical approach of Chapter 4 is supplemented in Chapter 5 with a discussion of the theoretical underpinnings of the optical properties of materials and how they can serve as a guide to new materials. Additional compounds for use as a

high index fluid are also presented. The principles of developing high index materials are applied to a different application in Chapter 6. Processes and materials for SFIL fabrication of photonic devices are discussed, and a polymer-based photonic crystal structure is presented. Finally, Chapter 7 provides conclusions from the research activities discussed in this work and suggests future directions for their applications.

1.6 REFERENCES

1. Bardeen, J.; Brattain, W. H. "The Transistor, A Semi-Conductor Triode." *Physical Review* **1948**, 74 (2), 230.
2. Shockley, W. "The theory of p - n junction in semiconductors and p - n junction transistors." *Bell Systems Technical Journal* **1949**, 28, 435.
3. Sze, S. M., *Modern semiconductor device physics*. Wiley: New York, **1998**; p 556.
4. Streetman, B. G.; Banerjee, S., *Solid state electronic devices*. 5th ed.; Prentice Hall: Upper Saddle River, N.J., **2000**; p 558.
5. Moore, G. E. "Cramming more components onto integrated circuits." *Electronics* **1965**, 38 (8).
6. *International Technology Roadmap for Semiconductors*, available at, <<http://www.itrs.net/Links/2005ITRS/Home2005.htm>> **2006**.
7. Moreau, W. M., *Semiconductor lithography : principles, practices, and materials*. Plenum Press: New York, **1988**; p 931.
8. Thompson, L. F.; Willson, C. G.; Bowden, M. J., *Introduction to microlithography*. 2nd ed.; American Chemical Society: Washington, DC, **1994**; p 527.

9. Mack, C. A., *Inside PROLITH : a comprehensive guide to optical lithography simulation*. FINLE Technologies: Austin, **1997**.
10. Lin, B. J. "Depth of focus in multilayered media - a long-neglected phenomenon aroused by immersion lithography." *Journal of Microlithography, Microfabrication, and Microsystems* **2004**, 3 (1), 21-27.
11. Reichmanis, E.; Thompson, L. F. "Polymer materials for microlithography." *Chemical Reviews (Washington, DC, United States)* **1989**, 89 (6), 1273-89.
12. Dammel, R., *Diazonaphthoquinone-based resists*. SPIE Optical Engineering Press: Bellingham, Wash., USA, **1993**; p 203.
13. Wallraff, G. M.; Hinsberg, W. D. "Lithographic Imaging Techniques for the Formation of Nanoscopic Features." *Chemical Reviews (Washington, D. C.)* **1999**, 99 (7), 1801-1821.
14. Frechet, J. M. J.; Ito, H.; Willson, C. G. "RESINES POUR UV LOINTAIN METTANT EN OEUVRE UN MECANISME D'AMPLIFICATION CHIMIQUE (Sensitive Deep UV Resist Incorporation Chemical Amplification)." *Colloque Internationale sur la Microlithographie: Microcircuit Engineering 82* **1982**, 260.
15. Ito, H.; Willson, C. G. "Chemical amplification in the design of dry developing resist materials." *Polymer Engineering & Science* **1983**, 23 (18), 1012-1018.
16. Frechet, J. M. J.; Eichler, E.; Ito, H.; Willson, C. G. "Poly(p-tert-butoxycarbonyloxystyrene): a convenient precursor to p-hydroxystyrene resins." *Polymer* **1983**, 24 (8), 995-1000.
17. Stewart, M. D.; Patterson, K.; Somervell, M. H.; Willson, C. G. "Organic imaging materials: a view of the future." *Journal of Physical Organic Chemistry* **2000**, 13 (12), 767-774.
18. Rai-Choudhury, P., *Handbook of microlithography, micromachining, and microfabrication*. SPIE Optical Engineering Press; Institution of Electrical Engineers: Bellingham, Wash., USA; London, UK, **1997**.

19. Thompson, L. F.; Willson, C. G.; Fréchet, J. M. J., *Materials for microlithography : radiation-sensitive polymers*. American Chemical Society: Washington, D.C., **1984**; p 494.
20. Hawryluk, A. M.; Seppala, L. G. "Soft x-ray projection lithography using an x-ray reduction camera." *Journal of Vacuum Science & Technology B: Microelectronics and Nanometer Structures* **1988**, 6 (6), 2162-2166.
21. Edita, T.; Kenneth, A. G.; SangHun, L.; Hector, M.; Phillip, J. B.; Paul, E. D.; Alastair, A. M.; Jeffrey, B.; David, A. "At-wavelength interferometry for extreme ultraviolet lithography." *Journal of Vacuum Science & Technology B: Microelectronics and Nanometer Structures* **1997**, 15 (6), 2455-2461.
22. Hawryluk, A. M.; Ceglio, N. M.; Markle, D. A. "EUV lithography." *Solid State Technology* **1997**, 40 (7), 151-159.
23. Hawryluk, A. M.; Ceglio, N. M.; Markle, D. A. "EUV lithography." *Solid State Technology* **1997**, 40 (8), 75-78.
24. Brueck, S. R. J.; Chen, X. "Spatial frequency analysis of optical lithography resolution enhancement techniques." *Journal of Vacuum Science & Technology, B: Microelectronics and Nanometer Structures* **1999**, 17 (3), 908-920.
25. Chan, M.; Kunz, R. R.; Doran, S. P.; Rothschild, M. "Photolithography at 0.10 and 0.13 μm using ArF excimer laser lithography in combination with resolution enhancement techniques." *Journal of Vacuum Science & Technology, B: Microelectronics and Nanometer Structures* **1997**, 15 (6), 2404-2411.
26. Shibuya, M. "Resolution enhancement techniques for optical lithography and optical imaging theory." *Optical Review* **1997**, 4 (1B), 151-160.
27. Mack, C. A. "Off-axis illumination." *Microlithography World* **2003**, 12 (3), 14-16.
28. Allen, R. D.; Wallraff, G. M.; Hinsberg, W. D.; Conley, W. E.; Kunz, R. R. "Designing high performance krypton monofluoride and argon monofluoride

- single-layer resists with methacrylate polymers." *Journal of Photopolymer Science and Technology* **1993**, 6 (4), 575-91.
29. Kunz, R. R.; Allen, R. D.; Hinsberg, W. D.; Wallraff, G. M. "Acid-catalyzed single-layer resists for argon fluoride lithography." *Proceedings of SPIE-The International Society for Optical Engineering* **1993**, 1925 (Advances in Resist Technology and Processing X), 167-75.
 30. Allen, R. D.; Wallraff, G. M.; Hofer, D. C.; Kunz, R. R. "Photoresists for 193-nm lithography." *IBM Journal of Research and Development* **1997**, 41 (1/2), 95-104.
 31. Patterson, K.; Okoroanyanwu, U.; Shimokawa, T.; Cho, S.; Byers, J.; Willson, C. G. "Improving performance of 193 nm photoresists based on alicyclic polymers." *Proceedings of SPIE-The International Society for Optical Engineering* **1998**, 3333 (Pt. 1, Advances in Resist Technology and Processing XV), 425-437.
 32. Nozaki, K.; Watanabe, K.; Yano, E.; Kotachi, A.; Takechi, S.; Hanyu, I. "A novel polymer for a 193-nm resist." *Journal of Photopolymer Science and Technology* **1996**, 9 (3), 509-522.
 33. Shida, N.; Ushirogouchi, T.; Asakawa, K.; Nakase, M. "Novel ArF excimer laser resists based on menthyl methacrylate terpolymer." *Journal of Photopolymer Science and Technology* **1996**, 9 (3), 457-464.
 34. Iwasa, S.; Maeda, K.; Nakano, K.; Ohfuji, T.; Hasegawa, E. "Design and characterization of alicyclic polymers with alkoxyethyl protecting groups for ArF chemically amplified resists." *Journal of Photopolymer Science and Technology* **1996**, 9 (3), 447-456.
 35. Yamachika, M.; Patterson, K.; Cho, S.; Rager, T.; Yamada, S.; Byers, J.; Paniez, P. J.; Mortini, B.; Gally, S.; Sassoulas, P. O.; Willson, C. G. "Improvement of post-exposure delay stability in alicyclic ArF excimer photoresists." *Journal of Photopolymer Science and Technology* **1999**, 12 (4), 553-560.
 36. Byers, J.; Patterson, K.; Cho, S.; McCallum, M.; Willson, C. G. "Recent advancements in cycloolefin based resists for ArF lithography." *Journal of Photopolymer Science and Technology* **1998**, 11 (3), 465-474.

37. Burns, R. L.; Punsalan, D.; Towidjaja, M. C.; Koros, W. J. "Strategies for purging the pellicle space for 157 nm lithography." *Journal of Vacuum Science & Technology B: Microelectronics and Nanometer Structures* **2002**, 20 (5), 1954-1960.
38. Switkes, M.; Rothschild, M. "Immersion lithography at 157 nm." *Journal of Vacuum Science & Technology, B: Microelectronics and Nanometer Structures* **2001**, 19 (6), 2353-2356.
39. Takanashi, A.; Harada, T.; Akeyama, M.; Kondo, Y.; Kurosaki, T.; Kuniyoshi, S.; Hosaka, S.; Kawamura, Y. "Pattern forming apparatus." U.S. Patent No. 4,480,910, **1984**.
40. Lin, B. J. "The future of subhalf-micrometer optical lithography." *Microelectronic Engineering* **1987**, 6 (1-4), 31-51.
41. Kawata, H.; Carter, J. M.; Yen, A.; Smith, H. I. "Optical projection lithography using lenses with numerical apertures greater than unity." *Microelectronic Engineering* **1989**, 9 (1-4), 31-36.
42. Owen, G.; Pease, R. F. W.; Markle, D. A.; Grenville, A.; Hsieh, R. L.; von Bunau, R.; Maluf, N. I. "1/8 μ m optical lithography." *Journal of Vacuum Science & Technology, B: Microelectronics and Nanometer Structures* **1992**, 10 (6), 3032-3036.
43. Hoffnagle, J. A.; Hinsberg, W. D.; Sanchez, M.; Houle, F. A. "Liquid immersion deep-ultraviolet interferometric lithography." *Journal of Vacuum Science & Technology, B: Microelectronics and Nanometer Structures* **1999**, 17 (6), 3306-3309.
44. Lin, B. J. "The k_3 coefficient in nonparaxial λ/NA scaling equations for resolution, depth of focus, and immersion lithography." *Journal of Microlithography, Microfabrication, and Microsystems* **2002**, 1 (1), 7-12.
45. Switkes, M.; Rothschild, M. "Resolution enhancement of 157-nm lithography by liquid immersion." *Proceedings of SPIE-The International Society for Optical Engineering* **2002**, 4691 (Pt. 1, Optical Microlithography XV), 459-465.

46. Raub, A. K.; Brueck, S. R. J. "Deep-UV immersion interferometric lithography." *Proceedings of SPIE-The International Society for Optical Engineering* **2003**, 5040 (Pt. 2, Optical Microlithography XVI), 667-678.
47. Smith, B. W.; Kang, H.; Bourov, A.; Cropanese, F.; Fan, Y. "Water immersion optical lithography for the 45nm node." *Proceedings of SPIE-The International Society for Optical Engineering* **2003**, 5040 (Pt. 2, Optical Microlithography XVI), 679-689.
48. Switkes, M.; Kunz, R. R.; Sinta, R. F.; Rothschild, M.; Gallagher-Wetmore, P. M.; Krukonis, V. J.; Williams, K. "Immersion liquids for lithography in the deep ultraviolet." *Proceedings of SPIE-The International Society for Optical Engineering* **2003**, 5040 (Pt. 2, Optical Microlithography XVI), 690-699.
49. Hafeman, S.; Neureuther, A. R. "Simulation of imaging and stray light effects in immersion lithography" **2003**; The International Society for Optical Engineering: Santa Clara, CA, United States, 2003; pp 700-712.
50. Wei, A.; Nellis, G.; Abdo, A.; Engelstad, R.; Chen, C.-F.; Switkes, M.; Rothschild, M. "Preliminary microfluidic simulation for immersion lithography." *Proceedings of SPIE-The International Society for Optical Engineering* **2003**, 5040 (Pt. 2, Optical Microlithography XVI), 713-723.
51. Owa, S.; Nagasaka, H. "Immersion lithography; its potential performance and issues." *Proceedings of SPIE-The International Society for Optical Engineering* **2003**, 5040 (Pt. 2, Optical Microlithography XVI), 724-733.
52. Hinsberg, W.; Wallraff, G. M.; Larson, C. E.; Davis, B. W.; Deline, V.; Raoux, S.; Miller, D.; Houle, F. A.; Hoffnagle, J.; Sanchez, M. I.; Rettner, C.; Sundberg, L. K.; Medeiros, D. R.; Dammel, R. R.; Conley, W. E. "Liquid immersion lithography - Evaluation of resist issues." *Proceedings of SPIE-The International Society for Optical Engineering* **2004**, 5376 (Pt. 1, Advances in Resist Technology and Processing XXI), 21-33.
53. Taylor, J. C.; Chambers, C. R.; Deschner, R.; LeSuer, R. J.; Conley, W. E.; Burns, S. D.; Willson, C. G. "Implications of immersion lithography on 193 nm photoresists." *Proceedings of SPIE-The International Society for Optical Engineering* **2004**, 5376 (Pt. 1, Advances in Resist Technology and Processing XXI), 34-43.

54. Vogt, B. D.; Soles, C. L.; Prabhu, V. M.; Jones, R. L.; Wu, W.-L.; Lin, E. K.; Goldfarb, D. L.; Angelopoulos, M. "Measurements of water distribution in thin lithographic films." *Proceedings of SPIE-The International Society for Optical Engineering* **2004**, 5376 (Pt. 1, Advances in Resist Technology and Processing XXI), 56-62.
55. LeSuer, R. J.; Fan, F.-R. F.; Bard, A. J.; Taylor, J. C.; Tsiartas, P.; Willson, G.; Conley, W. E.; Feit, G.; Kunz, R. R. "Using scanning electrochemical microscopy to probe chemistry at the solid-liquid interface in chemically amplified immersion lithography." *Proceedings of SPIE-The International Society for Optical Engineering* **2004**, 5376 (Pt. 1, Advances in Resist Technology and Processing XXI), 115-125.
56. "IBM claims to make first processors with immersion lithography." *EE Times*, available at <<http://www.eetimes.com/showArticle.jhtml?articleID=54201799>> **2004**.
57. Conley, W.; Bendik, J. "Is ArF the final wavelength?" *Proceedings of SPIE-The International Society for Optical Engineering* **2004**, 5376 (Pt. 1, Advances in Resist Technology and Processing XXI), 16-20.
58. Colburn, M.; Grot, A.; Amistoso, M. N.; Choi, B. J.; Bailey, T. C.; Ekerdt, J. G.; Sreenivasan, S. V.; Hollenhorst, J.; Willson, C. G. "Step and flash imprint lithography for sub-100-nm patterning." *Proceedings of SPIE-The International Society for Optical Engineering* **2000**, 3997 (Emerging Lithographic Technologies IV), 453-457.
59. Colburn, M.; Johnson, S.; Stewart, M.; Damle, S.; Bailey, T. C.; Choi, B.; Wedlake, M.; Michaelson, T.; Sreenivasan, S. V.; Ekerdt, J.; Willson, C. G. "Step and flash imprint lithography: a new approach to high-resolution patterning." *Proceedings of SPIE-The International Society for Optical Engineering* **1999**, 3676 (Pt. 1, Emerging Lithographic Technologies III), 379-389.
60. Johnson, S.; Resnick, D. J.; Mancini, D.; Nordquist, K.; Dauksher, W. J.; Gehoski, K.; Baker, J. H.; Dues, L.; Hooper, A.; Bailey, T. C.; Sreenivasan, S. V.; Ekerdt, J. G.; Willson, C. G. "Fabrication of multi-tiered structures on step and flash imprint lithography templates." *Microelectronic Engineering* **2003**, 67-68, 221-228.

61. Gates, B. D.; Xu, Q.; Stewart, M.; Ryan, D.; Willson, C. G.; Whitesides, G. M. "New approaches to nanofabrication: Molding, printing, and other techniques." *Chemical Reviews* **2005**, *105* (4), 1171-1196.
62. Colburn, M.; Suez, I.; Choi, B. J.; Meissl, M.; Bailey, T.; Sreenivasan, S. V.; Ekerdt, J. G.; Willson, C. G. "Characterization and modeling of volumetric and mechanical properties for step and flash imprint lithography photopolymers." *Journal of Vacuum Science & Technology, B: Microelectronics and Nanometer Structures* **2001**, *19* (6), 2685-2689.
63. Kim, E. K.; Stewart, M. D.; Wu, K.; Palmieri, F. L.; Dickey, M. D.; Ekerdt, J. G.; Willson, C. G. "Vinyl ether formulations for step and flash imprint lithography." *Journal of Vacuum Science & Technology, B: Microelectronics and Nanometer Structures--Processing, Measurement, and Phenomena* **2005**, *23* (6), 2967-2971.
64. Stewart, M. D.; Willson, C. G. "Imprint materials for nanoscale devices." *MRS Bulletin* **2005**, *30* (12), 947-952.
65. Stewart, M. D.; Wetzel, J. T.; Schmid, G. M.; Palmieri, F.; Thompson, E.; Kim, E. K.; Wang, D.; Sotodeh, K.; Jen, K.; Johnson, S. C.; Hao, J.; Dickey, M. D.; Nishimura, Y.; Laine, R. M.; Resnick, D. J.; Willson, C. G. "Direct imprinting of dielectric materials for dual damascene processing." *Proceedings of SPIE-The International Society for Optical Engineering* **2005**, *5751* (Pt. 1, Emerging Lithographic Technologies IX), 210-218.
66. Palmieri, F.; Stewart, M. D.; Wetzel, J.; Hao, J.; Nishimura, Y.; Jen, K.; Flannery, C.; Li, B.; Chao, H.-L.; Young, S.; Kim, W. C.; Ho, P. S.; Willson, C. G. "Multi-level step and flash imprint lithography for direct patterning of dielectrics" **2006**; International Society for Optical Engineering, Bellingham WA, WA 98227-0010, United States; San Jose, CA, United States, 2006; p 61510.
67. Schmid, G. M.; Stewart, M. D.; Wetzel, J.; Palmieri, F.; Hao, J.; Nishimura, Y.; Jen, K.; Kim, E. K.; Resnick, D. J.; Liddle, J. A.; Willson, C. G. "Implementation of an imprint damascene process for interconnect fabrication." *Journal of Vacuum Science and Technology B: Microelectronics and Nanometer Structures* **2006**, *24* (3), 1283-1291.
68. Stewart, M. D.; Johnson, S. C.; Sreenivasan, S. V.; Resnick, D. J.; Willson, C. G. "Nanofabrication with step and flash imprint lithography." *Journal of*

- Microlithography, Microfabrication, and Microsystems* **2005**, 4 (1), 011002/1-011002/6.
69. Khusnatdinov, N.; Doyle, G.; Miller, M.; Stacey, N.; Watts, M.; Labrake, D. L. "Fabrication of nano and micro optical elements by step and flash imprint lithography." *Proceedings of SPIE - The International Society for Optical Engineering* **2006**, 6110 (Micromachining Technology for Micro-Optics and Nano-Optics IV), 61100.
 70. Truskett, V. N.; Watts, M. P. C. "Trends in imprint lithography for biological applications." *Trends in Biotechnology* **2006**, 24 (7), 312-317.
 71. Taylor, J. C.; Hostetler, T.; Kornilovich, P.; Kramer, K. "Photonic crystals from step and flash imprint lithography." *Proceedings of SPIE-The International Society for Optical Engineering* **2006**, 6151 (Pt. 1, Emerging Lithographic Technologies X), 61510L/1-61510L/8.

CHAPTER 2: IMMERSION LITHOGRAPHY AS A VIABLE TECHNOLOGY

2.1 PRINCIPLES OF IMMERSION LITHOGRAPHY

The imaging benefits of immersion lithography come from a well known principle in optics. Snell's Law of refraction describes how light is transmitted across the interface between two materials with different refractive indices, and is given by

$$n_1 \sin \theta_1 = n_2 \sin \theta_2 \quad (2.1)$$

where n_1 is the index of refraction of the material through which the light is traveling, θ_1 is the angle with respect to normal at which the light is incident on the interface, n_2 is the index of refraction of the material into which the light is transmitted and θ_2 is the angle with respect to normal at which the light propagates in the incident material. Figure 2.1 illustrates this concept through a multilayer film stack, where the quantity $n_j \sin \theta_j$ remains constant at every interface. It should also be noted that part of the incident light is reflected from each interface at an angle equal to the angle of incidence, $\theta_i = \theta_r$. An infinite number of these interfacial reflections and transmissions combine to give the observed reflected and transmitted waves.

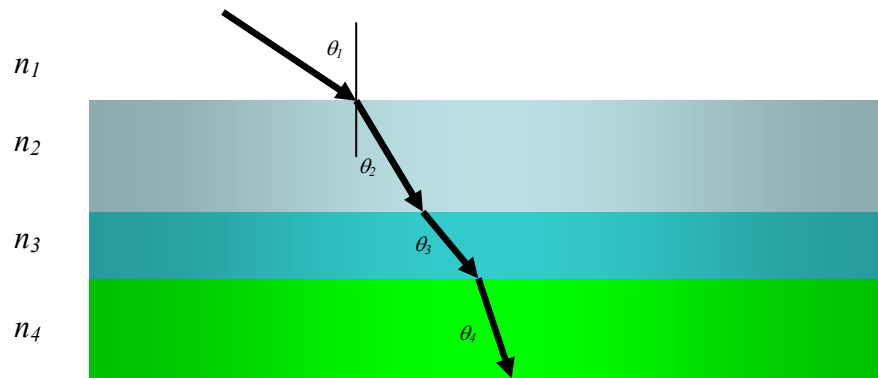


Figure 2.1 Snell's Law through a film stack.

Equation 2.1 defines two limits for light refraction through those interfaces. The first is that at normal incidence on the interface, $\theta_i = 0^\circ$, the transmitted light does not change direction after passing through the interface. The second is that at interfaces where $n_1 > n_2$, a maximum incident angle, called the critical angle, $\theta_c = \sin^{-1}(n_2/n_1)$, exists for which light can no longer pass through the interface. Light that is incident at an angle equal to or greater than the critical angle is said to be totally internally reflected by the interface.¹ Since the quantity $n_j \sin \theta_j$ is constant throughout a multilayer film stack, the material with the lowest index determines the critical angle.

Snell's Law is important in determining the resolution limits of a lithographic exposure tool, because of how a device pattern on a reticle is transferred into a photoresist. The imaging process begins when exposure radiation is transmitted through the reticle. When light passes through an aperture in an otherwise opaque screen, the transition between the light and the shadow of the screen is gradual and light and dark fringes form beyond the boundary of the geometrical shadow. This phenomenon is called

diffraction and the resulting pattern can be described by the light's intensity distribution normal to the aperture. The distribution is typically characterized by a central spot of high intensity surrounded by alternating regions of zero or lower intensity, Figure 2.2a. When the screen contains multiple apertures the diffraction pattern becomes more complicated. A central pattern, called the zero-order diffraction component, is formed along with similar looking side patterns of reduced intensity, Figure 2.2b. These higher-order components appear symmetrically around the zero-order, their spacing proportional to the wavelength of light and the inverse period, or spatial frequency, of the apertures.²

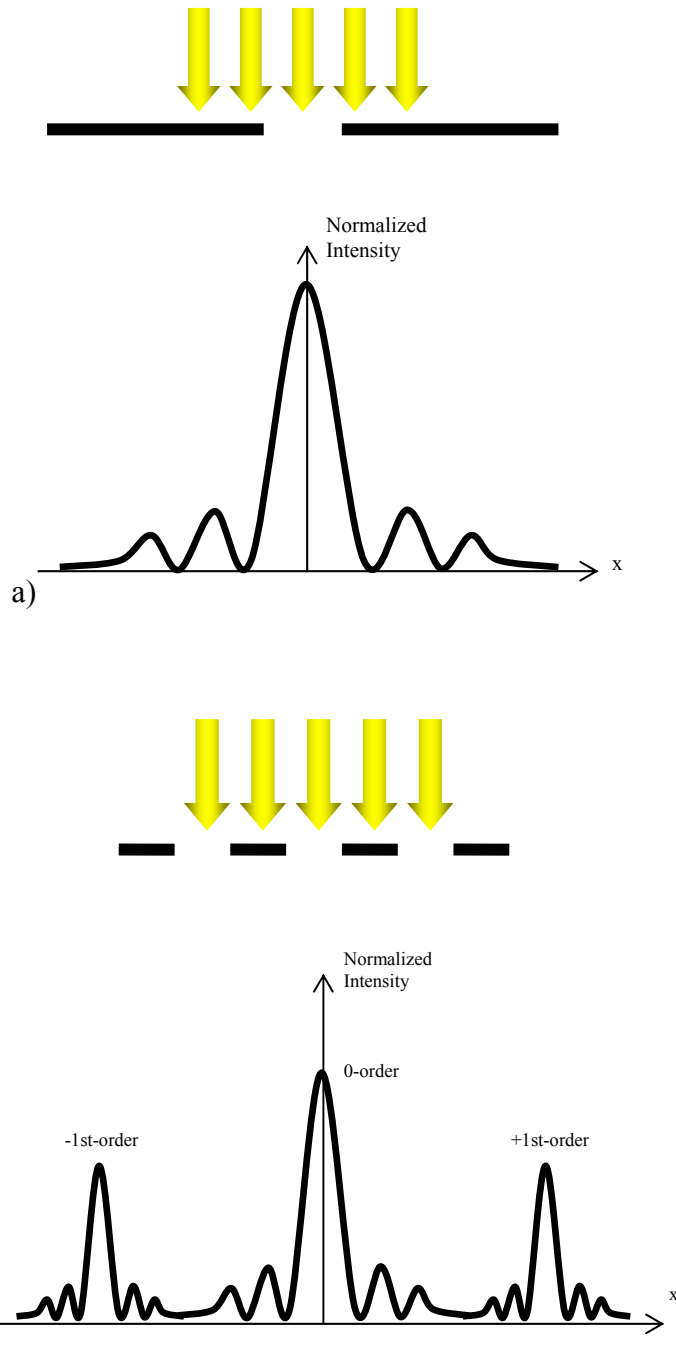


Figure 2.2 Intensity distribution of light transmitted through a screen with a) a single aperture and b) with multiple apertures.

When a reticle is illuminated in an exposure tool, it too forms a diffraction pattern with the zero-order propagating along the optical axis of the imaging lens and the higher orders traveling at angles away from the axis. An image of the device pattern is formed by the interference of the diffraction orders when they are focused into a photoresist by the lens, Figure 2.3.³ The propagation of the diffraction orders through the entire system can be modeled by Snell's Law, with the lens represented by its Lagrange invariant.⁴ The Lagrange invariant relates the entrance and exit angles of a light ray traveling through a lens to its magnification m by

$$m = \frac{n_o \sin \theta_o}{n_i \sin \theta_i} \quad (2.2)$$

where n_o is the index of refraction of the medium on the objective side of the lens, θ_o is the entrance angle with respect to the optical axis, n_i is the index of refraction of the medium on the image side and θ_i is the exit angle. The magnification is the inverse of the reduction factor of a lens, with a change in sign to account for focusing. As seen in Figure 2.3, the reticle is located on the objective side of the lens and the wafer is on the image side. The maximum exit angle of an imaging lens is typically used to determine the numerical aperture in the Rayleigh criterion and depth-of-focus expression.

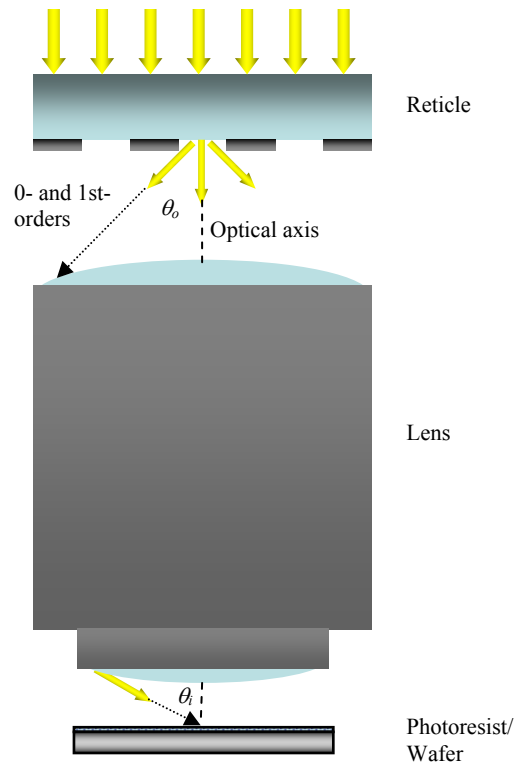


Figure 2.3 Illustration of an imaging system in a lithographic exposure tool.

As described in Chapter 1, the size of imaging lenses has been increased over time to give larger NA values. Since smaller features lead to larger spatial frequencies in reticle patterns and therefore larger θ_o values for the diffraction orders, larger lenses result in improved resolution. Still, these size increases can only go so far. As can be seen from Equations 2.1 and 2.2, the theoretical limit for an exposure system in air is $NA = 1$. Lenses built to accept entrance angles greater than those corresponding to the limit would have diffraction orders that are totally internally reflected at the image side. Furthermore, the practical limit is given as $NA = 0.95$ and this is being approached with current systems.^{5,6} However, there is a way to raise the limit. Recall that in a multilayer

film stack, the lowest index sets the critical angle. In the image side film stack shown in Figure 2.3, the lowest index material is the air in the gap between the final lens element and the photoresist. By filling that gap with a fluid so that $n_i > 1$, the theoretical limit for NA becomes n_i . Immersion lithography therefore enables the use of lenses that accept and emit light rays at angles greater than those handled by lenses designed to image in air. Imaging at NA s greater than one is now referred to as hyper- NA lithography.

Hyper- NA imaging is not the only benefit to immersion. In Equation 1.2, the DOF factor for a lithographic exposure decreases with smaller wavelengths or an increase in the NA due to an increase in lens size. Current exposure tools, whose resolution limits are fixed, can gain an improvement in DOF from immersion given by Equation 1.4. The gain comes from the reduction of the optical path length (OPL) through the gap between the lens and the photoresist.⁴ The OPL is the physical distance traveled by a light ray multiplied by the index of the medium it is traveling in. As the different diffraction orders travel through the lens they go through a complete 360° phase change every time the OPL equals a multiple of the wavelength. For higher orders with larger θ_o s and θ_s s, the OPLs are longer than those that propagate closer to the optical axis. The different path lengths result in phase differences between the diffraction orders at all but one point below the lens. This point defines a plane where the best image is formed. The range, above and below the plane where the phase differences are small enough for acceptable imaging, is the DOF. This range can be increased by decreasing the overall phase difference among the diffracted orders. For a set phase offset of θ_o , immersion decreases

θ_i and therefore also decreases the optical path length, leading to a smaller phase difference and larger DOF.

2.2 CHALLENGES IN IMMERSION LITHOGRAPHY

With the imaging benefits of immersion lithography established and the emergence of water as a potential immersion fluid at 193 nm, the semiconductor industry began to seriously consider its implementation as an alternative to 157 nm lithography. In December of 2002, SEMATECH hosted a workshop during which questions and concerns about the implementation of immersion into semiconductor manufacturing were discussed. This meeting produced a list of the initial top ten issues regarding immersion and led to the formation of task forces comprised of researchers from universities, national laboratories and the semiconductor industry to address them. The list of the top ten critical issues is given below.

Top Ten Critical Issues Facing Immersion Lithography (from December 2002 SEMATECH workshop)

1. Determination of fluid properties, absolute value of n , k , etc., to sufficient accuracy and precision.
2. Timing versus infrastructure versus competing technologies.
3. Strategy for NA versus field size, working distance, etc.
4. Formation, control and removal of microbubbles.
5. Chemical contamination of fluid and resist.
6. Out-gassing.

7. Determination of changing properties due to thermal and mechanical influences.
8. Determination of bubble effects (scattering, defects).
9. Polarization strategy and the impact on the tool.
10. Coupling of lens to stage – vibration coupled through fluid.

The first issue primarily involved the determination of exact values for the index of refraction, n , and the extinction coefficient, k , of water at the 193.39 nm operating wavelength of an ArF exposure tool. Precise knowledge of the indices of refraction of the materials in the imaging stack and their absorption coefficients is needed to optimize the exposure conditions. Index values for water in the DUV had been previously reported, but no explicit value at 193 nm was given.⁷ To obtain this, the National Institute of Standards and Technology performed measurements at six spectral lines from a Cu-Ne hollow cathode lamp with a minimum deviation technique through a fused silica prism and fit the data to a dispersion relation. For fully air-saturated HPLC grade water at 21.5 °C, the index value at 193.39 nm was determined to be $n = 1.43662 \pm 0.00002$.^{8,9} This work also determined the thermo-optic coefficient of water at 194.5 nm, $dn/dT = -1.00 \times 10^{-4} \pm 0.04 \times 10^{-4} (\text{°C})^{-1}$, addressing part of the seventh critical issue. The extinction coefficient is proportional to water's absorption coefficient, α , which determines the amount of light that passes through a unit length of material. A non-zero absorption coefficient means that the amount of light transmitted through the water is determined by the working distance between the final lens element and the photoresist. Higher transmittances from short working distances would result in faster exposures and

greater throughput, but also increase tool complexity and cost. The reported absorption coefficient from MIT Lincoln Labs was $\alpha = 0.036 \text{ cm}^{-1}$ base 10 at 193 nm, low enough for a 6 mm working distance at 95% transmittance.¹⁰ However, there was significant variation in this value depending on the source of the water. Impurities were cited as the likely cause of this variation, suggesting the need for a standardized purification process for immersion water.

The second and third issues were industry wide concerns best addressed by exposure tool manufacturers, as were issues nine and ten. For immersion to be adopted in semiconductor fabrication, production-grade tools and their supporting infrastructure would be needed in a timely fashion. Tool manufacturers needed to demonstrate full field projection optics compatible with immersion, and present feasible designs with high NAs .¹¹ In early 2005, a variety of projection systems with NAs up to 1.3 were demonstrated.¹²⁻¹⁵ At these high NA values, polarization effects were expected to become apparent during imaging.^{4, 16-18} Light in the p -polarization state, where the electric field is parallel with the plane of incidence, experiences a reduction in overlap and therefore in interference at the larger angles associated with high NAs . The resulting decrease in image quality requires polarization control during exposure. Vibration coupling through the fluid was also a tool specific issue. Despite these challenges, the first production hyper- NA exposure tool was shipped at the beginning of 2006 by Nikon Corp., with an NA of 1.07.

The fourth, sixth and eighth critical issues concern the impact of bubbles formed during immersion. Bubbles can be formed by dissolved gas coming out of solution,

entrainment of air during fluid filling and outgassing of volatile side products from the deprotection reaction.¹⁹ Degassing immersion water as part of a standardized purification process would reduce bubbles from the first process. The fluid filling process has been studied with computational fluid dynamics to determine the effects of gap height, fill velocity, contact angles and surface topography on bubble formation.²⁰⁻²² These studies provided fill regime maps based on velocity, contact angle and geometry to allow the design of fluid handling systems that prevent air entrainment. Outgassing causes lens contamination in conventional lithography, but because volatile side products have lower diffusion constants in water than in air, immersion would be expected to help alleviate this problem. However, if bubbles were to form on the surface of the photoresist and remain there during exposure, their presence could negatively impact the image in the resist.^{19, 23} Simulations showed that air bubbles would create unwanted light scatter; however, experiments using polymer particles as model bubbles resulted in few image distortions, suggesting that bubbles may not stay on the surface long enough to affect the exposure.^{24, 25} Furthermore, experiments using a model 193 nm photoresist showed little evidence for the formation of outgassing related bubbles.²⁶

Critical issue seven was concerned with changes in the optical properties of water due to thermal or mechanical changes during exposure. Simulations of the energy deposition during exposure revealed that a local temperature increase of 0.42 K could occur, which could lead to imaging errors because of water's non-zero thermo-optic coefficient.²⁷ Further work indicated that the primary imaging error from fluid heating was an effective focus shift along the direction of the exposure scan.²⁸ Pressure elevation

in the fluid from exposure was also predicted, resulting in an optical path length change of 0.1 nm.²⁹ Advanced process control to change focusing during exposure and using sufficiently rapid fluid flow to increase heat dissipation were both suggested as means to prevent potential imaging errors.

2.3 PHOTORESIST-WATER INTERACTIONS

The fifth critical issue on the SEMATECH list – chemical contamination of fluid and resist – is a topic of this dissertation. It was a serious concern regarding immersion since 193 nm photoresists have become complex formulations containing multiple small molecule components. In addition to the polymer resin, resist films include photoacid generators and their reaction products, base additives used to reduce image blur from acid diffusion and residual casting solvent left from the spin coating process. The percentages of each component in these formulations are precisely controlled to ensure repeatable imaging performance. Immersing resist films in water introduces the possibility of extraction of those components from the film, as well as the prospect of the resist absorbing water, both potentially degrading image quality. Extracted components also introduce a new source of lens contamination. Early imaging experiments showed that model 193 nm photoresists were capable of resolving 56 nm half-pitch, equal line-and-space patterns under immersion conditions.³⁰ However, these experiments did not quantify any component extraction or address contamination issues.

A sensitive measurement technique was needed to detect the presence of any extracted component in water. The first measurements were of PAG extraction from

model acrylic-based photoresists; one using the IBM structure in Figure 1.7 and another using the model structure from Tokyo Ohka Kogyo Co., Ltd. (TOK) (Kawasaki, Japan) shown in Figure 2.4.³¹ Near-edge X-ray absorption fine structure spectroscopy (NEXAFS) of the surface of resist films before and after immersion in water and showed qualitative evidence of PAG extraction. Quantitative measurements were conducted by a commercial lab, Exygen Research (State College, PA), which had previously developed a liquid chromatography/mass spectrometry (LCMS) technique to analyze waste streams for trace amounts of perfluorosulfonate anions from PAGs. They were contracted to analyze samples of aqueous solutions saturated with resist components and samples of water used to immerse a small portion of a resist film. The two PAGs studied, *tert*-butylphenyliodonium perfluorooctanesulfonate (TBI-PFOS) and triphenylsulfonium perfluorobutanesulfonate (TPS-PFBS), are shown in Figure 2.5. The saturated solutions showed concentrations of 30 – 2300 ppm of PAG. The LCMS measurements detected concentrations of 0.07 – 0.13 ppm of the PAGs in water contacted with unexposed resist films and concentrations of 0.066 – 0.27 ppm in water contacted with films that were exposed to 193 nm light. The immersion time was varied in these experiments from 1 minute to 90 minutes. While these measurements showed that water does extract PAG, the time scale of the experiments was long compared to exposure times and there was no way to distinguish PAG molecules from the reaction products. Detection of two base additives, triethanolamine and tri-*n*-dodecylamine, in the immersion water was also attempted, but results were inconclusive.

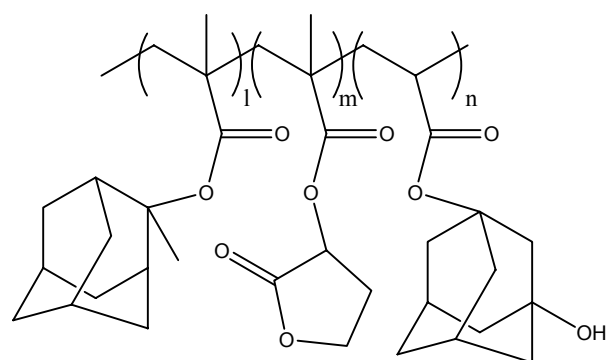


Figure 2.4 Structure of acrylic polymer from TOK.

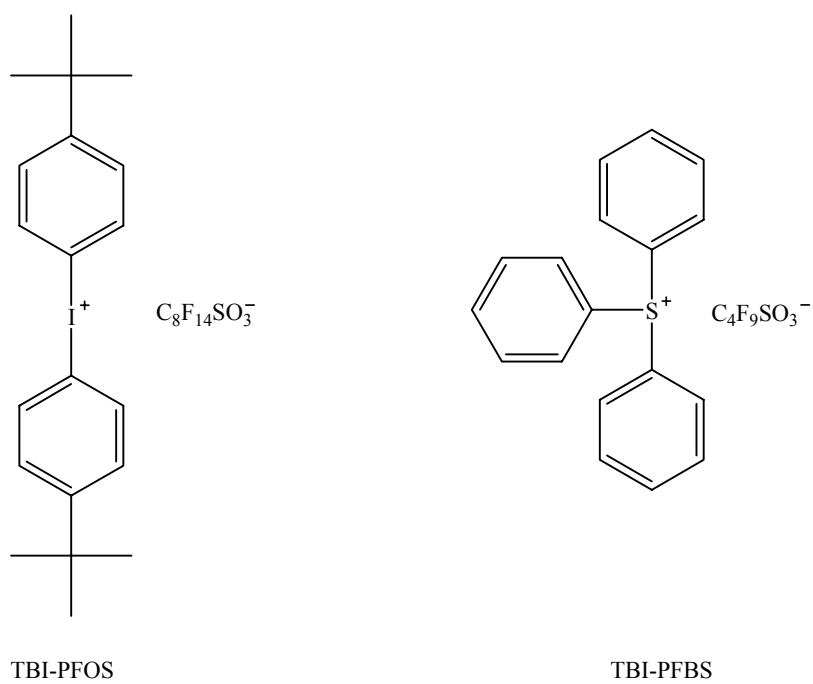


Figure 2.5 Structures of tert-butylphenyliodonium perfluorooctanesulfonate (TBI-PFOS) and triphenylsulfonium perfluorobutanesulfonate (TPS-PFBS) PAGs studied in photoresist extraction experiments.

In addition to component extraction, water absorption into the resist film was also observed. Using a quartz crystal microbalance (QCM) optical reflectance analysis, swelling of the resist films during immersion was quantified.³¹ The film swelling data were fit to a diffusion equation which showed three distinct diffusion regimes. Diffusion constants for water in the acrylic polymers were determined for each regime, and it was noted that the largest diffusion constant was approximately 15 times smaller than those typically observed for phenolic polymers used for 248 nm resists. Using secondary ion mass spectrometry and deuterium oxide (D_2O), the absorbed water was found to be distributed evenly across the thickness of the films. These observations were confirmed here by spectroscopic ellipsometry, which was used to monitor changes in thickness and refractive index of the TOK resist film during immersion.³² Within the first thirty seconds of immersion, the film thickness increased by several nanometers for both unexposed and exposed resists, Figure 2.6, which was consistent with the QCM and reflectance measurements. There was also a small decrease in the resist's refractive index over the same time period, Figure 2.7. While imaging experiments indicated that water absorption did not have a huge detrimental impact on resist performance, these two studies have shown that the changes in film thickness and index would have to be taken into account in future studies, along with changes in the water itself due to thermal and mechanical influences.

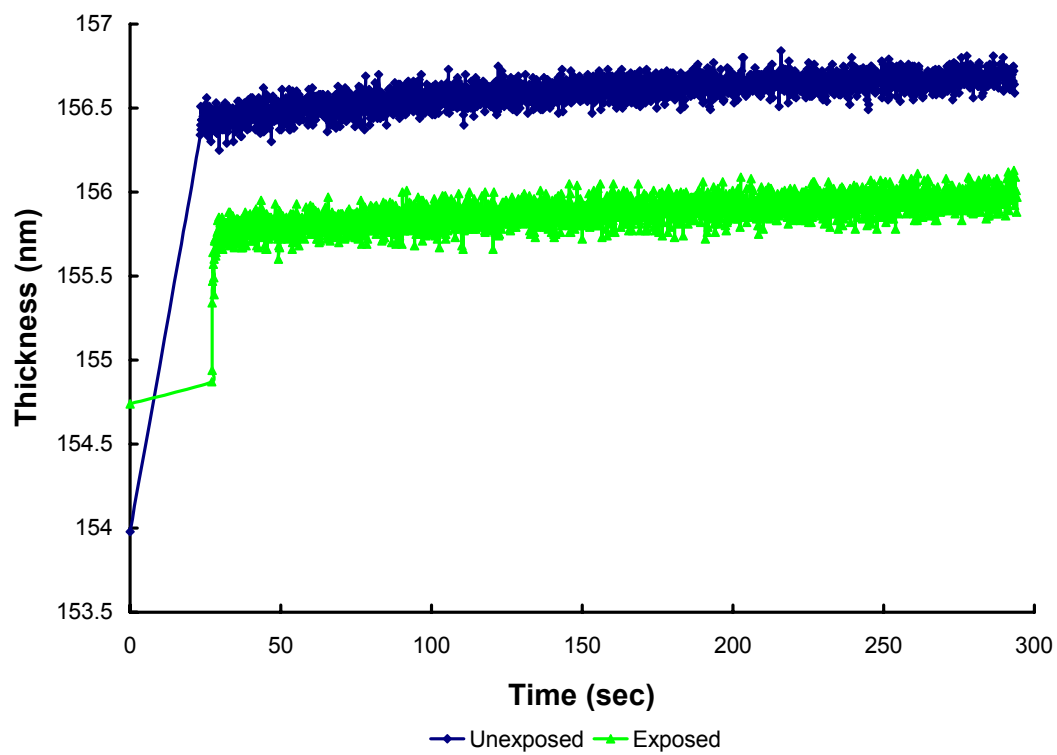


Figure 2.6 Film thickness vs. time of TOK resist during water immersion.

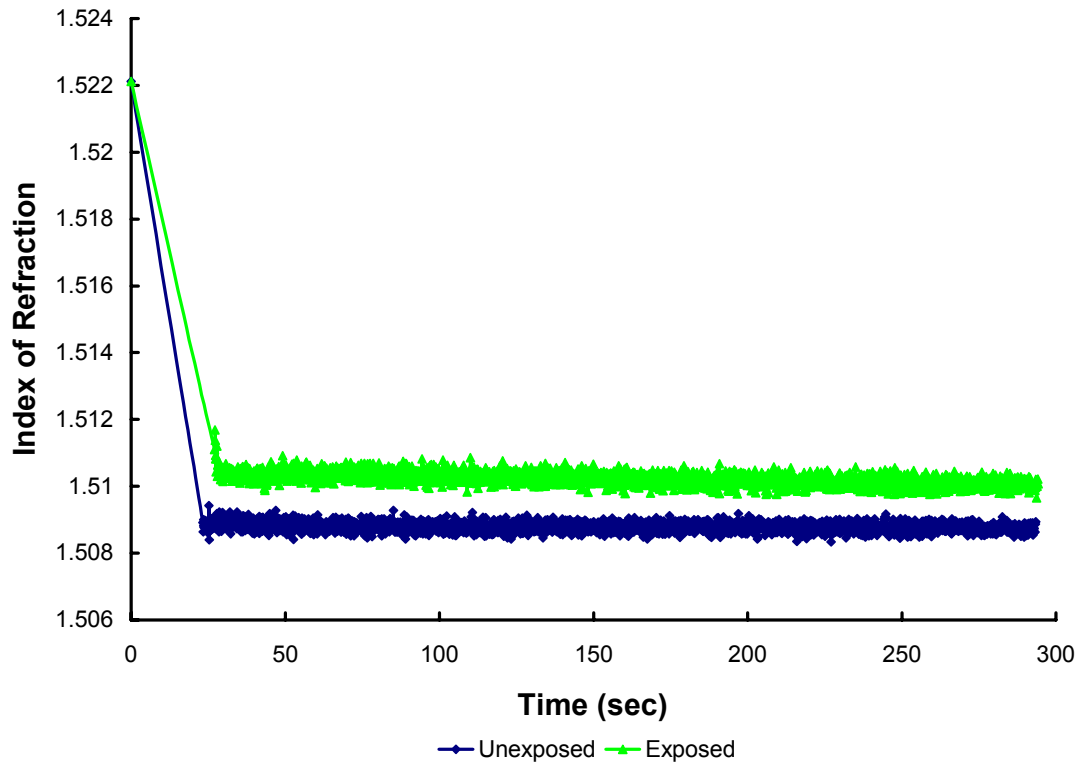


Figure 2.7 Refractive index vs. time of TOK resist during water immersion.

2.4 SUMMARY

The benefits of index matching in image formation have been known for some time, but the principles were only recently applied to semiconductor microlithography. Water immersion at 193 nm is providing a means for the semiconductor industry to continue following Moore's Law without the costly move to 157 nm lithography. While immersion presented significant challenges for adoption in large scale manufacturing, extensive studies have found most of the issues to be manageable. A remaining concern is the quantification of the extraction of resist components other than the PAG, as well as all components at times shorter than one minute. The next chapter provides a discussion

of how LCMS can be combined with two additional experimental techniques to create a more complete description of photoresist component extraction.

2.5 REFERENCES

1. Born, M.; Wolf, E., *Principles of optics : electromagnetic theory of propagation, interference and diffraction of light*. 7th expanded ed.; Cambridge University Press: Cambridge ; New York, **1999**; p 952.
2. Goodman, J. W., *Introduction to Fourier Optics*. McGraw-Hill: San Francisco, **1968**; p 287.
3. Mack, C. A., *Inside PROLITH : a comprehensive guide to optical lithography simulation*. FINLE Technologies: Austin, **1997**.
4. Mack, C. A.; Byers, J. D. "Exploring the capabilities of immersion lithography through simulation." *Proceedings of SPIE-The International Society for Optical Engineering* **2004**, 5377 (Pt. 1, Optical Microlithography XVII), 428-441.
5. Mulkens, J.; Streefkerk, B.; Hoogendorp, M.; Moerman, R.; Leenders, M.; de Jong, F.; Stavenga, M.; Boom, H. "Immersion lithography exposure systems: today's capabilities and tomorrow's expectations." *Proceedings of SPIE-The International Society for Optical Engineering* **2005**, 5754 (Pt. 2, Optical Microlithography XVIII), 710-724.
6. Sewell, H.; McCafferty, D.; Markoya, L.; Hendrickx, E.; Hermans, J.; Ronse, K. "32nm node technology development using interference immersion lithography." *Proceedings of SPIE-The International Society for Optical Engineering* **2005**, 5753 (Pt. 1, Advances in Resist Technology and Processing XXII), 491-501.
7. Querry, M. R.; Wieliczka, D. M.; Segelstein, D. J., Water (H₂O). In *Handbook of optical constants of solids*, Palik, E. D., Ed. Academic Press: Boston, **1991**; Vol. 2, p 1096 p.
8. Burnett, J. H.; Kaplan, S. "Measurement of the refractive index and thermo-optic coefficient of water near 193 nm." *Proceedings of SPIE-The International Society*

for *Optical Engineering* **2003**, 5040 (Pt. 3, Optical Microlithography XVI), 1742-1749.

9. Burnett, J. H.; Kaplan, S. G. "Measurement of the refractive index and thermo-optic coefficient of water near 193 nm." *Journal of Microlithography, Microfabrication, and Microsystems* **2004**, 3 (1), 68-72.
10. Switkes, M.; Kunz, R. R.; Sinta, R. F.; Rothschild, M.; Gallagher-Wetmore, P. M.; Krukoni, V. J.; Williams, K. "Immersion liquids for lithography in the deep ultraviolet." *Proceedings of SPIE-The International Society for Optical Engineering* **2003**, 5040 (Pt. 2, Optical Microlithography XVI), 690-699.
11. Owa, S.; Nagasaka, H. "Immersion lithography; its potential performance and issues." *Proceedings of SPIE-The International Society for Optical Engineering* **2003**, 5040 (Pt. 2, Optical Microlithography XVI), 724-733.
12. Owa, S.; Nagasaka, H.; Ishii, Y.; Shiraishi, K.; Hirukawa, S. "Full-field exposure tools for immersion lithography." *Proceedings of SPIE - The International Society for Optical Engineering* **2005**, 5754 (Pt. 2, Optical Microlithography XVIII), 655-668.
13. Rubingh, R.; Moers, M.; Suddendorf, M.; Vanoppen, P.; Kisteman, A.; Thier, M.; Blahnik, V.; Piper, E. "Lithographic performance of a dual stage, 0.93NA ArF step and scan system." *Proceedings of SPIE - The International Society for Optical Engineering* **2005**, 5754 (Pt. 2, Optical Microlithography XVIII), 681-692.
14. Nakano, H.; Hata, H.; Takahashi, K.; Arakawa, M.; Chibana, T.; Honda, T.; Chiba, K.; Mori, S. "Development of ArF immersion exposure tool." *Proceedings of SPIE - The International Society for Optical Engineering* **2005**, 5754 (Pt. 2, Optical Microlithography XVIII), 693-700.
15. Sekine, Y.; Kawashima, M.; Yamazoe, K.; Honda, T.; Ohkubo, A.; Kishikawa, Y.; Iwasaki, Y.; Suzuki, A. "Analysis of imaging properties for hyper-NA ArF immersion lithography." *Proceedings of SPIE-The International Society for Optical Engineering* **2005**, 5754 (Pt. 2, Optical Microlithography XVIII), 701-709.

16. Smith, B. W.; Kang, H.; Bourov, A.; Cropanese, F.; Fan, Y. "Water immersion optical lithography for the 45nm node." *Proceedings of SPIE-The International Society for Optical Engineering* **2003**, 5040 (Pt. 2, Optical Microlithography XVI), 679-689.
17. Hafeman, S.; Neureuther, A. R. "Simulation of imaging and stray light effects in immersion lithography." *Proceedings of SPIE - The International Society for Optical Engineering* **2003**, 5040 (Pt. 2, Optical Microlithography XVII), 700-712.
18. Smith, B. W.; Zavyalova, L.; Estroff, A. "Benefiting from polarization - Effects on high-NA imaging." *Proceedings of SPIE - The International Society for Optical Engineering* **2004**, 5377 (Pt. 1, Optical Microlithography XVII), 68-79.
19. Switkes, M.; Bloomstein, T. M.; Kunz, R. R.; Rothschild, M.; Ruberti, J. W.; Shedd, T. A.; Yeung, M. S. "Scattering in liquid immersion lithography." *Proceedings of SPIE-The International Society for Optical Engineering* **2004**, 5377 (Pt. 1, Optical Microlithography XVII), 469-476.
20. Wei, A.; Nellis, G.; Abdo, A.; Engelstad, R.; Chen, C.-F.; Switkes, M.; Rothschild, M. "Preliminary microfluidic simulation for immersion lithography." *Proceedings of SPIE-The International Society for Optical Engineering* **2003**, 5040 (Pt. 2, Optical Microlithography XVI), 713-723.
21. Wei, A. C.; Nellis, G. F.; Abdo, A. Y.; Engelstad, R. L.; Chen, C.-f.; Switkes, M.; Rothschild, M. "Microfluidic simulations for immersion lithography." *Journal of Microlithography, Microfabrication, and Microsystems* **2004**, 3 (1), 28-34.
22. Wei, A.; El-Morsi, M.; Nellis, G.; Abdo, A.; Engelstad, R. "Predicting air entrainment due to topography during the filling and scanning process for immersion lithography." *Journal of Vacuum Science & Technology, B: Microelectronics and Nanometer Structures--Processing, Measurement, and Phenomena* **2004**, 22 (6), 3444-3449.
23. Switkes, M.; Kunz, R. R.; Rothschild, M.; Sinta, R. F.; Yeung, M.; Baek, S. Y. "Extending optics to 50 nm and beyond with immersion lithography." *Journal of Vacuum Science & Technology, B: Microelectronics and Nanometer Structures--Processing, Measurement, and Phenomena* **2003**, 21 (6), 2794-2799.

24. Fan, Y.; Lafferty, N. V.; Bourov, A.; Zavyalova, L. V.; Smith, B. W. "Study of air-bubble-induced light scattering effect on image quality in 193-nm immersion lithography." *Proceedings of SPIE-The International Society for Optical Engineering* **2004**, 5377 (Pt. 1, Optical Microlithography XVII), 477-486.
25. Fan, Y.; Lafferty, N.; Bourov, A.; Zavyalova, L.; Smith Bruce, W. "Air bubble-induced light-scattering effect on image quality in 193 nm immersion lithography." *Applied Optics* **2005**, 44 (19), 3904-11.
26. Switkes, M.; Rothschild, M.; Shedd, T. A.; Burnett, H. B.; Yeung, M. S. "Bubbles in immersion lithography." *Journal of Vacuum Science & Technology, B: Microelectronics and Nanometer Structures--Processing, Measurement, and Phenomena* **2005**, 23 (6), 2409-2412.
27. Wei, A.; Abdo, A.; Nellis, G.; Engelstad, R.; Chang, J.; Lovell, E.; Beckman, W. "Simulating fluid flow characteristics during the scanning process for immersion lithography." *Journal of Vacuum Science & Technology, B: Microelectronics and Nanometer Structures--Processing, Measurement, and Phenomena* **2003**, 21 (6), 2788-2793.
28. Baek, S.-Y.; Wei, A.; Cole, D. C.; Nellis, G.; Yeung, M.; Abdo, A.; Engelstad, R. "Simulation of the coupled thermal/optical effects for liquid immersion micro/nanolithography." *Proceedings of SPIE - The International Society for Optical Engineering* **2004**, 5377 (Pt. 1, Optical Microlithography XVII), 415-427.
29. Nellis, G.; Wei, A. "Preliminary analysis of laser-pulse-induced pressure variation for immersion lithography." *Journal of Microlithography, Microfabrication and Microsystems* **2004**, 3 (1), 84-86.
30. Raub, A. K.; Brueck, S. R. J. "Deep-UV immersion interferometric lithography." *Proceedings of SPIE-The International Society for Optical Engineering* **2003**, 5040 (Pt. 2, Optical Microlithography XVI), 667-678.
31. Hinsberg, W.; Wallraff, G. M.; Larson, C. E.; Davis, B. W.; Deline, V.; Raoux, S.; Miller, D.; Houle, F. A.; Hoffnagle, J.; Sanchez, M. I.; Rettner, C.; Sundberg, L. K.; Medeiros, D. R.; Dammel, R. R.; Conley, W. E. "Liquid immersion lithography - Evaluation of resist issues." *Proceedings of SPIE-The International Society for Optical Engineering* **2004**, 5376 (Pt. 1, Advances in Resist Technology and Processing XXI), 21-33.

32. Taylor, J. C.; Chambers, C. R.; Deschner, R.; LeSuer, R. J.; Conley, W. E.; Burns, S. D.; Willson, C. G. "Implications of immersion lithography on 193 nm photoresists." *Proceedings of SPIE-The International Society for Optical Engineering* **2004**, 5376 (Pt. 1, Advances in Resist Technology and Processing XXI), 34-43.

CHAPTER 3: DETECTION OF PHOTORESIST COMPONENT EXTRACTION DURING IMMERSION

3.1 TECHNIQUES FOR EXTRACTION MEASUREMENTS

Three experimental techniques have been used to investigate component extraction from model 193 nm photoresist formulations. The first of these, liquid chromatography/mass spectroscopy (LCMS), has been utilized by several researchers to study the mass transfer of resist components into water, but only results for PAGs with perfluorinated sulfonate anions have been obtained. Two additional techniques, scanning electrochemical microscopy (SECM) and liquid scintillation counting (LSC), have been used to further examine PAG extraction and to study other components. These techniques are discussed below.

3.1.1 LIQUID CHROMATOGRAPHY/MASS SPECTROSCOPY

Due to concerns regarding the long-term effects of perfluorinated sulfonates on the environment, highly sensitive LCMS analytical methods have been developed by a commercial laboratory, Exygen Research (State College, PA), to examine waste water streams from semiconductor fabrication plants. Their analysis, used in the IBM study discussed in Chapter 2, was adopted by SEMATECH for immersion resist characterization. While the LCMS results showed qualitative evidence of PAG extraction during immersion, different studies used different experimental procedures, making meaningful comparison of results difficult.¹ Also, the detection of other resist components using LCMS was not successful. The Exygen LCMS analysis was used in

this study to allow direct comparison of its results to those from other methods used to detect a perfluorinated sulfonate anion.

3.1.2 SCANNING ELECTROCHEMICAL MICROSCOPY

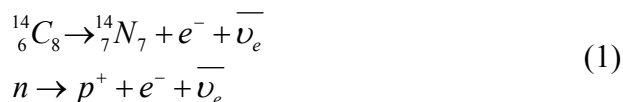
Scanning electrochemical microscopy provides the capability to probe the local chemistry at a solid/liquid interface under real-time conditions.² In SECM, the response of an ultramicroelectrode is monitored as a function of distance from a substrate where the species of interest is being generated. Three modes of scanning electrochemical microscopy (SECM) – potentiometric, voltammetric and conductometric – were used to analyze the diffusion of photoacid and PAG from the surface of a photoresist film into water. In the potentiometric mode, changes in the pH of the water due to formation of photoacid were observed. The voltammetric mode was used to measure PAG concentration by detection of a common PAG cation and the conductometric mode measured changes in overall ion concentration at the resist-water interface. The scanning electrochemical microscope and electrode fabrication have been described elsewhere.³

3.1.3 LIQUID SCINTILLATION COUNTING

The LCMS and SECM methods described above were useful in detecting PAG extraction, but another technique was needed to study other resist components, specifically residual casting solvent (RCS) and base additive. Previous work involving the measurement of RCS concentration gradients in resist films used a radiochemical analysis to detect carbon-14 labeled analogs of common casting solvents.⁴⁻⁶ Synthesis of

labeled analogs of a PAG and base in addition to the casting solvents allowed this method to be applied to the measurement of resist component extraction.

Carbon-14 (^{14}C) can be detected by liquid scintillation counting (LSC). This involves counting radioactive decay events from a ^{14}C -labeled analyte in a solution of scintillation cocktail. Carbon-14 radiation results from beta decay, where an unstable neutron in the ^{14}C nucleus decays into a proton, electron and antineutrino. This results in the formation of a stable nitrogen nucleus and the emission of the electron, called a beta particle. The mechanism is shown by the following reactions,



The scintillation cocktail contains a mixture of linear alkane-based solvents and primary and secondary photo-emitters. Solvent molecules absorb energy from the beta particles, and then the energy is transferred to the photo-emitters. These then emit photons which are detected by photomultiplier tubes in a liquid scintillation counter. The photons are counted over a specified period of time, after which an average rate given in counts per minute (*CPM*) is determined. The counting rate is converted into a decay, or disintegration, rate (*DPM*) by subtracting out a *CPM* factor for the level of background radiation and dividing by an efficiency factor. The *DPM* value is then converted into micro Curies (μCi) – the Ci is the SI unit for the decay rate, or activity – and divided by the analyte's specific activity (*SA*), the activity per unit mass in $\mu\text{Ci/g}$, to give the total mass in the sample being counted.⁷

Unlike the LCMS and SECM methods, the detection limits for LSC are not determined by the physiochemical properties of a particular analyte. They are determined by the strength of the signal from the sample, *i.e.*, its *CPM* compared to that of the background, the length of time a sample is counted and the efficiency of the counting process. The *CPM* of a particular sample is set by the mass of analyte present and the analyte's *SA*. A longer counting time allows for more total counts from analyte decay to be detected relative to those from the background. The efficiency of the process is reduced when decay events are quenched by beta particle or photon absorption and therefore not counted. During a measurement the efficiency is determined by the scintillation counter according to the "H-number" method, developed by Horrocks and discussed elsewhere.^{6, 8, 9} Since the *CPM* and efficiency are set by experimental procedure, increased counting time is the most direct way to improve the detection limits. By counting for sufficient time periods, LSC allowed for quantification of PAG and base extraction from model resist films and determination of a maximum limit for possible RCS extraction.

3.2 MATERIALS: PHOTORESIST FORMULATIONS AND FILM PREPARATION

Model 193 nm photoresist materials for component extraction experiments were provided by Tokyo Ohka Kogyo Co. (TOK) (Kawasaki, Japan) and AZ Electronic Materials (Somerville, New Jersey). The standard TOK resists, designated TOK-ILP01 and TOK-ILP04 in Figure 3.1, were formulated from acrylic ter-polymer and tetra-polymer resins, triphenylsulfonium perfluorobutanesulfonate PAG (commonly called

TPS nonaflate) and triethanolamine base additive dissolved in a 60/40 wt% mixture of propylene glycol monomethyl ether acetate (PGMEA) and ethyl lactate. Alternative formulations with tripentylamine or tri-n-dodecylamine as the base additive were also provided. The AZ formulation, T-518 in Figure 3.1, also included an acrylic polymer, TPS nonaflate and diethanolamine dissolved in ethyl lactate. The standard resists were formulated at a 6 wt% total solids concentration, a PAG loading of 5 wt% of the polymer, and a base loading of 0.3 wt% of the polymer. For LCMS and SECM measurements, the PAG loading in T-518 films was varied from 0 – 5 wt%.

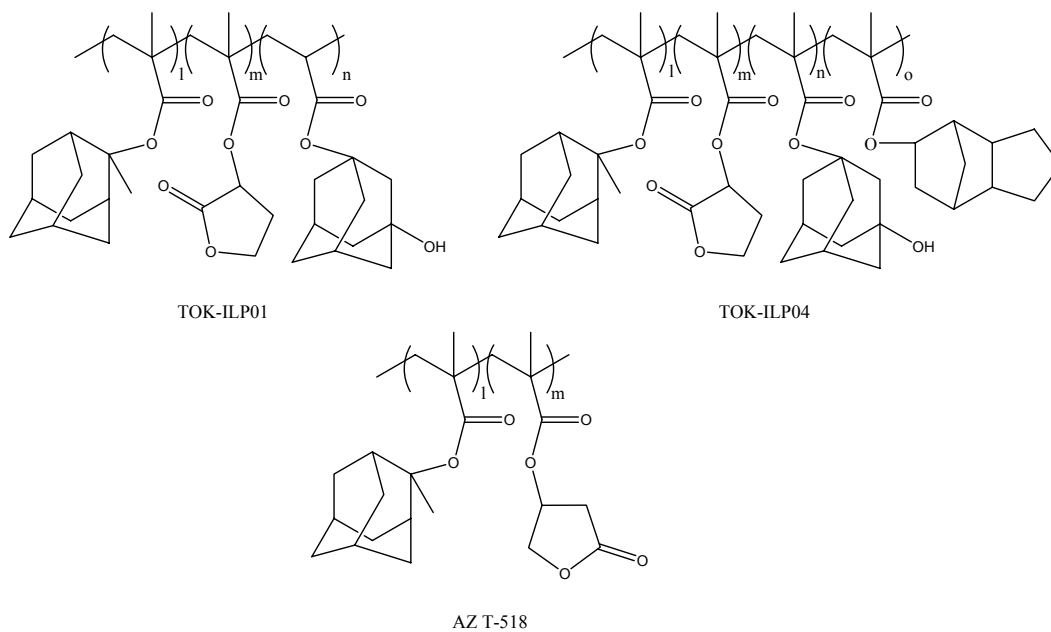


Figure 3.1 Model 193 nm photoresist polymers from TOK and AZ.

Three samples of each resist were made for LSC measurements, one with an aliquot of ^{14}C -labeled casting solvent, one with ^{14}C -TPS nonaflate and the last with ^{14}C -tripentylamine. The TOK resists had 0.5 g of ^{14}C -PGMEA; the resulting SA of the PGMEA in the TOK resists was 1.54 $\mu\text{Ci/g}$. The same amount of ^{14}C -ethyl lactate was added to the Clariant resist for a final ethyl lactate SA of 1.31 $\mu\text{Ci/g}$. The synthesis of the radiolabeled casting solvents has been described elsewhere.^{4, 10} For the other samples only radiolabeled PAG and base were used in the formulations. The SA of the ^{14}C -TPS nonaflate was 8.60 $\mu\text{Ci/g}$ and that of the ^{14}C -tripentylamine was 49.8 $\mu\text{Ci/g}$. The synthesis of the labeled TPS nonaflate and tripentylamine is reported in Appendix A. Additional PGMEA and ethyl lactate were obtained from Aldrich Co. (Milwaukee, Wisconsin). Additional triethanolamine obtained from Acros Co. (Morris Plains, New Jersey). The structures of the labeled materials are shown in Figure 3.2.

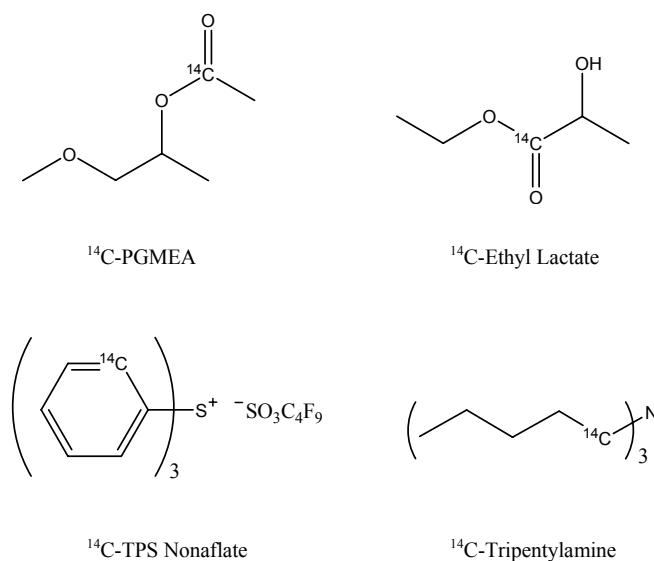


Figure 3.2 Structures of radiolabeled photoresist components.

Resist films were cast onto quartz plates for LCMS and SECM experiments and on 2 in silicon wafers for LSC experiments using a Headway Research, Inc. EC101DT spin coater at a speed of 2000 rpm for 30 s. The films were then subjected to a post apply bake (PAB) for 90 s at 115 °C resulting in a film thickness of approximately 150 nm. Film thickness was measured using a J. A. Woollam M-2000 variable angle spectroscopic ellipsometer. Ellipsometric data were collected over a spectral range of 400 to 1000 nm and fit using WVASE32 software from Woollam; see Chapter 4 for a discussion of ellipsometry.

3.3 EXPERIMENTAL PROCEDURES FOR EXTRACTION MEASUREMENTS

The LCMS and SECM experiments were conducted with Milli-Q water (18 M Ω). Square wave voltammetry was performed using a CHI 600 electrochemical instrument (Austin, TX). The working electrode used in voltammetry experiments was a 25 μ m diameter Hg drop plated onto a Pt microelectrode as described previously and a Pt wire was used as a counter electrode.^{11, 12} Potentials were referenced versus a Ag/AgCl electrode. pH measurements were made by measuring the potential between an Sb microelectrode (100 μ m diameter) and a saturated calomel electrode using a high input impedance potentiometer. Conductivity measurements were performed using a modification of the method originally described by Johnson and Enke and adapted by Calhoun *et al.*^{13, 14} Data acquisition and pulse generation were accomplished using home-built software and electronics based on previous designs.¹³⁻¹⁵ A more detailed

description of the application of DC pulses to measure solution conductivity at solid/liquid interfaces is given elsewhere.¹⁶ LCMS analysis of water samples was performed by Exygen Research (3058 Research Dr, State College, PA, 16801).

The cell used in this work has been described previously.² A 6.5 mm diameter hole was drilled in a Teflon well. A quartz plate was used as the bottom of the well resulting in a cell volume of 100 μL and a surface area in contact with water of 0.33 cm^2 . Samples were irradiated from below the quartz plate such that the incident light and the electrode were perpendicular to the substrate plane. The exposure was conducted using 193 nm light from a Lambda Physik (Ft. Lauderdale, FL) excimer laser (26 kV, 120 mJ/cm^2 , 10-50 ns pulse length, 1 to 10 Hz pulse rate). Light was directed through a fiber optic cable onto the underside of the conductivity cell resulting in an average energy output per pulse ranging from 1 to 2 mJ/cm^2 . Flood exposure was performed using a 3500 W unfiltered EXFO Novacure[®] lamp (Mississauga, Ontario, Canada).

Wafers coated with resists containing radiolabeled components were placed into a 2 in glass Petri dish lid and covered with a 7 mL puddle of deionized (DI) water for contact times ranging from 30 s to 30 min. The water was then transferred to a scintillation vial containing 12.5 mL Scintiverse BD scintillation cocktail (Fisher Scientific Co. Hampton, NH) and decay events were counted over 20 min using a Beckman 1801 liquid scintillation counter for the RCS and most PAG samples. A Beckman LS 6500 counter was used to count the labeled base samples, the sub-30 s immersion time samples and the thickness dependence samples, for four to five hours. Results from the two instruments for similar conditions were in agreement. A sample of

scintillation cocktail containing 7 mL of DI water was also counted to determine the level of background radiation present. To confirm the amounts of radiolabeled components in the resists, films not subjected to a PAB were dissolved in 5 mL of unlabeled casting solvent. The wafer and Petri dish were rinsed two times with 5 mL and one time with 4.5 mL of scintillation cocktail to complete transfer of the sample into a scintillation vial and counted as described above.

The PAG extraction experiment on TOK-ILP01 was repeated twice with slight variations. First, a 248 nm excimer laser was used to flood expose the resist films immediately after immersion. In the second repetition, a 30 sec prerinse immersion was performed before immersing four films from 30 sec to 5 min. The prerinse on TOK-ILP01 was also performed for the base extraction. Thickness dependence on PAG and base leaching was measured using films of TOK-ILP04 with thicknesses ranging from approximately 140 – 50 nm that were immersed for 30 s. A custom built polycarbonate immersion cell based on a previously published design was used to improve time resolution to 10 s.¹ A 4 mL aliquot of DI water was injected into the 2 mm high space in the cell over films of AZ T-518 and was allowed to sit for a specified time before being collected with a 10 mL syringe.

3.4 COMPONENT EXTRACTION FROM MODEL 193 NM PHOTORESIST FILMS BY WATER

The results from the three measurements techniques are described below. The SECM techniques provided a qualitative description of PAG/photoacid extraction. Quantitative results were obtained from the LCMS and LSC measurements.

3.4.1 LIQUID CHROMATOGRAPHY/MASS SPECTROSCOPY RESULTS

The dependence of PAG and photoacid extraction on immersion contact time was analyzed using LCMS detection of the nonaflate anion. Aliquots of water, 100 μL , were left in contact with exposed and unexposed films of T-518 with PAG loadings of 0 to 5% from 10 to 120 seconds. The results of the LCMS analyses of these samples are shown in Figure 3.3. The concentration of nonaflate anion in the immersion water was reported in parts per billion (ppb).

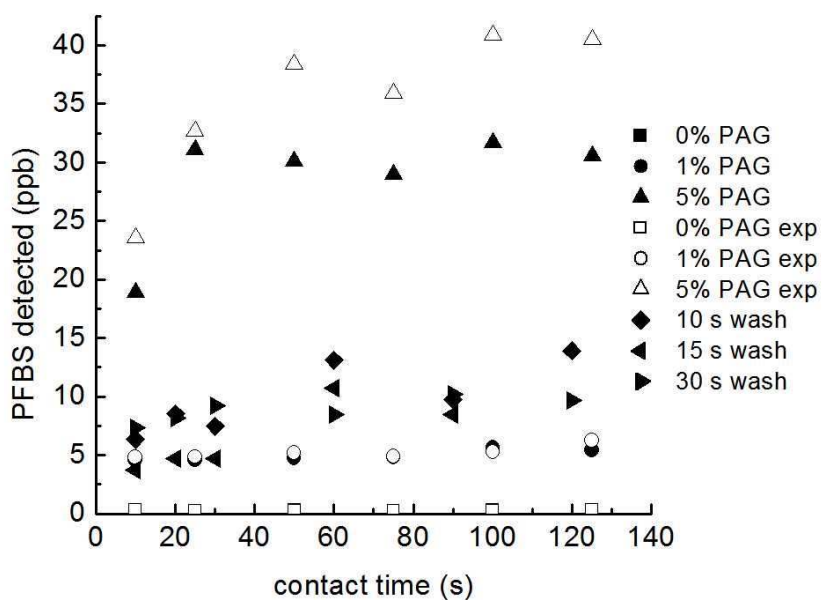


Figure 3.3 Concentration of nonaflate anion from extracted PAG/photoacid in immersion water vs. contact time.

As expected, no nonaflate was observed in the water samples that were in contact with films containing no PAG. The amount of nonaflate in the water was dependent on

the resist formulation and a nearly five times increase in nonaflate was observed between the 1 wt% and 5 wt% PAG loaded films. The 5 wt% PAG formulation displayed an increase in PAG concentration until a near steady-state value was obtained after a contact time of 30 seconds. One cannot observe a significant difference between the exposed and unexposed 1 wt% PAG-loaded films, however, the amount of nonaflate leached from the exposed 5 wt% film was approximately 20% higher than the corresponding unexposed film. To confirm that PAG was leaching out of the film only during the first few seconds of contact with water, 5 wt% PAG-loaded, unexposed, resist-coated wafers were bathed in deionized water for 10 to 30 seconds and air dried prior to performing the water contact/leaching experiment. As shown in Figure 3.3, washing unexposed wafers for 10 seconds decreases the amount of nonaflate detected by approximately 80%. Within the accuracy of this measurement, increasing the wash time to 30 seconds does not reduce the amount of PAG leached from the film any further.

3.4.2 SCANNING ELECTROCHEMICAL MICROSCOPY RESULTS

Three modes of scanning electrochemical microscopy (SECM) – potentiometric, voltammetric and conductometric – were used to analyze the diffusion of photoacid and PAG from a photoresist into immersion water. In the potentiometric mode, an antimony fiber with a diameter of 100 μm was sealed in glass and used to measure changes in pH close to a resist-coated wafer submerged in water. The use of antimony as a pH sensitive electrode is well established and Sb microelectrodes have been used previously in SECM methodology.¹⁷ pH measurements of water in contact with TOK-ILP01 are shown in

Figure 3.4. The Sb microelectrode was positioned approximately 50 μm above the resist and the pH was measured as a function of time and UV exposure. Upon flood exposure using a mercury arc lamp, the pH of the water layer decreased. The solution pH increased slightly when the lamp was turned off, indicating that the acidic species generated during exposure were diffusing away from the electrode. The fact that the pH of the exposed solution did not return to its original value suggests that the PAG was present in the water layer by the time the cell is exposed to UV light. Repeat experiments showed the same qualitative behavior but had varying initial pH values, which was most likely due to difficulties in measuring the pH of pure, unbuffered water accurately. The transient nature of this experiment and fluctuating background make precise pH measurements difficult and the determination of moles of H^+ hard to quantify.

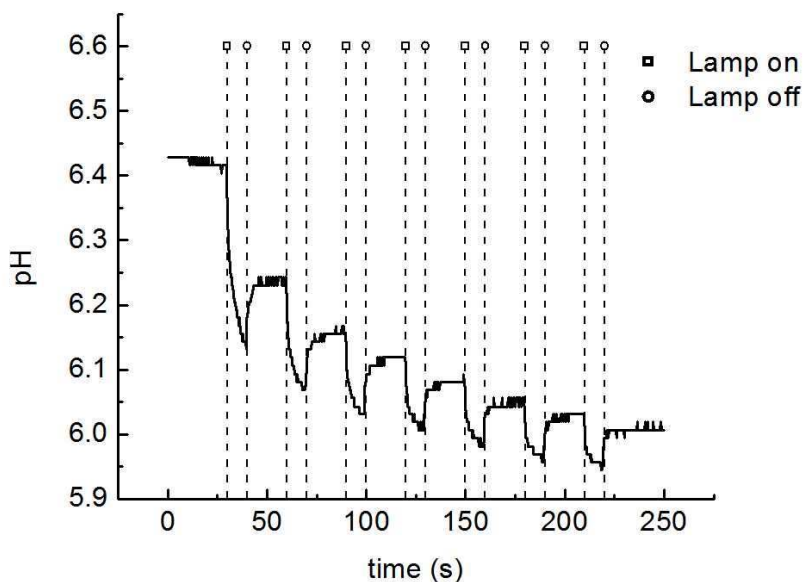


Figure 3.4 pH measurements of liquid layer above a film of TOK-ILP01.

In the voltammetric SECM mode, the solution concentration of photoacid generator was measured by triphenylsulfonium cation (TPS) reduction at a Hg drop microelectrode. The electrochemistry of TPS has been reported previously and a reduction wave occurs at -1.45 V versus a Ag/AgCl reference electrode.¹⁸ Square wave voltammograms of water in contact with a wafer coated with TOK-ILP01 are shown in Figure 3.5, where the Hg drop microelectrode was positioned at various distances from the wafer surface. As the microelectrode approached the surface, the reduction wave for TPS grew. While the voltammograms were a qualitative confirmation that TPS was leaching from the resist, it was difficult to quantify the amount for two reasons: the current due to TPS reduction was only slightly larger than the background current and the true geometry of the Hg drop was not known. At the distance marked 0 μm , it is not clear whether the tip of the Hg hemisphere is touching the surface or if the drop has been compressed between the glass of the microelectrode and the wafer, which could result in a larger current since a larger area of the wafer would be probed. Despite the inability to obtain quantitative data, both pH and voltammetric measurements clearly showed the presence of PAG and/or photoacid in the immersion water.

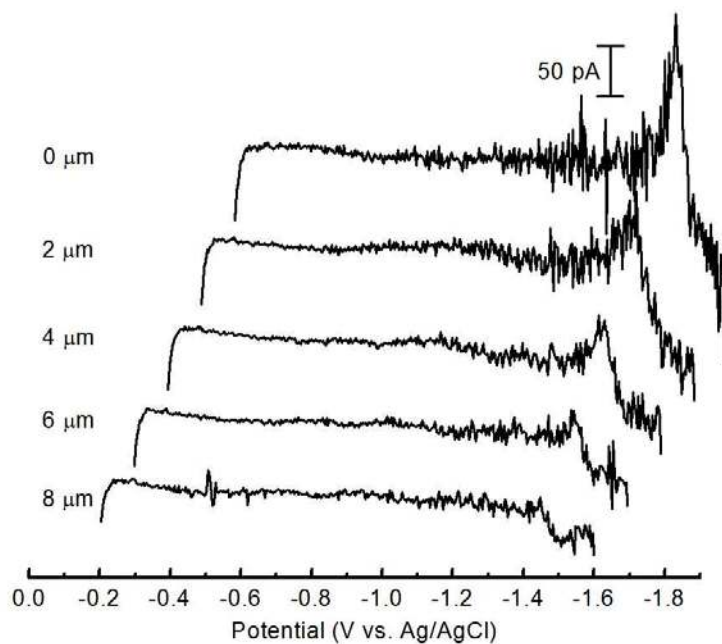


Figure 3.5 Square wave voltammograms at a Hg hemisphere microelectrode above a film of TOK-ILP01, the distance between the electrode and the film is noted in the legend.

Both transient and steady state conductometric SECM modes were used to investigate changes in ion concentration at the resist/immersion water interface. In the steady state measurements, the solution conductivity was measured as a function of distance from the surface. Figure 3.6 shows an approach curve where the conductance was normalized by the conductance remote from the surface and the distance was normalized by the radius of the tip (in this case 12.5 μm). The theoretical response (solid line) for conductance approach curves has been previously shown to follow the expected feedback for an approach to an insulating surface.^{19, 20} As the microelectrode approaches an insulating surface, the surface blocks diffusion and migration pathways to the tip,

minimizing the conductance measured at the tip. In an inhomogeneous solution, such as when ions would leach from the surface, the increase in local conductance around the tip would result in a normalized conductance that is higher than the theory predicts. Approaching films of T-518 with 4 wt% PAG loading followed the theory until the tip was approximately 10 μm from the film. This abrupt, distance independent, conductivity is due to geometric effects. The microelectrode plane was not absolutely parallel to the substrate plane. In this case, the glass sheath of the microelectrode touched the glass substrate, limiting the distance of closest approach. The squares in Figure 3.6 show an approach curve recorded while the cell was exposed to 1.5 mJ/cm^2 193 nm light pulses at a rate of 1 Hz. There is a clear increase in conductance as the electrode approached the film. If the electrode was placed remote from the film, however, and the solution conductance was monitored as a function of time, it increased under these exposure conditions. The source of this increase is unclear but is likely due to the geometry of the experimental setup, where the laser beam was incident on the electrode surface. Excitation of the platinum electrode surface may induce photoemission and water electrolysis can occur, resulting in what appears to be a conductance change.²¹ A background scan was obtained by performing an approach curve remote from any surface, such that only the time-dependent behavior would be recorded. Correcting the approach curve for this background effect showed that even under illumination the approach followed the theory for a homogeneous solution, circles in Figure 3.6.

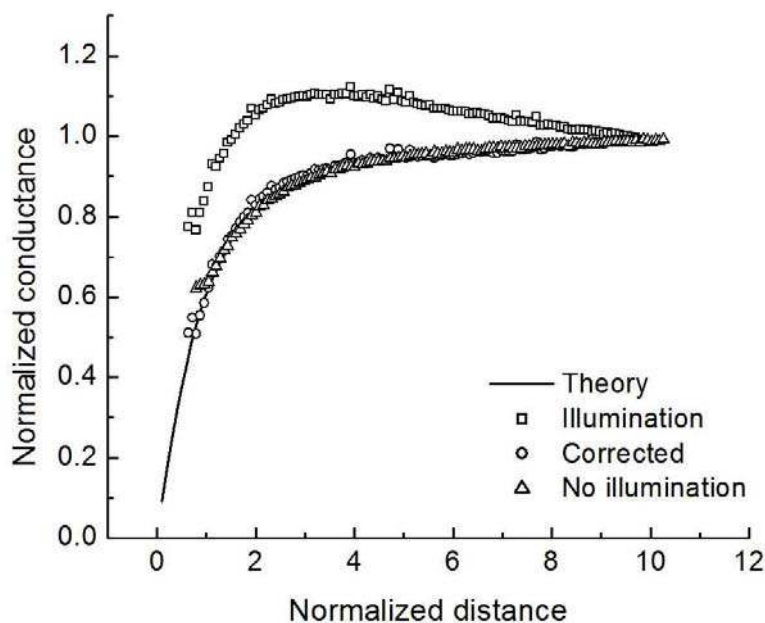


Figure 3.6 Conductivity approach curves of 4 wt% PAG loaded T-518 immersed in 18 M Ω water.

Transient conductance measurements were used to monitor changes in ion concentration in the water layer during exposure of the resist to 193 nm light. A 100 μm diameter Pt electrode was placed at a fixed distance (100 μm) from the surface and conductance was measured as a function of time. Under these conditions, and assuming a limiting molar conductivity of 100 S cm² mol⁻¹, the minimum detection limit of TPS nonaflate is on the order of 1 μM . An estimate of 100 S cm² mol⁻¹ for the limiting molar conductivity of TPS nonaflate was determined by comparing the conductivity response of TPS nonaflate solutions to that of KCl solutions under identical conditions, the limiting molar conductivity of KCl in water is known.²² Conductance measurements of water in

contact with unexposed resist films with PAG loading were not statistically different from similar measurements over resist films with no PAG. Note that the time required to position the microelectrode, which in this case was 30 seconds, determines the earliest point at which a conductance measurement can be made. Figure 3.7 shows the conductance response when various formulations of T-518 were irradiated with 190 mJ/cm² of 193 nm light over 10 seconds (10 Hz pulse rate). Greater PAG loading yielded a higher conductance during exposure and slopes of the solution conductance versus time plots followed a linear dependence with PAG loading in the film (Figure 3.7 inset). The two TOK films, ILP01 and ILP04 with tri-n-dodecylamine replacing triethanolamine and designated TOK3 and TOK4, respectively, had similar slopes that are approximately 30% higher than the corresponding 5 wt% AZ formulation.

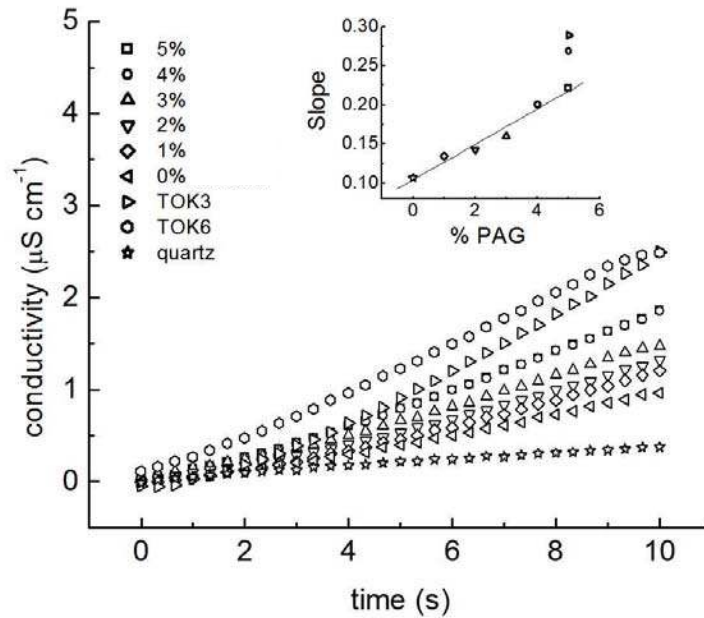


Figure 3.7 Change in conductivity of immersion water over various resist formulations and quartz. Inset is plot of the slopes of the conductivity versus time plot.

3.4.3 LIQUID SCINTILLATION COUNTING RESULTS

Liquid scintillation counting was used to provide quantitative information regarding extraction of three photoresist components, residual casting solvent, PAG and base additive during immersion. The mass in grams of a radiolabeled resist component in a sample was determined using Equation 2,

$$Mass = \left(\frac{CPM - CPM_b}{Efficiency} \right) \left(\frac{1 \mu Ci}{2.22 \times 10^6 DPM} \right) / SA \quad (2)$$

where CPM is the counting rate measured by the scintillation counter, CPM_b is the level of background radiation, $Efficiency$ is determined from the amount of quenching

measured by the LSC instrumentation and SA is the specific activity of the component being analyzed. The first bracketed term in Equation 2 is the DPM value for the sample and the second is the conversion factor between DPM and activity.

The amount of each component present in the resist films was determined first. LSC measurements of the amount of residual casting solvent in films of TOK-ILP01 cast onto 2 inch wafers had an average of 424 ± 27 CPM with a counting efficiency of 93%. This corresponded to an average RCS mass of 177 ± 12 μg . For the amount of PAG in TOK-ILP01, an average of 473 ± 10 CPM with an efficiency of 88% was obtained, which corresponded to 25 ± 0.5 μg of PAG in the film. Measurements of the amount of base in TOK-ILP01 resulted in an average CPM value of 179 ± 5 with an efficiency of 90% for a total of 1.48 ± 0.04 μg of tripropylamine in the films. The errors for the quantification were determined from the counting error and the sample-to-sample variation. The radioactive decay process was assumed to follow a Poisson distribution, so the standard deviation of the activity for each sample analyzed by LSC was determined by dividing the square root of the total number of counts detected by the counting time.⁸ The sample-to-sample variation was determined by the repetition of the measurements of seven to ten samples.

Next, the extent of RCS extraction was examined. For immersion times from 30 – 1800 s, no statistically detectable amount of RCS was seen in the immersion water from any of the formulations tested. This was determined by comparing the total number of counts measured from each sample over a twenty minute period to the total number measured for the background. Since the radioactive decay process follows a Poisson

distribution, the standard deviation (σ) of the radiation level of a sample is determined from the square root of the number of decay events.⁸ The results of the LSC measurements showed that the immersion water exhibited radiation levels within two or three standard deviations of those measured for the background, Figure 3.8.

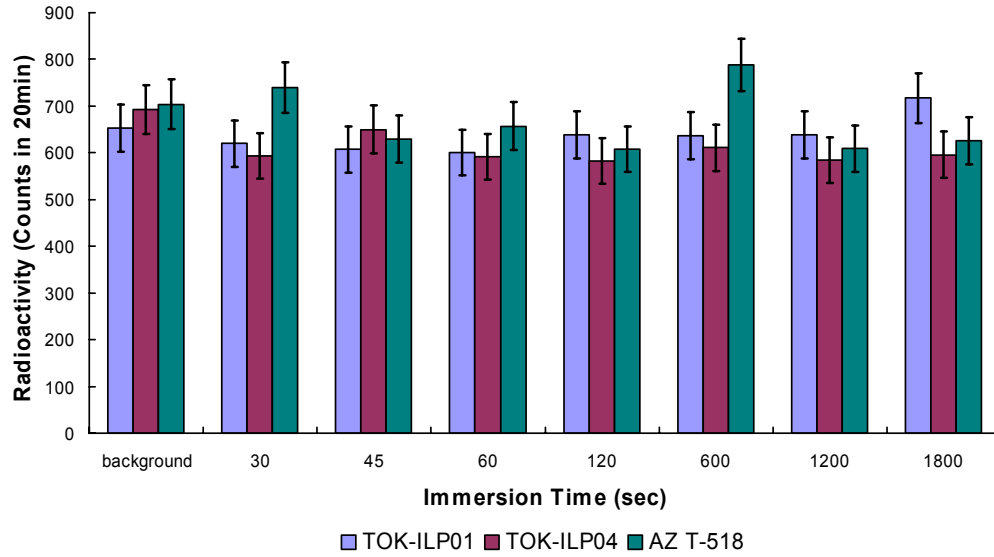


Figure 3.8 Radioactivity expressed as total counts in 20 min from background and from water samples that immersed resist films with ¹⁴C-labeled RCS for various times.

A detection limit for each LSC measurement was determined by Equation 3,

$$Mass_{\min} > \left(\frac{2\sqrt{CPM_b \times t}}{t} \right) \left(\frac{1\mu Ci}{2.22 \times 10^6 DPM} \right) / SA \quad (3)$$

where t is the total time in minutes that the background level was counted and the first term on the right hand side is the 95% error limit of the CPM_b measurement. Under the conditions of these experiments, no more than 0.8 μg of RCS could have been extracted

from a resist film coated onto a two inch wafer. Normalized to surface area, this corresponds to a limit of 40 ng/cm^2 . An increase in the sensitivity of these measurements by an order of magnitude would require either an equal increase in the magnitude of the SA of the radiolabeled casting solvent or a sample counting time of approximately 33 h.

The results of the ^{14}C -PAG extraction experiments from unexposed films of all three model resists showed a significant signal in each of the immersion water samples. Figure 3.9 shows that after only a 30 s immersion, a statistically significant amount of ^{14}C -PAG was detected. The amount of PAG extracted from each resist then remained essentially constant after 30 s for increasing immersion times up to 30 min. Figure 3.10 shows leaching from AZ T-518 occurring primarily in the first 10 s of immersion. For a counting efficiency of 91%, the amounts of PAG extracted from films of TOK-ILP01 and TOK-ILP04, averaged over immersion time, was determined to be 30 ng/cm^2 . Under the same conditions, 52 ng/cm^2 of PAG leached from the AZ T-518. Detection limits for the PAG extraction experiments were determined from Equation 3 to be 7 ng/cm^2 .

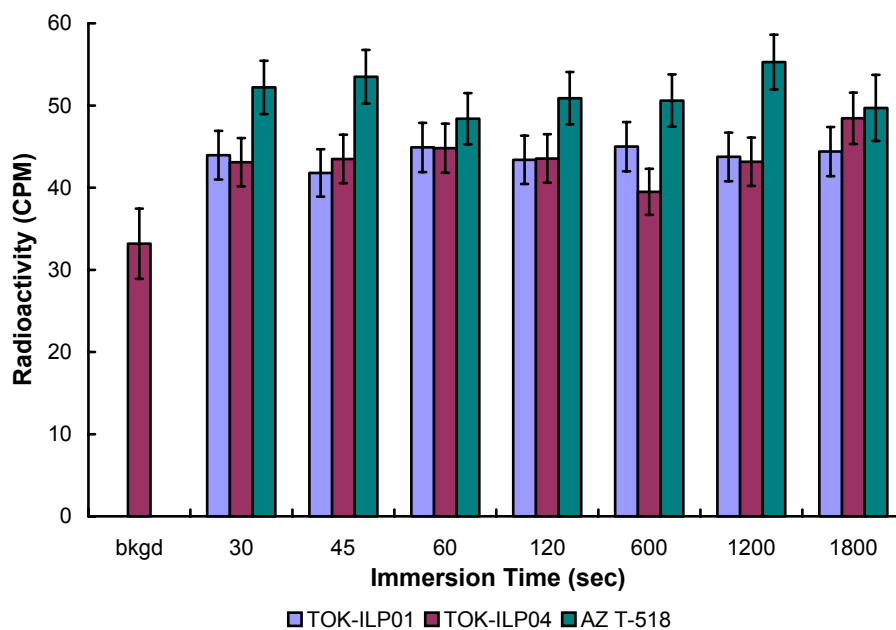


Figure 3.9 Radioactivity in *CPM* of immersion water containing extracted ^{14}C -PAG vs. immersion time.

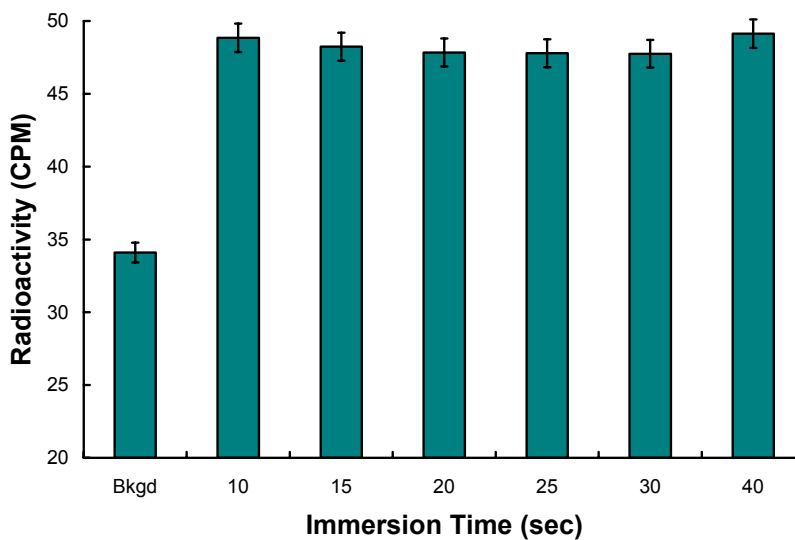


Figure 3.10 Radioactivity in *CPM* of immersion water containing extracted ^{14}C -PAG from AZ T-518 vs. immersion time.

Figure 3.11 compares leaching of PAG and photoacid from unexposed and exposed samples of TOK-ILP01, respectively, as determined by LSC. Contrary to LCMS measurements, no statistically significant difference between the amount of PAG extracted from the exposed resist and that extracted from the unexposed samples was observed using LSC, but it should be noted that LCMS could detect only the anion and LCS could detect only the phenyl ring on the cation. Accurate measurement of photoacid leaching using this method would require the synthesis of a PAG with a radiolabeled anion. Several films of TOK-ILP01 were also subjected to a 30 s prerinse before immersion. Figure 3.12 shows that the LSC measurements of the prerinse water reported radioactivity levels comparable to those reported for the initial PAG extraction experiments, but the activity level of the immersion water was no greater than background. This shows that essentially all the PAG that was extracted from a photoresist film is removed within the first 30 s of immersion. Figure 3.13 shows the thickness dependence of PAG extraction from films of TOK-ILP04. The radioactivity levels in the immersion water stayed constant with decreasing film thickness, indicating that PAG was only being extracted from the surface of the film.

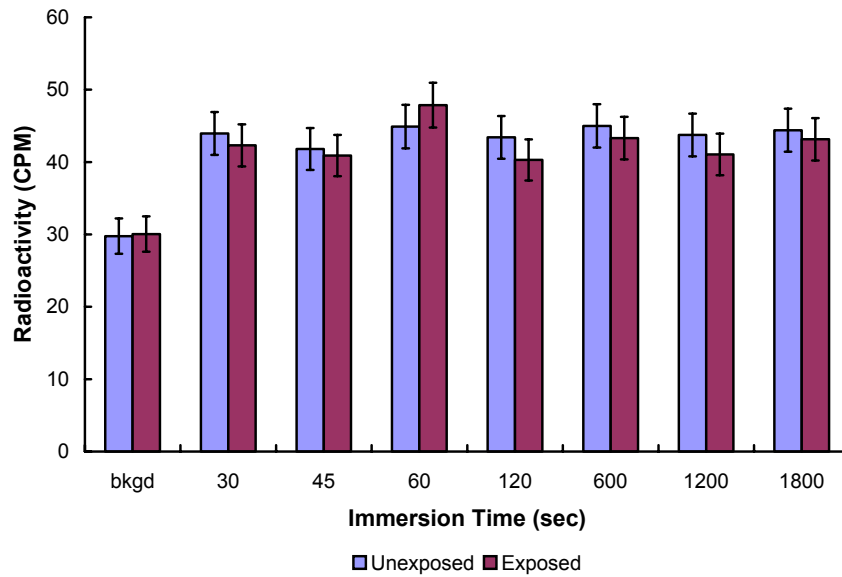


Figure 3.11 Radioactivity in *CPM* of immersion water containing extracted ^{14}C -PAG from unexposed and exposed films of TOK-ILP01 vs. immersion time.

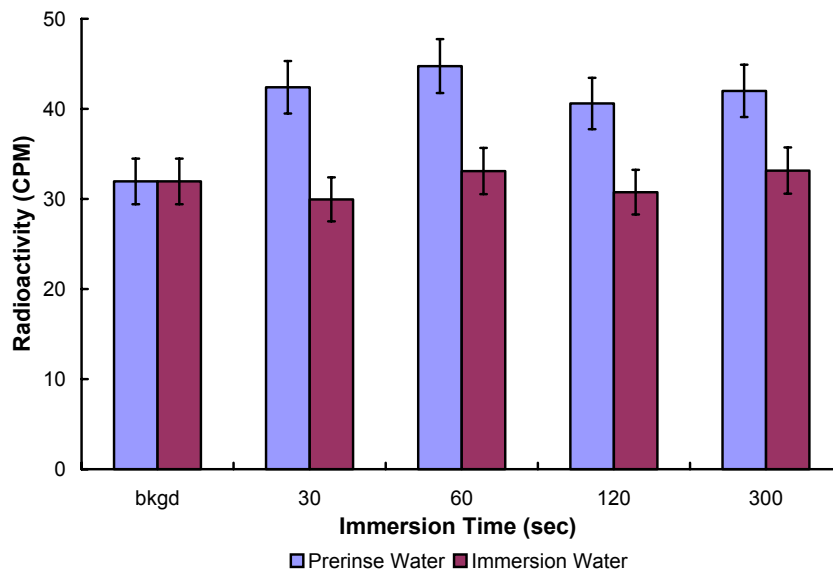


Figure 3.12 Radioactivity in *CPM* of 30 s pre-rinse and immersion water containing extracted ^{14}C -PAG from films of TOK-ILP01 vs. immersion time.

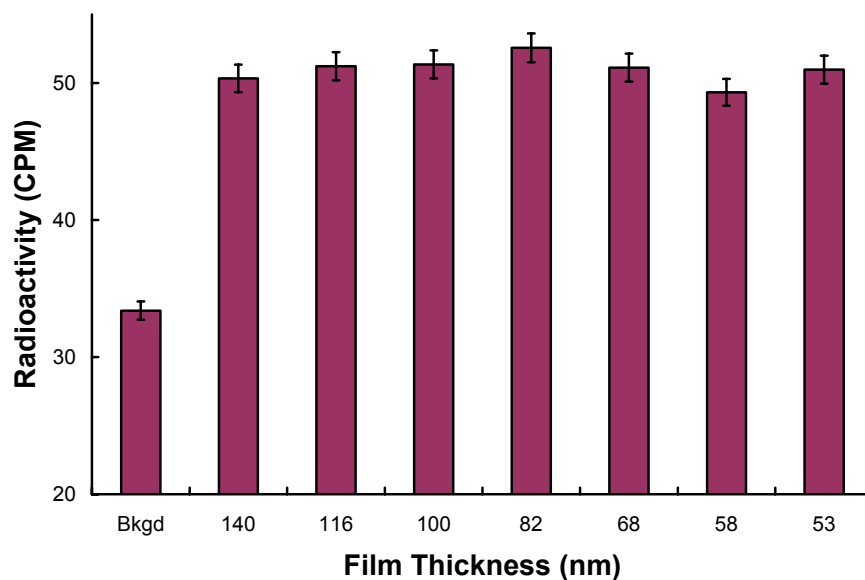


Figure 3.13 Radioactivity in *CPM* of immersion water containing extracted ^{14}C -PAG from films of TOK-ILP04 vs. film thickness.

The results of the ^{14}C -base extraction experiments are summarized in Figure 3.14. The radioactivity level in the immersion water shows that after 30 s of immersion a small, but detectable amount of base was extracted from each resist. The level did not increase with immersion time, again indicating that the extraction is complete within 30 s. The amount extracted, with a counting efficiency of 96% and averaged over immersion time, was $0.04\ \mu\text{g}$ or $2\ \text{ng}/\text{cm}^2$ of ^{14}C -tripentylamine from each resist. Sub-30 s measurements showed no detectable signal from labeled base in the immersion water until 25 s of immersion time.

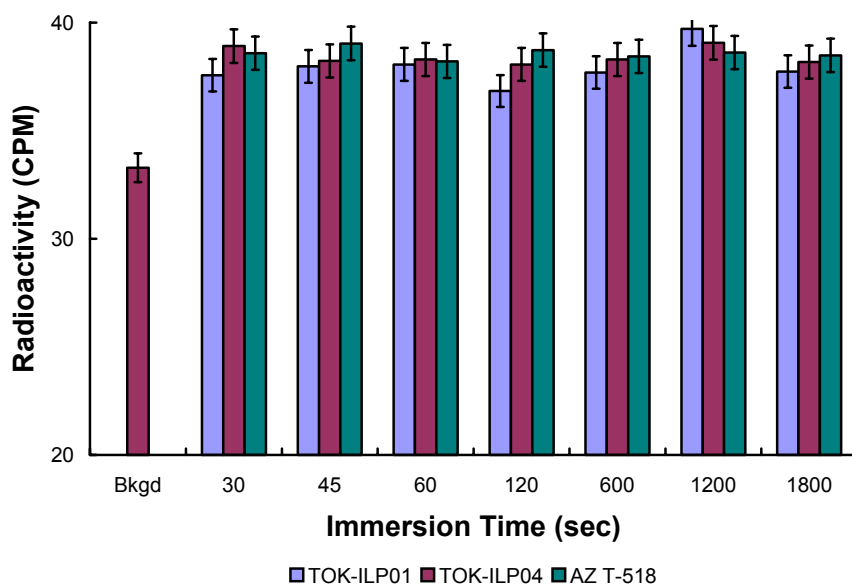


Figure 3.14 Radioactivity in *CPM* of immersion water containing extracted ^{14}C -base vs. immersion time.

Figure 3.15 shows that LSC measurements of prerinse and immersion water from films of TOK-ILP01 gave similar levels of radioactivity from extracted base. The level again did not increase with immersion time and was consistent with those shown in Figure 3.14. Figure 3.15 indicates that the base, unlike the PAG, will continue to be extracted from a film during subsequent immersion. This was confirmed by immersing a single film of TOK-ILP01 five separate times. In each sample of immersion water from that film, a level of extracted base consistent with the data in Figures 3.14 and 3.15 was detected. Results from thickness dependent base extraction measurements are shown in Figure 3.16. As the thickness of the TOK-ILP04 films decreased, the radioactivity level in the immersion water increased, indicating that an increasing amount of tripropylamine

was extracted. This is opposite to what one would expect for bulk diffusion of base through the film, suggesting the possibility of a thin film effect.

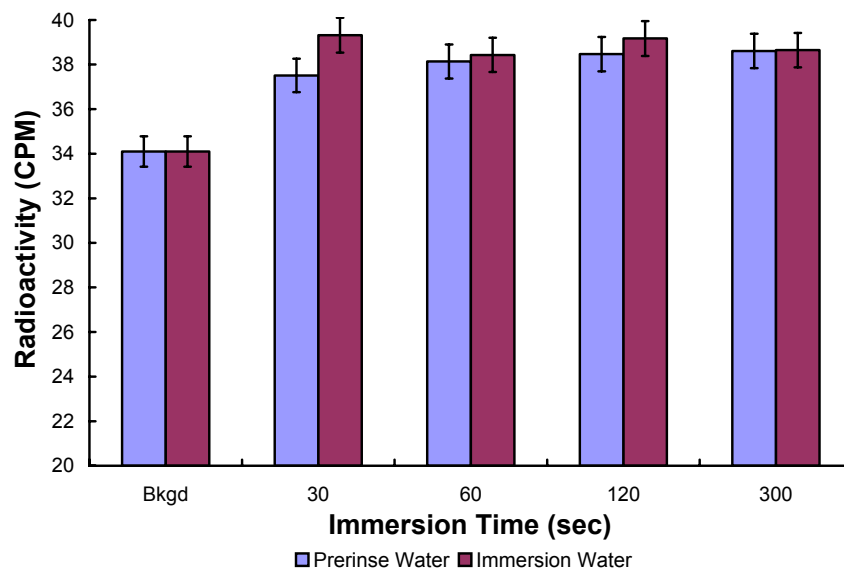


Figure 3.15 Radioactivity in CPM of 30 s pre-rinse and immersion water containing extracted ^{14}C -base from films of TOK-ILP01 vs. immersion time.

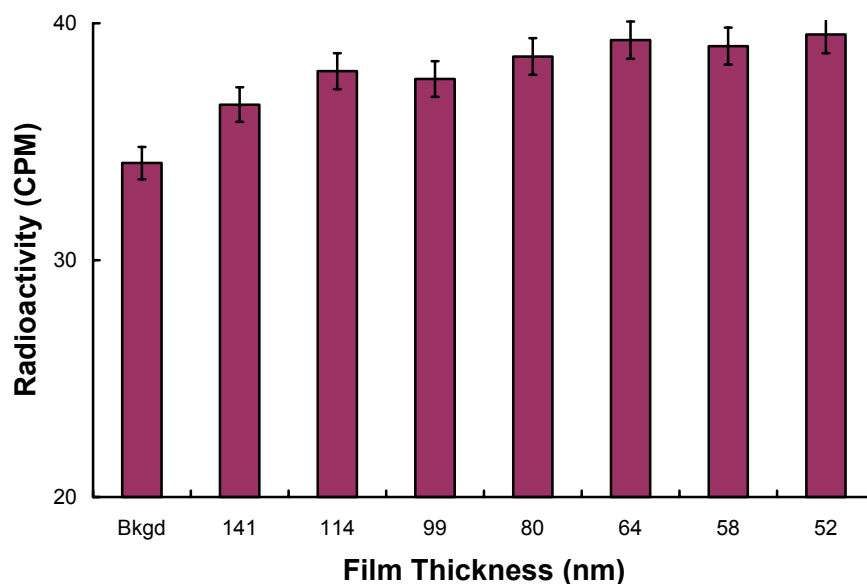


Figure 3.16 Radioactivity in *CPM* of immersion water containing extracted ^{14}C -base from films of TOK-ILP04 vs. film thickness.

3.5 DISCUSSION OF PHOTORESIST COMPONENT EXTRACTION

The extraction of components from model 193 nm photoresists was studied with three different analytical techniques. While each method provided qualitative evidence of extraction, quantification was made difficult by several factors. The SECM modes all allowed for real-time monitoring of the resist/immersion water interfacial region and, in combination, differentiated between the extraction of PAG and photoacid. However, the sensitivity limit of SECM is in the micromolar region, which is not sufficient for the samples measured. LCMS has parts per billion sensitivity limits for the PFBS anion, but is indifferent to the counterion and thus cannot differentiate between PAG and photoacid. LSC methods provide the opportunity to investigate multiple photoresist components, depending on synthetic capability and the availability of radiolabeled precursors.

Detection limits are set by the specific activity of radiolabeled material used and the time invested in the counting procedure. Using highly radioactive samples and very long counting times provides very high, tunable sensitivity. However, the synthesis of ^{14}C -isotope labeled chemicals for LSC requires a significant commitment.

The challenge of accurate quantification becomes apparent when the results of LCMS are compared to those of LSC. The result from the former method, analyzing 100 μL drops, indicated that an order of magnitude less PAG was extracted from TOK-ILP04 than what was detected by the latter, analyzing 7 mL baths. To probe this discrepancy, several additional experiments were carried out. First, a nominally 100 ng/ml sample of radiolabeled TPS nonaflate was prepared and analyzed by both LSC and LCMS. LCMS detected a concentration of 74 ng/mL and the concentration determined by LSC measurements was 105 ng/mL, demonstrating that the two techniques provide comparable results within about 20% accuracy. In the second experiment, an extraction was performed using the full wafer immersion procedure and this solution was analyzed using LCMS. The amount of extracted PAG detected was 30 ng/cm². In the last, 100 μL drops were analyzed by LSC. Samples containing just one drop showed no detectable signal from labeled PAG, but a sample containing six drops collected from different areas of the same film did. This amount was again consistent with those from the previous LSC measurements. This indicates an error in the analysis of extremely small samples and led to the use of LSC as the primary method of leaching quantification.

Results from previous studies of concentration gradients and diffusion in photoresist films support the observations from this work.²³ A modified Fujita-Doolittle

solvent diffusion model developed to generate residual casting solvent concentration profiles in a resist film showed a significant decrease in the RCS concentration at the resist surface relative to the bulk value after the PAB.^{24, 25} This results in densification of the resist film which reduces the mass transport rate at the surface, leading to the expectation that very little RCS could be extracted from any resist film. A similar inhomogeneity has also been seen in the PAG concentration profile. The PAG concentration profile throughout the film depends upon the nature of the resist and the physicochemical properties of the PAG. Early work showed that polar PAGs such as triphenylsulfonium hexafluoroantimonate tended to show a depletion at the surface of a resist film formulated with non-polar polymers such as polystyrene.²⁶ More recent work using near edge x-ray absorption fine structure showed that ionic PAGs with high fluorine content tend to aggregate to the surface of resist films.²⁷ As the PAG used in this study is similar to those used in the latter work, it is expected to aggregate at the surface and be more susceptible to extraction. Also, the amounts of PAG extracted from the resists are consistent with what would be expected based on previously published values of diffusion coefficients for PAGs and photoacid generators.^{28, 29} By assuming a homogeneous distribution of PAG throughout the film, an upper limit of 4 – 6 nm is estimated for the depth from which PAG is leached.

The aggregation of PAG at the surface of a resist film and subsequent depletion was observed in preliminary studies using X-ray photoelectron spectra (XPS). The XPS data was collected with a PHI 5700 ESCA system and are given in Figure 3.17. A film of AZ T-518 with 5 wt% PAG loading was coated onto a wafer which was split in half.

One half of the wafer was immersed in water for 30 s. Relative amounts of fluorine in the film were obtained by assuming a constant carbon concentration and normalizing the fluorine signal by the carbon signal. In both the washed and unwashed samples, the fluorine signal decreases with increasing angle, suggesting a higher fluorine concentration at the surface than in the bulk of the film. As expected, the washed sample displays lower fluorine signals at all angles relative to the unwashed sample.

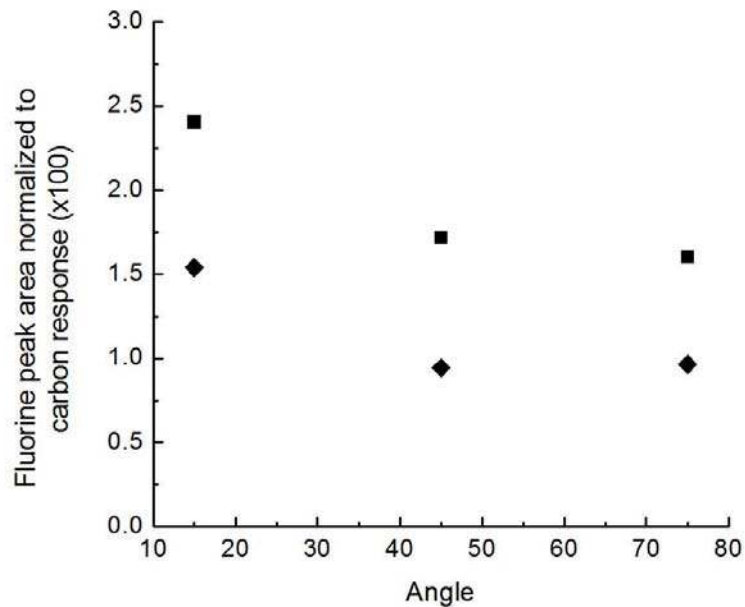


Figure 3.17 XPS analysis of fluorine content in wafers coated with AZ T-518 both washed (◆) and unwashed (■).

Unlike for the RCS and PAG, there was not a clear interpretation for the results of the base extraction measurements. At first, there appeared to be an upper limit to the amount of base extracted from the resist films since the amount did not increase with

immersion time. Yet multiple immersions of the same film continued to show evidence of base extraction. The results for the film thickness-dependence measurements were also counterintuitive. It was not apparent why more base should come out of thinner films than thicker films. Attempts were made to vary the amount of water used for the immersions in addition to the thickness variation, but no consistent trend was found. It was noted that when larger volumes of water were used for the immersion, an oily-appearing film formed at the surface of the water. However, much of that film remained as a residue on the wafer after the water was collected so it could not be analyzed. It is possible that the residue was base, but there is no confirmation of that as yet. Since there has not been a thorough study of base diffusion in photoresists, the nature of these results remains unexplained. It is clear that further work is needed to elucidate the behavior of a base additive in a photoresist in general, as well as under immersion conditions.

3.6 SUMMARY

Liquid chromatography/mass spectrometry, scanning electrochemical microscopy and liquid scintillation counting were used to analyze photoresist component extraction phenomena from model resists for 193 nm immersion lithography. Qualitative confirmation of PAG and photoacid extraction was observed using all techniques. While the LCMS technique was capable of providing quantitative results for PAG extraction, only the LSC method was able to do so for all three photoresist components studied. In the discrepancy between the two techniques, the LSC results showed greater PAG extraction. Therefore, the LSC results were used for quantification so that measurements

of the amounts of each component extracted were consistent and would represent at least a worst case scenario among all of the results. As such, the amount of PAG leaching from a resist film was 30-50 ng/cm², depending upon formulation. Base leaching was also quantified at 2 ng/cm², independent of the formulation. No statistically significant residual casting solvent was seen to be extracted from the resists. The behavior of the extraction as a function of immersion time suggested that PAG leaching occurs only at the surface and that after a 30 second rinse of a film, no additional extraction will be observed for upwards of 30 minutes. Base leaching also occurs within the first 30 seconds of immersion, but unlike the PAG, it continues to be leached from the film during subsequent immersions. The differences in the behavior of the PAG and base leaching suggest that the base is extracted from these resist films through a more complex mechanism than simply being rinsed from the surface, as the PAG appears to be.

3.7 REFERENCES

1. Dammel, R. R.; Houlihan, F. M.; Sakamuri, R.; Rentkiewicz, D.; Romano, A. "193 nm immersion lithography - Taking the plunge." *Journal of Photopolymer Science and Technology* **2004**, *17* (4), 587-602.
2. LeSuer, R. J.; Fan, F.-R. F.; Bard, A. J.; Taylor, J. C.; Tsiartas, P.; Willson, G.; Conley, W. E.; Feit, G.; Kunz, R. R. "Using scanning electrochemical microscopy to probe chemistry at the solid-liquid interface in chemically amplified immersion lithography." *Proceedings of SPIE-The International Society for Optical Engineering* **2004**, 5376 (Pt. 1, Advances in Resist Technology and Processing XXI), 115-125.
3. Bard, A. J.; Mirkin, M. V., *Scanning Electrochemical Microscopy*. Marcel Dekker: New York, **2001**; p 650.

4. Gardiner, A. B. *Measurement of Concentration Gradients in Photoresist Films and Study of the Influence of these Gradients on Photoresist Performance*. PhD Dissertation, The University of Texas at Austin, Austin, TX, USA, **1999**.
5. Fender, N.; Brock, P. J.; Chau, W.; Bangsaruntip, S.; Mahorowala, A. P.; Wallraff, G. M.; Hinsberg, W. D.; Larson, C. E.; Ito, H.; Breyta, G.; Burnham, K.; Truong, H.; Lawson, P.; Allen, R. D. "Characterization of new aromatic polymers for 157-nm photoresist applications." *Proceedings of SPIE-The International Society for Optical Engineering* **2001**, 4345 (Pt. 1, Advances in Resist Technology and Processing XVIII), 417-427.
6. Burns, S. D. *Understanding Fundamental Mechanisms of Photoresist Dissolution*. PhD Dissertation, The University of Texas at Austin, Austin, TX, USA, **2003**.
7. Howard, P. L., *Basic Liquid Scintillation Counting*. American Society of Clinical Pathologists: Chicago, **1976**; p 59.
8. Horrocks, D. L., *Applications of Liquid Scintillation Counting*. Academic Press: New York, **1974**; p 346.
9. Horrocks, D. L., In *Liquid Scintillation: Science and Technology*, Noujaim, A. A.; Ediss, C.; Weibe, L. I., Eds. Academic Press: New York, **1976**; p 352.
10. Hinsberg, W. D.; MacDonald, S. A.; Clecak, N. J.; Snyder, C. D. "Airborne Contamination of a Chemically Amplified Resist. 2. Effect of Polymer Film Properties on Contamination Rate." *Chemistry of Materials* **1994**, 6 (4), 481-8.
11. Mauzeroll, J.; Buda, M.; Bard, A. J.; Prieto, F.; Rueda, M. "Detection of Tl(I) Transport through a Gramicidin-Dioleoylphosphatidylcholine Monolayer Using the Substrate Generation-Tip Collection Mode of Scanning Electrochemical Microscopy." *Langmuir* **2002**, 18 (24), 9453-9461.
12. Selzer, Y.; Mandler, D. "Scanning Electrochemical Microscopy. Theory of the Feedback Mode for Hemispherical Ultramicroelectrodes: Steady-State and Transient Behavior." *Analytical Chemistry* **2000**, 72 (11), 2383-2390.

13. Johnson, D. E.; Enke, C. G. "Bipolar pulse technique for fast conductance measurements." *Analytical Chemistry* **1970**, *42* (3), 329-35.
14. Calhoun, R. K.; Holler, F. J.; Geiger, R. F., Jr.; Nieman, T. A.; Caserta, K. J. "Wide-range bipolar pulse conductance instrument employing current and voltage models with sampled or integrated signal acquisition." *Analytica Chimica Acta* **1991**, *252* (1-2), 29-40.
15. Caserta, K. J.; Holler, F. J.; Crouch, S. R.; Enke, C. G. "Computer controlled bipolar pulse conductivity system for applications in chemical rate determinations." *Analytical Chemistry* **1978**, *50* (11), 1534-41.
16. LeSuer, R. J.; Fan, F.-R. F.; Bard, A. J. "Scanning Electrochemical Microscopy, 52. Bipolar Conductance Technique at Ultramicroelectrodes for Resistance Measurements." *Analytical Chemistry* **2004**, *76* (23), 6894-6901.
17. Horrocks, B. R.; Mirkin, M. V.; Pierce, D. T.; Bard, A. J.; Nagy, G.; Toth, K. "Scanning electrochemical microscopy. 19. Ion-selective potentiometric microscopy." *Analytical Chemistry* **1993**, *65* (9), 1213-24.
18. McKinney, P. S.; Rosenthal, S. "Electrochemical reduction of the triphenyl-sulfonium ion." *Journal of Electroanalytical Chemistry and Interfacial Electrochemistry* **1968**, *16* (2), 261-70.
19. Horrocks, B. R.; Schmidtke, D.; Heller, A.; Bard, A. J. "Scanning electrochemical microscopy. 24. Enzyme ultramicroelectrodes for the measurement of hydrogen peroxide at surfaces." *Analytical Chemistry* **1993**, *65* (24), 3605-14.
20. Alpuche-Aviles, M. A.; Wipf, D. O. "Impedance Feedback Control for Scanning Electrochemical Microscopy." *Analytical Chemistry* **2001**, *73* (20), 4873-4881.
21. Gurevich, I. U. I. A.; Pleskov, I. U. V.; Rotenberg, Z. A., *Photoelectrochemistry*. Consultants Bureau: New York, **1980**; p 239.
22. Lind, J. E., Jr.; Zwolenik, J. J.; Fuoss, R. M. "Calibration of conductance cells at 25 Deg with aqueous solutions of potassium chloride." *Journal of the American Chemical Society* **1959**, *81*, 1557-9.

23. Gardiner, A. B.; Burns, S.; Qin, A.; Willson, C. G. "Determination of residual casting solvent concentration gradients in resist films by a "halt development" technique." *Journal of Vacuum Science & Technology, B: Microelectronics and Nanometer Structures* **2001**, *19* (1), 136-141.
24. Mack, C. A. *Modeling solvent effects in optical lithography*. PhD Dissertation, The University of Texas at Austin, Austin, TX, USA, **1998**.
25. Mueller, K. E. *Diffusion in polymers using quartz crystal microbalance techniques*. PhD Dissertation, The University of Texas at Austin, Austin, TX, USA, **1998**.
26. Hult, A.; MacDonald, S. A.; Willson, C. G. "Photoinitiated interfacial cationic polymerization." *Macromolecules* **1985**, *18* (10), 1804-9.
27. Lenhart, J. L.; Jones, R. L.; Lin, E. K.; Soles, C. L.; Wu, W.-l.; Fischer, D. A.; Sambasivan, S.; Goldfarb, D. L.; Angelopoulos, M. "Probing surface and bulk chemistry in resist films using near edge x-ray absorption fine structure." *Journal of Vacuum Science & Technology, B: Microelectronics and Nanometer Structures* **2002**, *20* (6), 2920-2926.
28. Mueller, K. E.; Koros, W. J.; Mack, C. A.; Willson, C. G. "Diffusivity measurements in polymers, part IV: acid diffusion in chemically amplified resists." *Proceedings of SPIE-The International Society for Optical Engineering* **1997**, *3049* (Advances in Resist Technology and Processing XIV), 706-711.
29. Stewart, M. D. *Catalyst diffusion in positive-tone chemically amplified photoresists*. PhD Dissertation, The University of Texas at Austin, Austin, TX, USA, **2003**.

CHAPTER 4: SECOND GENERATION FLUIDS FOR IMMERSION LITHOGRAPHY

4.1 INTRODUCTION TO SECOND GENERATION IMMERSION LITHOGRAPHY

The benefits of immersion lithography and the success in resolving its critical issues have resulted in its supplantation of 157 nm lithography as the technology of choice for the 45 nm technology node. This success has also generated interest in extending its capabilities beyond that enabled by water. The most straightforward path to achieving improvement would be to replace water with a higher refractive index fluid. This approach would be feasible since many of the initial demonstrations of immersion used fluids other than water.¹⁻⁴ However, since significant investments have been made in developing the water immersion process, many aspects of the process would not be directly transferable to a new material. One example is the fluid handling systems for immersion exposure tools, which would have to be completely redesigned for use with a different fluid.

The requirements for new immersion fluids were described by French, *et al.*⁵ Fluids intended to replace water, dubbed second generation immersion fluids, should have a refractive index of $n = 1.65$, an absorption coefficient of $\alpha < 0.15 \text{ cm}^{-1}$ and a thermo-optic coefficient of $dn/dT < 250 \text{ ppm/K}$. For fluid handling purposes, the surface tension and wetting properties should be as close to water as possible and the viscosity should not be more than three times that of water. Other considerations are a cost of ownership of one to two dollars per circuit layer printed, minimal photochemical effects

and no negative impact from interactions with photoresists. Second generation fluids are expected to facilitate patterning of 38 nm features. To achieve smaller features, a third generation of fluids with a refractive index of $n = 1.9$ would be needed, with the other properties equivalent to a second generation fluid. There are two additional considerations for next generation immersion lithography that are not directly related to the fluids. At either of the target index values, the fluid would no longer be the lowest index component of the imaging system. The final lens element, $n \approx 1.56$, would have to be replaced with a higher index material or a lens element with a large, concave curvature to achieve the higher NA values needed for imaging 38 nm features and below. Both options are challenging as a high index material suitable for lenses has yet to be identified and a large curvature would likely complicate fluid handling.^{6, 7} Also, for third generation immersion, a high index photoresist would be required since current resists have $n \approx 1.7$.⁸

These considerations were apparent in the first proposals for new immersion fluids, which suggested using an additive in water to increase its index of refraction. Common organic compounds, metal salts and acids, heavy metal cations stabilized with surfactants and nanoparticles were all suggested as possible high index additives.⁹⁻¹³ Of these options, the largest indices were obtained with aqueous solutions of ionic species. However, the larger index values were accompanied by significant increases in the absorbance of the solutions over that of water. Also, metal contamination has been a serious and ongoing concern in semiconductor fabrication, so metal-containing ionic additives would not be a viable option in manufacturing.¹⁴⁻¹⁶

While these studies provided valuable information about the optical properties of some aqueous solutions at the 193 nm wavelength, none of this information led directly to a fluid with the target properties. In the following study, a systematic survey of the optical properties of solutions of common ionic compounds was performed. The information from this survey was intended to show how optical properties changed with different ionic species. The viscosities and contact angles of these solutions were also measured to determine the impact of an additive on fluid handling. The trends seen were used to guide the development of semiconductor-friendly ionic additives in which metal cations were replaced with quaternary ammonium cations.

4.2 CHARACTERIZATION OF OPTICAL AND PHYSICAL PROPERTIES OF FLUIDS

The optical properties of the fluids studied were measured using spectroscopic ellipsometry and transmission spectroscopy. Ellipsometry measures changes in the polarization of a beam of light before and after reflection from a sample, and relates those changes to characteristics of the sample.¹⁷⁻¹⁹ The sample is typically composed of thin films coated onto a reflective substrate. The polarization of a light wave is determined by the rotation of its electric field vector around its axis of propagation. (Since a wave's magnetic field is completely specified by its electric field, discussions of polarization often neglect the former for simplicity.) While electromagnetic waves are typically represented as two-dimensional oscillations, they can be three-dimensional, with the field vectors rotating around the axis of propagation. If the electric field vector rotates so that a head-on view of the wave would produce a circle, it is said to be circularly polarized. If

the vector does not rotate but oscillates in a single plane, it is then said to be linearly polarized. Any intermediate case is referred to as elliptically polarized light. These cases are illustrated in Figure 4.1. A wave of any polarization can be described as the superposition of two perpendicular, linearly polarized waves.

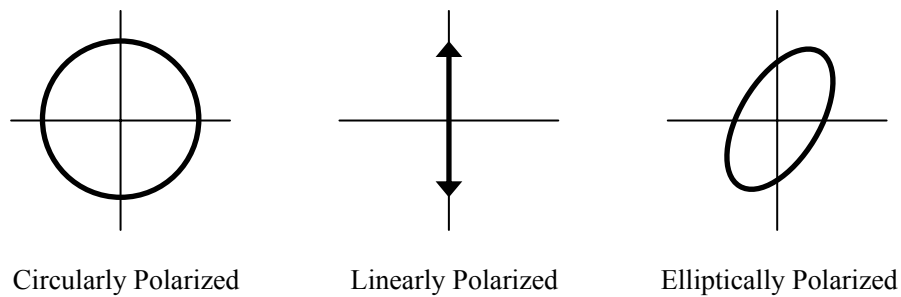


Figure 4.1 Possible polarizations for an electric field vector.

These two component waves, called the p - and s -waves, are defined for ellipsometry relative to the plane in which the light beam is incident on the sample. As discussed in Chapter 2, when a light wave is incident on an interface between two media, part of the energy in the wave is transmitted across the interface and part is reflected. This energy transfer is observed as a reduction in the amplitudes, and in some cases a phase shift, of the reflected and transmitted waves compared to that of the incident wave. The reflection and transmission occur in a common plane normal to the interface, called the plane of incidence. The p - and s -waves are defined relative to the plane of incidence, with the electric field vector of the p -wave parallel to the plane and the electric field vector of the s -wave perpendicular, see Figure 4.2. (Note: the polarization state of light is sometimes given the designation transverse electric, TE, or transverse magnetic, TM.

They are commonly used in literature relating to photonics. For ellipsometry, TE corresponds to the s -wave and TM corresponds to the p -wave.)

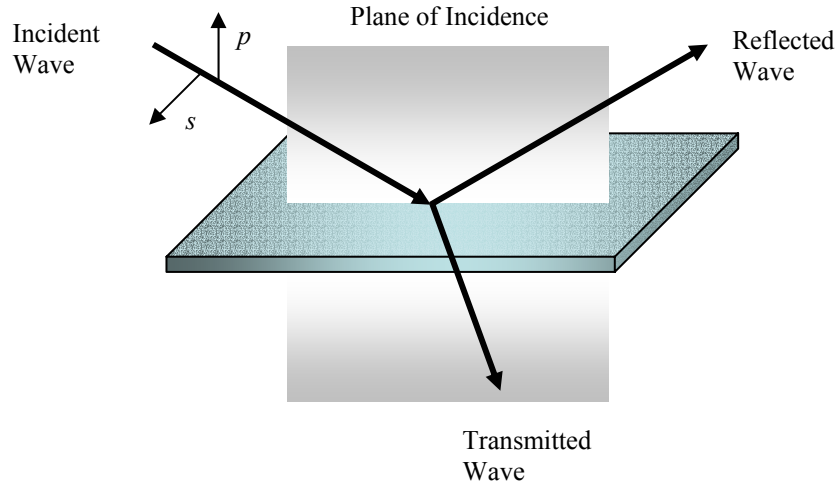


Figure 4.2 The electric field vectors of the p - and s -waves relative to the plane of incidence.

The p - and s -components of a wave need not be in phase with each other, and the phase shift which may occur during reflection need not be the same for both. Also, the amplitude reduction will not necessarily be the same, and depends on the angle of incidence. Ellipsometry measures two parameters, Ψ and Δ , which compare the amplitudes and phase differences of the p - and s -waves before and after reflection from a sample according to the following expressions,

$$\tan \Psi = \frac{|R^p|}{|R^s|} \quad (4.1)$$

$$\Delta = \delta_1 - \delta_2 \quad (4.2)$$

In Equation 4.1, $|R^P|$ and $|R^S|$ are the magnitudes of the total reflection coefficients for the p - and s -waves, respectively. The total reflection coefficient for a film stack is the ratio of the amplitude of the reflected wave to that of the incident wave, and is analogous to the well known Fresnel reflection coefficient for a single interface.²⁰ In Equation 4.2, δ_1 is the phase difference between the p - and s -waves before reflection and δ_2 is the phase difference after.

The thicknesses and optical properties of the films composing a sample analyzed by ellipsometry are determined from the total reflection coefficients, which are typically complex values. The fundamental equation of ellipsometry relates Ψ and Δ to the ratio of the total amplitude reflection coefficients by the following,

$$\tan \Psi(e^{i\Delta}) = \frac{R^P}{R^S} \quad (4.3)$$

The expressions relating R^P and R^S to the angle of incidence, thicknesses and optical properties are given elsewhere.¹⁹ Since ellipsometry measures the characteristics of the light rather than the sample, a model must be used to relate the two. With enough *a priori* knowledge of the structure of the sample and reasonable guesses for the unknowns, a regression analysis can be used to match a model of the expected behavior of Ψ and Δ to the experimental data.

The Ψ and Δ data are collected on an instrument called an ellipsometer. There are several configurations for an ellipsometer, and research-grade tools usually have a broadband source for spectroscopic measurements and the capability to scan at multiple angles of incidence.¹⁷ This flexibility allows many different types of samples to be

analyzed on a single instrument. Once the ellipsometric data has been collected, a model of the sample describing the thicknesses and optical properties of the individual films is created. The optical properties can be represented by actual tabulated values for well known materials or by dispersion relations, *i.e.*, mathematical expressions with only a few adjustable parameters that describe their behavior over a specific wavelength range. Initial guesses are made for the unknown film thicknesses and optical property parameters and used to calculate expected Ψ and Δ values. A regression analysis then varies the parameters to match the modeled data to the experimental according to the mean-squared error merit function (MSE). The MSE indicates how closely the modeled data falls within a standard deviation of the experimental, with lower MSE values corresponding to better fits.¹⁷ Also, the regression analysis will calculate 90% confidence intervals for the varied parameters, allowing the quality of each to be assessed along with the overall fit. For the 90% confidence interval, a reasonable fit is indicated by a value that is at least an order of magnitude less than the parameter. While the ellipsometric technique is an indirect measurement of thickness and optical properties, it has been shown to be very reliable.²¹

The refractive index values for the solutions studied were determined from measurements using a J. A. Woollam M-2000 variable angle spectroscopic ellipsometer (VASE). The angle of incidence was set at 70° and data was collected over a spectral range of 190 nm – 1000 nm. The angle of 70° was chosen since it is typically close to the Brewster angle, the angle at which R^p goes to zero. In the region close to the Brewster angle, both errors and noise in the measurement are reduced. Data analysis was

performed using the WVASE32 software package, also provided by J. A. Woollam Co., Inc. The fluids were measured by first filling a 2 in diameter Fluoroware cup with 5 – 7 mL until a flat surface was obtained and then leveling the base of the ellipsometer in order to align the detector to the fluid surface. This procedure deviates from typical operation in which the sample is mounted on a stage and its tilt is adjusted to align the sample to the detector. The curved and opaque bottom surface of the cup scattered light transmitted through the air – fluid interface and ensured that only reflections from the top surface of the fluid were collected and analyzed. This technique was adapted from the “rough surface” technique developed at Woollam.²² Using this approach, the fluid sample is modeled as a semi-infinite substrate with a single interface with the ambient. The index values were determined by a Cauchy model, which represents the normal dispersion of the refractive index over a particular wavelength range with a quadratic expression,

$$n(\lambda) = A + \frac{B}{\lambda^2} + \frac{C}{\lambda^4} \quad (4.4)$$

where A , B and C are empirical coefficients and the wavelength is in units of microns (μm). This technique is convenient when evaporation and/or contamination from the ambient are not significant concerns. The accuracy of this method was verified by comparing the index values measured for water to those measured by the prism minimum deviation methods used by the National Institute of Standards and Technology (NIST) and by the J. A. Woollam Co with a VUV-VASE® system, Figure 4.3.²²⁻²⁵ At 193 nm, the index value for HPLC grade water was found to be $n = 1.438 \pm 0.008$, where the error represents the 90% confidence limits of the fit of the ellipsometric parameters.

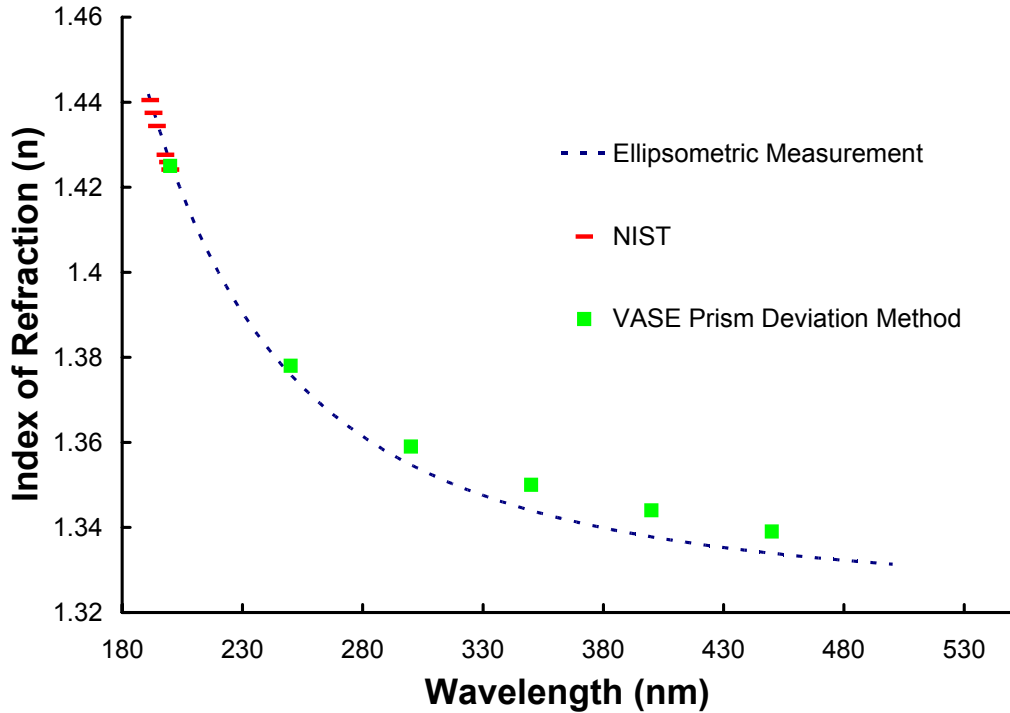


Figure 4.3 Index of refraction of water vs. wavelength determined by direct ellipsometric measurement and by prism deviation methods used by NIST and with the Woollam VUV-VASE®.

Typically, ellipsometric measurements also allow the determination of a material's extinction coefficient, from which its absorption coefficient can be calculated. However, the “rough surface” technique described above does not provide a reliable measurement for an extinction coefficient several orders of magnitude less than that of the index value measured, as is the case with water.²² Therefore, the fluid absorption coefficients were determined by transmission measurements with an Acton Research Corporation CAMS-507 Spectrophotometer (CAMS). The measurements from the CAMS have been shown to be in good agreement with ellipsometric measurements.²⁶

The absorption coefficient is found from Lambert's Law,²⁷

$$\frac{dI}{dz} = -\alpha I \quad (4.5)$$

where I is the intensity of light propagating in the z direction through the material being analyzed. The intensity is the energy flux from the light perpendicular to the direction of propagation and is proportional to the square of its amplitude. The solution to Equation 4.5 is

$$I(z) = I_0 \exp(-\alpha z) \quad (4.6)$$

where I_0 is the intensity at $z = 0$. However, absorption coefficients are conventionally reported in base 10, so Equation 4.6 can be restated as

$$I(z) = I_0 10^{(-\alpha z)} \quad (4.7)$$

where α now includes a factor of $\ln 10$. The quantity αz is known as the sample's absorbance and the ratio of $I(z)/I_0$ is referred to as its transmittance, T . Transmittance values are typically given as a percentage; that convention was used here. For dilute solutions, the absorbance is directly proportional to the molar concentration of the absorbing species, according to Beer's Law. The absorbance is determined by taking the ratio of the intensities of light transmitted through a solution and through a reference with no absorbing species. This approach implicitly accounts for transmission losses due to interfacial reflections as part of the measurement.

At high concentrations, interactions between molecules and changes in the refractive index cause deviations from the linear relationship of Beer's Law.^{27, 28} Since changing the refractive index was the purpose of the ionic additives in the fluids studied,

Beer's Law was not expected to be valid. Therefore, the absorption coefficient for the entire solution was determined. The measurements were carried out by collecting transmittance data referenced to the ambient nitrogen environment over a spectral range from 180nm to 250nm. Cylindrical quartz cuvettes with a 1 cm path length, purchased from Hellma Cells, Inc (Plainview, NY), were used to hold the fluids. Each cuvette was rinsed three times with HPLC grade water prior to being filled with a sample. Transmission losses due to interfacial reflections were determined by calculating the transmittance at each interface from the Fresnel equation at normal incidence,

$$T_i = 1 - \left(\frac{n_{t_i} - n_{o_i}}{n_{t_i} + n_{o_i}} \right)^2 \quad (4.8)$$

where T_i is the transmittance of interface i , n_{t_i} is refractive index of the medium into which the light is transmitted, and n_{o_i} is the refractive index of the medium from which the light is incident. The measured transmittance was then corrected for these losses using the following expression,

$$T_{sample} = \frac{T_{measured}}{T_1 T_2 T_3 T_4} \quad (4.9)$$

and the absorption coefficient was calculated from Equation 4.7. The four interfaces are shown in Figure 4.4.

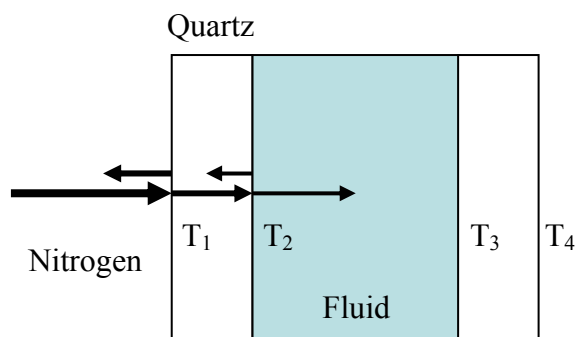


Figure 4.4 Interfaces in quartz cuvettes contributing to transmission losses.

The nitrogen environment was assumed to have an index of $n = 1$, and the index values for quartz tabulated in WVASE32 were used for the cuvette. Transmission measurements of empty cuvettes showed they approached 100% transparency above 190 nm once corrected for interfacial reflections, Figure 4.5. Below 190 nm quartz becomes opaque, so the transmittance begins to drop. Measurements of HPLC grade water showed that at 193 nm its absorption coefficient was $\alpha = 0.094 \text{ cm}^{-1}$, with a standard deviation of 0.005 cm^{-1} for the measurement, Figure 4.6. This value was in agreement with previously reported values for typical samples.^{4, 5} After extensive purification, the absorption coefficient has been reported to be as low as 0.01 cm^{-1} .

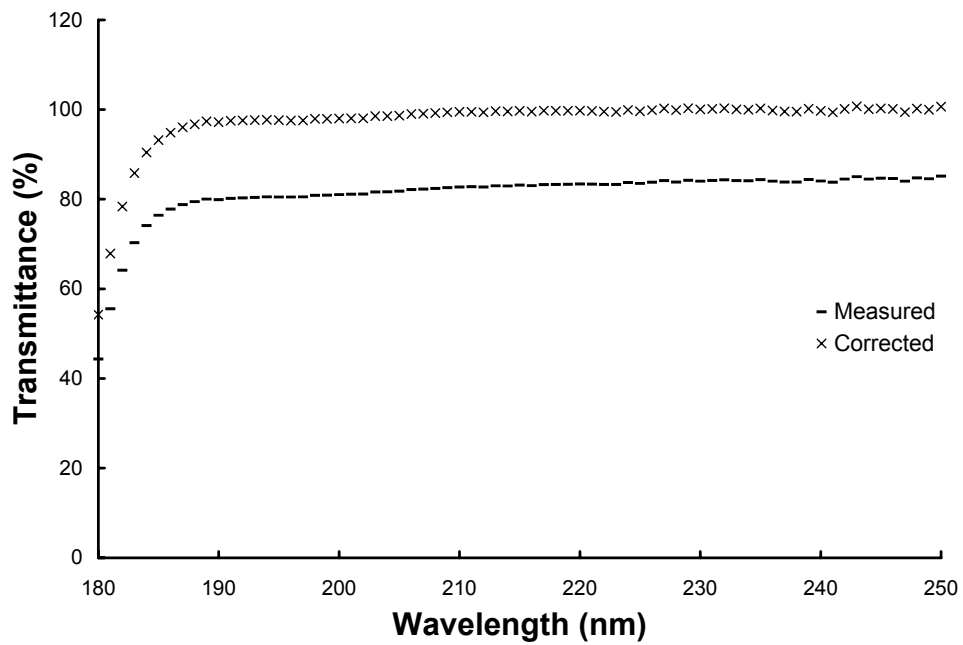


Figure 4.5 Transmittance of empty quartz cuvette vs. wavelength, both measured and corrected for interfacial reflections.

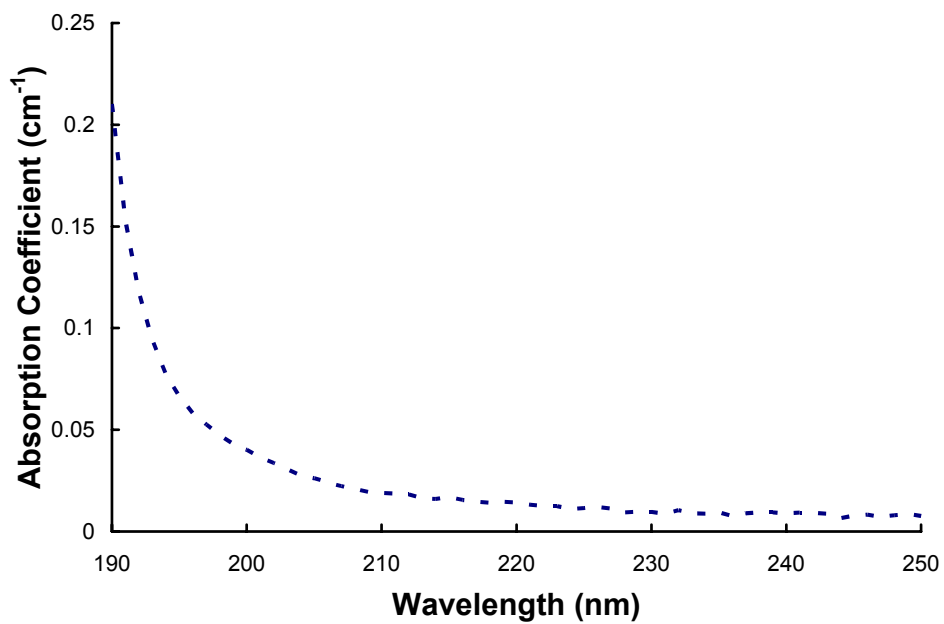


Figure 4.6 Absorption coefficient of water vs. wavelength.

In addition to the optical properties of the fluids, the viscosities and contact angles were measured. The kinematic viscosity was measured according to ASTM Standard D 446 using Cannon-Fenske viscometers of sizes 25, 75 and 150. Fluids of known viscosity were measured first to confirm the validity of the viscometer constants reported in the ASTM standard. Contact angle measurements were made on a Ramé-Hart Inc. NRL C.A. goniometer. Pre-cleaned glass slides from Fisher Scientific (Fairlawn, NJ) were used as the substrate after an isopropyl alcohol rinse.

HPLC grade water obtained from EMD Chemicals, Inc. (Gibbstown, NJ) was used as the primary fluid for the high index fluids experimentation. Alkali metal, ammonium and tetramethylammonium halide and acetate salts and acids were obtained from Fisher Scientific and Sigma-Aldrich Co. (St. Louis, MO). Solutions of 2 M concentrations were made in aliquots of 10 mL or 25 mL and diluted as needed. Quaternary ammonium salts were obtained from SACHEM, Inc. (Austin, TX) either in solution and tested as received or as hydroxide solutions that were neutralized with glacial acetic acid, also obtained from Fisher Scientific. Methylsulfonate salt solutions were also prepared at SACHEM by neutralization of methanesulfonic acid with a metal hydroxide solution containing the desired cation.

4.3 SURVEY OF IONIC ADDITIVES

The refractive index was first measured for several solutions of sodium chloride of varying concentrations to identify an appropriate concentration for the comparison of different species. Figure 4.7 shows that as the concentration of the ionic additive was

increased, the index of refraction tended to increase. However, the index values of the low concentration solutions were equivalent to that of water to within the experimental error of the measurements. These results are consistent with mixing rules for the index of refraction, such as the Lorentz – Lorenz Equation,²⁹

$$\frac{n_{12}^2 - 1}{n_{12}^2 + 2} = \phi_1 \frac{n_1^2 - 1}{n_1^2 + 2} + \phi_2 \frac{n_2^2 - 1}{n_2^2 + 2} \quad (4.10)$$

where n_{12} , n_1 and n_2 are the refractive indices of the solution, solvent and solute, respectively and ϕ_i is the volume fraction. This equation predicts only a small difference between the solution index and that of water for low additive concentrations. Therefore, a 2 M concentration of additive was chosen for the analysis and comparison of the solutions so that the index values would be significantly different from that of water.

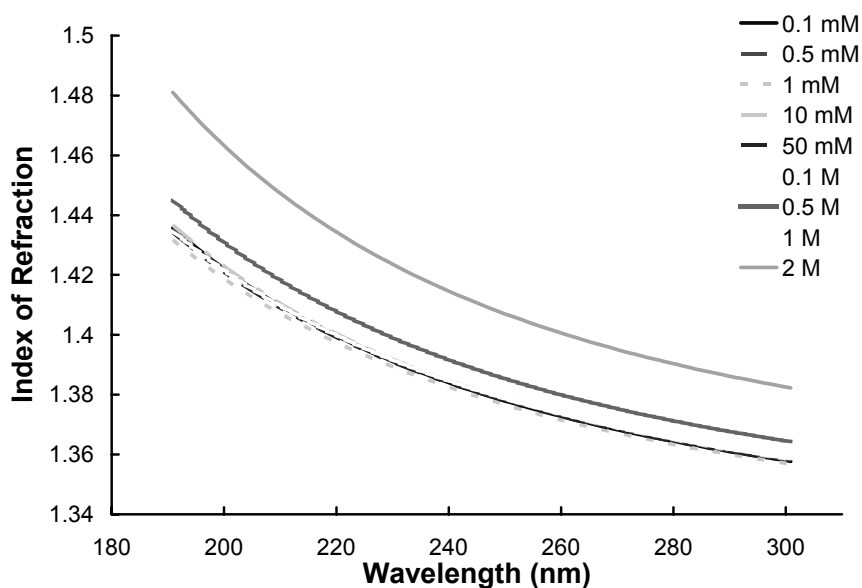


Figure 4.7 Refractive index dispersion curves for sodium chloride solutions of different concentrations.

It has been noted that the convention of using volume fraction in the mixing rules for optical properties is not intuitive. Its use apparently arose due to a concept called the refractivity, or specific refraction, in which an expression involving a material's refractive index is normalized by its density to produce a constant quantity. A combination of empirical and theoretical results led to the following quantity as the preferred expression of refractivity,

$$\frac{1}{\rho} \frac{n^2 - 1}{n^2 + 2} = \text{const.} \quad (4.11)$$

and is credited to H. A. Lorentz and L. Lorenz. It is analogous to an expression for the dielectric function derived by Clausius and Mossotti for low frequencies. Since Equation 4.11 was taken to be true under most conditions, it followed that it should hold for a mixture and that the mixture's refractivity should be determined by the constituent refractivities and their mass fractions.³⁰ Eventually, the density and mass fraction terms were combined and expressed as volume fraction, as in Equation 4.10, to more conveniently address systems where volume additivity does not hold.

The first series of ionic additives tested were chloride salts. Figure 4.8 shows the dispersion curves for the refractive indices of 2 M solutions of lithium, sodium, potassium, rubidium, cesium, ammonium (NH₄) and tetramethylammonium (TMA) chloride. These dispersion curves were grouped closely together and had similar curvature. At 193 nm, the indices ranged from $n = 1.47 - 1.50$. Figure 4.9 shows the dispersion curves for 2 M solutions of bromide salts of the same series of cations. Again, the dispersion curves were grouped together and had similar curvature. The index values

at 193 nm were higher than those of the corresponding chloride solutions and ranged from $n = 1.52 - 1.55$. The dispersion curves of 2 M acetate salts are shown in Figure 4.10. The curvatures were again similar, but they were not grouped as tightly as those for the chloride and bromide solutions. The index values at 193 nm spanned a slightly wider range as well, with $n = 1.47 - 1.52$. The index value for each 2 M solution of chloride, bromide and acetate salt at 193 nm is shown in Figure 4.11. Based on the results in Figures 4.8 through 4.11, varying the cation of the additive has a small effect on the value of the solution's refractive index. An increase in the index values of the solutions with increasing atomic radius was observed for monatomic cations. Early screening of Group I metal-halogen salts showed that fluoride-containing salts had essentially no effect on the index values at 193 nm and that iodide salts had absorption peaks above 193 nm, so they were not included as part of the main survey.

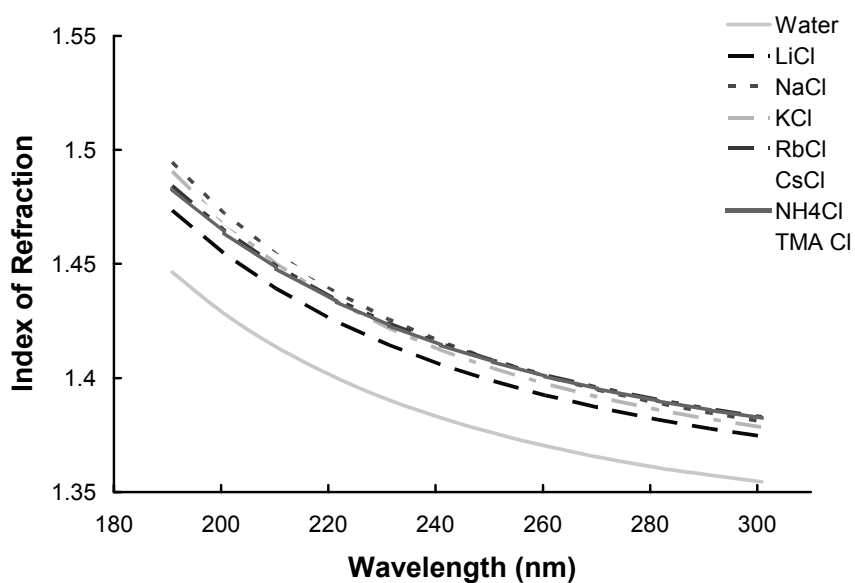


Figure 4.8 Dispersion curves for refractive indices of 2 M chloride salt solutions.

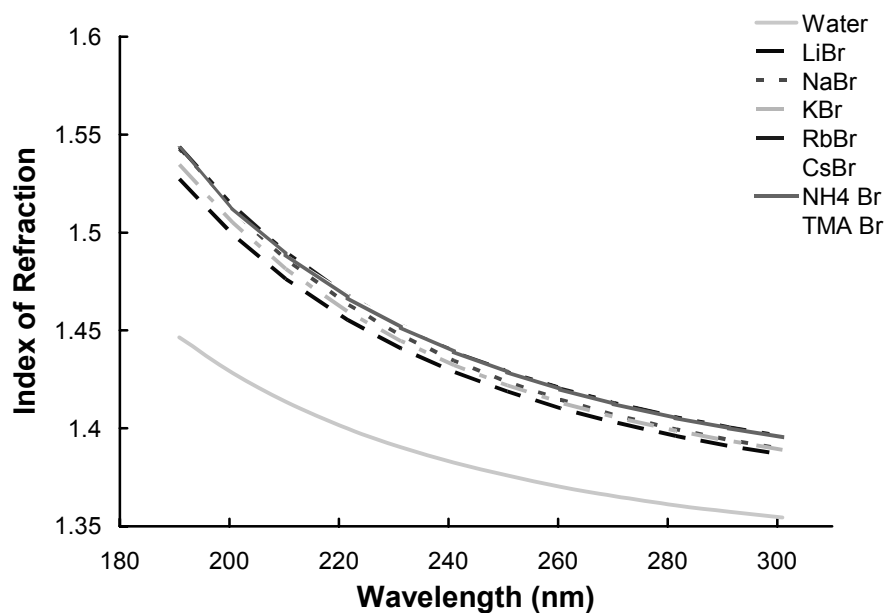


Figure 4.9 Dispersion curves for refractive indices of 2 M bromide salt solutions.

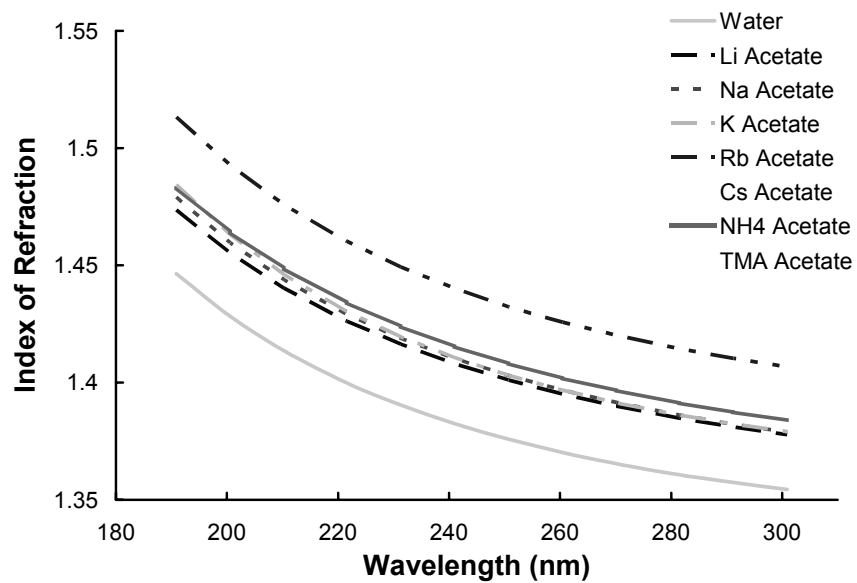


Figure 4.10 Dispersion curves for refractive indices of 2 M acetate salt solutions.

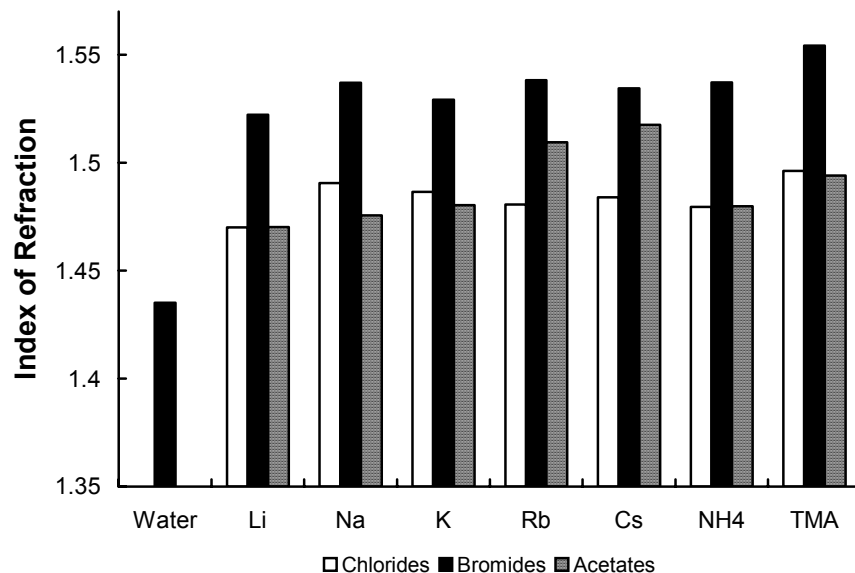


Figure 4.11 Refractive index values of 2 M chloride, bromide and acetate salt solutions vs. cation at 193 nm.

The previous results suggested that an additive's anion had a more pronounced effect on the solution's refractive index than the cation did. To further investigate the effect of the anions, two addition series of solutions were tested. First, 2 M solutions of hydrochloric, nitric, sulfuric and phosphoric acid were compared. Figure 4.12 shows that the dispersion curves were grouped closely together at wavelengths down to 260 nm and began to deviate from each other after. The refractive indices of a series of sodium salts with complex anions were then measured, Figure 4.13. Sodium thiocyanate (SCN⁻), sodium thiosulfate (S₂O₃²⁻) and sodium sulfite solutions had the highest index values, all above $n = 1.5$. The solutions of sodium bisulfate (HSO₄⁻) and sodium perchlorate (ClO₄⁻) had the lowest index values, similar to those of sulfuric and phosphoric acid. The index values of the acid solutions at 193 nm ranged from $n = 1.46 - 1.49$ and the values for the

sodium solutions were $n = 1.45 - 1.55$, Figures 4.14 and 4.15. The wider range of index values indicated that the anions in these solutions had a stronger influence on the refractive index than the cations.

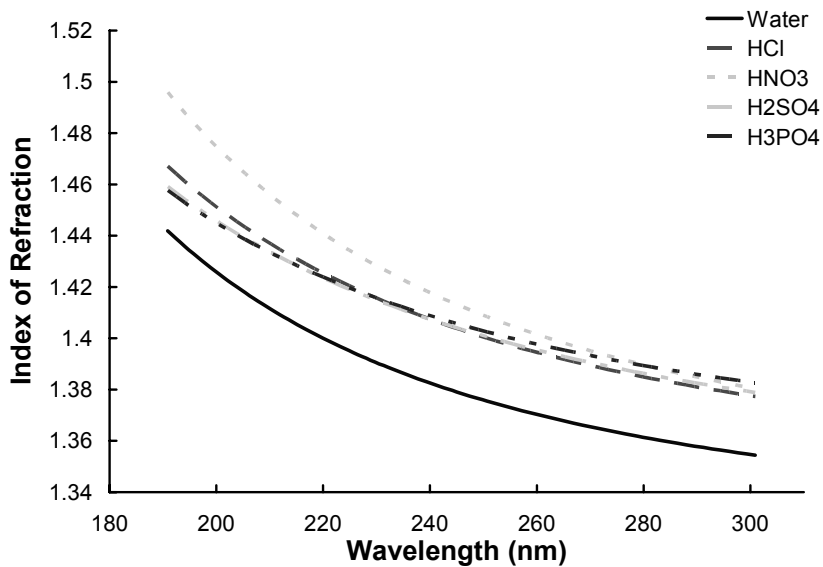


Figure 4.12 Dispersion curves for refractive indices of 2 M acid solutions.

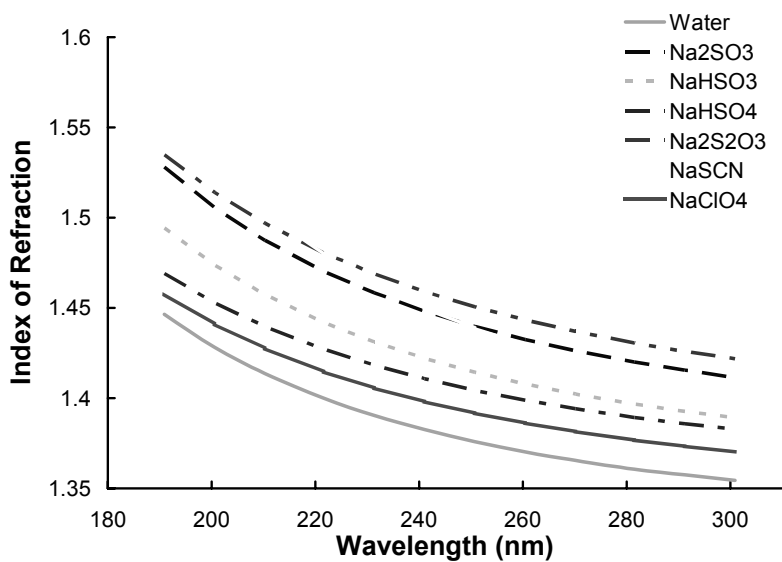


Figure 4.13 Dispersion curves for refractive indices of 2 M sodium salt solutions.

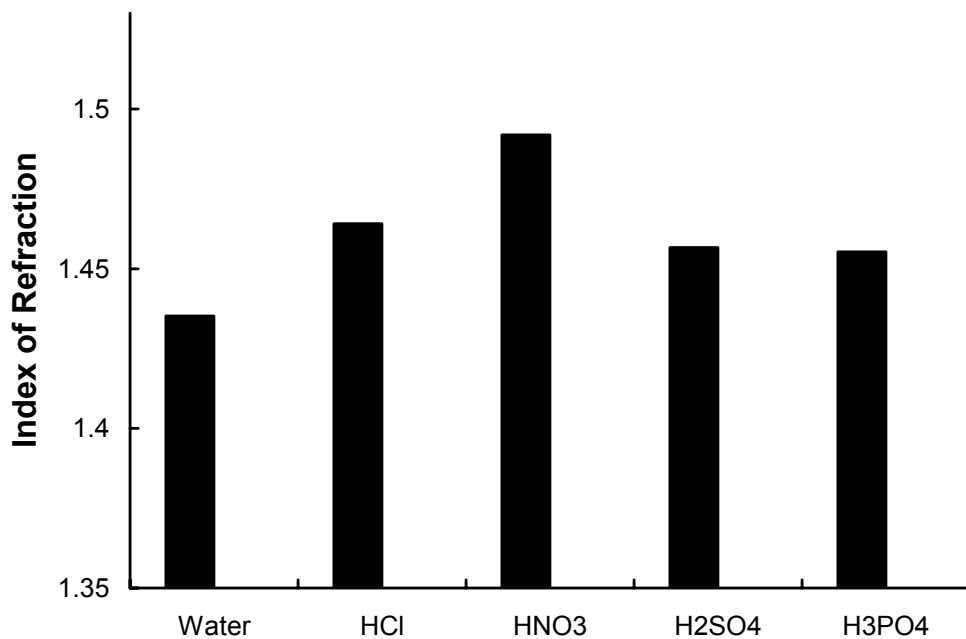


Figure 4.14 Refractive index values of 2 M acid solutions vs. anion at 193 nm.

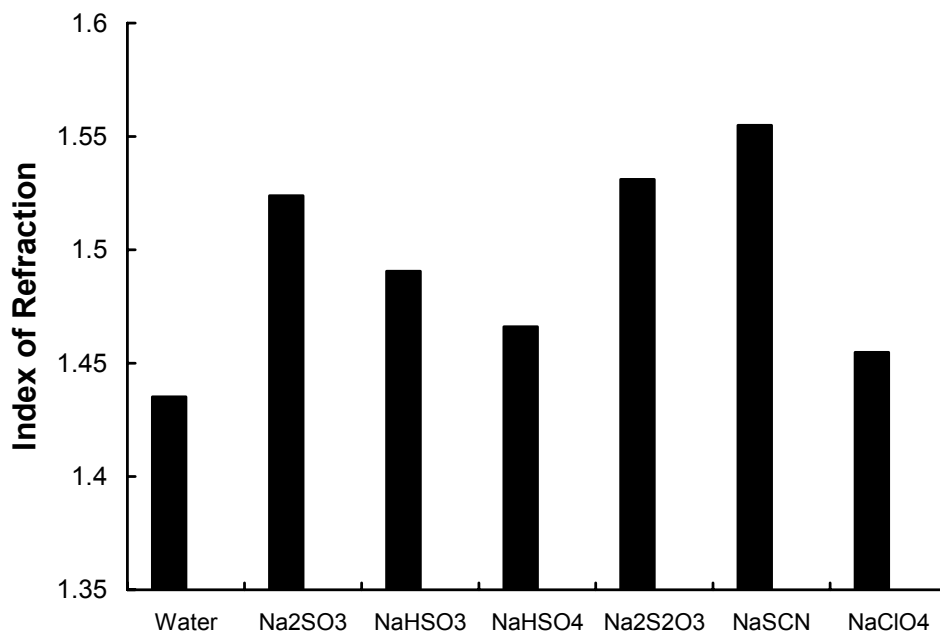


Figure 4.15 Refractive index values of 2 M sodium salt solutions vs. anion at 193 nm.

Once the refractive indices of these ionic solutions were determined, their absorbance values were then measured and compared. First, the sodium chloride solutions of different concentrations were used to determine an appropriate concentration range for absorbance measurements. Figure 4.16 shows the absorption spectra of NaCl solutions with concentrations from 0.1 mM – 2 M. In contrast to the refractive index measurements, the absorption coefficient was very sensitive to concentration, and above 1 mM these solutions were too opaque to obtain a measurement at 193 nm. Therefore, a concentration of 1 mM was initially chosen for the absorbance measurements of the ionic solutions; however, the concentrations of the bromide salt, acid and sodium salt solutions had to be further reduced to 0.1 mM to obtain reasonable measurements.

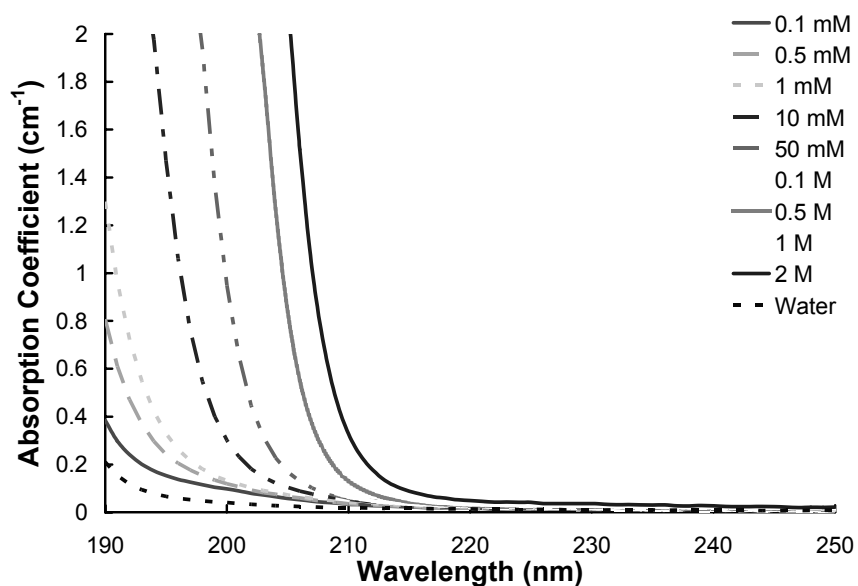


Figure 4.16 Absorption spectra of sodium chloride solutions of different concentration vs. wavelength.

The absorption spectra for 1 mM chloride salt solutions are shown in Figure 4.17. As was seen for refractive index dispersion curves, the absorption coefficient curves for each solution were grouped tightly together and had similar curvature. This behavior was also observed for the bromide and acetate salt solutions, Figures 4.18 and 4.19. The absorption coefficients values for these solutions at 193 nm are given in Figure 4.20. The chloride salt solutions had absorption coefficient values in the range of $\alpha = 0.4 - 0.5 \text{ cm}^{-1}$, for the bromide series $\alpha = 1.3 - 1.4 \text{ cm}^{-1}$, and for the acetate salts $\alpha = 0.6 - 0.8 \text{ cm}^{-1}$, which correspond to transmittances of approximately 35%, 5% and 20%, respectively. Similar to the effect on the index, varying the cation in all three of these series increased the absorption coefficient values slightly with increasing cation atomic radius. Additionally, the anion dictated the overall shape and strength of the absorption spectra.

The solutions with the complex cations NH_4^+ and TMA^+ behaved similarly to those with the larger monatomic cations.

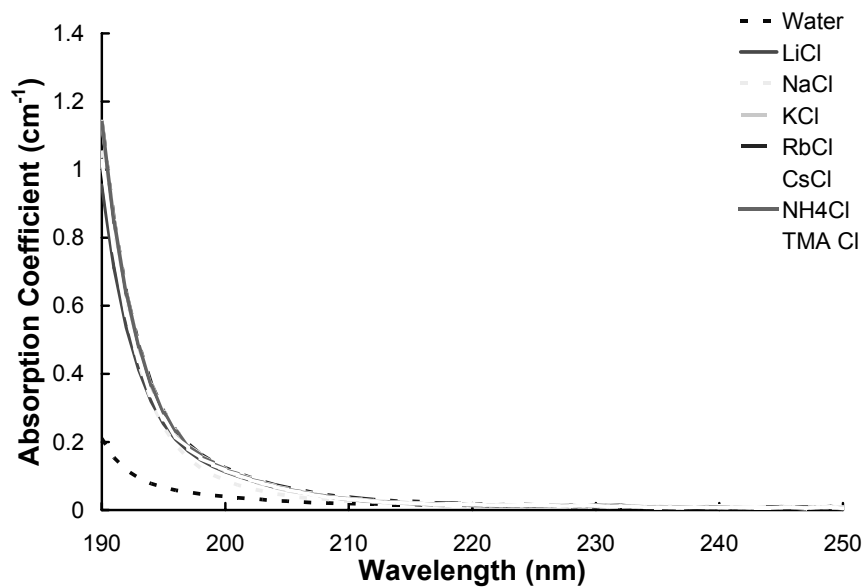


Figure 4.17 Absorption spectra of 1 mM chloride salt solutions.

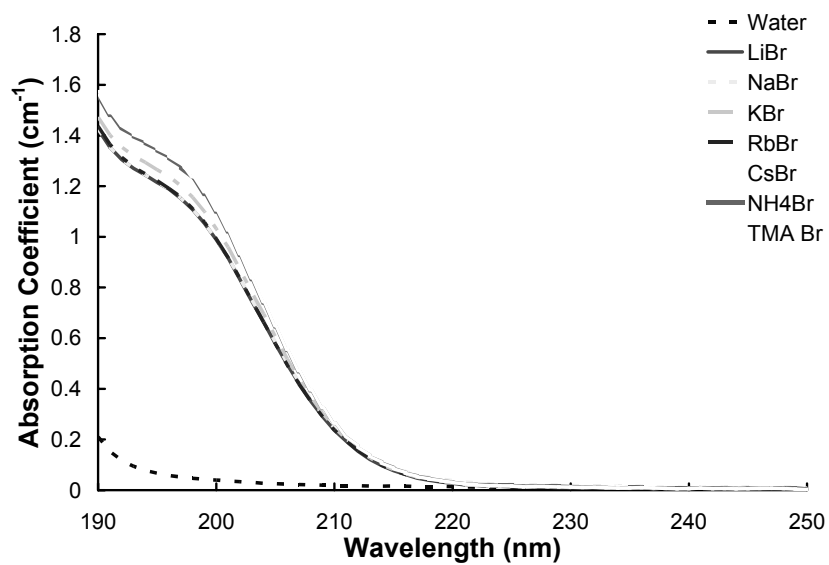


Figure 4.18 Absorption spectra of 0.1 mM bromide salt solutions.

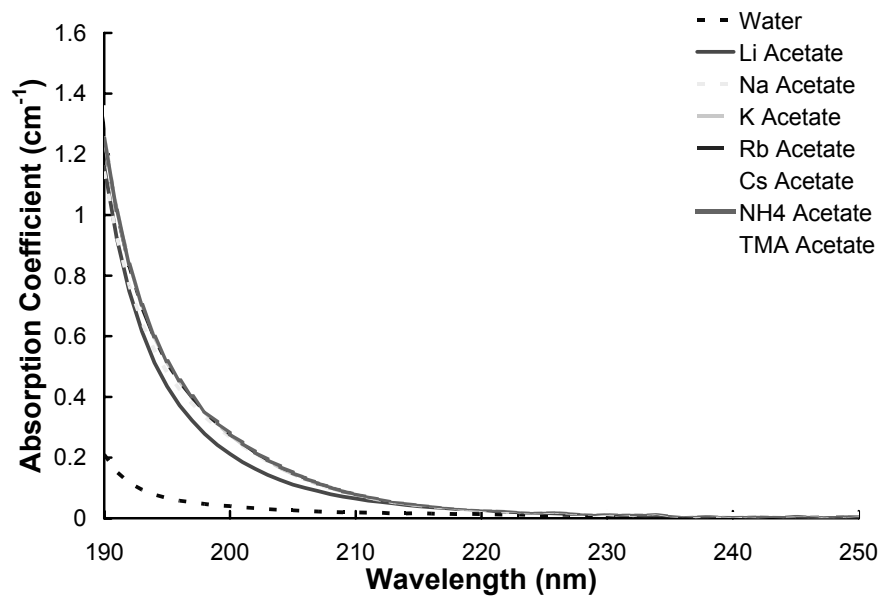


Figure 4.19 Absorption spectra of 1 mM acetate salt solutions.

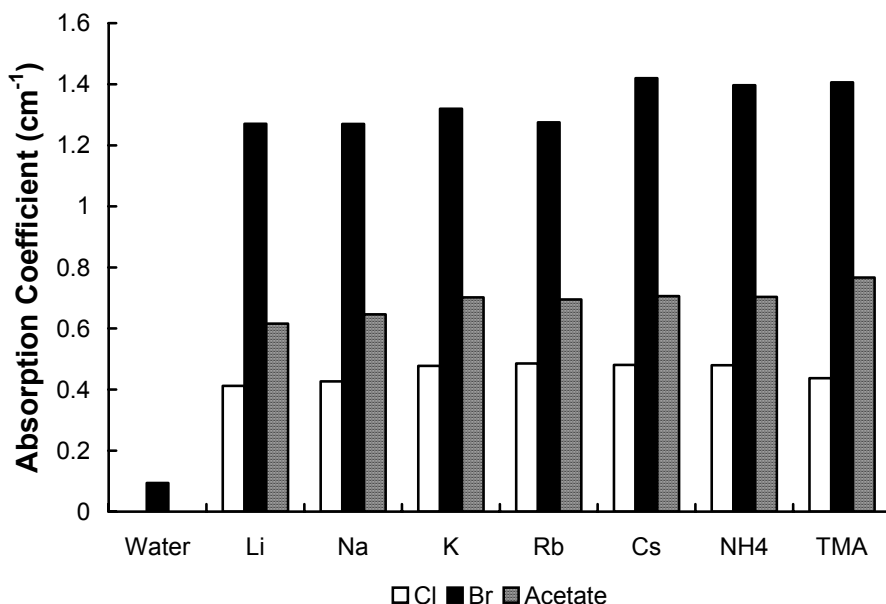


Figure 4.20 Absorption coefficients of 1 mM chloride, 0.1 mM bromide and 1 mM acetate salt solutions at 193 nm vs. cation.

The effect of the additive's anion was again investigated by measuring the absorption spectra of the acid and sodium salt solutions. The absorption spectra for the acids at 0.1 mM concentration are shown in Figure 4.21. Figure 4.22 shows the spectra for 0.1 mM sodium salts. Again, the dispersion curves had different shapes and were not grouped tightly together. The absorption spectra of the nitric acid, sodium thiosulfate and sodium thiocyanate solutions had peaks in the wavelength range over which the measurements were taken and the absorption coefficients were larger than those of the other solutions, at 193 nm $\alpha = 0.8 - 1.3 \text{ cm}^{-1}$, Figures 4.23 and 4.24. The spectra of the sulfuric acid, phosphoric acid, sodium bisulfate and sodium perchlorate solutions were very similar to each other and had almost identical absorption coefficient values at 193

nm, approximately $\alpha = 0.2 \text{ cm}^{-1}$. The absorption coefficient values of the sodium sulfite and bisulfite solutions were slightly higher at $\alpha = 0.3 \text{ cm}^{-1}$ and 0.4 cm^{-1} , respectively. From Figures 4.17 – 4.24, the anion of the ionic additive had a much stronger influence on the absorption spectra of the solutions than did the cation. Varying the anion resulted in absorbance values corresponding to solution transmittances ranging from as high as 66% to as low as 5%, while varying the cation changed the solution transmittance by three percentage points or less. The trends observed are consistent with previous studies of the effects of different ions on the absorption spectra of solutions.^{31, 32}

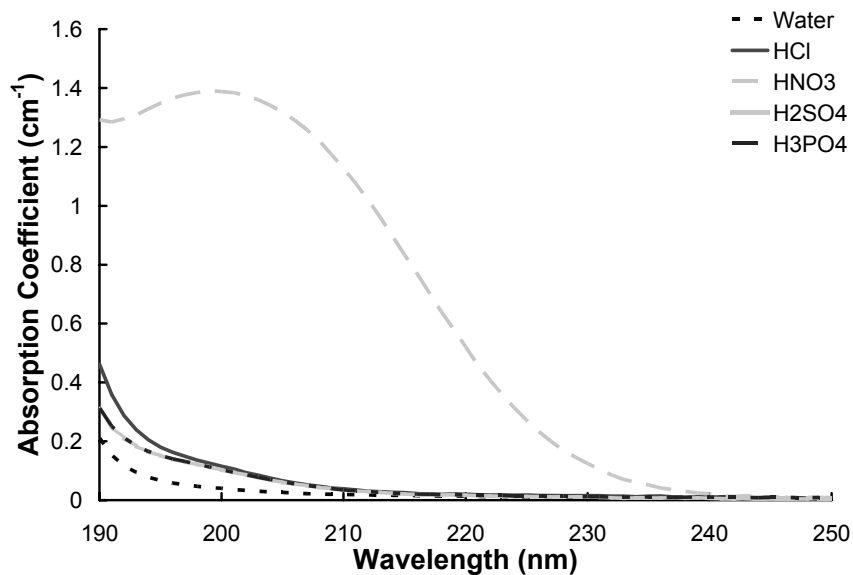


Figure 4.21 Absorption spectra of 0.1 mM acid solutions.

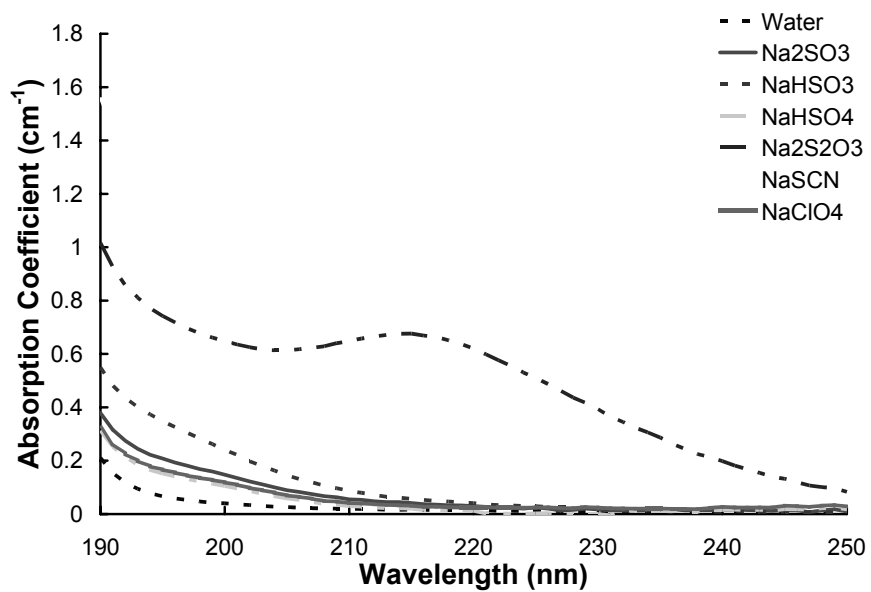


Figure 4.22 Absorption spectra of 0.1 mM sodium solutions.

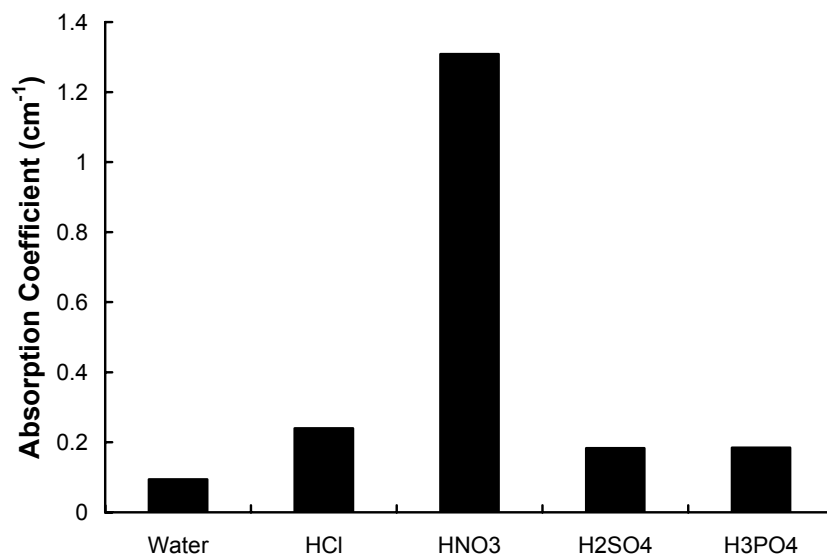


Figure 4.23 Absorption coefficients of 0.1 mM acid solutions at 193 nm vs. anion.

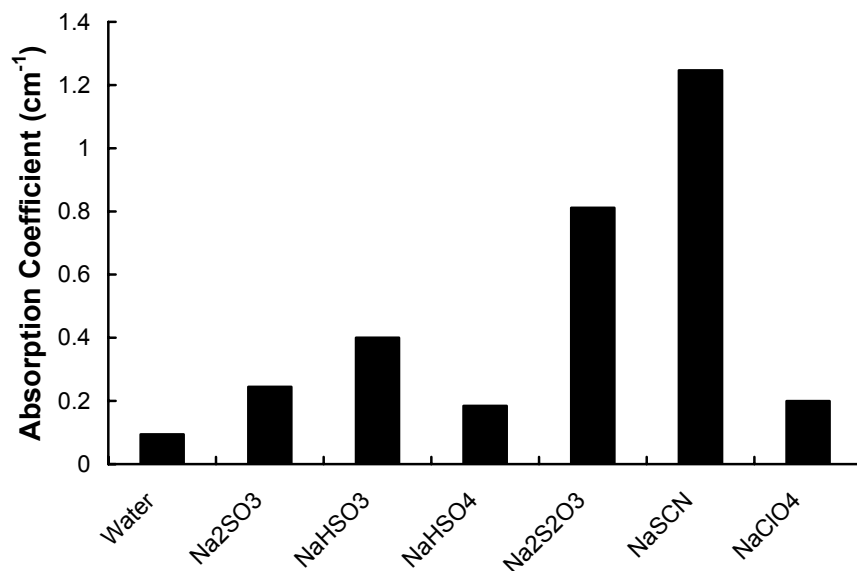


Figure 4.24 Absorption coefficients of 0.1 mM sodium salt solutions at 193 nm vs. anion.

Once the optical properties of the solutions were determined, the kinematic viscosities (ν) and contact angles were measured. Table 4.1 shows the kinematic viscosities for HPLC grade water, the 2 M chloride, bromide, acetate and sodium salt solution series. The chloride and bromide solutions had viscosities close to that of water, while the acetates were slightly higher. All of the sodium salts with complex anions except for sodium thiocyanate were almost twice as viscous as water. For an immersion fluid, a viscosity three times that of water is acceptable.⁵ The contact angles of the same solutions are shown in Table 4.2. For most solutions, the contact angle was essentially the same as that of water, while for more complex anions the contact angle increased slightly. No specification for contact angle other than being similar to water has been reported.

Table 4.1 Kinematic viscosities of 2 M ionic solutions.

Solution (2 M)	ν (mm²/s)		Solution (2 M)	ν (mm²/s)
Water	1.05			
LiCl	1.30		LiBr	1.57
NaCl	1.14		NaBr	1.01
KCl	0.93		KBr	0.82
RbCl	0.79		RbBr	0.74
CsCl	0.72		CsBr	0.68
NH ₄ Cl	0.96		NH ₄ Br	1.07
TMACl	1.55		TMABr	1.29
Na Acetate	2.26		Na ₂ SO ₃	2.57
K Acetate	1.44		NaHSO ₃	1.79
Rb Acetate	1.31		NaHSO ₄	1.76
Cs Acetate	1.16		NaS ₂ O ₃	1.93
NH ₄ Acetate	1.44		NaSCN	1.08

Table 4.2 Contact angles of 2 M ionic solutions.

Solution (2 M)	Contact Angle		Solution (2 M)	Contact Angle
Water	36 ± 5°			
LiCl	40°		Li Acetate	34°
NaCl	35°		Na Acetate	37°
KCl	40°		K Acetate	36°
RbCl	49°		Rb Acetate	35°
CsCl	38°		Cs Acetate	40°
NH ₄ Cl	42°		NH ₄ Acetate	43°
TMA Cl	33°		TMA Acetate	38°
NaBr	38°		Na ₂ SO ₃	46°
KBr	36°		NaHSO ₃	43°
RbBr	36°		NaHSO ₄	44°
CsBr	34°		NaS ₂ O ₃	52°
TMA Br	30°		NaSCN	39°

4.3 DEVELOPMENT OF ADDITIVE FOR AQUEOUS 2ND GENERATION IMMERSION FLUID

An aqueous solution of an ionic additive for a second generation immersion fluid must not only meet the stated requirements, but must also be compatible with semiconductor processing environment. The ionic compounds surveyed above resulted in solutions with refractive indices significantly higher than that of water, but would require concentrations greater than 2 M to achieve the target of $n = 1.65$. Yet even at concentrations of 0.1 mM, nearly all of these solutions were too strongly absorbing to be viable immersion fluids. In addition to failing to meet the optical property requirements, the metal salts would be prohibited in a fabrication facility. However, salts containing the tetramethylammonium cation would be compatible with semiconductor processing, as evidenced by the use of tetramethylammonium hydroxide as the standard photoresist developer in lithography processes. Therefore, the scope of the survey was narrowed to additives with quaternary ammonium cations.

First, samples of different quaternary ammonium salt solutions including TMA, methyltriethylammonium (MtEA), tetrapropylammonium (TPA) and tetrabutylammonium (TBA) acetate were obtained from SACHEM, Inc., and the refractive indices were measured. The solutions were obtained at different concentrations, so index data were measured and then adjusted using Equation 4.10 to represent 5 mole % solutions of each cation, Figure 4.25. The index values at 193 nm are shown in Figure 4.26. The absorption spectra and absorption coefficient values at 193 nm for solutions diluted to 1 mM are shown in Figures 4.27 and 4.28. The dispersion curves were similar to those of the previously measured acetate salts. However, there

was a trend of increases in both index and absorbance with increasing size of the quaternary ammonium cation.

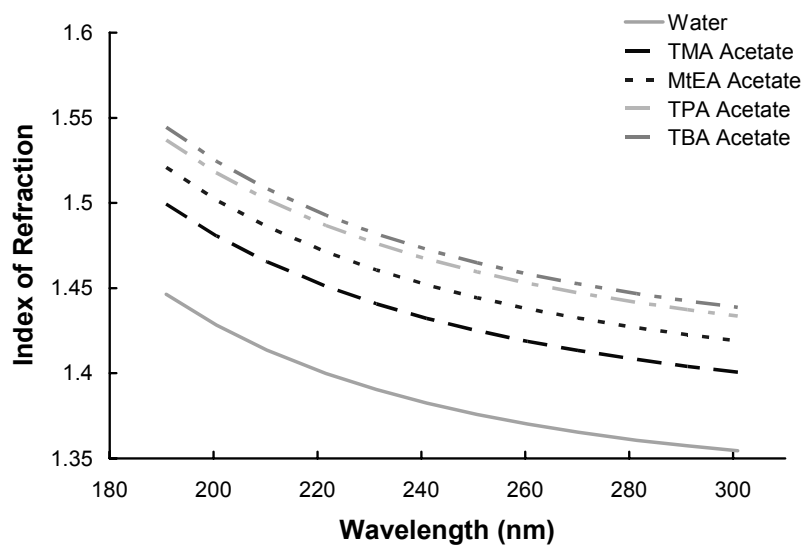


Figure 4.25 Dispersion curves for refractive indices of 5 mol% quaternary ammonium acetate salt solutions.

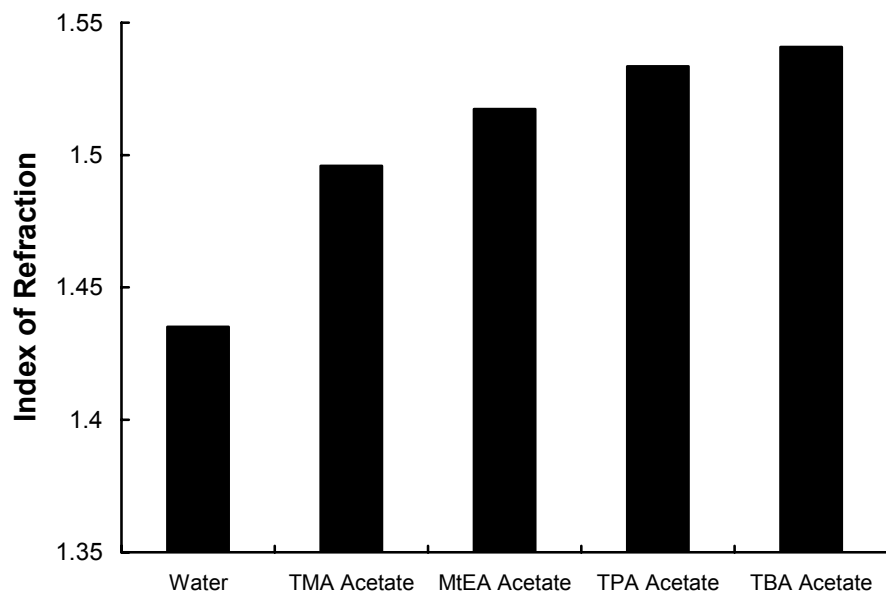


Figure 4.26 Index values of 5 mol% quaternary ammonium acetate salt solutions at 193 nm vs. cation.

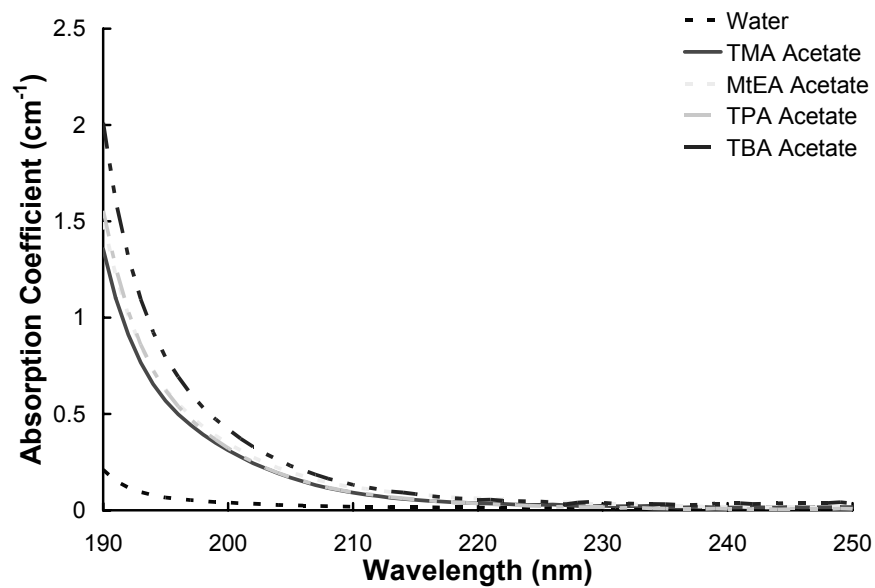


Figure 4.27 Absorption spectra of 1 mM quaternary ammonium acetate salt solutions.

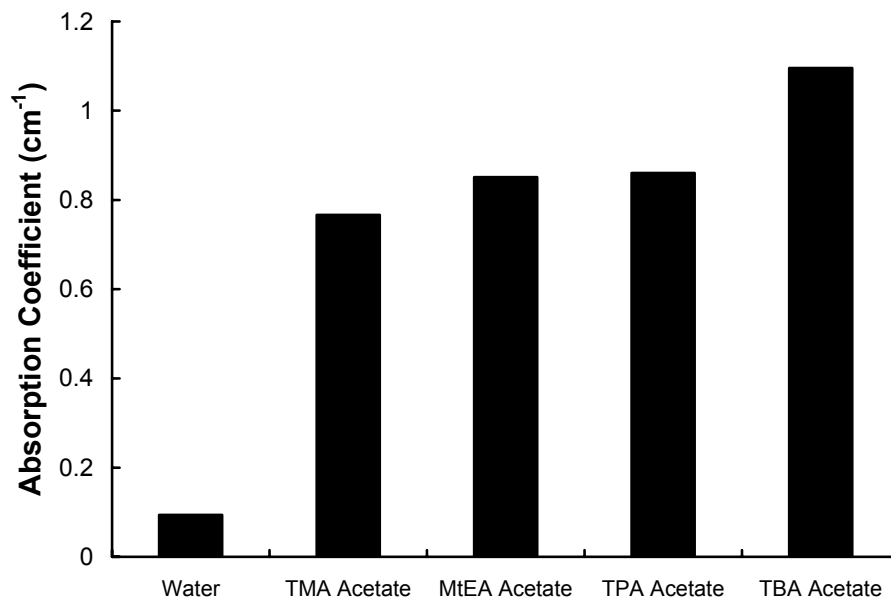


Figure 4.28 Absorption coefficient values of 1 mM quaternary ammonium acetate salt solutions at 193 nm vs. cation.

The refractive indices for several additional quaternary ammonium salt solutions were also measured, Figures 4.29 and 4.30. The kinematic viscosities and contact angles of all of these solutions were then measured, Tables 4.3 and 4.4; note that a tetraethylammonium (TEA) acetate solution was tested in place of the MtEA acetate. The viscosities of the quaternary ammonium salt solutions were found to be higher than that of water, with the solutions becoming more viscous as the alkyl chain length on the cation increased. The contact angles were also seen to decrease with increasing alkyl chain length. The index data suggested that larger alkyl chains on the cation would be beneficial, and the absorption data seemed to confirm this trend as there were only

modest increases in α . However, the increases in viscosity for all but the TMA cation were greater than the 3x criterion for a 2nd generation fluid.

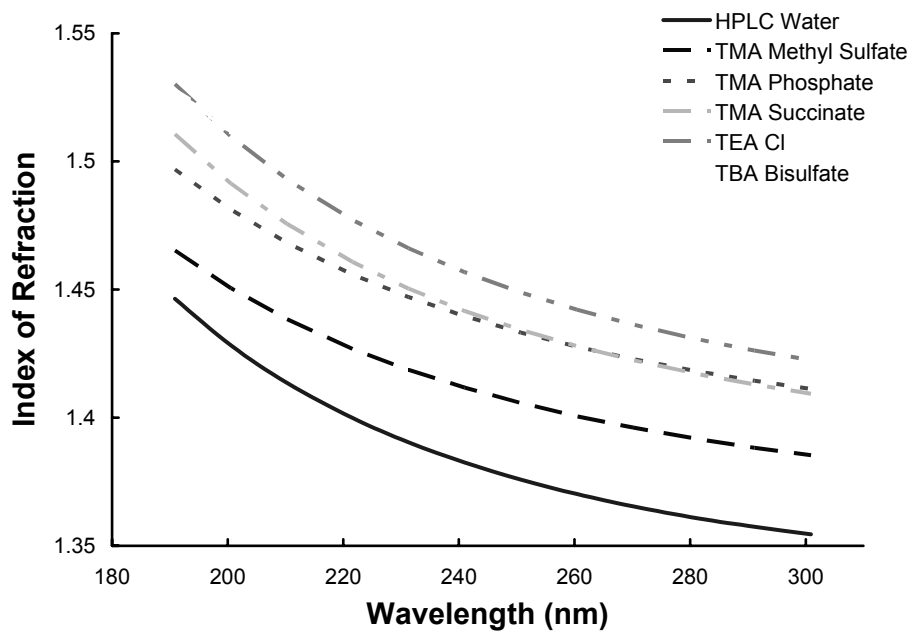


Figure 4.29 Dispersion curves for refractive indices of additional 5 mol% quaternary ammonium salt solutions.

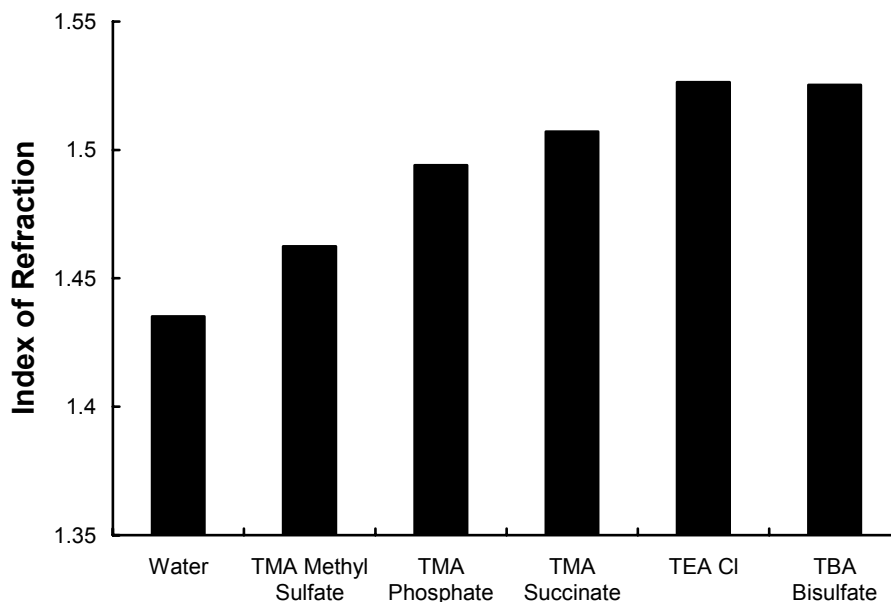


Figure 4.30 Index values of 5 mol% quaternary ammonium salt solutions at 193 nm.

Table 4.3 Kinematic viscosities of quaternary ammonium salt solutions.

Solution (2 M)	ν (mm ² /s)	Solution (2 M)	ν (mm ² /s)
Water	1.05		
2.35 M TMA Acetate	3.09	2 M TMA Methyl Sulfate	1.68
2.08 M TEA Acetate	6.70	1.36 M TMA Phosphate	3.67
1.76 M TPA Acetate	21.1	50 wt% TEA Cl	9.70
1.9 M TBA Acetate	20.9	55 wt% TBA Bisulfate	18.6

Table 4.4 Contact angles of quaternary ammonium salt solutions.

Solution (2 M)	Contact Angle	Solution (2 M)	Contact Angle
Water	36°		
2.35 M TMA Acetate	43°	2 M TMA Methyl Sulfate	39°
2.08 M TEA Acetate	33°	1.36 M TMA Phosphate	34°
1.76 M TPA Acetate	24°	50 wt% TEA Cl	44°
1.9 M TBA Acetate	19°	55 wt% TBA Bisulfate	21°

Based on the data presented above and a screening of the absorption of some additional acids, researchers from SACHEM, Inc. prepared solutions of additives with a methylsulfonate anion for characterization. At a 2 M concentration, methanesulfonic acid was found to have an index value at 193 nm just above water, $n = 1.46$, but an absorption coefficient of only $\alpha = 0.4 \text{ cm}^{-1}$. For comparison, sulfuric acid at the same concentration was found to have an absorption coefficient of above $\alpha = 2 \text{ cm}^{-1}$. To test the potential of the methylsulfonate anion, the first solutions were prepared with large, monatomic cations. These solutions included 2 M cesium, barium and lanthanum methylsulfonate. The increasing oxidation states of these cations enabled larger concentrations of the anion to be achieved at the same overall salt concentrations. This resulted in a significant increase in the refractive index from one solution to the next. For a saturated (approximately 2.82 M) solution of lanthanum methylsulfonate, an index of $n = 1.58$ was achieved, Figures 4.31 and 4.32. The absorption coefficients were also measured, with the unexpected result that the absorption of the barium and lanthanum solutions was less than that of the cesium solution, Figures 4.33 and 4.34. Impurities resulting from the synthesis of the solutions were suspected of contributing to the high absorption coefficient of the cesium solution, so additional purification steps were taken in the development of the barium and lanthanum solutions. The high purity of the saturated lanthanum methylsulfonate solution resulted in an absorption coefficient less than that measured for the acid, $\alpha = 0.3 \text{ cm}^{-1}$. The surface tensions of these solutions were measured with a pendant drop technique, and the viscosities measured with a cone-and-plate geometry on a Paar Physica rheometer, Table 4.5. The surface tensions were

found to be significantly less than that of water, and the viscosities of the solutions containing lanthanum were over an order of magnitude higher than that of water.

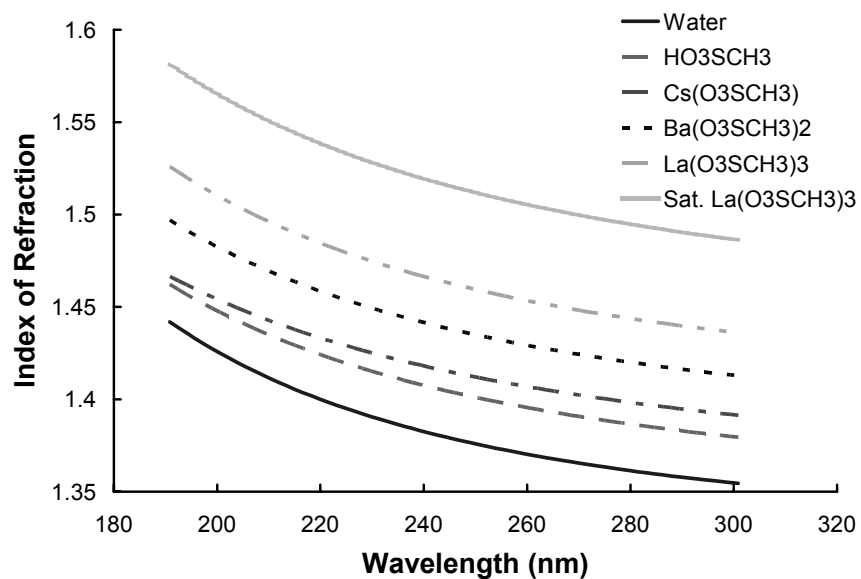


Figure 4.31 Refractive index dispersion curves for 2 M methylsulfonate salt solutions.

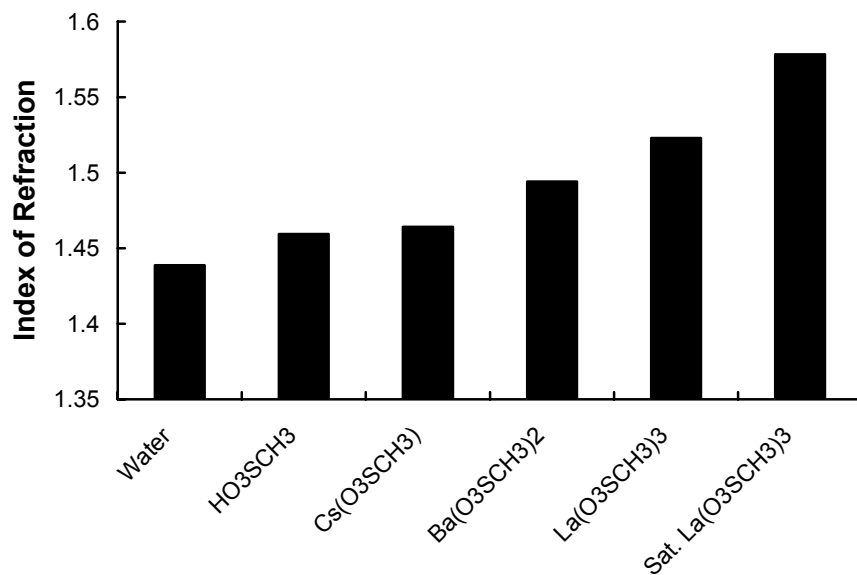


Figure 4.32 Index values of 2 M methylsulfonate salt solutions at 193 nm vs. cation.

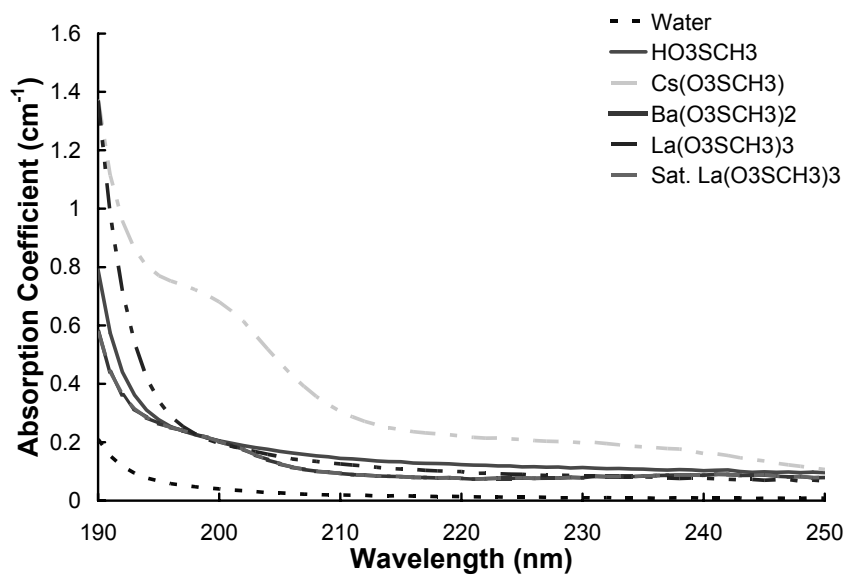


Figure 4.33 Absorption spectra for 2 M methylsulfonate salt solutions.

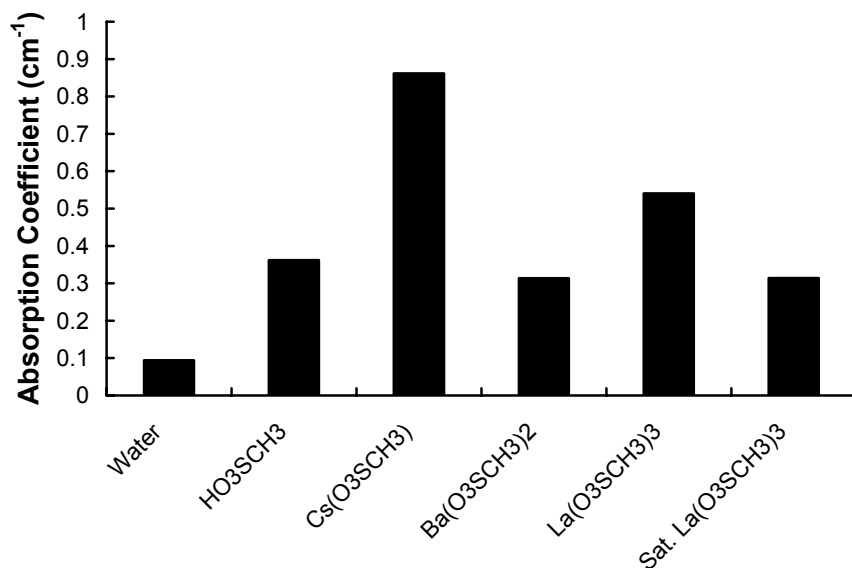


Figure 4.34 Absorption coefficients of 2 M methylsulfonate salt solutions at 193 nm vs. cation.

Table 4.5 Surface tension and viscosity of methylsulfonate solutions.

Solution	Surface Tension (dyne/cm ²)	Viscosity (mm ² /s)
Water	72.8	
2M CH ₃ SO ₃ H	20.6	1.1
2M Cs(O ₃ SCH ₃)	24.2	0.9
2M Ba(O ₃ SCH ₃) ₂	23.7	1.8
2M La(O ₃ SCH ₃) ₃	28.8	30.4
2.82M La(O ₃ SCH ₃) ₃	28.2	55.6

A second generation of the methylsulfonate solutions was prepared with quaternary ammonium cations in place of the metals. The index values for these saturated solutions were slightly less than that of the saturated lanthanum methylsulfonate solution, $n = 1.55 - 1.56$, Figures 4.35 – 4.36. The absorption coefficients were found to

be higher, $\alpha = 0.5 - 0.9 \text{ cm}^{-1}$, Figures 4.37 – 4.38. The surface tension and viscosity values for these solutions are given in Table 4.6. For these solutions, the surface tension was still lower than that of water and the viscosities were higher, but the values were closer to those of water than for the metal containing solutions. The metal containing methylsulfonate solutions were used in an interferometric imaging system at the Rochester Institute of Technology to generate images of a 65 nm half-pitch line and space pattern, Figure 4.39.³³ Using the saturated lanthanum methylsulfonate solution, 45 nm, 34.5 nm and 32 nm half-pitch images were achieved, Figure 4.40. Using a quaternary ammonium methylsulfonate salt solution, initial imaging of a 34.5 nm line and space pattern was performed, Figure 4.41.

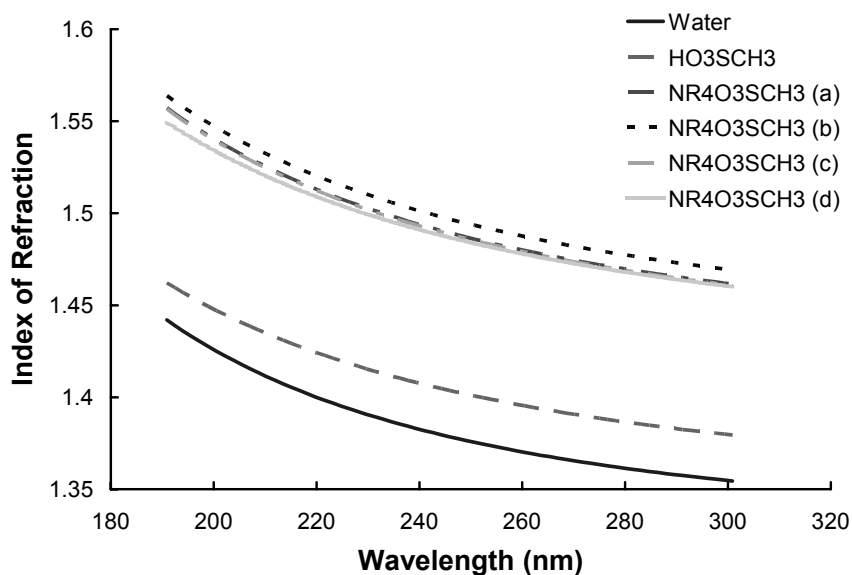


Figure 4.35 Refractive index dispersion curves for saturated quaternary ammonium methylsulfonate salt solutions, where R = H or alkyl chain.

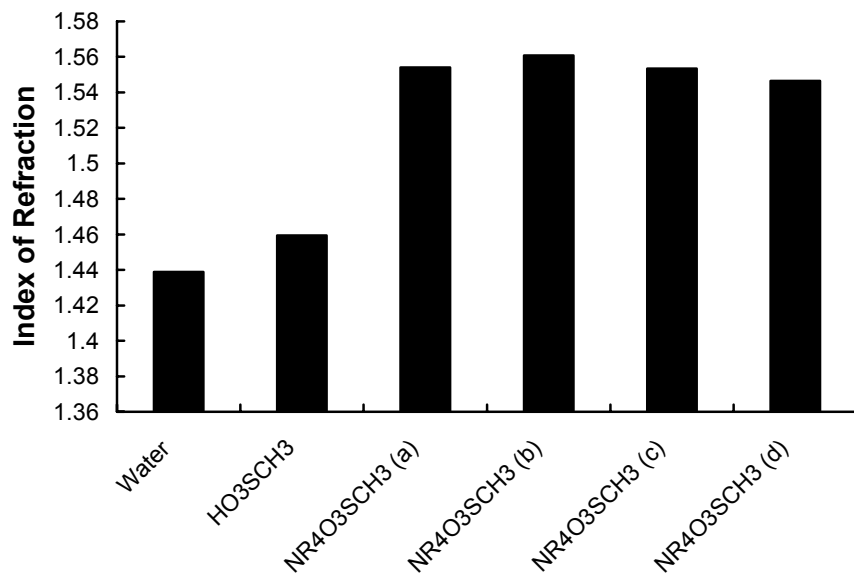


Figure 4.36 Index values of saturated quaternary ammonium methylsulfonate salt solutions at 193 nm, where R = H or alkyl chain.

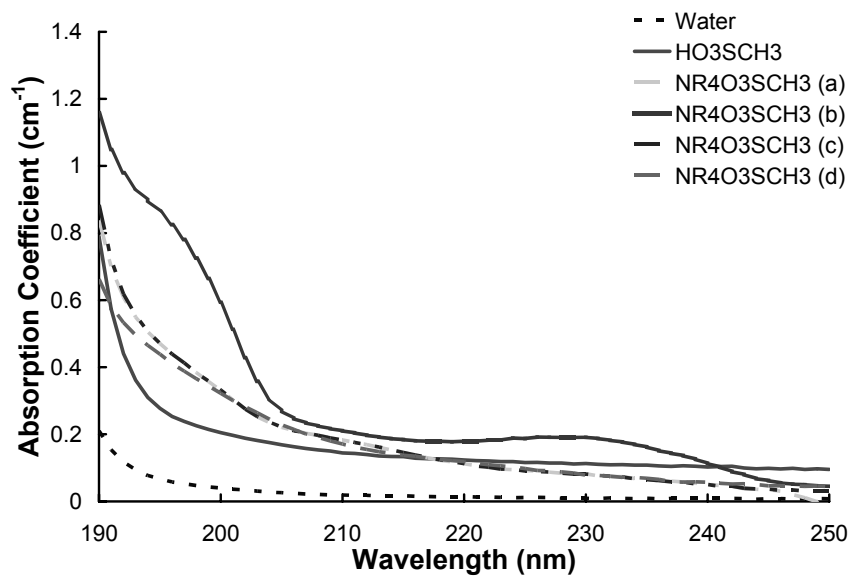


Figure 4.37 Absorption spectra for saturated quaternary ammonium methylsulfonate salt solutions, where R = H or alkyl chain.

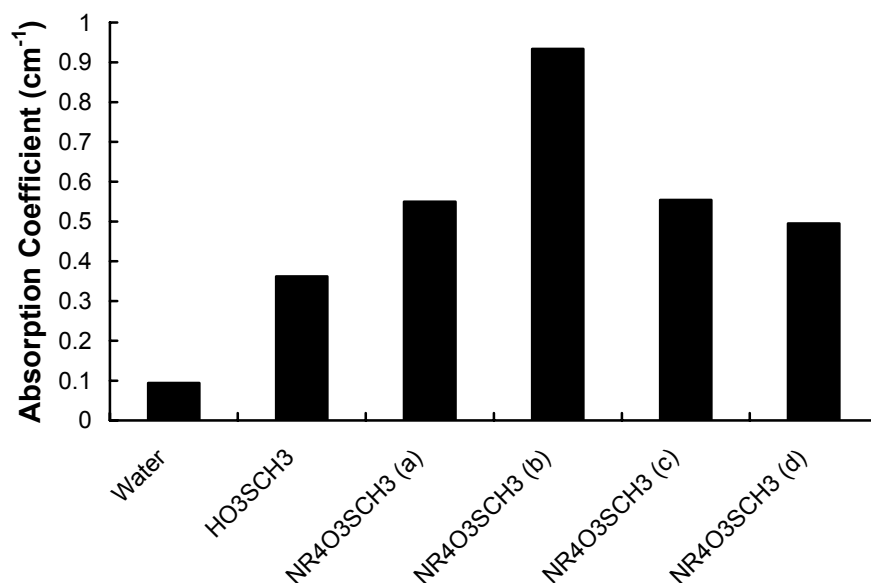


Figure 4.38 Absorption coefficients of saturated quaternary ammonium methylsulfonate salt solutions at 193 nm, where R = H or alkyl chain.

Table 4.6 Surface tension and viscosity of methylsulfonate solutions.

Solution	Surface Tension (dyne/cm ²)	Viscosity (mm ² /s)
Water	72.8	
NR ₄ O ₃ SCH ₃ (a)	40.1	6.5
NR ₄ O ₃ SCH ₃ (b)	38.7	7.9
NR ₄ O ₃ SCH ₃ (c)	37.2	7.3
NR ₄ O ₃ SCH ₃ (d)	36.2	12.3

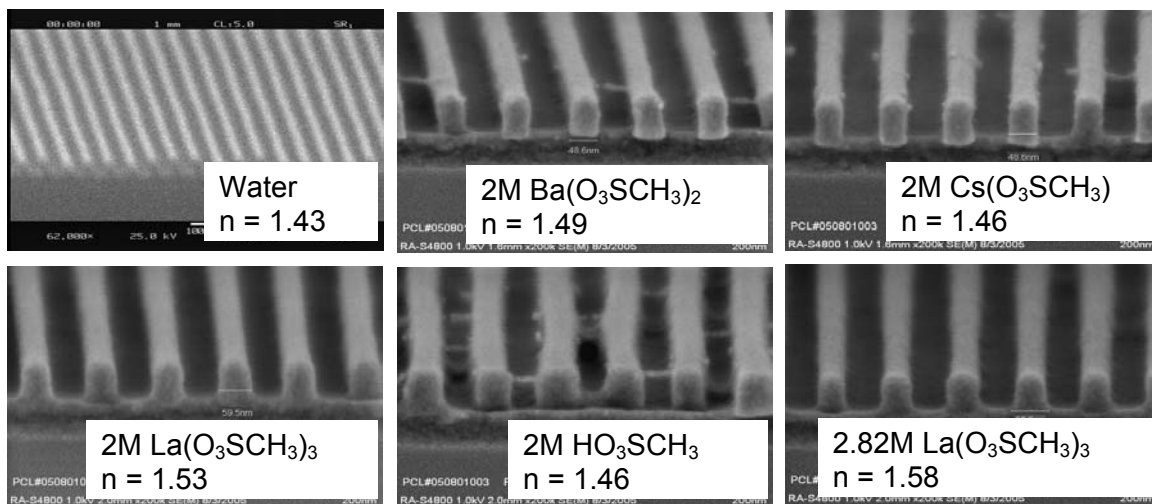


Figure 4.39 Scanning electron micrographs (SEM) of 65 nm half-pitch lines and spaces imaged with methanesulfonate solutions.

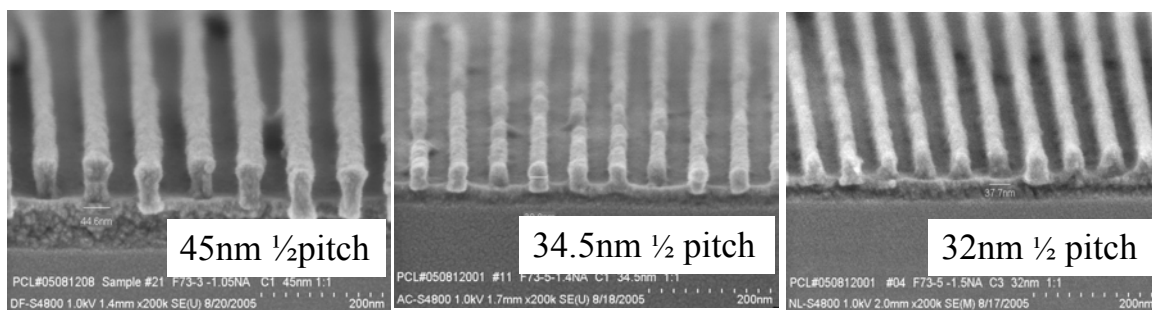


Figure 4.40 SEM micrographs of line and space patterns imaged with saturated lanthanum methanesulfonate solution.

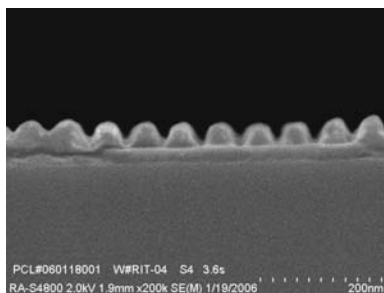


Figure 4.41 SEM micrograph of 34.5 nm half-pitch line and space pattern imaged with $\text{NR}_4\text{O}_3\text{SCH}_3$ (c).

4.5 SUMMARY

The results of the ionic additive survey showed first that the optical properties of these solutions were most significantly affected by the anion. Solutions with the same anion had similar curvature to the dispersion and small variations in the magnitude. The cation had a less significant effect, but it was seen that larger ions led to slightly higher values of the index and absorption coefficient. Complex ions showed a wider range of behavior than monatomic ones. In particular, it was noted that anions containing oxygen seemed to have lower absorption coefficients than those without. Solutions with complex ions also had larger differences in surface tension and viscosity when compared to water.

Solutions with the methylsulfonate anion were found to have high refractive index values with moderate absorption coefficients, and purification was found to reduce them. Saturated solutions of lanthanum and quaternary ammonium methylsulfonate had refractive index values of 1.56 – 1.58 at 193 nm, with absorption coefficients as low as $\alpha = 0.3 - 0.4 \text{ cm}^{-1}$. These are some of the highest refractive index values coupled with low absorption coefficients to be reported for aqueous solutions.³⁴ With these potential

immersion fluids, line and space patterns down to 32 nm half-pitch were successfully imaged with an interferometric imaging system.

While advances were made in the search for an additive for a second generation immersion fluid, the solutions tested did not meet all of the targets. At best, the solutions tested were twice as absorbing as water and showed significant differences in surface tension and viscosity. Also, further increases in refractive index are not likely since the solutions with the highest reported values were saturated. Increased purification of the solutions and the use of a different cation to improve fluid properties may result in a solution which meets most of the criteria. However, a solely empirical approach like this survey is not likely to yield an ideal additive quickly since it is time and resource intensive. Therefore, a better understanding of the nature of the refractive index and the absorption coefficient is developed in the next chapter to facilitate a more efficient search for an immersion fluid additive.

4.6 REFERENCES

1. Hoffnagle, J. A.; Hinsberg, W. D.; Sanchez, M.; Houle, F. A. "Liquid immersion deep-ultraviolet interferometric lithography." *Journal of Vacuum Science & Technology, B: Microelectronics and Nanometer Structures* **1999**, *17* (6), 3306-3309.
2. Switkes, M.; Rothschild, M. "Immersion lithography at 157 nm." *Journal of Vacuum Science & Technology, B: Microelectronics and Nanometer Structures* **2001**, *19* (6), 2353-2356.
3. Switkes, M.; Rothschild, M. "Resolution enhancement of 157-nm lithography by liquid immersion." *Proceedings of SPIE-The International Society for Optical Engineering* **2002**, *4691* (Pt. 1, Optical Microlithography XV), 459-465.

4. Switkes, M.; Kunz, R. R.; Sinta, R. F.; Rothschild, M.; Gallagher-Wetmore, P. M.; Krukonis, V. J.; Williams, K. "Immersion liquids for lithography in the deep ultraviolet." *Proceedings of SPIE-The International Society for Optical Engineering* **2003**, 5040 (Pt. 2, Optical Microlithography XVI), 690-699.
5. French, R. H.; Sewell, H.; Yang, M. K.; Peng, S.; McCafferty, D.; Qiu, W.; Wheland, R. C.; Lemon, M. F.; Markoya, L.; Crawford, M. K. "Imaging of 32-nm 1:1 lines and spaces using 193-nm immersion interference lithography with second-generation immersion fluids to achieve a numerical aperture of 1.5 and a k_1 of 0.25." *Journal of Microlithography, Microfabrication and Microsystems* **2005**, 4 (3), 031103.
6. Burnett, J. H.; Kaplan, S. G.; Shirley, E. L.; Tompkins, P. J.; Webb, J. E. "High-index materials for 193 nm immersion lithography." *Proceedings of SPIE-The International Society for Optical Engineering* **2005**, 5754 (Pt. 2, Optical Microlithography XVIII), 611-621.
7. Smith, B. W.; Fan, Y.; Slocum, M.; Zavyalova, L. "25 nm immersion lithography at 193 nm wavelength." *Proceedings of SPIE-The International Society for Optical Engineering* **2005**, 5754 (Pt. 1, Optical Microlithography XVIII), 141-147.
8. Whittaker, A. K.; Blakey, I.; Liu, H.; Hill, D. J. T.; George, G. A.; Conley, W.; Zimmerman, P. "High-RI resist polymers for 193 nm immersion lithography." *Proceedings of SPIE-The International Society for Optical Engineering* **2005**, 5753 (Pt. 2, Advances in Resist Technology and Processing XXII), 827-835.
9. Conley, W.; Bendik, J. "Is ArF the final wavelength?" *Proceedings of SPIE-The International Society for Optical Engineering* **2004**, 5376 (Pt. 1, Advances in Resist Technology and Processing XXI), 16-20.
10. Smith, B. W.; Bourov, A.; Fan, Y.; Zavyalova, L. V.; Lafferty, N. V.; Cropanese, F. C. "Approaching the numerical aperture of water - Immersion lithography at 193 nm." *Proceedings of SPIE-The International Society for Optical Engineering* **2004**, 5377 (Pt. 1, Optical Microlithography XVII), 273-284.
11. Zhou, J.; Fan, Y.; Bourov, A.; Lafferty, N.; Cropanese, F.; Zavyalova, L.; Estroff, A.; Smith, B. W. "Immersion lithography fluids for high NA 193 nm

- lithography." *Proceedings of SPIE-The International Society for Optical Engineering* **2005**, 5754 (Pt. 2, Optical Microlithography XVIII), 630-637.
12. Lee, K.; Kunjappu, J.; Jockusch, S.; Turro, N. J.; Widerschpan, T.; Zhou, J.; Smith, B. W.; Zimmerman, P.; Conley, W. "Amplification of the index of refraction of aqueous immersion fluids by ionic surfactants." *Proceedings of SPIE-The International Society for Optical Engineering* **2005**, 5753 (Pt. 1, Advances in Resist Technology and Processing XXII), 537-553.
 13. Chumanov, G.; Evanoff, D. D., Jr.; Luzinov, I.; Klep, V.; Zdryko, B.; Conley, W.; Zimmerman, P. "Nanocomposite liquids for 193 nm immersion lithography: a progress report." *Proceedings of SPIE-The International Society for Optical Engineering* **2005**, 5753 (Pt. 2, Advances in Resist Technology and Processing XXII), 847-850.
 14. Eisele, K. M.; Klausmann, E. "Effects of heavy metal contamination from corrosive gas and dopant handling equipment in silicon wafer processing." *Solid State Technology* **1984**, 27 (10), 177-80.
 15. Gruver, R. A.; Gaylord, R. H.; Bilyou, B. W.; Albaugh, K. B. "Relationship of wafer surface contamination to metallic contamination in process liquids." *Proceedings - Institute of Environmental Sciences* **1992**, 38th (Vol. 1), 460-5.
 16. Hill, M.; Hellmann, D.; Rother, M. "Quartz glass components and heavy-metal contamination." *Solid State Technology* **1994**, 37 (3), 49-50,52.
 17. Tompkins, H. G.; McGahan, W. A., *Spectroscopic Ellipsometry and Reflectometry: A User's Guide*. Wiley: New York, **1999**; p 228.
 18. Styrkas, D.; Doran, S. J.; Gilchrist, V.; Keddie, J. L.; Lu, J. R.; Murphy, E.; Sackin, R.; Su, T.-J.; Tzitzinou, A. "Application of ellipsometry to polymers at interfaces and in thin films." In *Polymer Surfaces and Interfaces III*, Richards, R. W.; Peace, S. K., Eds. Wiley-Interscience: New York, **1999**; pp 1-42.
 19. Azzam, R. M. A.; Bashara, N. M., *Ellipsometry and polarized light*. North-Holland Pub. Co.: Amsterdam, **1977**; p 529.

20. Born, M.; Wolf, E., *Principles of optics: electromagnetic theory of propagation, interference and diffraction of light*. 7th expanded ed.; Cambridge University Press: Cambridge; New York, **1999**; p 952.
21. Burns, S. D. *Understanding Fundamental Mechanisms of Photoresist Dissolution*. PhD Dissertation, The University of Texas at Austin, Austin, TX, USA, **2003**.
22. Synowicki, R. A.; Pribil, G. K.; Cooney, G.; Herzinger, C. M.; Green, S. E.; French, R. H.; Yang, M. K.; Burnett, J. H.; Kaplan, S. "Fluid refractive index measurements using rough surface and prism minimum deviation techniques." *Journal of Vacuum Science and Technology B: Microelectronics and Nanometer Structures* **2004**, 22 (6), 3450-3453.
23. Burnett, J. H.; Kaplan, S. "Measurement of the refractive index and thermo-optic coefficient of water near 193 nm." *Proceedings of SPIE-The International Society for Optical Engineering* **2003**, 5040 (Pt. 3, Optical Microlithography XVI), 1742-1749.
24. Burnett, J. H.; Kaplan, S. G. "Measurement of the refractive index and thermo-optic coefficient of water near 193 nm." *Journal of Microlithography, Microfabrication, and Microsystems* **2004**, 3 (1), 68-72.
25. French, R. H.; Yang, M. K.; Lemon, M. F.; Synowicki, R. A.; Pribil, G. K.; Cooney, G. T.; Herzinger, C. M.; Green, S. E.; Burnett, J. H.; Kaplan, S. "Immersion fluid refractive indices using prism minimum deviation techniques." *Proceedings of SPIE - The International Society for Optical Engineering* **2004**, 5377 (Pt. 3, Optical Microlithography XVII), 1689-1694.
26. Brodsky, C.; Byers, J.; Conley, W.; Hung, R.; Yamada, S.; Patterson, K.; Somervell, M.; Trinque, B.; Tran, H. V.; Cho, S.; Chiba, T.; Lin, S.-H.; Jamieson, A.; Johnson, H.; Vander Heyden, T.; Willson, C. G. "157 nm resist materials: Progress report." *Journal of Vacuum Science & Technology, B: Microelectronics and Nanometer Structures* **2000**, 18 (6), 3396-3401.
27. Mack, C. A., *Inside PROLITH : a comprehensive guide to optical lithography simulation*. FINLE Technologies: Austin, **1997**.

28. Skoog, D. A.; West, D. M., *Fundamentals of analytical chemistry*. 3rd ed.; Holt, Rinehart, and Winston: New York, **1976**; p 804.
29. Heller, W. "Remarks on refractive index mixture rules." *Journal of Physical Chemistry* **1965**, *69* (4), 1123-9.
30. Lorentz, H. A., *The theory of electrons and its applications to the phenomena of light and radiant heat*. 2nd ed.; Dover Publications: New York, **1952**; p 343.
31. Stein, G.; Treinin, A. "Absorption spectra of anions in solution. III. Ionic effects." *Transactions of the Faraday Society* **1960**, *56*, 1393-403.
32. Rabinowitch, E. "Electron-transfer spectra and their photochemical effects." *Reviews of Modern Physics* **1942**, *14*, 112-31.
33. Bourov, A.; Fan, Y.; Cropanese, F. C.; Lafferty, N. V.; Zavyalova, L.; Kang, H.; Smith, B. W. "Immersion microlithography at 193 nm with a Talbot prism interferometer." *Proceedings of SPIE - The International Society for Optical Engineering* **2004**, *5377* (Pt. 3, Optical Microlithography XVII), 1573-1578.
34. Zhou, J.; Fan, Y.; Bourov, A.; Smith Bruce, W. "Inorganic immersion fluids for ultrahigh numerical aperture 193 nm lithography." *Applied Optics* **2006**, *45* (13), 3077-82.

CHAPTER 5: THEORETICAL CONSIDERATIONS FOR HIGH REFRACTIVE INDICES AND LOW ABSORPTION COEFFICIENTS

5.1 INTRODUCTION

The empirical survey from the previous chapter led to the identification of methanesulfonic acid-based salts as possible high index/low absorbance additives. Their aqueous solutions were found to have some of the highest index values paired with some of the lowest absorption coefficients measured for potential ionic additives. However, neither target value was achieved, nor were the physical properties sufficiently similar to those of water. Furthermore, the observation that every increase in refractive index was accompanied by an increase in absorbance suggested that it may not be possible to consider the two properties independently. That is not surprising since there is indeed a fundamental connection between the two properties. This connection is apparent from the description of light interacting with a medium, where the two are expressed as a single quantity called the complex index of refraction, and is described by the Kramers-Kronig relation. From these descriptions, models of their behavior versus wavelength have been formulated; typically to fit experimental data obtained from techniques such as ellipsometry. In this chapter the nature of the complex index of refraction is introduced, and the Kramers-Kronig relation is discussed. Several models for optical properties are also briefly reviewed and are then used to calculate spectra that are representative of an ideal high index/low absorbance additive. Finally, initial experimental results from a new class of additives developed based on insights from these theoretical considerations are presented.

5.2 THE COMPLEX INDEX OF REFRACTION

The refractive index and absorption coefficient are quantities that describe the propagation of light through a medium. The refractive index is defined as the ratio of the speed of light in vacuum c to its phase velocity in the medium; the absorption coefficient is the attenuation of the light's intensity, as described in the previous chapter. They can be related to the properties that describe the medium's response to an external electromagnetic field by the solution of a wave equation for light propagating through the medium. The wave equation is obtained from Maxwell's equations written in terms of macroscopic quantities and the medium's properties. Descriptions of how properties relate to the fundamental physical processes occurring during the interaction between the light and medium can then be used to formulate models for the optical properties. A general discussion taken from Wooten's treatment is presented here.¹

The macroscopic form of Maxwell's equations in cgs units are given below,

$$\nabla \cdot \mathbf{E} = 4\pi\rho^{total} \quad (5.1)$$

$$\nabla \times \mathbf{E} = -\frac{1}{c} \frac{\partial \mathbf{B}}{\partial t} \quad (5.2)$$

$$\nabla \cdot \mathbf{B} = 0 \quad (5.3)$$

$$\nabla \times \mathbf{B} = \frac{1}{c} \frac{\partial \mathbf{E}}{\partial t} + \frac{4\pi}{c} \mathbf{J}^{total} \quad (5.4)$$

where \mathbf{E} is the total electric field strength, \mathbf{B} is the magnetic induction, ρ^{total} is the total charge density and \mathbf{J}^{total} is the total current density. The charge and current density can be split into bound and free contributions, *e.g.*, contributions from bound and conduction electrons in a solid. For the charge density, the bound contribution comes from the

polarization \mathbf{P} , or the dipole moment per unit volume of the medium, and the free contribution comes from an external source of charge, Equation 5.5.

$$\rho^{total} = -\nabla \cdot \mathbf{P} + \rho^{ext} \quad (5.5)$$

The bound contribution to the current density comes from the magnetic dipole moment per unit volume of the medium, called the magnetization \mathbf{M} , and any time-dependent polarization. The free contribution also has two parts, one from the motion of any conduction electrons in the medium, including any electrons that have absorbed radiation, and one from an external source. The total current density is given in Equation 5.6.

$$\mathbf{J}^{total} = \frac{\partial \mathbf{P}}{\partial t} + c\nabla \times \mathbf{M} + \mathbf{J}^{cond} + \mathbf{J}^{ext} \quad (5.6)$$

The total electric field present in the medium is a combination of any external field, such as an incident light wave, and the resulting induced field. The external field is represented by a vector called the displacement \mathbf{D} and the induced field comes from the polarization, Equation 5.7. Similarly, a vector for the total magnetic field strength \mathbf{H} is defined by the magnetic induction and the magnetization, Equation 5.8.

$$\mathbf{E} = \mathbf{D} - 4\pi\mathbf{P} \quad (5.7)$$

$$\mathbf{H} = \mathbf{B} - 4\pi\mathbf{M} \quad (5.8)$$

At this point, it is typically observed that the polarization and \mathbf{J}^{cond} should be related to the electric field strength and the magnetization to the magnetic field strength. For an isotropic medium that responds linearly to a field, it is assumed that the following relationships hold true,

$$\mathbf{P} = \chi_e \mathbf{E} \quad (5.9)$$

$$\mathbf{M} = \chi_m \mathbf{H} \quad (5.10)$$

$$\mathbf{J}^{cond} = \sigma \mathbf{E} \quad (5.11)$$

where χ_e is termed the medium's electric susceptibility, χ_m is its magnetic susceptibility and σ is its conductivity. In the limit of zero frequency σ can usually be assumed to be the electrical conductivity, but in response to transverse electromagnetic waves it represents absorption. The displacement and magnetic induction are also assumed to be linearly related to the electric and magnetic field strengths in the medium,

$$\mathbf{D} = \epsilon \mathbf{E} \quad (5.12)$$

$$\mathbf{B} = \mu \mathbf{H} \quad (5.13)$$

where ϵ is the dielectric function and μ is the magnetic permeability of the medium. The magnetic permeability is essentially equal to 1 for non-magnetic materials, so it is neglected in later calculations but included here for completeness.

Using Equations 5.5 – 5.8 and 5.11 – 5.13, Equations 5.1 – 5.4 can be rewritten to include the medium's properties. In the absence of any external sources, $\rho^{ext} = \mathbf{J}^{cond} = 0$, they can be combined to obtain a wave equation for light propagating through the medium, Equation 5.14.

$$\nabla^2 \mathbf{E} = \frac{\epsilon \mu}{c^2} \frac{\partial^2 \mathbf{E}}{\partial t^2} + \frac{4\pi \sigma \mu}{c^2} \frac{\partial \mathbf{E}}{\partial t} \quad (5.14)$$

If the incident light is assumed to be a plane wave,

$$\mathbf{E} = \mathbf{E}_0 \exp i(\hat{\mathbf{q}} \cdot \mathbf{r} - \omega t) \quad (5.15)$$

where \mathbf{E}_0 is the amplitude, $\hat{\mathbf{q}}$ is the wave vector, \mathbf{r} is the unit vector and ω is the angular frequency of the light, the solution of Equation 5.14 results in the following expression for the magnitude of the wave vector,

$$\hat{q}^2 = \mu \frac{\omega^2}{c^2} \left(\varepsilon + i \frac{4\pi\sigma}{\omega} \right) \quad (5.16)$$

Thus the expression for the plane wave propagating through the medium becomes

$$\mathbf{E} = \mathbf{E}_0 \exp \left(i \frac{\omega}{c} \sqrt{\mu \left(\varepsilon + i \frac{4\pi\sigma}{\omega} \right)} \mathbf{q} \cdot \mathbf{r} \right) \exp(-i\omega t) \quad (5.17)$$

For convenience, the quantity in parenthesis in Equation 5.16 is often expressed as a single parameter called the complex dielectric function,

$$\hat{\varepsilon} = \varepsilon_1 + i\varepsilon_2 = \varepsilon + i \frac{4\pi\sigma}{\omega} \quad (5.18)$$

For a transparent insulator, where $\sigma = 0$, and using the definition of the angular frequency, $\omega = 2\pi\nu/\lambda$, where ν is the phase velocity of light in the medium, Equation 5.17 becomes

$$\mathbf{E} = \mathbf{E}_0 \exp \left(i \frac{2\pi}{\lambda} \frac{\nu}{c} \sqrt{\mu\varepsilon} \mathbf{q} \cdot \mathbf{r} \right) \exp(-i\omega t) \quad (5.19)$$

Comparing Equation 5.19 to a standard expression for a plane wave, it can be seen that²

$$\nu = \frac{c}{\sqrt{\varepsilon\mu}} \quad (5.20)$$

The quantity $\sqrt{\varepsilon\mu}$ is therefore equal to the refractive index, n , of a transparent medium.

When the frequency of the light is high enough for absorption to occur, *i.e.*, the conductivity is not zero, a complex index of refraction \hat{n} can also be defined. It is related to the complex dielectric function by Maxwell's relation,³

$$\hat{\epsilon}\mu = \hat{n}^2 = (n + ik)^2 \quad (5.21)$$

where k is the extinction coefficient. Equation 5.17 can then be rewritten in terms of the refractive index and extinction coefficient,

$$\mathbf{E} = \mathbf{E}_0 \exp i \left(\frac{\omega}{c} n \mathbf{q} \cdot \mathbf{r} - \omega t \right) \exp \left(- \left(\frac{\omega}{c} k \mathbf{q} \cdot \mathbf{r} \right) \right) \quad (5.22)$$

in which the first exponential describes the propagation of a wave whose phase velocity is c/n and the second describes the attenuation of the wave. The extinction coefficient is therefore related to the absorption coefficient, given by the following expression,⁴

$$\alpha = \frac{4\pi k}{\ln 10 \lambda} \quad (5.23)$$

The factor of $\ln 10$ converts α into the conventional base 10 units from base e . Since α and k are equivalent, the extinction coefficient will be used from here on for simplicity.

Using Equations 5.18 and 5.21, the refractive index and extinction coefficient are related to a medium's dielectric function, magnetic permeability and conductivity,

$$\epsilon_1 = n^2 - k^2 / \mu = \epsilon \quad (5.24)$$

$$\epsilon_2 = 2nk / \mu = 4\pi\sigma / \omega \quad (5.25)$$

These expressions indicate that n and k are not independent quantities. This result is an important consideration for the development of high index, low absorbance fluids for next generation immersion lithography. It indicates that the optical properties of an

additive cannot be optimized independently of each other. The relation between n and k results from a principle known as causality, which leads to one quantity being fully specified by complete knowledge of the other.

5.3 THE KRAMERS-KRONIG RELATION

Causality is a fundamental assumption in physics regarding the effect of an interaction between two entities. Nussenzveig describes several causality conditions, the simplest and most general being primitive causality, “The effect cannot precede the cause.”⁵ A more specific condition is relativistic or macroscopic causality, “No signal can propagate with velocity greater than c .”⁵ For a general scattering system, Toll gives the causality condition as, “no scattered wave can appear until the primary wave has reached some part of the scatter,” and for a refractive medium he gives a condition equivalent to macroscopic causality, “a source at the time $t = 0$ can produce no electromagnetic disturbance whatsoever at the plane $x = x_0$ in advance of the time $t = x_0/c$.”⁶

The relevance of these conditions to the refractive index and extinction coefficient is evidenced when a medium is viewed as a collection of resonators that can both scatter and absorb radiation.⁷ The resonators consist of electrons that are bound to atomic nuclei at some equilibrium position and subject to viscous damping. When light of a certain frequency is incident on those resonators, it forces them to oscillate at that frequency. To return to their equilibrium positions they reemit waves at the same frequency. When the frequency is far from the natural, or resonance, frequency of the electron, the reemitted

waves are slightly out of phase with the incident radiation. The interference of these scattered waves with the incident waves causes a phase shift observable as a change in the phase velocity of the light as it propagates passed the resonators, giving rise to the refractive index. The phase shift is dependent on both the resonance frequency and the incident frequency, so the phase velocity and therefore n are dependent on the wavelength of light.⁸ This phenomenon is called dispersion. When the incident frequency approaches the resonance frequency the phase shift increases to the point that the scattered waves destructively interfere with the incident waves, resulting in absorption. This classical interpretation of a medium serves as the basis for many of the models describing the optical properties.

The causality conditions state that for a resonator to absorb part of a light wave, that wave must first reach the resonator. They also state that for two waves to interfere, they must first reach each other. The refractive index dictates when a wave will reach a resonator, and the extinction coefficient dictates how much light will be left to interfere with incident waves once it is scattered by the resonator. To satisfy the condition of causality, n and k must be related. Toll presents a physical argument emphasizing this point, based on his statement of macroscopic causality. If a beam of light taken to be the superposition of waves of all wavelengths, \mathbf{E} , is incident on a medium at time $t = 0$, there can be no field leaving the medium for any $t < 0$. If the medium were to act as a perfect absorber for some frequency ω , the amplitude of the component \mathbf{E}_ω would disappear for $t > 0$ passed the medium. If n and k were assumed to be independent for the medium, the absorption of one particular wave would not affect the phase shifts occurring for all other

waves. Since an individual wave extends over all time unless it destructively interferes with other waves at certain intervals, the resulting field leaving the medium $\mathbf{E}_r = \mathbf{E} - \mathbf{E}_\omega$ would have a component that exists for $t < 0$ composed of waves that should have canceled by \mathbf{E}_ω . To avoid the existence of a field passed the medium before the incident field reaches it, all other components of \mathbf{E} must experience an additional phase shift as \mathbf{E}_ω is attenuated so that their superposition results in no field for $t < 0$.^{5,6}

The causality condition for n and k was formally stated by Kramers and Kronig, Equation 5.26,^{7,9}

$$n(\omega) - 1 = \frac{2}{\pi} P \int_0^\infty \frac{\omega' k(\omega')}{\omega'^2 - \omega^2} d\omega' \quad (5.26)$$

where n at an angular frequency ω is given by integrating k over all frequencies ω' , and P denotes Cauchy's principle value of the integral, given by the following,⁵

$$P \int_0^\infty = \lim_{\beta \rightarrow 0} \left(\int_0^{\omega-\beta} + \int_{\omega+\beta}^\infty \right) \quad (5.27)$$

The Kramers-Kronig relation is considered to be the first known dispersion relation, a formula that relates a dispersive process to an absorption process. These relationships have since found many applications in physics, including determining n from measurements of k .¹⁰⁻¹³

5.4 MODELS FOR OPTICAL PROPERTIES

The relation of n and k to the macroscopic quantities ϵ , μ , and σ through the complex dielectric function provide a starting point for the development of models that describe their behavior according to the fundamental physics occurring as light interacts

with a medium. The Kramers-Kronig relation provides a check for the models, as well as an additional tool for their formulation. The first models describing the dispersion of n and k were empirical and not consistent with the Kramers-Kronig relation. The Cauchy model for dispersion, Equation 4.4, is an example of such model. In wavelength regions where the Cauchy model provides a good description of the index, an Urbach absorption tail is usually used for the extinction coefficient,¹⁴

$$k(\lambda) = A_k \exp B_k \left(\frac{1240}{\lambda} - \frac{1240}{\lambda_o} \right) \quad (5.28)$$

where λ is in units of nm and A_k , B_k and λ_o are fitting parameters. Note that the parameters A_k and λ_o are completely correlated, so Equation 5.28 has only two adjustable parameters.² These two expressions provide a good mathematical fit to n and k in spectral regions far from a resonance, but in the vicinity of a resonance frequency a more rigorous model is needed.

The Lorentz oscillator model is commonly used to illustrate the absorption and dispersion behavior in a dielectric or semiconductor medium. It is particularly useful in that its derivation provides expressions for both dispersion and absorption in terms of the complex dielectric function that are Kramers-Kronig consistent, and they in turn provide insight into the microscopic nature of the two processes. In the Lorentz model an electron bound to an atomic nucleus is considered to be a small mass bound to a infinitely large mass by a spring.^{1, 8} The motion of the electron in response to an electric field can be described by a second order differential equation,

$$m \frac{d^2 \mathbf{r}}{dt^2} + m\Gamma \frac{d\mathbf{r}}{dt} + m\omega_o^2 \mathbf{r} = -e\mathbf{E}_{loc} \quad (5.29)$$

where m is the electron's mass, \mathbf{r} is the displacement of the electron, Γ represents an energy loss mechanism due to scattering, ω_o is the resonance frequency, e is the magnitude of the electric charge and \mathbf{E}_{loc} is the local electric field acting on the electron. The term $m\Gamma(d\mathbf{r}/dt)$ represents viscous damping and the term $m\omega_o^2 \mathbf{r}$ is a Hooke's law restoring force. If the electric field is taken to be a harmonic wave of the form $\mathbf{E}_{loc} = \mathbf{E}_o e^{i\omega t}$ and the oscillations of the electron are assumed to have the same form, then the solution of Equation 5.29 is

$$\hat{\mathbf{r}} = \frac{-e\mathbf{E}_{loc} / m}{(\omega_o^2 - \omega^2) - i\Gamma \omega} \quad (5.30)$$

The dipole moment of a one-electron atom is defined as the product of the magnitude of one of the charges and the distance between them,

$$\hat{\mathbf{p}} = -e\hat{\mathbf{r}} = \frac{e^2 \mathbf{E}_{loc}}{m} \frac{1}{(\omega_o^2 - \omega^2) - i\Gamma \omega} \quad (5.31)$$

The frequency-dependent atomic polarizability is defined by a linear relationship between the dipole moment and the electric field, $\hat{\mathbf{p}} = \hat{\alpha}(\omega)\mathbf{E}_{loc}$, and is therefore

$$\hat{\alpha}(\omega) = \frac{e^2}{m} \frac{1}{(\omega_o^2 - \omega^2) - i\Gamma \omega} \quad (5.32)$$

Recalling that the polarization is the dipole moment per unit volume, it is then directly related to the atomic polarizability,

$$\hat{\mathbf{P}} = N \langle \hat{\mathbf{p}} \rangle = N \hat{\alpha} \langle \mathbf{E}_{loc} \rangle \quad (5.33)$$

where N is the number of atoms per unit volume. By making the assumption that $\langle \mathbf{E}_{loc} \rangle = \mathbf{E}$ and recalling Equations 5.7 and 5.12, it can be seen that

$$\hat{\mathbf{D}} = \hat{\epsilon} \mathbf{E} = \mathbf{E} + 4\pi \hat{\mathbf{P}} \quad (5.34)$$

$$\hat{\epsilon} = \epsilon_1 - i\epsilon_2 = 1 + 4\pi N \hat{\alpha} \quad (5.35)$$

Using Equation 5.32, the complex dielectric function can be expressed by

$$\hat{\epsilon}(\omega) = 1 + \frac{4\pi N e^2}{m} \frac{1}{(\omega_o^2 - \omega^2) - i\Gamma\omega} \quad (5.36)$$

Solving for the real and imaginary parts of the dielectric constant and using Equations 5.24 and 5.25, the following relationships for n and k are obtained,

$$\epsilon_1 = n^2 - k^2 = 1 + \frac{4\pi N e^2}{m} \frac{(\omega_o^2 - \omega^2)}{(\omega_o^2 - \omega^2)^2 + \Gamma^2 \omega^2} \quad (5.37)$$

$$\epsilon_2 = 2nk = \frac{4\pi N e^2}{m} \frac{\Gamma \omega}{(\omega_o^2 - \omega^2)^2 + \Gamma^2 \omega^2} \quad (5.38)$$

The dispersion function for the complex dielectric constant can be generalized for systems with multiple electrons oscillating at different resonance frequencies by

$$\hat{\epsilon} = 1 + \frac{4\pi e^2}{m} \sum_j \frac{N_j}{(\omega_j^2 - \omega^2) - i\Gamma_j \omega} \quad (5.39)$$

where N_j is the density of electrons with resonance frequency ω_j and $\sum_j N_j = N$. The

real and imaginary parts then become summations of their respective forms,

$$\epsilon_1 = n^2 - k^2 = 1 + \frac{4\pi e^2}{m} \sum_j \frac{N_j (\omega_j^2 - \omega^2)}{(\omega_j^2 - \omega^2)^2 + \Gamma_j^2 \omega^2} \quad (5.40)$$

$$\varepsilon_2 = 2nk = \frac{4\pi e^2}{m} \sum_j \frac{N_j \Gamma_j \omega}{(\omega_j^2 - \omega^2)^2 + \Gamma_j^2 \omega^2} \quad (5.41)$$

Using Equations 5.37 and 5.38 and assuming a resonance frequency at a wavelength of 200 nm and values of $\Gamma = 1 \times 10^{14}$ and $4\pi N e^2/m = 1 \times 10^{31}$, examples of the dispersion curves for the complex dielectric function and the complex index of refraction can be calculated, Figures 5.1 and 5.2. From these curves, several observations can be made. First, in regions far from ω_0 both n and ε_1 increase gradually with decreasing wavelength and k and ε_2 asymptotically approach zero; this is referred to as normal dispersion. Close to the resonance they experience a sharp change, rising to a maximum just before the maximum of either k or ε_2 , and then decreasing rapidly to a minimum before returning to normal dispersion. This behavior is called anomalous dispersion. At wavelengths below ω_0 it is seen that $n < 1$, indicating that $v > c$ and suggesting a violation of the macroscopic causality condition. In this region the energy associated with the light is high enough to overcome the energy binding the electrons to their nuclei and the electrons become free, *e.g.*, like conduction electrons in a metal. An applied field induces what is called a plasma oscillation in these free electrons – where the oscillations are weakly damped in phase and extend over a spatial region significantly larger than the wavelength of light – rather than a harmonic oscillation. Under these conditions, n is considered to be representative of the group velocity of light rather than its phase velocity. The actual mechanism for the phenomenon causing $n < 1$, called superluminality, is unclear. Two possible explanations are that it is a result of an unequal response by a medium to the front and back of a wave, creating an outgoing signal

containing information from the incident wave and the medium, or just of a particular superposition of different frequencies in the anomalous dispersion region which create the illusion of superluminality. In either case the velocity of the energy in the light has not been found to be greater than c , and there is no evidence yet of an actual violation of causality.¹⁵⁻¹⁷

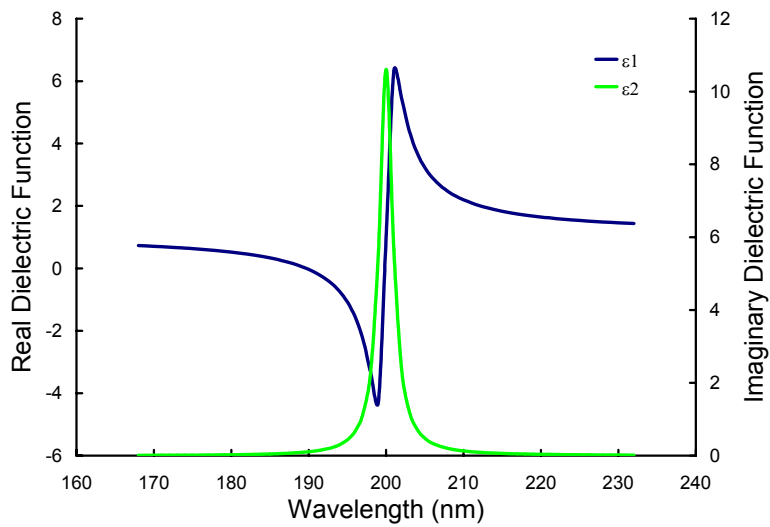


Figure 5.1 Dispersion curves calculated from Equations 5.37 and 5.38 for ϵ_1 and ϵ_2 versus wavelength.

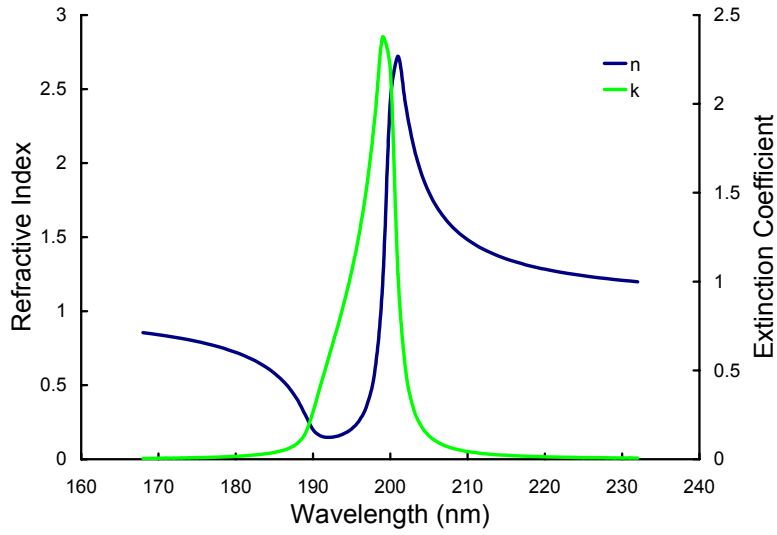


Figure 5.2 Dispersion curves calculated from Equations 5.37 and 5.38 for n and k versus wavelength.

Figure 5.1 shows that there is both a minimum and a maximum for ε_1 . From the derivative of Equation 5.37, their locations $\omega_{\min/\max}$ can be determined,

$$\pm \Gamma/2 = \omega_o - \omega_{\min/\max} \quad (5.42)$$

Equation 5.42 also shows that Γ is the width of the region of anomalous dispersion.

From Equation 5.38, the maximum value of ε_2 is seen to be the following,

$$\varepsilon_{2,\max} = \frac{4\pi N e^2 / m}{\Gamma \omega_o} \quad (5.43)$$

and Γ is essentially the full width at half maximum of ε_2 . Since ε_2 represents absorption in a material, ω_o can be said to designate an electronic transition resulting from the absorption of a photon with energy $\hbar\omega_o$. The broadening of that transition due to

contributions from other transitions such as rotational and vibrational is then represented by Γ . The quantity $4\pi Ne^2/m$ can be viewed as the amplitude for that absorption.

The Lorentz model provides an intuitive description of the behavior of a material's optical properties, but it is not the only model available. Indeed, the WVASE32 software program used for data analysis with ellipsometers from the J. A. Woollam Co. contains 27 different functions associated with 18 different model types to describe a broad range of materials. Many are based on the Lorentz model, such as the Drude model for metals. In this model the conduction electrons in a metal are not considered bound to a particular nucleus, so they do not have a resonance frequency. By setting $\omega_o = 0$ in Equations 5.37 and 5.38, defining the quantity $\omega_p = (4\pi Ne^2/m)^{1/2}$ as the plasma frequency and stating that $\Gamma = \tau^{-1}$ where τ is the mean free collision time between electrons, the Drude model is given directly from the Lorentz,¹

$$\varepsilon_1 = n^2 - k^2 = 1 - \frac{\omega_p^2 \tau^2}{1 + \tau^2 \omega^2} \quad (5.44)$$

$$\varepsilon_2 = 2nk = \frac{\omega_p^2}{\omega(1 + \tau^2 \omega^2)} \quad (5.45)$$

For amorphous materials, more complex models are built from the Lorentzian expression for absorption, Equation 5.38. The Tauc-Lorentz model combines Tauc's joint density of states expression for ε_2 ,¹⁸

$$\varepsilon_2 = A(\omega - \omega_g)^2 / \omega^2 \quad (5.46)$$

where ω_g represents a cut-off frequency below which no absorption occurs, with the Lorentzian expression to give,^{19, 20}

$$\varepsilon_2 = 2nk = \frac{A_{TL}}{\omega} \frac{\Gamma(\omega - \omega_g)^2}{(\omega_o^2 - \omega^2)^2 + \Gamma^2\omega^2} \quad (5.47)$$

for $\omega > \omega_g$ and $\varepsilon_2 = 0$ for $\omega < \omega_g$, and the real part of the dielectric function is determined by the Kramers-Kronig relation. The Cody-Lorentz model includes a Kramers-Kronig consistent Urbach absorption tail to describe ε_2 below ω_g .²¹ These increasingly sophisticated models are needed to better describe mediums such as semiconductors whose electronic structures are represented by bands instead of discrete states, whereas Lorentzian or even Gaussian representations of absorption can adequately describe insulators.²²

5.5 CALCULATIONS OF DISPERSION CURVES FOR HIGH INDEX/LOW ABSORBANCE ADDITIVE

Maxwell's equations have shown how the complex index of refraction arises from the interaction between light and matter. The Kramers-Kronig relation has established the dependence of n and k on each other. The Lorentz model provides a phenomenological account of the microscopic processes leading to these macroscopically observable quantities. The result is a description of the refractive index and extinction coefficient which clearly shows they cannot be considered independently. However, it also shows that the presence of absorption is not necessarily detrimental to the development of a high index/low absorbance additive. Referring back to Figure 5.2, the presence of an absorption peak causes a sharp increase in the value of the index before the peak and an offset where the index is larger above the peak than below it. An ideal additive for next generation immersion lithography would therefore not show a complete

absence of absorption, but would have a strong peak in the vacuum ultraviolet (VUV) region with a sharp cut-off just below 193 nm. Such a peak would lead to a large increase in the composite fluid's refractive index at 193 nm without a significant increase in the absorbance. Also, additional absorption peaks at even lower wavelengths would contribute to further index increases since the offset is additive. Figure 5.3 shows this result as a peak of increasing amplitude at 171 nm is added to a peak at 188 nm.

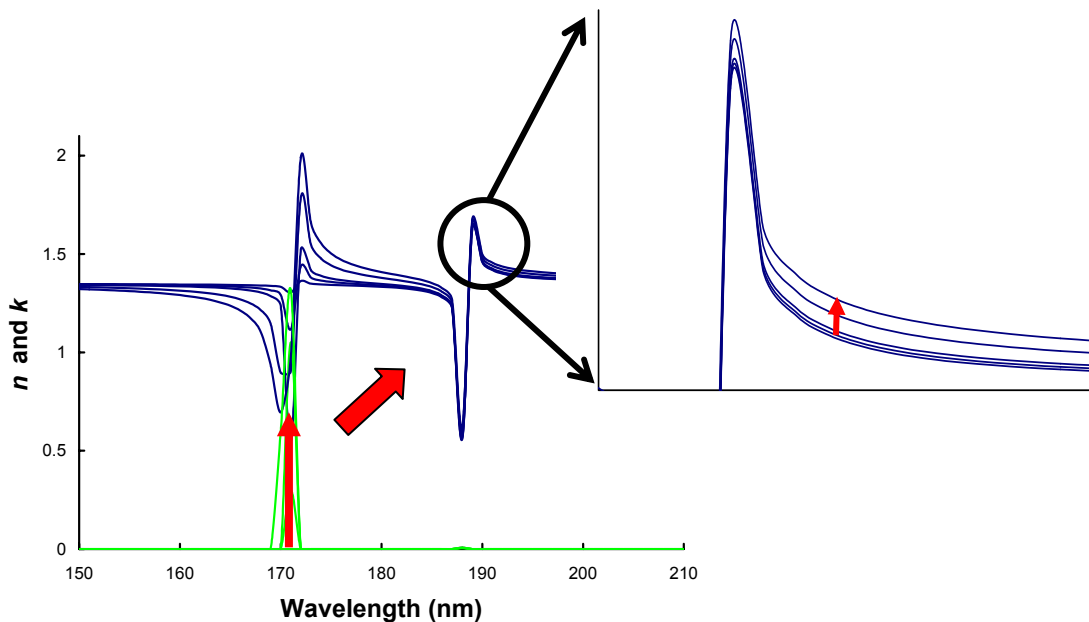


Figure 5.3 Index offset at higher wavelengths increases as amplitude of absorption peak at lower wavelengths increases, indicating benefit of additional absorption in immersion additives.

Identifying a compound with these characteristics presents a challenge as it is difficult to obtain absorption data in the VUV region and little is currently available. Previous work to identify transparent polymers for use with 157 nm lithography used

qualitative models based on density functional theory calculations to screen structures for appropriate transparency, with the results for promising candidates verified experimentally.²³ An inverse approach could be useful for identifying possible additive structures. A model using Lorentz oscillators to specify the location and strength of absorption peaks that result in a target index value and extinction coefficient for an additive could be created. If those absorption peaks were then related to known electronic transitions, a structure or necessary parts of a structure would start to emerge. Proposed structures and any modifications, for example to improve solubility, could then be analyzed before any synthesis or experimental measurements need occur.

The first step to this approach would be to verify that it is possible to create a reasonable representation of spectra from the Lorentz model. Since the material to be modeled starts as an unknown, its density and therefore N are unknown. The dispersion behavior outside of the VUV also cannot be determined *a priori*, so a complete set of oscillators cannot be specified. The Kramers-Kronig relation requires that the extinction coefficient be known at all wavelengths for the index to be determined at just one. To overcome these deficiencies, the Lorentz model is parameterized in the following manner,

$$\hat{\epsilon} = \epsilon_o + \sum_j \frac{A_j}{(E_j^2 - E^2) - i\Gamma_j E} \quad (5.48)$$

where ϵ_o is a real constant used to account for contributions to ϵ_1 from resonances not explicitly included in the model calculations, A_j is an amplitude term approximating the quantity $4\pi N e^2/m$, $E = \hbar\omega$ and Γ_j is the peak broadening. The conversion to photon

energy allows the parameters in Equation 5.48 to be expressed as $O(1)$ rather than $O(10^{30})$. To evaluate the Lorentz model, Equation 5.48 was used to model the dispersion behavior of water.

The *Handbook of Optical Constants of Solids* provides a compilation of n and k data for water collected up to the year 1991; Figure 5.4 shows the values from the x-ray region into the visible.²⁴ Water has a relatively constant refractive index through the visible region, $n = 1.33$, and is transparent into the deep UV, confirming the measurements reported in Chapter 4. At a wavelength of 150 nm, it has a strong absorption peak to which its index value of 1.435 at 193 nm can be attributed. Below 150 nm there is a broad absorption peak centered at 85 nm, with three distinct shoulders at 125 nm, 70 nm and 50 nm, Figure 5.5. The absorption at 85 nm and below can be attributed to the photoionization of water, which has peaks at energies of 12.62 eV (98 nm), 14.74 eV (84 nm), 18.51 eV (67 nm), 32.2 eV (39 nm) and 48 eV (26 nm).²⁵ The absorption at 150 nm and 125 nm will then be assumed to be from electronic transitions, possibly Rydberg states though the nature of the excitations is not fully understood.²⁶

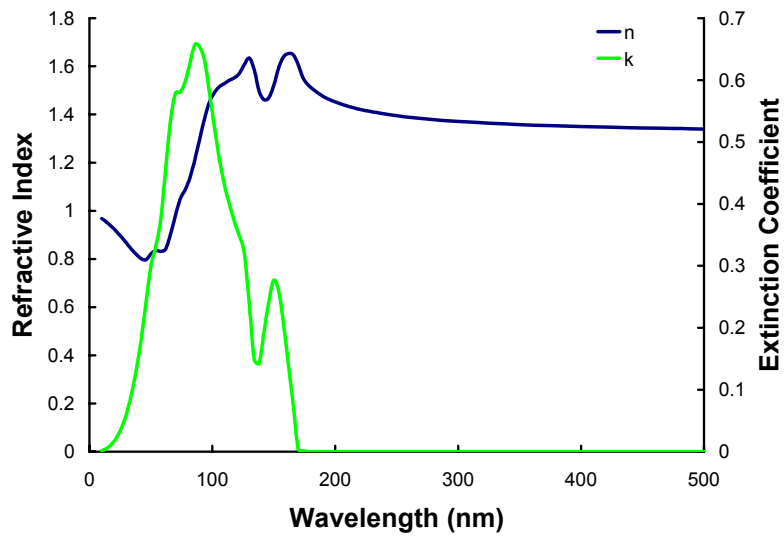


Figure 5.4 Refractive index and extinction coefficient values for water from the *Handbook of Optical Constants*.²⁴

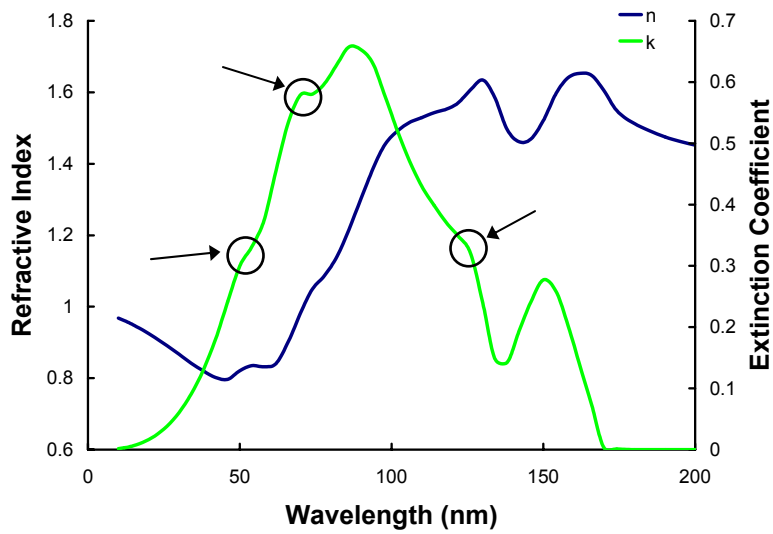


Figure 5.5 Absorption peak shoulders at 125 nm, 70 nm and 50 nm.

A two-oscillator model was used to represent the first two absorption peaks for water. The parameters, determined by trial-and-error, for the model are given in Table 5.1, and the calculated dispersion curves of n and k are compared with the reported values in Figures 5.6 and 5.7. This initial model reasonably described the shapes of both of the dispersion curves and was in good agreement with the magnitudes of the absorption peaks. However, it did not accurately represent the values of the refractive index, underestimating it below 190 nm and overestimating above. Also, it predicted that k would asymptotically approach zero rather than dropping off sharply at 170 nm. The calculated index values could be improved with the addition of a third oscillator with no broadening, $\Gamma_j = 0$. This type of oscillator is called a pole oscillator, and is used in the WVASE32 program as an additional means to represent contributions to the real part of the dielectric function from absorption outside of the spectral region being modeled. In this case, a pole oscillator could be used to represent the absorption due to ionization. The parameters for this three-oscillator model are given in Table 5.2, and the calculated dispersion curves are shown in Figures 5.8 and 5.9. Referring to the mean squared error (MSE) for the values of the refractive index,

$$MSE = \frac{1}{m} \sum_{j=1}^m \left(\left(\frac{n_{\text{calculated}}}{n_{\text{reported}}} \right)_m - 1 \right)^2 \quad (5.49)$$

the three-oscillator model increased the accuracy of the representation by an order of magnitude with $MSE = 4 \times 10^{-4}$ versus an $MSE = 0.004$ for the two oscillator model. There was no significant change in the MSE value for the extinction coefficient.

Table 5.1 Parameters for two-oscillator Lorentz model of water.

Oscillator j	E_j	A_j	Γ_j	ϵ_0
1	8.2	6	1	1.8
2	9.9	8	1	

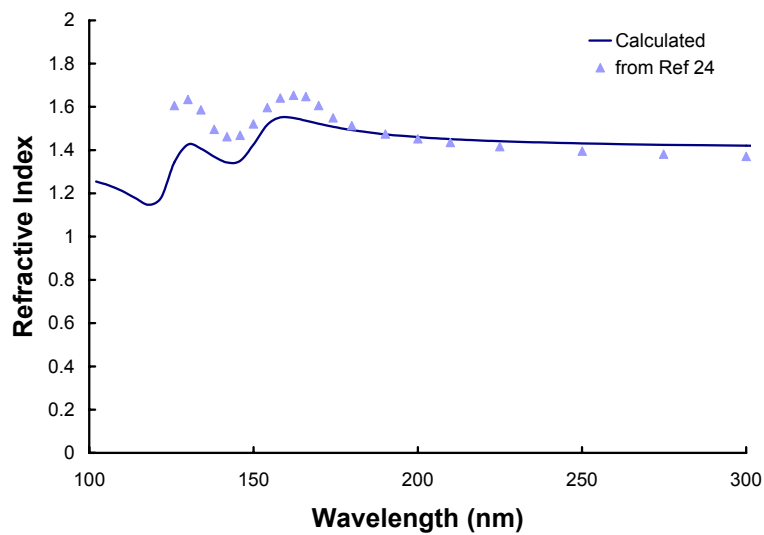


Figure 5.6 Dispersion of the refractive index of water calculated from two-oscillator Lorentz model compared to reported values from the *Handbook of Optical Constants*.

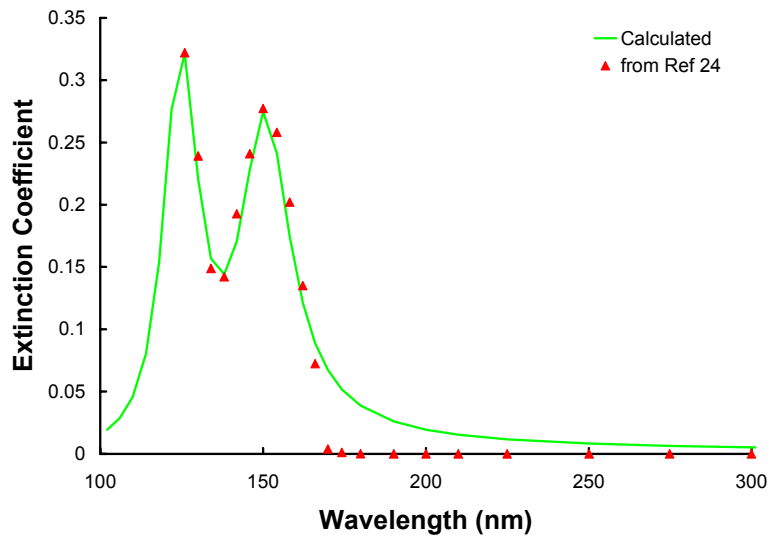


Figure 5.7 Dispersion of the extinction coefficient of water calculated from two-oscillator Lorentz model compared to reported values from the *Handbook of Optical Constants*.

Table 5.2 Parameters for three-oscillator Lorentz model of water.

Oscillator j	E_j	A_j	Γ_j	ϵ_o
1	8.2	6.2	1	1
2	10	10	1	
Pole	120	14	0	

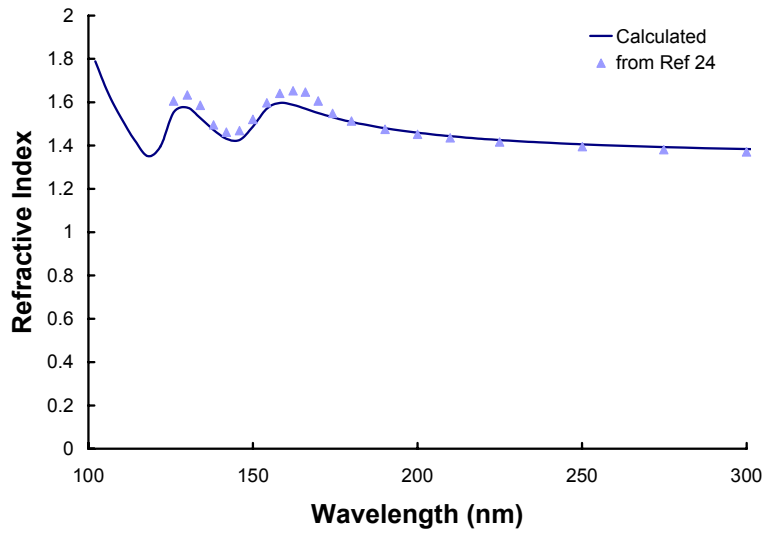


Figure 5.8 Dispersion of the refractive index of water calculated from three-oscillator Lorentz model compared to reported values from the *Handbook of Optical Constants*.

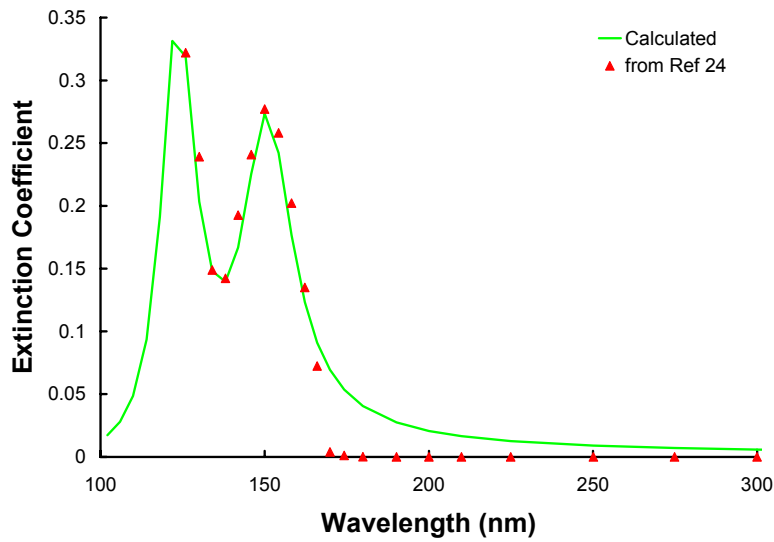


Figure 5.9 Dispersion of the extinction coefficient of water calculated from three-oscillator Lorentz model compared to reported values from the *Handbook of Optical Constants*.

The representation of water's optical properties with a three-oscillator Lorentz model illustrates the limitations of any such model. Absorption outside of the spectral range of interest can have a significant impact on the optical properties inside that range. Some general assumptions must be made about a material's behavior in the absence of experimental data to create a reasonable model. The mathematical expression of the model may not accurately describe the observed behavior in all regions, such as the asymptotic decrease of the calculated extinction coefficient at wavelengths above the absorption peak. The cut-off frequency in the Tauc-Lorentz and Cody-Lorentz models is intended to address this particular discrepancy, but it is also not useful unless the absorption behavior is already known. In the view of creating spectra for an ideal immersion additive, the Lorentz model would present a worst case prediction of an additive's absorption at 193 nm, as long as reasonable values for ϵ_0 and any pole oscillators could be specified.

The primary assumption regarding the nature of a high index/low absorbance additive for an aqueous-based immersion fluid was that it would be organic. This assumption was made for two reasons. The first was that it was already known that aliphatic compounds are transparent into the DUV, hence their use as 193 nm photoresists. The second was that several industrial research groups presented data for proprietary organic-based second generation immersion fluids which had index values approaching $n = 1.64$ at 193 nm and absorption coefficient values approaching the target of $\alpha = 0.15 \text{ cm}^{-1}$.²⁷⁻³⁰ While these fluids appeared to achieve the target optical properties, they had the distinct disadvantage of being sensitive to oxygen, exposure to which caused

significant increases in the absorption coefficients. A later study investigating the use of cyclic hydrocarbons as third generation immersion fluids identified the proposed second generation fluids as compounds such as cyclohexane and decahydronaphthalene, or decalin.³¹⁻³³ It also identified the source of the increased absorbance after oxygen exposure as a charge-transfer complex formed with the cyclic hydrocarbon, and noted that these lack photostability.³⁴

A Lorentz model for an ideal immersion additive was formulated by first ascertaining reasonable values for the location of a pole oscillator to represent ionization and for ϵ_0 . The ionization potentials for common organic compounds ranges from 8 eV to 14 eV, with most aliphatic compounds having a potential close to 10 eV.^{35, 36} The parameter ϵ_0 in Equation 5.48 is usually taken to represent the static dielectric constant of a material, the value of ϵ_l at low frequencies typically associated with electric currents. For water, $\epsilon_l = 64$ according to the *Handbook of Optical Constants*.²⁴ The significantly lower values for ϵ_0 used in the Lorentz models in Figures 5.6 – 5.9 are a result of the depression of the refractive index due to large absorption peaks in the microwave and IR regions of the spectrum. A compilation of dielectric constant data for organic compounds reported a range of $\epsilon_l = 1 - 40$.³⁷ Since the static dielectric constant of water would have fallen at the large end of the range for organic compounds, ϵ_0 for the additive model was also set to one. A pole oscillator was designated at 124 nm, or 10 eV. It was given an initial amplitude of $A = 85$ so that the refractive index in the UV and into the visible would start at $n = 1.4$, a low value for organics, before any oscillators were added.

The spectral range for calculating the model was 130 nm to 330 nm, and the three-oscillator Lorentz model given in Table 5.2 was used to represent water. The refractive index and extinction coefficient values for a solution of the additive and water was calculated using the Maxwell-Garnett effective-medium approximation (ema),

$$\frac{\hat{\epsilon}_{solution} - \hat{\epsilon}_{water}}{\hat{\epsilon}_{solution} + 2\hat{\epsilon}_{water}} = f \frac{\hat{\epsilon}_{additive} - \hat{\epsilon}_{water}}{\hat{\epsilon}_{additive} + 2\hat{\epsilon}_{water}} \quad (5.50)$$

where $\hat{\epsilon}$ is the complex dielectric function and f is the volume fraction of the additive.³⁸⁻

⁴² The Maxwell-Garnett ema was derived to describe systems in which the composite can be considered a matrix of the host component in which small, uniform particles of the additive are imbedded. The particles are assumed to be spherical, and their radii assumed to be smaller than their spacing which is also assumed to be smaller than the wavelengths at which the composite is being analyzed. Water was desired to be the major component of the solution to better maintain its physical properties, so the volume fraction was set at $f = 0.3$. The target index value for the solution was $n = 1.65$ and the target extinction coefficient was $k = 0.125$, which is five times the value of k predicted for water by the Lorentz model.

The first oscillator was placed at $E_o = 6.85$ eV (181 nm). The amplitude of this peak was varied from 1 – 50 for five different values of Γ , from 0.1 – 3, to investigate the effect of these two parameters on the solution's optical properties. The results for n and k at 193 nm are shown in Figures 5.10 and 5.11. Increasing the amplitude of the absorption peak increased both n and k for all values of Γ , with the increase in n being essentially linear. Figures 5.10 and 5.11 show that the target n and k values could be reached with Γ

= 0.1 – 1. Figure 5.12 shows the dispersion curves for the additive with one absorption peak calculated with $A = 21.5$ and $\Gamma = 1$, which resulted in $n = 1.65$ and $k = 0.13$ for the solution. Comparing Figure 5.12 to Figure 5.4, the magnitude of the absorption peak was larger than the ionization peak for water at 85 nm. As these oscillators were intended to represent electronic transitions rather than ionization, a maximum allowable value of $k = 0.45$ was chosen for the calculated absorption peaks above 155 nm, where ionization can start to take place.

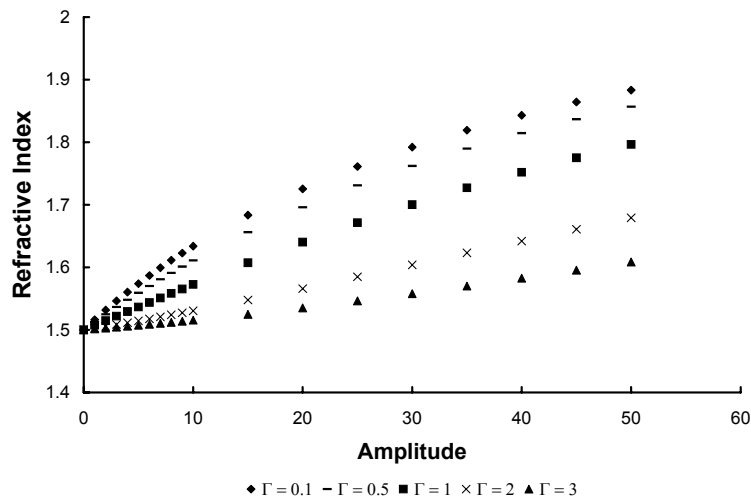


Figure 5.10 Refractive index at 193 nm of modeled solution versus amplitude of first absorption peak for different broadening values.

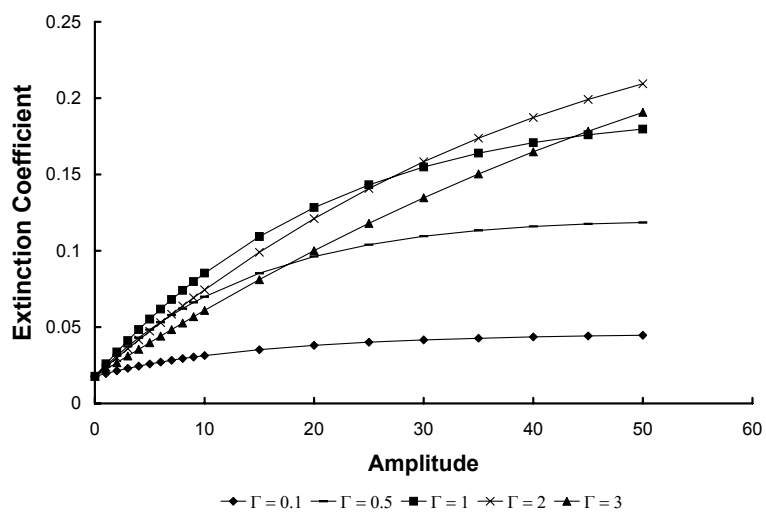


Figure 5.11 Extinction coefficient at 193 nm of modeled solution versus amplitude of first absorption peak for different broadening values.

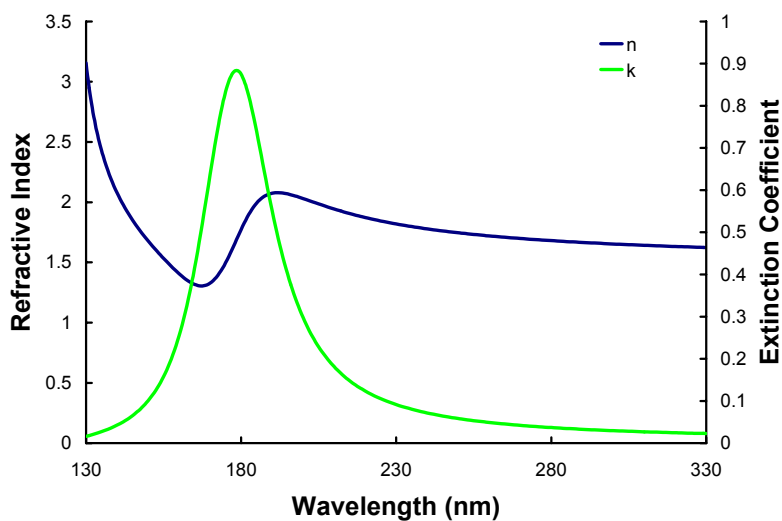


Figure 5.12 Dispersion curves for additive with one absorption peak at $E_0 = 6.85$ eV, $A = 21.5$ and $\Gamma = 1$.

A model with five oscillators was created to represent the additive. Multiple oscillators were needed to achieve significant absorption in the wavelength region of 130 nm to 190 nm without excessive k values. The initial parameters for the model are given in Table 5.3. The dispersion curves calculated from this model are shown in Figure 5.13. The n and k values for the solution were calculated to be $n = 1.61$ and $k = 0.05$. To better match the target n value, the Microsoft Excel Solver function was used to vary the parameters of the five oscillators. The parameters from one result are given in Table 5.4 and the dispersion curves are shown in Figure 5.14. The dispersion curves for the solution are shown in Figure 5.15, the optical properties at 193 nm were $n = 1.65$ and $k = 0.087$.

Table 5.3 Initial parameters for Lorentz model of additive.

Oscillator j	E_j	A_j	Γ_j	ϵ_o
Pole	10	85	0	1
1	6.85	0.2	0.1	
2	7	2	0.5	
3	7.25	5	1	
4	8	8	1	
5	9.5	25	1	

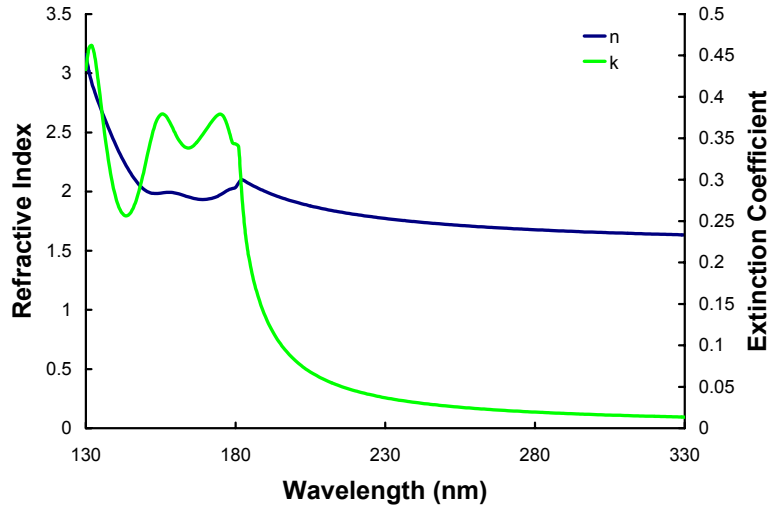


Figure 5.13 Dispersion curves for Lorentz model of additive calculated from parameters in Table 5.3.

Table 5.4 Parameters for Lorentz model of additive found by Excel Solver.

Oscillator j	E_j	A_j	Γ_j	ϵ_0
Pole	10	85	0	1
1	6.667	0.319	0.146	
2	6.547	2.094	0.382	
3	7.038	6.057	0.834	
4	7.832	8.034	0.961	
5	9.342	25.017	0.989	

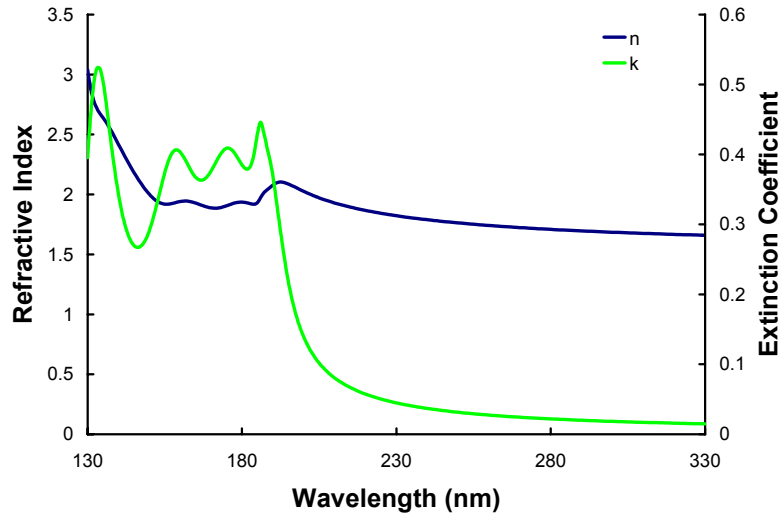


Figure 5.14 Dispersion curves for Lorentz model of additive calculated from parameters in Table 5.4.

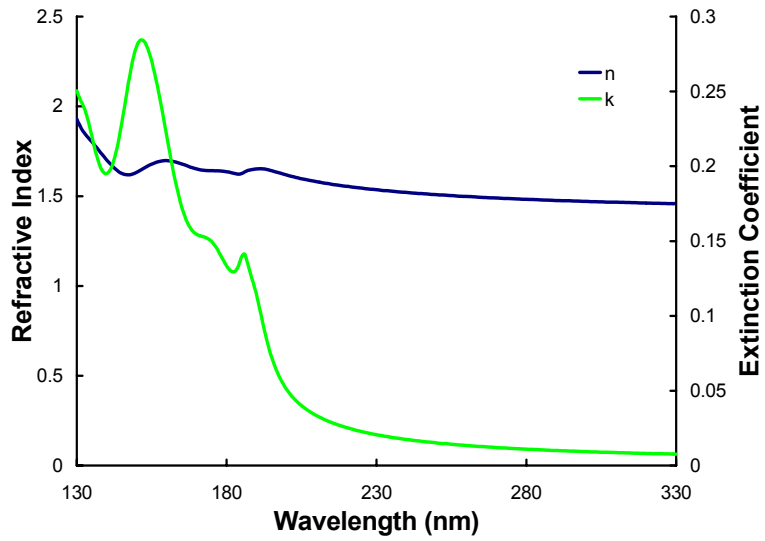


Figure 5.15 Dispersion curves for model solution of the additive and water, with $n = 1.65$ and $k = 0.087$.

The parameters for the Lorentz model in Table 5.4 are not a unique set leading to the target index value. Several iterations of the solution were found, and different starting parameters led to different results. The general characteristics of the spectra were similar among the different solutions, with narrower peaks close to 180 nm and larger, broader peaks below. These results were intended to be used as guide to identify possible additive structures. Gas phase vacuum UV absorption data showed that most saturated hydrocarbons do not begin to absorb until 180 nm, while unsaturated compounds begin to absorb at 200nm.⁴³⁻⁴⁵ Ketones were also found to have absorption peaks at 200 nm.⁴⁶ Some cyclic ethers such as dioxane and tetrahydropyran had absorption peaks at 180 nm, suggesting a possible structure.⁴⁷⁻⁴⁹ In a study of the use of crown ethers to enhance the solubility of heavy metal cations in water for high index fluids, it was found that the ethers themselves had index values of $n = 1.68$.⁵⁰ However, their absorption as tested was too high. It was suggested that structural modifications could lead to a shift in the absorption to lower wavelengths. The combined results of the recent studies of organic immersion fluids and the Lorentz model calculations indicated that saturated cyclic hydrocarbons would be leading candidates for use in second generation immersion fluids. In the next section, possible additives based on these structures are introduced.

5.6 NEW ADDITIVE STRUCTURES

The compounds cyclohexane and decalin served as the basis for several possible second generation fluids since they have a high index with low absorbance. Their index values at 193 nm are $n = 1.56$ and $n = 1.64$ respectively. Figures 5.16 and 5.17 show the

dispersion of their index and absorption coefficients along with those of hexane, as measured by the procedures described in Chapter 4. As discussed above, these materials form a charge-transfer complex with oxygen that significantly increases their absorbance at 193 nm.³¹ To obtain the measurements in Figure 5.17, each compound was purified with an activated silica gel column to remove unsaturated impurities and was bubbled with argon for at least 10 minutes. This sensitivity to oxygen presents a major obstacle to the adoption of these materials as immersion fluids. Their cost and the need for complex recycling systems and different fluid handling systems also detract from their promising optical properties. In an attempt to achieve these optical properties in water, solutions of sulfonic acid salts of cyclohexane and decalin were tested. Sodium cyclohexanesulfonate was obtained from Sigma Aldrich at a 98% purity level. Sodium decalinsulfonate was prepared from decahydro-2-naphthol. The refractive index for a 20 wt% solution of sodium cyclohexanesulfonate in HPLC-grade water and a 5 wt% solution of sodium decalinsulfonate were measured, Figure 5.18. The absorbance of these solutions was measured on a Hewlett-Packard 8452 UV-Vis spectrophotometer with HPLC-grade water used as a reference, Figure 5.19. The sodium decalinsulfonate solution was diluted to approximated 0.5 wt% for the absorbance measurements. These solutions had a moderate increase in refractive index over water. The absorbance was high for both, but did not decrease when the solutions were bubbled with argon. Greater increases in the index values would be expected at higher additive loading, but the two salts appeared to form micelles at concentrations above those tested. Using the Lorentz-Lorenz equation (Equation 4.10) to estimate the refractive indices of the two salts at 193 nm, $n = 1.62$ for

sodium cyclohexanesulfonate and $n = 2.02$ for sodium decalinsulfonate. Based on these index values, a 40% solution by volume of sodium decalinsulfonate would be required to meet the target fluid index value. For these salts to be considered as viable additives for a second generation immersion fluid, their purity level would need to be improved to attempt to reduce their absorption at 193 nm and their solubility would need to be increased while decreasing their tendency to form micelles.

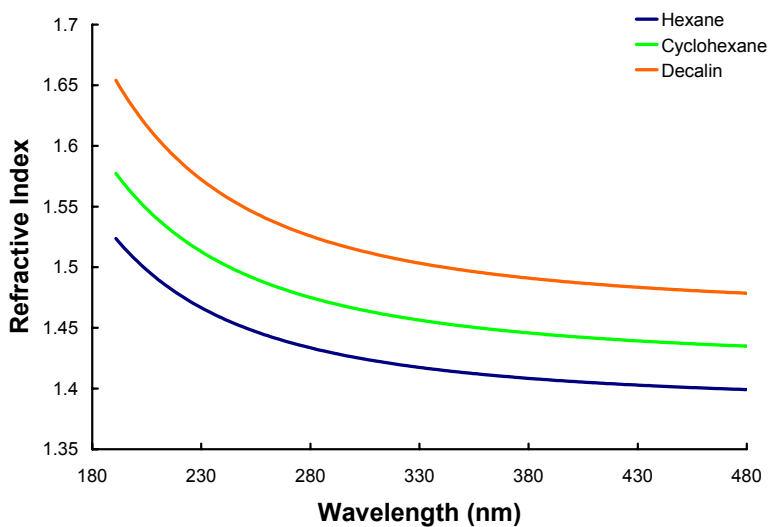


Figure 5.16 Refractive index dispersion curves for hexane, cyclohexane and decalin.

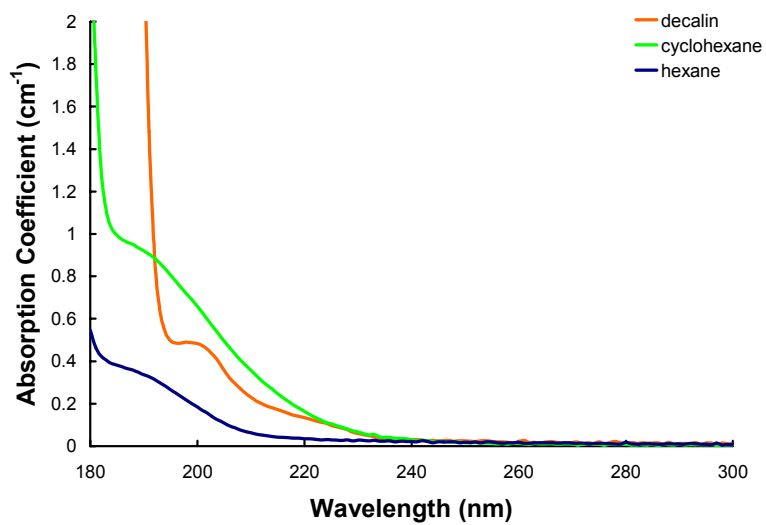


Figure 5.17 Absorption coefficients of hexane, cyclohexane and decalin.

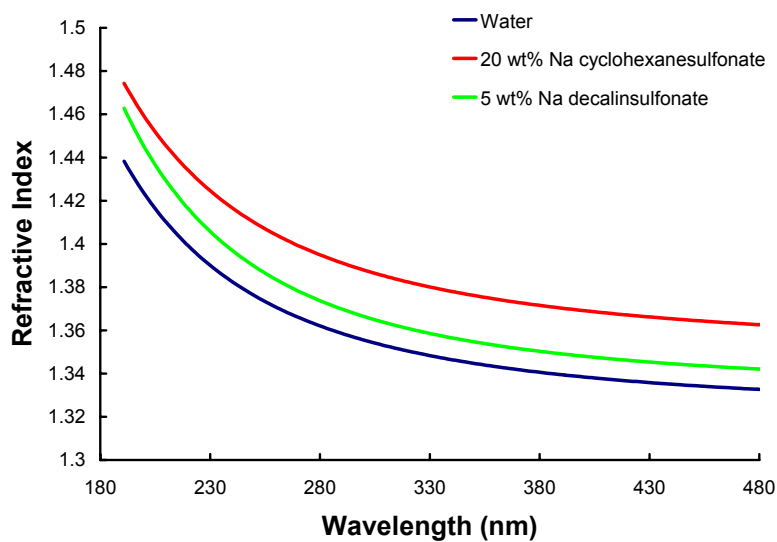


Figure 5.18 Refractive index dispersion of solutions of sodium cyclohexanesulfonate and sodium decalinsulfonate compared to that of water.

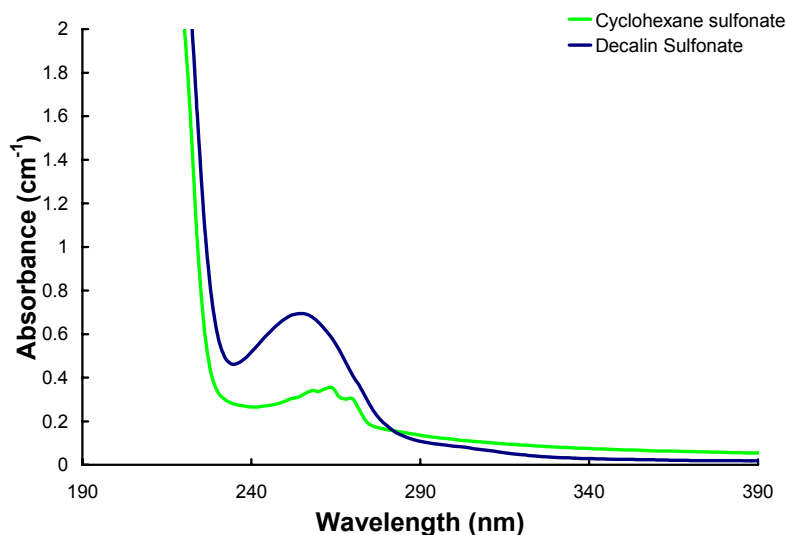


Figure 5.19 Absorbance of sodium cyclohexanesulfonate and sodium decalinsulfonate referenced to water.

5.7 SUMMARY

Second and third generation immersion lithography depend on the development of materials that have high refractive indices at 193 nm and are still sufficiently transparent for imaging. Identifying materials with these characteristics presented a challenge as the two are related. An investigation into the nature of the refractive index and absorption coefficient revealed that the scattering of electromagnetic waves at a subatomic level causes both a phase shift and attenuation of the waves which are observed as a change in the velocity of light as it propagates through a medium and a reduction in its intensity. This leads to a direct relationship between the two properties given by the Kramers-Kronig relation, and a classical description of their behavior by oscillator models such as the Lorentz model. The models show that in regions where a material is transparent, its refractive index increases slightly as the wavelength of light decreases. In a region of

absorption the index changes more drastically and experiences anomalous dispersion, a sharp decrease with decreasing wavelength. The result is an index value that is greater in the wavelength region above the absorption peak than below it, and a small region where the index has significantly increased and the absorbance has not. The implication for an immersion fluid, or a material for any application requiring a high index and low absorbance, is that absorption at lower wavelengths is beneficial to and necessary for a high index at the wavelength of interest. Using the Lorentz model, dispersion curves with several absorption peaks in the region between 130 nm and 180 nm were calculated to represent the optical properties of an additive for a water-based second generation immersion fluid with $n = 1.65$. The calculated absorption behavior was similar to that found for cyclic hydrocarbons in gas phase. These materials had previously been suggested as candidates for both second and third generation immersion fluids, but sensitivity to oxygen has complicated their use. Aqueous solutions of sulfonic acid salts of two compounds, cyclohexane and decalin, were prepared and tested, but the high concentrations needed to meet the target index could not be reached. These salts are promising candidates if their solubility in water can be improved. Additional compounds could also be identified if the Lorentz model calculations were paired with density functional theory calculations as had been done to investigate structures for 157 nm lithography.

5.8 REFERENCES

1. Wooten, F., *Optical Properties of Solids*. Academic Press: New York, **1972**; p 260.
2. Tompkins, H. G.; McGahan, W. A., *Spectroscopic Ellipsometry and Reflectometry: A User's Guide*. Wiley: New York, **1999**; p 228.
3. Böttcher, C. J. F., *Theory of electric polarization*. Elsevier Scientific Pub. Co.: Amsterdam, **1952**.
4. Born, M.; Wolf, E., *Principles of optics: electromagnetic theory of propagation, interference and diffraction of light*. 7th expanded ed.; Cambridge University Press: Cambridge; New York, **1999**; p 952.
5. Nussenzveig, H. M., *Causality and Dispersion Relations*. Academic Press: New York, **1972**.
6. Toll, J. S. "Causality and the Dispersion Relation: Logical Foundations." *Physical Review* **1956**, 104 (6), 1760.
7. Kronig, R. d. L. "The theory of dispersion of x-rays." *Journal of the Optical Society of America* **1926**, 12, 547-57.
8. Lorentz, H. A., *The theory of electrons and its applications to the phenomena of light and radiant heat*. 2nd ed.; Dover Publications: New York, **1952**; p 343.
9. Kramers, H. A. "La diffusion de la lumiere par les atomes." *Atti. Congr. Int. Fis.* **1927**, 2, 545-557.
10. Peiponen, K. E.; Vartiainen, E. M. "Kramers-Kronig relations in optical data inversion." *Physical Review B* **1991**, 44 (15), 8301.
11. Milton, G. W.; Eyre, D. J.; Mantese, J. V. "Finite Frequency Range Kramers Kronig Relations: Bounds on the Dispersion." *Physical Review Letters* **1997**, 79 (16), 3062-3065.

12. King, F. W. "Efficient numerical approach to the evaluation of Kramers-Kronig transforms." *Journal of the Optical Society of America B: Optical Physics* **2002**, *19* (10), 2427-2436.
13. Lucarini, V., *Kramers-Kronig relations in optical materials research*. Springer: Berlin, **2005**; p 160.
14. Urbach, F. "The long-wave-length edge of photographic sensitivity and of the electronic absorption of solids." *Physical Review* **1953**, *92*, 1324.
15. Chiao, R. Y.; Boyce, J. "Superluminality, paraelectricity, and Earnshaw's theorem in media with inverted populations." *Physical Review Letters* **1994**, *73* (25), 3383-6.
16. Wang, L.-G.; Liu, N.-H.; Lin, Q.; Zhu, S.-Y. "Superluminal propagation of light pulses: a result of interference." *Physical Review E: Statistical, Nonlinear, and Soft Matter Physics* **2003**, *68* (6-2), 066606/1-066606/10.
17. Mugnai, D.; Mochi, I. "Superluminal X-wave propagation: energy localization and velocity." *Physical Review E: Statistical, Nonlinear, and Soft Matter Physics* **2006**, *73* (1-2), 016606/1-016606/5.
18. Tauc, J.; Grigorovici, R.; Vancu, A. "Optical Properties and Electronic Structure of Amorphous Germanium." *Physica Status Solidi (B)* **1966**, *15* (2), 627-637.
19. Jellison, G. E., Jr.; Modine, F. A. "Parameterization of the optical functions of amorphous materials in the interband region." *Applied Physics Letters* **1996**, *69* (3), 371-373.
20. Jellison, G. E., Jr.; Modine, F. A. "Parameterization of the optical functions of amorphous materials in the interband region. [Erratum to document cited in CA125:207104]." *Applied Physics Letters* **1996**, *69* (14), 2137.
21. Ferlauto, A. S.; Ferreira, G. M.; Pearce, J. M.; Wronski, C. R.; Collins, R. W.; Deng, X.; Ganguly, G. "Analytical model for the optical functions of amorphous semiconductors from the near-infrared to ultraviolet: Applications in thin film photovoltaics." *Journal of Applied Physics* **2002**, *92* (5), 2424-2436.

22. Kim, C. C.; Garland, J. W.; Abad, H.; Racciah, P. M. "Modeling the optical dielectric function of semiconductors: Extension of the critical-point parabolic-band approximation." *Physical Review B* **1992**, *45* (20), 11749.
23. Brodsky, C.; Byers, J.; Conley, W.; Hung, R.; Yamada, S.; Patterson, K.; Somervell, M.; Trinqué, B.; Tran, H. V.; Cho, S.; Chiba, T.; Lin, S.-H.; Jamieson, A.; Johnson, H.; Vander Heyden, T.; Willson, C. G. "157 nm resist materials: Progress report." *Journal of Vacuum Science & Technology, B: Microelectronics and Nanometer Structures* **2000**, *18* (6), 3396-3401.
24. Querry, M. R.; Wieliczka, D. M.; Segelstein, D. J. "Water (H₂O)." In *Handbook of Optical Constants of Solids*, Palik, E. D., Ed. Academic Press: Boston, **1991**; Vol. 2, p 1096.
25. Chipman, D. M. "Ionization potentials of water from valence bond and molecular orbital wave functions." *J. Am. Chem. Soc.* **1978**, *100* (9), 2650-2654.
26. Garrett, B. C.; Dixon, D. A.; Camaioni, D. M.; Chipman, D. M.; Johnson, M. A.; Jonah, C. D.; Kimmel, G. A.; Miller, J. H.; Rescigno, T. N.; Rossky, P. J.; Xantheas, S. S.; Colson, S. D.; Laufer, A. H.; Ray, D.; Barbara, P. F.; Bartels, D. M.; Becker, K. H.; Bowen, K. H., Jr.; Bradforth, S. E.; Carmichael, I.; Coe, J. V.; Corrales, L. R.; Cowin, J. P.; Dupuis, M.; Eisenthal, K. B.; Franz, J. A.; Gutowski, M. S.; Jordan, K. D.; Kay, B. D.; LaVerne, J. A.; Lymar, S. V.; Madey, T. E.; McCurdy, C. W.; Meisel, D.; Mukamel, S.; Nilsson, A. R.; Orlando, T. M.; Petrik, N. G.; Pimblott, S. M.; Rustad, J. R.; Schenter, G. K.; Singer, S. J.; Tokmakoff, A.; Wang, L.-S.; Wittig, C.; Zwier, T. S. "Role of water in electron-initiated processes and radical chemistry: issues and scientific advances." *Chemical Reviews (Washington, DC, United States)* **2005**, *105* (1), 355-389.
27. Budhlall, B.; Parris, G.; Zhang, P.; Gao, X.; Zarkov, Z.; Ross, B.; Kaplan, S.; Burnett, J. "High refractive index immersion fluids for 193 nm immersion lithography." *Proceedings of SPIE-The International Society for Optical Engineering* **2005**, *5754* (Pt. 2, Optical Microlithography XVIII), 622-629.
28. French, R. H.; Sewell, H.; Yang, M. K.; Peng, S.; McCafferty, D.; Qiu, W.; Wheland, R. C.; Lemon, M. F.; Markoya, L.; Crawford, M. K. "Imaging of 32-nm 1:1 lines and spaces using 193-nm immersion interference lithography with second-generation immersion fluids to achieve a numerical aperture of 1.5 and a

- k_1 of 0.25." *Journal of Microlithography, Microfabrication and Microsystems* **2005**, 4 (3), 031103.
29. Miyamatsu, T.; Wang, Y.; Shima, M.; Kusumoto, S.; Chiba, T.; Nakagawa, H.; Hieda, K.; Shimokawa, T. "Material design for immersion lithography with high refractive index fluid (HIF)." *Proceedings of SPIE-The International Society for Optical Engineering* **2005**, 5753 (Pt. 1, Advances in Resist Technology and Processing XXII), 10-19.
 30. Peng, S.; French, R. H.; Qiu, W.; Wheland, R. C.; Yang, M.; Lemon, M. F.; Crawford, M. K. "Second generation fluids for 193 nm immersion lithography." *Proceedings of SPIE-The International Society for Optical Engineering* **2005**, 5754 (Pt. 1, Optical Microlithography XVIII), 427-434.
 31. Gejo, J. L.; Kunjappu, J.; Turro, N. J.; Conley, W. "Outlook for Potential Third Generation Immersion Fluids" 3rd International Symposium on Immersion Lithography, **2006**; SEMATECH: 2006.
 32. French, R. H.; Peng, S.; Wheland, R. C. "Use of highly purified hydrocarbons in vacuum ultraviolet applications." U.S. Patent No. 2005-141285 2005286031, 09/14/2005, **2005**.
 33. Zhang, P.; Budhlall, B. M.; Parris, G. E.; Barber, L. C. "Immersion lithography fluids." U.S. Patent No. 2005-30132 2005173682, 01/07/2005, **2005**.
 34. Parsons, B. F.; Chandler, D. W. "On the Dissociation of van der Waals Clusters of X₂-Cyclohexane (X = O, Cl) Following Charge-Transfer Excitation in the Ultraviolet." *J. Phys. Chem. A* **2003**, 107 (49), 10544-10553.
 35. Morrison, J. D.; Nicholson, A. J. C. "Ionization efficiency. II. The ionization potentials of some organic molecules." *Journal of Chemical Physics* **1952**, 20, 1021-3.
 36. Dewar, M. J. S.; Worley, S. D. "Photoelectron spectra of molecules. I. Ionization potentials of some organic molecules and their interpretation." *Journal of Chemical Physics* **1969**, 50 (2), 654-67.

37. Sild, S.; Karelson, M. "A General QSPR Treatment for Dielectric Constants of Organic Compounds." *J. Chem. Inf. Model.* **2002**, *42* (2), 360-367.
38. Maxwell-Garnett, J. C. "Colours in Metal Glasses and in Metallic Films." *Philosophical Transactions of the Royal Society of London. Series A, Containing Papers of a Mathematical or Physical Character* **1904**, *203*, 385-420.
39. Maxwell-Garnett, J. C. "Colours in Metal Glasses, in Metallic Films, and in Metallic Solutions. II." *Philosophical Transactions of the Royal Society of London. Series A, Containing Papers of a Mathematical or Physical Character* **1906**, *205*, 237-288.
40. Stroud, D. "Generalized effective-medium approach to the conductivity of an inhomogeneous material." *Physical Review B* **1975**, *12* (8), 3368.
41. Gittleman, J. I.; Abeles, B. "Comparison of the effective medium and the Maxwell-Garnett predictions for the dielectric constants of granular metals." *Physical Review B: Solid State* **1977**, *15* (6), 3273-5.
42. Gehr, R. J.; Boyd, R. W. "Optical Properties of Nanostructured Optical Materials." *Chemistry of Materials* **1996**, *8* (8), 1807-1819.
43. Pickett, L. W.; Muntz, M.; McPherson, E. M. "Vacuum ultraviolet absorption spectra of cyclic compounds. I. Cyclohexane, cyclohexene, cyclopentane, cyclopentene, and benzene." *Journal of the American Chemical Society* **1951**, *73*, 4862-5.
44. Raymond, J. W. "Rydberg States in Cyclic Alkanes." *The Journal of Chemical Physics* **1972**, *56* (8), 3912-3920.
45. Stokes, S.; Pickett, L. W. "Absorption of bicycloheptane and bicycloheptene in the vacuum ultraviolet." *Journal of Chemical Physics* **1955**, *23*, 258-60.
46. O'Toole, L.; Brint, P.; Kosmidis, C.; Boulakis, G.; Tsekeris, P. "Vacuum-ultraviolet absorption spectra of propanone, butanone and the cyclic ketones $C_nH_{2n-2}O$ ($n = 4, 5, 6, 7$)." *Journal of the Chemical Society, Faraday Transactions* **1991**, *87* (20), 3343-51.

47. Pickett, L. W.; Hoeflich, N. J.; Liu, T.-C. "Vacuum ultraviolet absorption spectra of cyclic compounds. II. Tetrahydrofuran, tetrahydropyran, 1,4-dioxan, and furan." *Journal of the American Chemical Society* **1951**, *73*, 4865-9.
48. Hernandez, G. J. "Vacuum-ultraviolet absorption spectra of the cyclic ethers: trimethylene oxide, tetrahydrofuran, and tetrahydropyran." *Journal of Chemical Physics* **1963**, *38*, 2233-42.
49. Hernandez, G. J.; Duncan, A. B. F. "Vacuum ultraviolet absorption spectra of 1,4-dioxane and 1,3-dioxane." *Journal of Chemical Physics* **1962**, *36*, 1504-8.
50. Lopez-Gejo, J.; Kunjappu, J. T.; Turro, N. J.; Conley, W. "Amplification of the index of refraction of aqueous immersion fluids with crown ethers: A progress report." *Proceedings of SPIE-The International Society for Optical Engineering* **2006**, *6153* (Pt. 1, Advances in Resist Technology and Processing XXIII), 61530.

CHAPTER 6: FABRICATION OF POLYMER-BASED PHOTONIC CRYSTALS BY STEP AND FLASH IMPRINT LITHOGRAPHY

6.1 INTRODUCTION TO PHOTONIC CRYSTALS

Composite materials whose structural arrangements give rise to unique properties are called metamaterials. For a subset called photonic crystals, two otherwise transparent materials are arranged in such a way that certain wavelengths of light are forbidden from propagating through the composite.¹ This type of phenomenon has been well known for one-dimensional systems where a multilayer dielectric mirror comprised of alternating high and low refractive index films would act as a near-perfect mirror for specific wavelengths. In 1987, Eli Yablonovitch and Sajeev John expanded the concept to theoretical systems with three-dimensional periodicity of their dielectric functions.^{2, 3} The descriptions developed for these systems were analogous to those used to for semiconductors; the dielectric periodicity was represented by a crystal lattice of “atoms” of one dielectric in a matrix of the other and Maxwell’s equations were solved in a manner similar to the Schrödinger equation to find bands of allowed electromagnetic modes that could propagate through the crystal.⁴⁻⁶ For wavelengths on the same order of magnitude as the lattice spacing, the multiple interfacial reflections caused by the dielectric periodicity result in destructive interference that completely reflects those wavelengths from the crystal, thereby creating a gap in the so-called photonic bands.

Yablonovitch proposed creating photonic crystal structures in semiconductor materials so that they would have overlapping photonic and electronic band gaps which would suppress unwanted spontaneous emission in devices like solar cells and

semiconductor lasers.² John proposed using photonic crystals to study strong localization of light.³ With the development of a two-dimensional crystal configuration, other applications such as low-loss waveguides capable of guiding light around sharp bends, highly-efficient LEDs, fast optical switches and modulators and high-Q microcavities were also proposed.⁷⁻¹⁰ However, a lack of naturally occurring photonic crystals with useful band gaps has necessitated the development of materials and fabrication processes to enable the creation of these devices.¹¹

One-dimensional photonic crystals can be fabricated with thin film deposition techniques such as spin coating or evaporation, but have limited application since the band gap exists for only a narrow range of wavelengths at near normal incidence. Two-dimensional photonic crystals, see Figure 6.1, are compatible with planar fabrication processes such as microlithography and etching. Depending on the dielectric contrast, *i.e.*, the ratio of the higher refractive index to the lower, a 2D crystal's band gap can range from a narrow gap that is dependent on both the direction of propagation and polarization state of the incident light to a complete band gap for all in-plane directions and polarization states.¹²⁻¹⁶ This range gives the 2D configuration considerable flexibility, as several applications for crystals with moderate contrast such as narrow-band filters and highly sensitive probes have been proposed in addition to the previously mentioned uses.¹⁷ The fabrication of three-dimensional crystals has typically relied on layer-by-layer application of 2D methods, laser holography or self-assembly of colloidal systems.^{1, 18, 19} The 3D systems do not have the polarization dependence of the 2D crystals, but there are a limited number of crystals structures that can have complete band

gaps without sufficiently high dielectric contrast.⁷ The fabrication challenges associated with them have limited the accessibility of 3D photonic crystals relative to 2D systems, but their primary function of light confinement in all directions can usually be achieved by combining conventional index guiding in the out-of-plane direction with a 2D crystal.²⁰

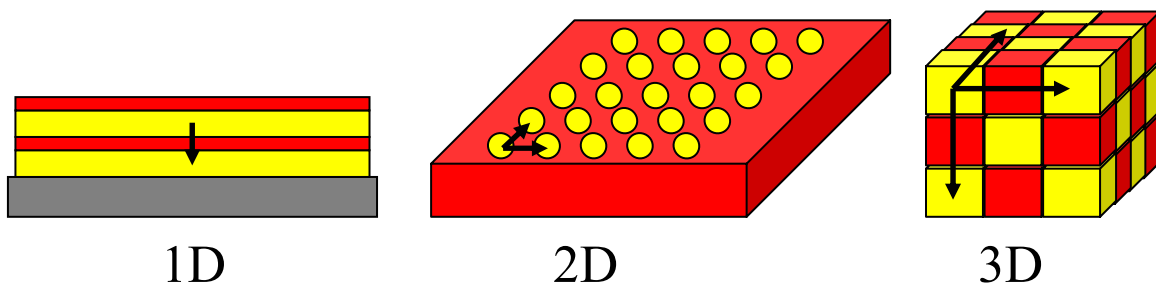


Figure 6.1 Possible configurations for photonic crystals with one-, two- and three-dimensional dielectric periodicity.

6.2 FABRICATION OF 2D PHOTONIC CRYSTALS WITH STEP AND FLASH IMPRINT LITHOGRAPHY

Joannopoulos *et al.* state that “One interesting feature of electromagnetism in dielectric media is that there is no fundamental length scale other than the assumption that the system is macroscopic.”⁷ The consequence for photonic crystals is that it is theoretically possible to have a band gap in any region of the electromagnetic spectrum as long as there is dielectric periodicity with appropriate spacing. The availability of sub-micron patterning techniques and transparent, high index semiconductors has made 2D photonic crystals with IR band gaps for telecommunications applications common.²¹⁻²⁶

However, for devices such as high efficiency LEDs for lighting and displays, band gaps

in the visible region are needed. Creating a photonic crystal with such a band gap is more challenging since it requires feature sizes that are approximately half those needed for IR band gaps.⁷ Patterning techniques such as e-beam and ion beam lithography have the resolution to print the necessary nanometer scale features but are slow, whereas high resolution, high throughput optical lithography is becoming increasingly complex and costly.

An alternative would be to use step and flash imprint lithography (SFIL), which achieves the resolution of the direct write processes with higher throughput, to create 2D photonic crystals.²⁷ In addition, it has previously been demonstrated that SFIL is capable of producing other optical elements such as wire grid polarizers and micro lens arrays.²⁸ It is also compatible with a wide range of materials, from semiconductor, oxide and polymer substrates to directly patternable functional materials.²⁹ This material flexibility compliments the design flexibility of 2D photonic crystals, where polymers could be used for moderate dielectric contrast, oxides for higher contrast and composites for tunable refractive indices.^{30, 31}

An SFIL process for fabricating photonic crystals requires the creation of a template, optimization of the imprint process and development of etch recipes for any pattern transfer steps. Templates can be obtained from commercial lithography reticle vendors, but are typically very expensive and require a significant amount of time for the vendor to process. Recently, SEMATECH sponsored a project for the creation of SFIL templates in collaboration with the Microelectronics Research Center (MRC) at the University of Texas at Austin. To assist in that work, a template with a photonic crystal

pattern was developed using a negative tone ebeam resist. Once fabricated, that template was then used to develop an imprint process for fabricating polymer photonic crystals. Pattern transfer was demonstrated in two polymer samples, one containing an additive to raise the polymer's index in the visible region.

6.3 SFIL TEMPLATE FOR 2D PHOTONIC CRYSTAL

The template creation process consists of several steps. The first is determining the design of the device to be fabricated. For a photonic crystal, this involves choosing a crystal configuration and optimizing its lattice parameters to obtain the desired photonic band structure for the material to be patterned. Once the design is complete, blank templates compatible with the imprint tool must be obtained. The design pattern is created on the template using e-beam lithography. Finally the pattern is transferred into the template by dry etch processes and verified.

6.3.1 DESIGN OF PHOTONIC CRYSTAL STRUCTURE

One of the most common configurations for 2D photonic crystals is an array of air holes drilled into a dielectric slab, which allows for maximum dielectric contrast.²¹⁻²⁶ Since SFIL is inherently negative tone, this type of configuration would require a template with posts protruding from the surface. Such features are conveniently obtained using a negative tone resist, and therefore provided an appropriate model system for template fabrication. Of the possible arrangements, a triangular lattice is known to have a complete photonic band gap when the dielectric contrast is high enough, and is

commonly used for device demonstrations.^{16, 22, 32-35} Therefore, the triangular lattice of air holes was chosen for the crystal configuration, see Figure 6.2.

The actual dimensions of a photonic crystal lattice are determined by the wavelength range to be encompassed by the band gap. To emphasize the resolution of SFIL, a band gap in the visible region was targeted with two common wavelengths of 632 nm from a helium-neon laser and 532 nm from a frequency-doubled Nd:YAG laser chosen as design wavelengths. The crystal dimensions, the lattice constant and the hole radii, were determined from band structure calculations using the *BandSOLVE 3.0* simulation tool from the RSoft Photonics Suite (RSoft Design Group, Inc., Ossining, NY). These band structures arise from the mathematical description of light propagation through the crystals.

As discussed previously, photonic crystals are treated in an analogous manner to semiconductors.⁷ Their dielectric periodicity is represented by a crystal lattice complete with reciprocal space and Brillouin zones that define regions of symmetry in the crystal structure. To determine how electromagnetic waves propagate through them, Maxwell's equations are combined to obtain a wave equation in the form of an eigenvalue problem for the magnetic field strength. The wave equation is solved at points along the Brillouin zone to determine which frequencies exist in the crystal. As each new frequency is found it is connected to a frequency at the previous point to create a band structure of the dispersion of the waves through the crystal. The solution of Maxwell's equations as an eigenvalue problem and the representation of the allowed frequencies as a band structure follow the analogy with semiconductors as they rely on the same theories used to

determine electronic energy levels from Schrödinger's equation. A complete description of the methods for calculating band structures is given elsewhere.^{7, 36, 37}

The first step in the band structure calculations was to lay out a crystal lattice, such as that shown in Figure 6.2 where a is the lattice constant and r is the hole radius as defined by a unit cell of the crystal. Figure 6.2 also shows the first Brillouin zone for the unit cell with an irreducible region shaded in blue. The indices Γ , M and K mark the path along which the eigenvalue wave equation is solved to determine the band structure. As stated previously, there is no fundamental length scale governing these problems. The band structure calculated for a particular lattice is valid at any length scale as long as all of the dimensions of the lattice and the frequencies in the band structure are scaled by the same parameter. The lattice constant is the conventional parameter used for scaling. The default values in the *BandSOLVE* program are $a = 1 \mu\text{m}$ and $r = 0.2a$, and were used for the initial calculations. The next step was to specify the refractive index of the dielectric slab. Theoretically, any index value could have been used and the resulting band structure rescaled, but the frequencies do not scale linearly with n . Since the structure was ultimately to be transferred into a poly(methyl methacrylate) (PMMA) slab, its index of $n = 1.5$ was chosen for the initial design. The initial band structure calculated in *BandSOLVE* for the given parameters is shown in Figure 6.3. The frequencies were plotted against each point along the irreducible Brillouin zone and reported as a non-dimensional quantity $\omega a / 2\pi c$. Thus a given a determines the frequency range of the band structure and a desired ω determines the needed a .

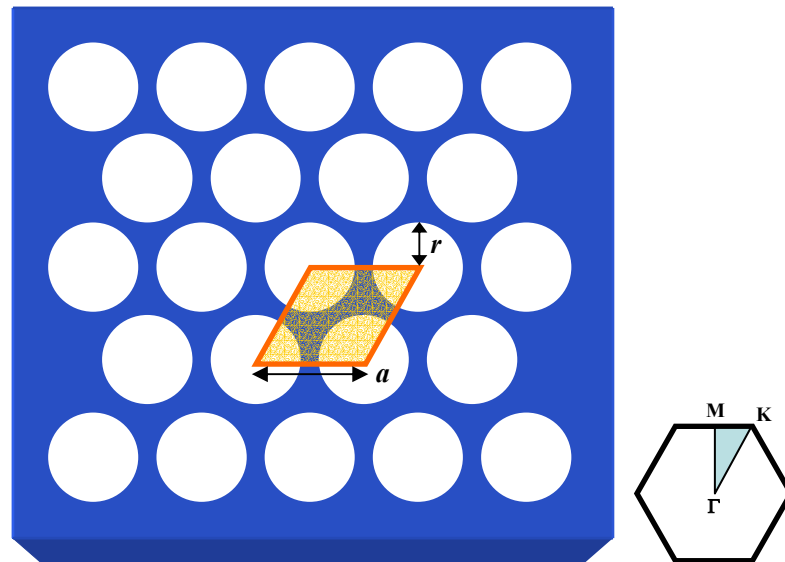


Figure 6.2 Two-dimensional photonic crystal with triangular lattice of air holes in a dielectric slab. The unit cell of the lattice is shown in orange and the first Brillouin zone is shown in the right inset.

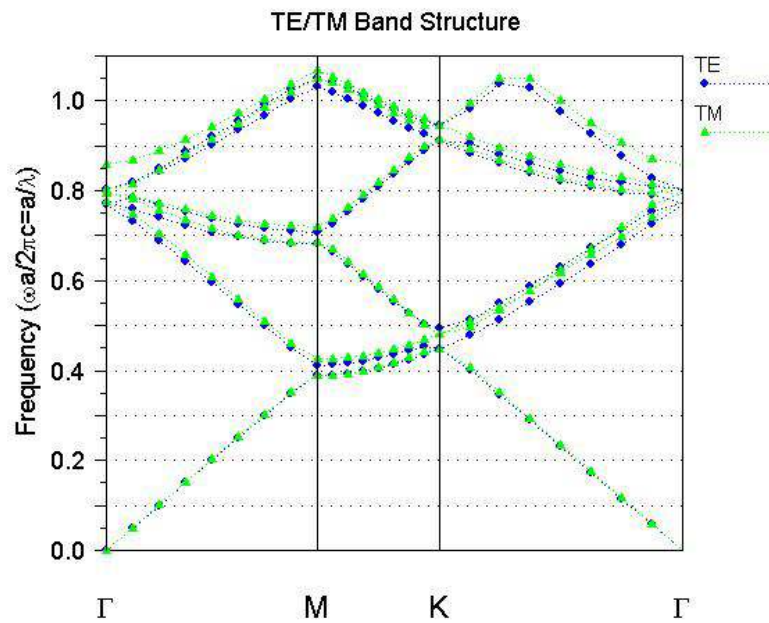


Figure 6.3 Photonic crystal band structure for 2D triangular lattice of air holes in PMMA slab of $n = 1.5$.

Notice that the frequency bands in Figure 6.3 were divided into TE and TM components. The 2D photonic crystal configuration is sensitive to the polarization state of the incident waves and each state satisfies a different, simplified wave equation. For moderate dielectric contrast, *e.g.*, $n_{high}/n_{low} < 2.7$, a band gap is only expected for the TM polarization state.¹⁶ In *BandSOLVE*, the TM state is defined as that which has its electric field vector parallel to the radial direction of the air holes as shown in Figure 6.2 and the TE state as that which has its electric field vector perpendicular. A complete band gap is considered to exist when two adjacent bands do not touch and the maximum point on the lower band is less than the minimum point on the upper band. For example, in the band structure above the first two TE bands, counted from the bottom up, intersect at the K point and the maximum point of the first TM band is at a higher frequency than the minimum of the second band, Figure 6.4. While there is no complete band gap for this initial photonic crystal configuration, there is a small, direction-dependent gap. Inspection of Figure 6.3 showed that at the M point, neither the first two TE nor the TM bands intersected, Figure 6.5. There are no frequencies in the range of 0.39 – 0.41 that exist between the Γ point and the M point for either polarization state, so waves in that narrow range traveling along the $\Gamma - M$ path would experience reflection.

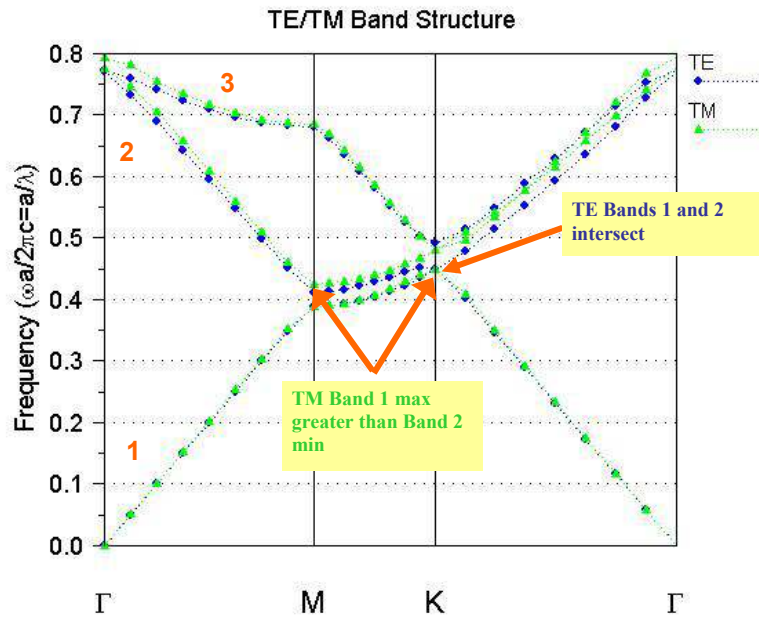


Figure 6.4 Close-up of initial band structure showing no complete band gap exists since adjacent bands either intersect or overlap.

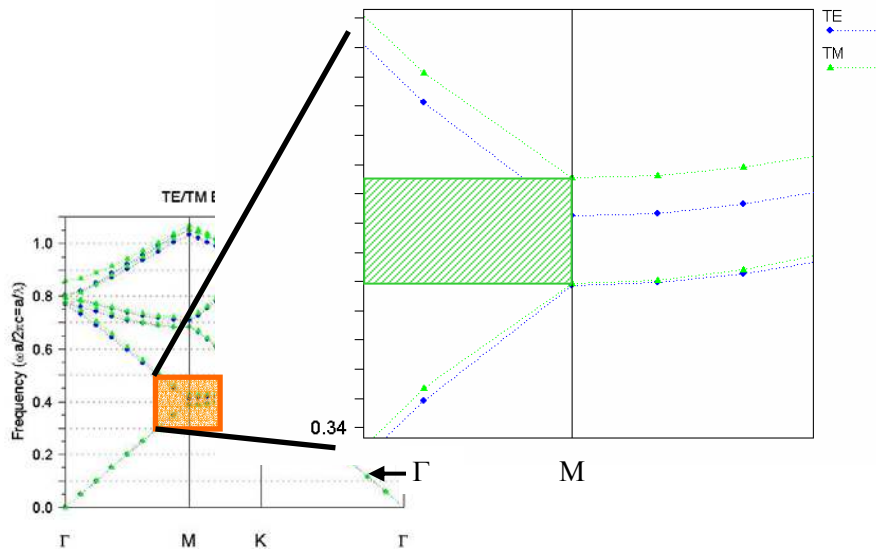


Figure 6.5 Direction dependent band gaps following $\Gamma - M$ path along Brillouin zone.

A complete band gap for the TM state in the lattice was obtained by varying the ratio of the hole radius to the lattice constant. As the ratio was increased, the separation between the first and second TM bands increased until a gap opened. The gap was open for a range of $r/a = 0.275 - 0.49$. This is shown as a gap map in Figure 6.6. A gap map compresses a series of band structures calculated during a parameter scan into one plot that shows the gap width, *i.e.*, the range of frequencies encompassed by the band gap, for each value of the parameter. The maximum gap width for a 2D, triangular lattice photonic crystal in a PMMA slab was found at $r/a = 0.37$ for a range of $\omega a/2\pi c = 0.49 - 0.51$. For the design wavelengths of 532 nm and 632 nm, that would correspond to $a = 266$ nm and 316 nm and $r = 98$ nm and 117 nm, respectively. In anticipation of an increase in the hole radii due to feature shrinkage during imprint and etch steps, a smaller ratio of $r/a = 0.3$ was chosen for the target template feature sizes.³⁸ That ratio corresponded to $a = 250$ nm and 292 nm and $r = 75$ nm and 87.6 nm, respectively.

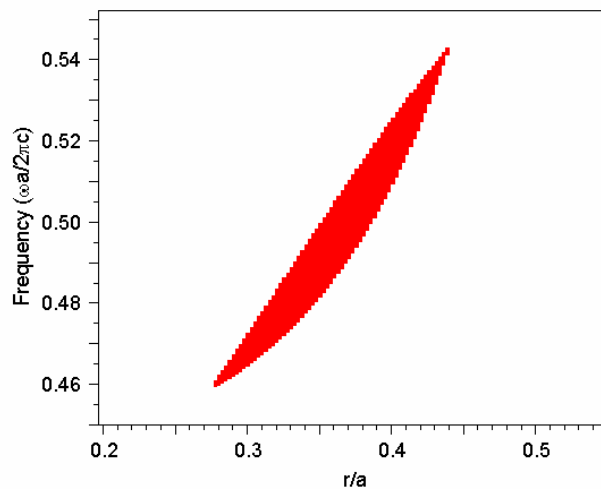


Figure 6.6 Gap map for triangular lattice of air holes in PMMA slab.

Once the dimensions for the lattice were determined, four separate structures were designed for inclusion on the template. Each structure included an array of posts with a length of $50a$ and a width of $40a$. In two of the structures, a line defect was introduced by removing one row of posts from the middle of the array to simulate a photonic crystal waveguide. These types of defects allow light that falls into the band gap to actually propagate through the crystal, potentially enabling waveguiding around sharp bends. They are also highly dispersive, *i.e.*, the observed group velocity of the guided light changes significantly with wavelength and is much less than that expected in a conventional waveguide of the same material. This characteristic is expected to be useful in combination with nonlinear optical phenomena.³³ The line defects were introduced along the $\Gamma - K$ direction of the crystal, though the orientation should not matter for a direction-independent band gap.

Two ridges nominally 500 nm wide and 0.5 cm in length were placed on either side of the arrays. These ridges aided in the location of the photonic crystal arrays, provided an easily cross-sectioned set of features to monitor etch depth and simulated a ridge waveguide on a negative tone template. Figure 6.7 shows the layout of these structures. As designed, they provide for confinement of light in the plane of the crystal structure. To achieve total confinement, conventional index guiding is needed in the vertical direction.²⁰ Index guiding is achieved through total internal reflection, so the top and bottom of the finished structure need to be clad with some lower refractive index material. Maximum index contrast for any photonic structure is obtained with air, so the top can be left exposed. For a PMMA structure ($n = 1.5$), the bottom cladding layer

needs to have a sufficiently low index. According to simulations from the RSoft Photonics Suite, the bottom cladding layer should have an index of $n = 1.3$ and the PMMA structure should have a thickness of $1 \mu\text{m}$. A higher cladding index or smaller film thickness would lead to significant coupling of light into the substrate and loss of signal intensity. An index of $n = 1.3$ is currently attainable only with polytetrafluoroethylene, or Teflon. Since the imprint process requires good adhesion among the components of the film stack on which the pattern is to be imprinted, the successful use of Teflon in the process will need to be verified. For this work a more conventional oxide cladding was employed by using silicon wafers with a $1 \mu\text{m}$ thick thermal SiO_2 layer (Addison Engineering, Inc., San Jose, CA) as the imprint substrates. For an oxide index of $n = 1.46$, the index of the PMMA would need to be increased to approximately $n = 1.56$ with a film thickness of $2 \mu\text{m}$ for adequate vertical confinement.

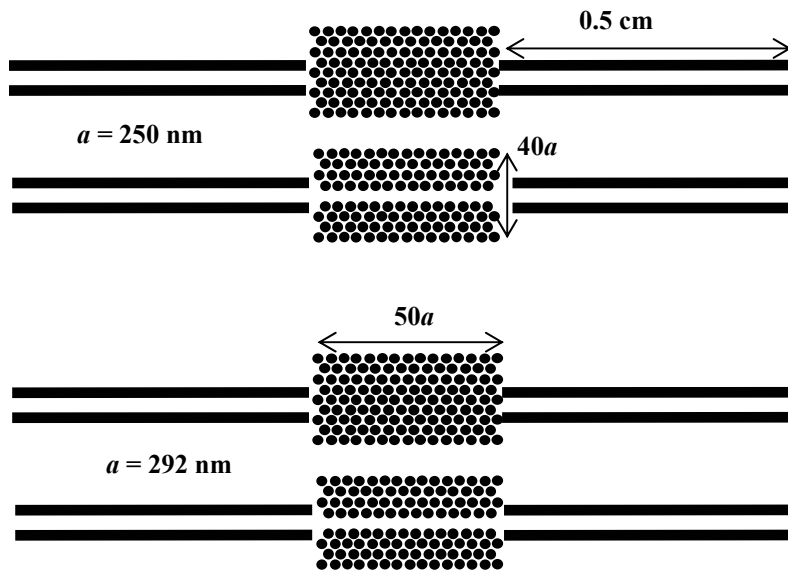


Figure 6.7 Layout of structures for photonic crystal template.

6.3.2 PREPARATION OF TEMPLATE BLANK

Templates for the Molecular Imprints Imprio SFIL tools are created from 65 x 65 mm² quartz plates that are 6.35 mm thick and have a raised area called a mesa in the center on which the features are created. These blanks can either be obtained from commercial sources or made from surplus 6 x 6 in² quartz plates used for photolithography reticles. The templates used for this work were created from a surplus reticle plate according to the procedure described in the template fabrication report submitted to SEMATECH.³⁹ Materials used for the template fabrication were available through the MRC unless otherwise noted. These surplus plates were obtained with chromium and photoresist already coated on the surface. The resist was removed with acetone, but the chromium left for mesa patterning. The plate was then recoated with AZ 5209E photoresist by spinning at 500 rpm and completely wetting the surface with acetone, then reducing the speed to 150 rpm to apply the resist, and finally coating at 900 rpm for 1.5 min. A post apply bake at 120°C was performed for 5 min and then the plate was allowed to cool for 5 min. The mesa area was patterned by contact printing using a mask with a 25 x 25 mm² area defined by chromium and a 6 min exposure at 10,000 mV/cm² from a mercury arc lamp. The resist was developed by applying AZ 726 MIF developer during spinning at 200 rpm until the surface was covered, then puddle developing for approximately 1 min. The developer was rinsed away by spinning the plate at 300 rpm and spraying with DI water, and dried by baking at 120°C for 5 min. The exposed chromium was removed by a wet etch using a commercial chromium etchant (typically a solution of 25 wt% ceric ammonium nitrate and 10 wt% perchloric

acid). A 15 μm high mesa was formed by a 3 hr wet etch in a buffered oxide etch solution (6:1 40 wt% NH_4F to 49 wt% HF). This process creates four mesas on the plates. The individual template blanks were obtained by recoating a protective layer of photoresist over the surface of the plate and then sending it to Applied Laser Solutions (Union City, CA) to be diced into four 65 x 65 mm^2 pieces.

6.3.3 ELECTRON BEAM LITHOGRAPHY PATTERNING

Once the template blanks were obtained, the photonic crystal structures shown in Figure 6.7 were patterned using e-beam lithography. The patterning involved several steps. First, the structures were drawn and the e-beam exposure was optimized through a series of dose tests. Once the appropriate dose was determined, the template was prepared for patterning. After exposure, the resist was developed and the template dried in preparation for dry etching.

The photonic crystal structures were drawn using an AutoCAD program and converted to a file type compatible with the e-beam tool's operating software according to the instructions in Reference 39. The structures were then patterned on 4" silicon wafers at a range of electron doses to determine the proper e-beam exposure conditions. The wafers were first treated with hexamethyldisilazane (HMDS) vapor in a YES HMDS oven at 150°C for 2 min to improve adhesion of the photoresist. They were spin coated with NEB 31A3 negative tone e-beam resist at 3000 rpm for 60s followed by a post apply bake (PAB) at 110°C for 2 min. After exposure, a post exposure bake (PEB) at 90°C for

3 min was performed. The resist was then developed by soaking the wafers in CD-26 (0.26 N TMAH) developer for approximately 50 s, and then quenched in DI water.

The exposures were performed on a JEOL JBX-6000FS/E electron beam lithography system with the accelerating energy set at 50 KeV and the current at 75 pA. The dose was ranged from 7 – 14 $\mu\text{C}/\text{cm}^2$. For exposure doses above 9 $\mu\text{C}/\text{cm}^2$, the individual features did not resolve clearly. An example is shown in Figure 6.8, which shows scanning electron micrograph (SEM) of a field exposed at 10 $\mu\text{C}/\text{cm}^2$ with a nominal feature size of 150 nm ($r = 75$ nm). For the fields exposed at 7 – 9 $\mu\text{C}/\text{cm}^2$, the diameters of the post features were measured and plotted against the dose in Figure 6.9. Assuming a linear increase in feature size with dose between the 7 $\mu\text{C}/\text{cm}^2$ and 7.5 $\mu\text{C}/\text{cm}^2$ points on the chart in Figure 6.9, it was determined that that and exposure of 7.25 $\mu\text{C}/\text{cm}^2$ was needed to achieve the target post sizes of 150 nm and 175 nm ($r = 87.5$ nm). Figure 6.10 shows the measured feature sizes for fields exposed at 7.3 $\mu\text{C}/\text{cm}^2$.

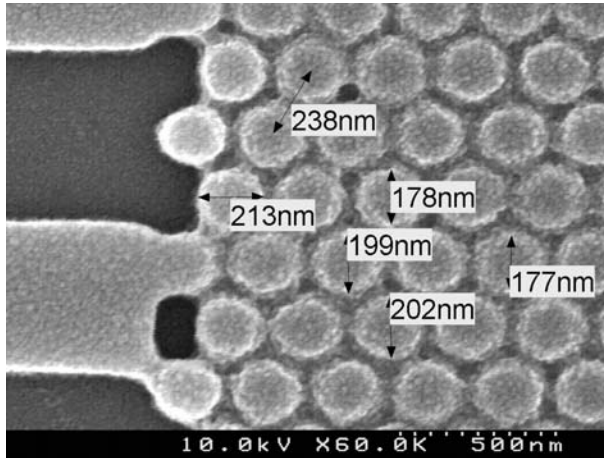


Figure 6.8 Scanning electron micrograph of photonic crystal structure exposed at $10 \mu\text{C}/\text{cm}^2$ with 150 nm nominal feature sizes.

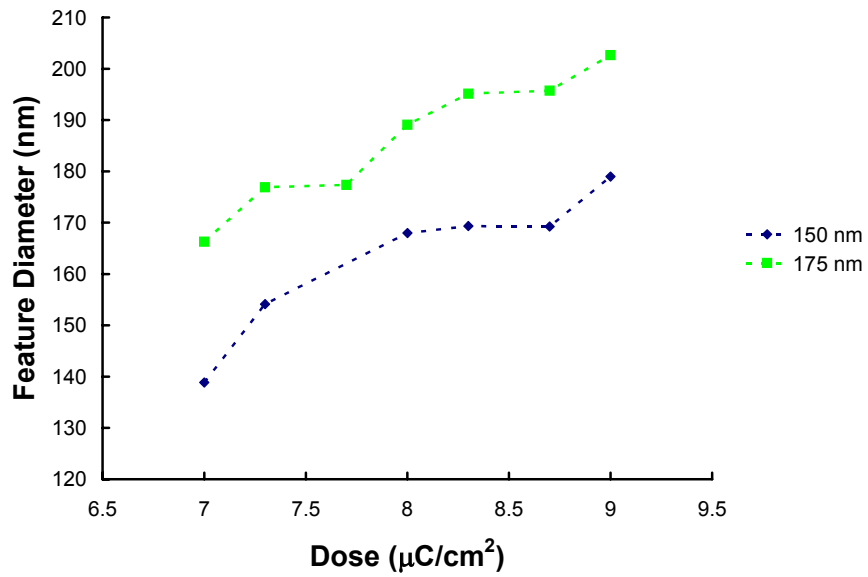


Figure 6.9 Feature diameter vs. e-beam exposure dose for 150 nm and 175 nm posts.

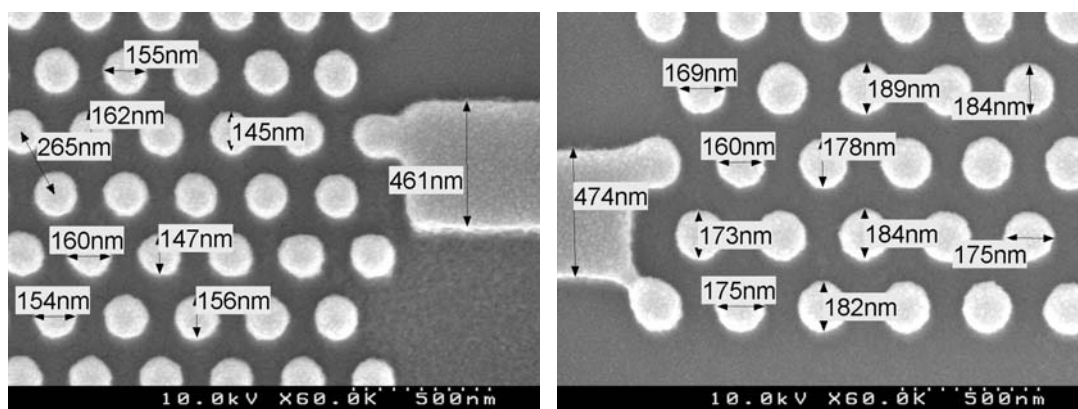


Figure 6.10 SEMs of nominally 150 nm and 175 nm posts exposed at $7.3 \mu\text{C}/\text{cm}^2$.

The template blanks were prepared for patterning by the same procedures as the wafers with two exceptions. First, a 15 nm film of chromium was deposited on the template surface by evaporation in a CHA metal deposition tool before coating with resist. The chromium served as a charge dissipation layer during the exposure to avoid a buildup of electrons at the resist–quartz interface. Second, the PAB and PEB temperatures were increased by 15°C and both timed at 4 min. The initial attempt at the template fabrication followed the bake recipes used for the wafers; the resulting pattern had no discernable photonic crystal structure and the ridges were oversized and almost completely merged together, Figure 6.11. It was found that as a result of the non-negligible thickness, thermal mass and insulating characteristic of the template plate, the surface took approximately 1 min to reach an equilibrium temperature that was about 15°C cooler than the set temperature of the hotplate. Once the exposure was complete, the resist was developed as described previously and the surface dried by light blow drying with an N_2 gun. The template fabrication procedure is summarized in Table 6.1.

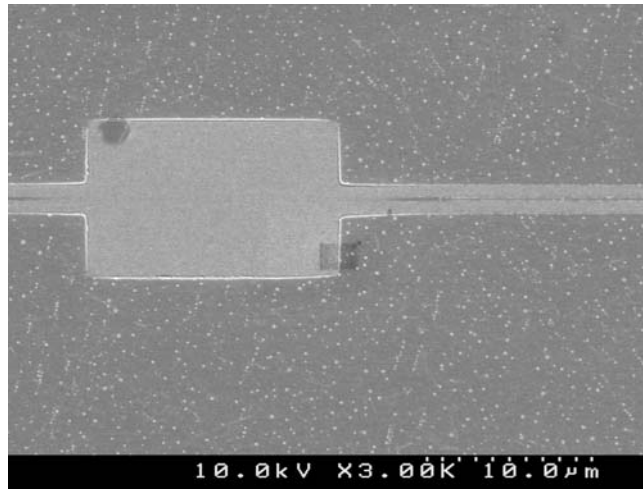


Figure 6.11 SEM of test imprint from first template showing no photonic crystal structure and oversized ridges almost merged together.

Table 6.1 Template fabrication procedure for NEB 31A3 resist.

Step	Process	Conditions
1	<i>Chromium Deposition</i>	thickness = 15 nm
2	<i>HMDS Treatment</i>	T = 150 °C t = 2 min
3	<i>Spin Coating</i>	Speed = 3000 rpm t = 60 s
4	<i>PAB</i>	T = 125 °C t = 4 min
5	<i>E-beam Exposure</i>	Dose = 7.25 $\mu\text{C}/\text{cm}^2$
6	<i>PEB</i>	T = 110 °C t = 4 min
7	<i>Development</i>	t = 50 s DI rinse

6.3.4 DRY ETCH PATTERN TRANSFER

Pattern transfer into the quartz was achieved by a three step dry etch process in a Trion Oracle III reactive ion etch (RIE) system. The first etch step was a descum step to remove resist scum from the development. The second was a chromium etch to reveal the quartz surface. The final step was the quartz etch to transfer the pattern into the template. The process conditions used for each etch step are given in Table 6.2.

Table 6.2 Process conditions for etch transfer into template.

Etch Process	Gas Flow Rates (sccm)	Pressure (mT)	RF Power (W)	Time (s)
<i>Descum</i>	O ₂ = 2 He = 70	35	20	30
<i>Chromium</i>	Cl ₂ = 40 O ₂ = 10	30	80	200
<i>Quartz</i>	He = 40 CF ₄ = 15	15	130	400

6.3.5 PATTERN VERIFICATION

After the template fabrication was completed, the photonic crystal structure on the final template was verified by direct examination in a Hitachi S-4500 field emission scanning electron microscope and by examination of test imprints. To obtain clear images of the template surface, a larger amount of gold was deposited on the surface than is typical (approximately 1 min sputter time versus 20 s for a polymer on Si) and a piece of copper tape was used to ground the template surface to the SEM stage. Four micrographs of the template are shown in Figure 6.12. The first two show examples of

structures with and without a line defect. The second two show close-up views of the structures. Note that the structure set was actually repeated three times on the template mesa since there was a large area available for patterning, so the micrographs only show a few examples. The images in Figure 6.12 also showed some color variation in the post arrays. This was most likely due to residual resist and chromium on the posts causing some height variation. Some scumming was also evident around a few arrays, but not all. This could have been the result of incomplete development at these locations or some precipitation of photoresist during the rinse.

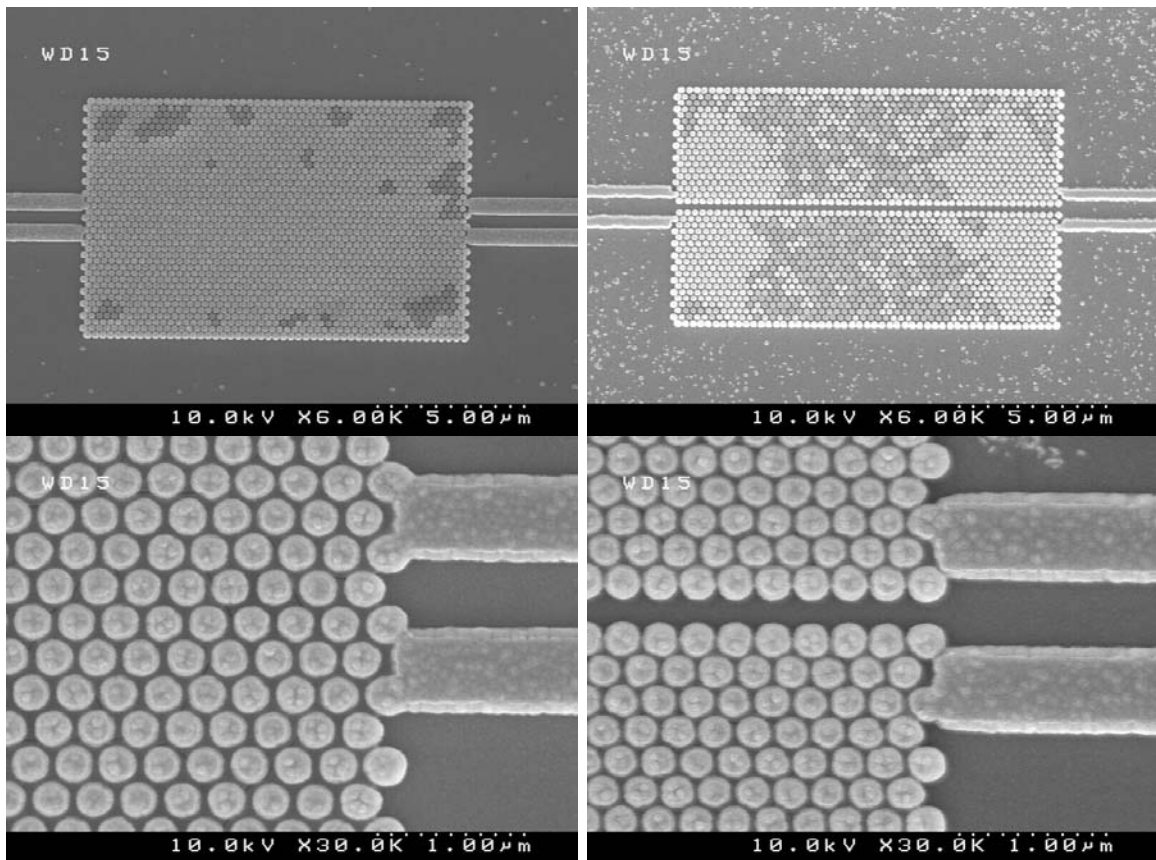


Figure 6.12 SEM micrographs of photonic crystal structures on SFIL template.

The feature sizes were verified by making test imprints. The test imprints were made in a mixture of 65 wt% isobornyl acrylate (Sigma-Aldrich, St. Louis, MO), 30 wt% ethylene glycol diacrylate (Sigma-Aldrich) and Darocur 1173 photoinitiator (Ciba Specialty Chemicals, Newport, DE) on silicon wafers treated with AP410 adhesion promoter (Silicon Resources, Inc., Chandler, AZ). The adhesion promoter was applied by spin coating at 3000 rpm for 30 s followed by a PAB at 100°C for 30 s. A drop of the imprintable mixture was then placed on the wafer and the template placed on top. The mixture was allowed to fill the area under the mesa and then photocured by a blanket exposure from a mercury arc lamp for 90 s. Figure 6.13 shows a complete view of one of the photonic crystal arrays and Figure 6.14 shows the measurements of features for both nominal 150 nm and 175 nm structures. These measurements revealed that the imprinted feature sizes in the test imprint formulation matched well with the target sizes. Figure 6.15 shows a cross-section of the guide ridges and an imprint depth of approximately 200 nm.

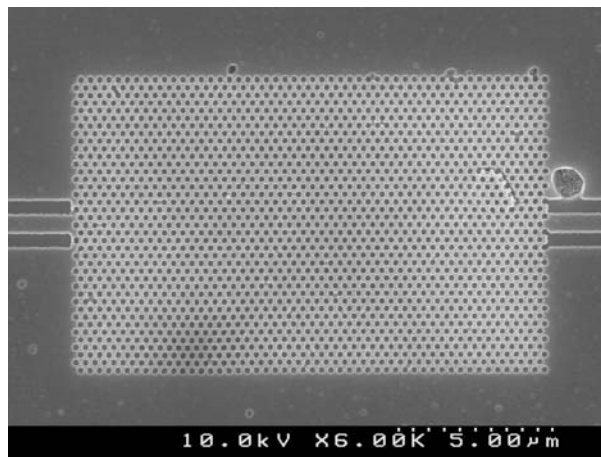


Figure 6.13 Micrograph of photonic crystal structure in test imprint.

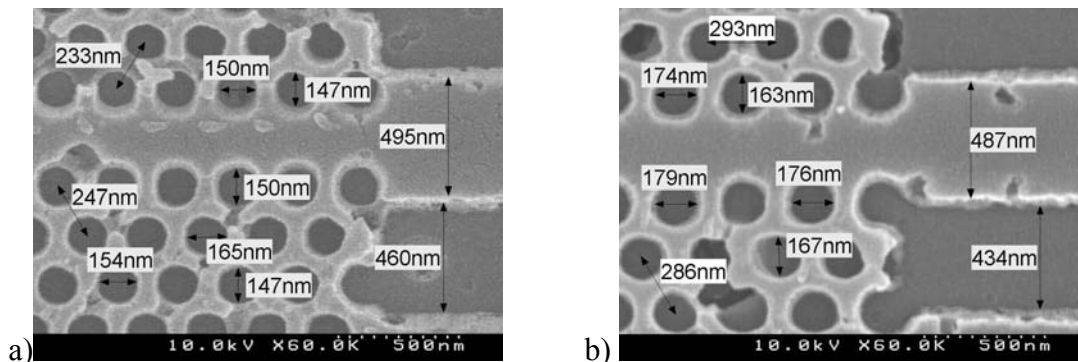


Figure 6.14 Micrographs of a) 150 nm nominal photonic crystal features and b) 175 nm nominal features.

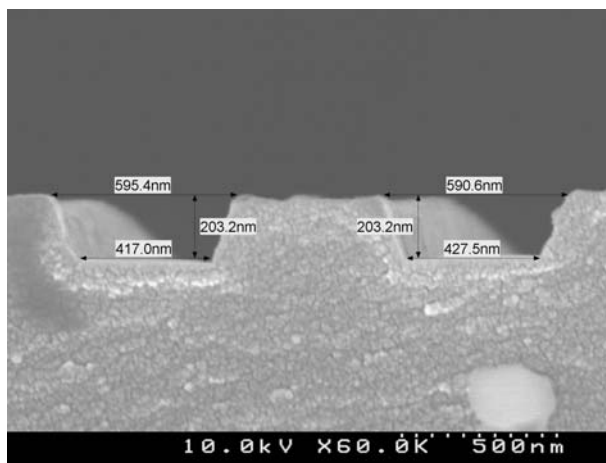


Figure 6.15 Cross-section micrograph of guide ridges showing 200 nm imprint depth.

6.4 FABRICATION OF POLYMER PHOTONIC CRYSTAL

Following the completion of the photonic crystal template, SFIL patterning of a polymer-based photonic crystal pattern was demonstrated. Two polymer samples were used for the demonstration, with one containing an additive that increased the polymer's refractive index. The photonic crystal structures were imprinted into a standard SFIL

imprint material and then etched into the polymer samples. The final feature sizes were then used to determine what band gap should exist according to the previous calculations.

6.4.1 MATERIALS

The polymer used for this demonstration was a 350,000 molecular weight (MW) PMMA (Polysciences, Inc., Warrington, PA). PMMA was chosen for its compatibility as a transfer layer with the acrylate imprint materials used in the SFIL process, as well as its transparency through the visible spectrum. A 7 wt% PMMA solution in chlorobenzene (Sigma-Aldrich) was prepared and films were spin coated at 2500 rpm for 45 s with a PAB at 180°C for 90 s for a thickness of 750 nm. Double side polished 4" silicon wafers were used for imprinting. The high index additive was an organic laser dye, 3-(2'-benzothiazolyl)-7-diethylaminocoumarin, or coumarin 6 (Acros Organics, Morris Plains, NJ). In addition to the coumarin 6 dye, several proprietary benzoxazinone dyes from Clariant Corporation were investigated. These dyes were chosen as high index additives because they exhibited sharp absorption edges in the visible region which could lead to significant index increases, as described in the previous chapter. Their structures are shown in Figure 6.16. Absorption spectra were measured for the coumarin 6 and two of the Clariant dyes dissolved in acetonitrile at approximately 10 µg/mL, Figures 6.17 and 6.18. The coumarin 6 and several Clariant dyes were added to PMMA solutions at a 10 wt% loading relative to the polymer. Composite films were prepared by the same procedure as the polymer, and their refractive indices and extinction coefficients were measured by ellipsometry, Figure 6.19 and 6.20. The coumarin 6 composite had higher

index values that the others, with $n = 1.56$ at 532 nm and 1.54 at 632 nm. The Clariant dye composites experienced a more modest increase in the refractive index close to their absorption peak at 350 nm, but all had larger n values than PMMA throughout the spectral region measured. The Clariant dyes would be useful additives for applications requiring the use of wavelengths below 532 nm where the coumarin 6 starts to exhibit significant absorption. For the current demonstration, the coumarin 6 additive was chosen as an example for fabrication. Assuming a constant index value of $n = 1.55$, a gap map for the PMMA/coumarin 6 composite was also calculated, Figure 6.21.

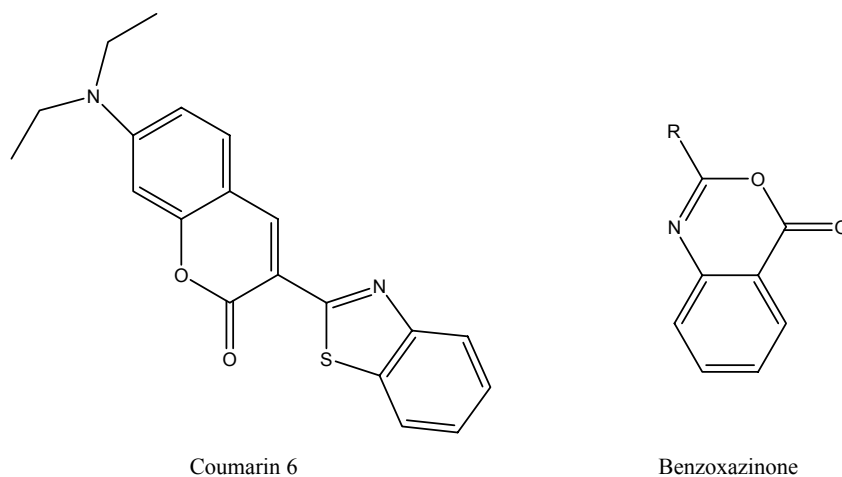


Figure 6.16 Structures of coumarin 6 and generic Clariant benzoxazine dye.

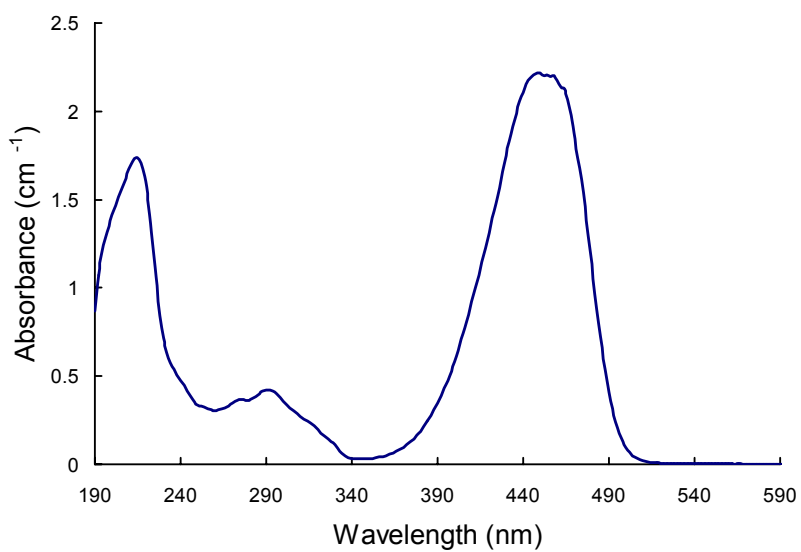


Figure 6.17 Absorption spectrum of coumarin 6.

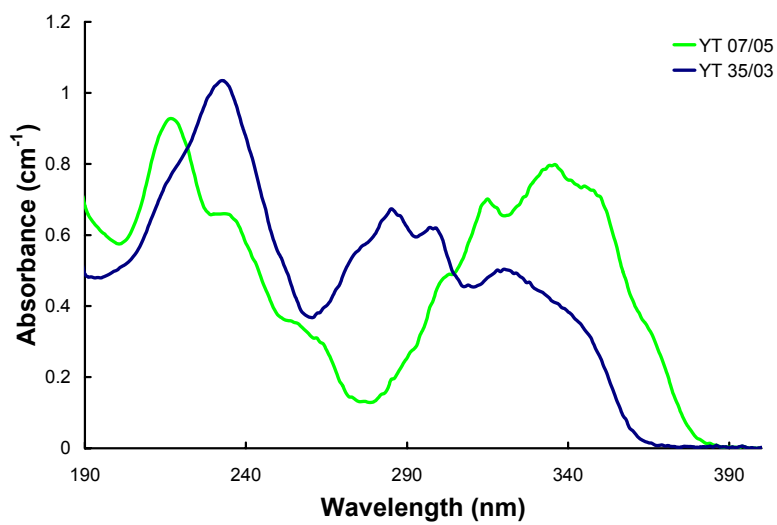


Figure 6.18 Absorption spectra for two Clariant benzoxazine dyes.

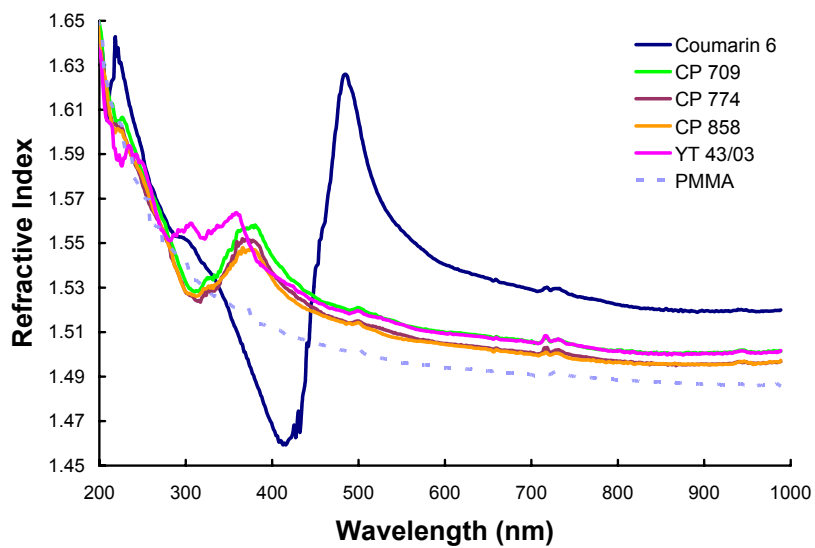


Figure 6.19 Refractive index dispersion curves for PMMA and dye composite films.

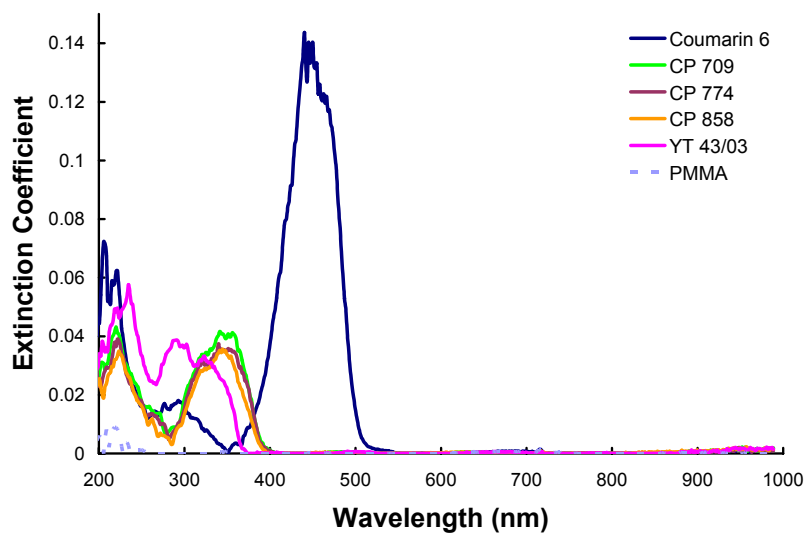


Figure 6.20 Extinction coefficient dispersion curves for PMMA and dye composite films.

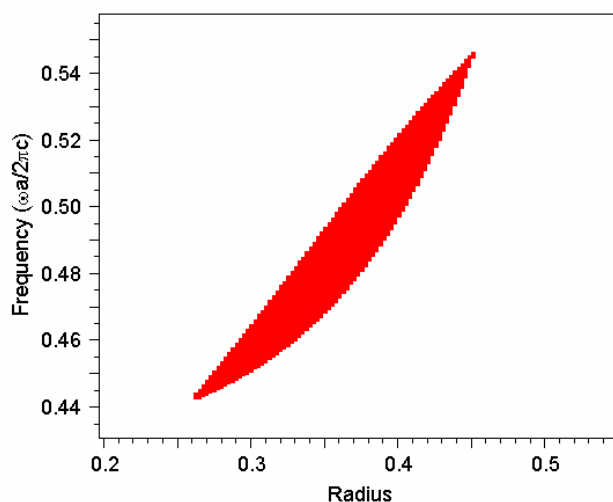


Figure 6.21 Gap map for triangular lattice in PMMA/coumarin 6 composite.

6.4.2 SFIL PROCESS

The imprinting was performed on a Molecular Imprints Imprio 100 imprint tool. Before imprinting, the template was treated with a fluorinated self-assembled monolayer (FSAM) release layer by soaking it for approximately one hour in a 0.5 wt% (tridecafluoro-1,1,2,2-tetra-hydrooctyl)dimethylchlorosilane (Gelest, Inc., Morrisville, PA) solution in toluene followed by an N₂ dry. The template was loaded onto the tool and leveled based on a 16 point measurement. A coated wafer was then loaded and also leveled based on the 16 point measurement. The imprint material used was Molecular Imprints' standard silicon-containing etch barrier, called Sil-Mat. The imprint recipe used a standard drop pattern with 0.23 μL of the Sil-Mat dispensed. A 12 N imprint force was used with a 180 s delay after the template contacted the Sil-Mat, followed by a 10 s exposure to photocure. The typical separation force between the template and the polymerized Sil-Mat was approximately 25 N. The resulted imprint films were 210 –

230 nm thick according to ellipsometric measurements, so the etch barrier residual layer was thin compared to the imprint. Figure 6.22 shows several imprinted fields, and Figure 6.23 shows a close-up view with measurements of the feature sizes. From the micrographs in Figure 6.22, taken after over one hundred imprints had been made with the template, it could be seen that defects had formed in some of the structures but others maintained their integrity over time. The feature measurements from the fields in Figure 6.23 indicated that after imprint the hole dimensions were, on average, within 10% of their nominal values. This result is consistent with previous studies of feature shrinkage do to polymerization induced densification of the imprint film.^{38, 40}

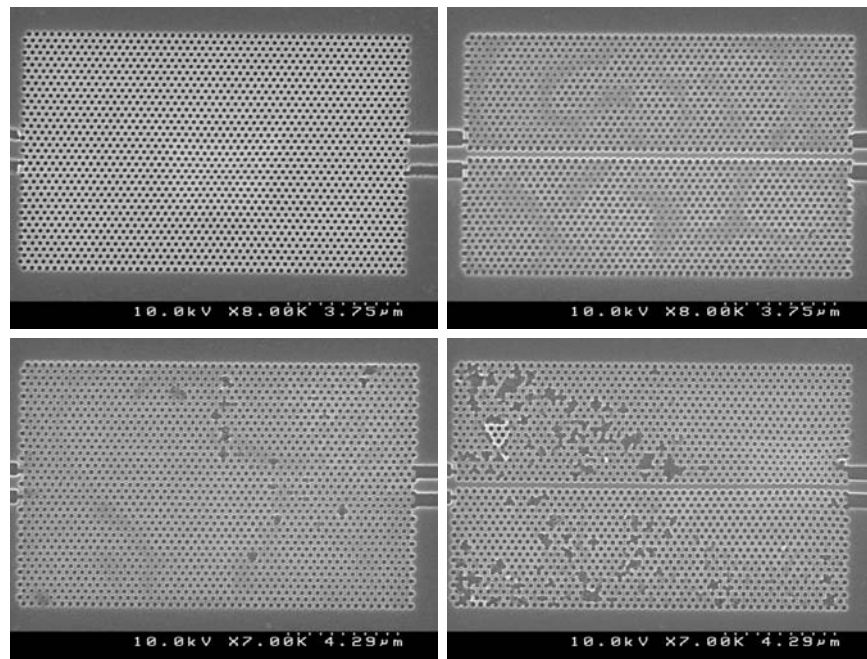


Figure 6.22 SEM micrographs of imprinted photonic crystal structures showing defect-free and defect-containing fields after over one hundred imprints.

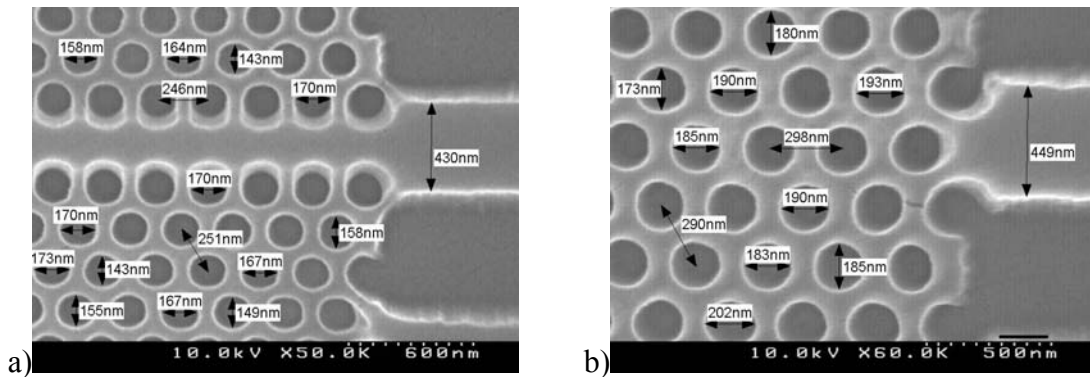


Figure 6.23 SEM micrographs showing feature measurements of a) 150 nm nominal features and b) 175 nm nominal features.

6.4.3 BREAKTHROUGH AND TRANSFER ETCHES

The final step in the polymer photonic crystal fabrication process was to transfer the imprinted patterns into the polymer underneath. This required a two step etch process. The first was to breakthrough the residual etch barrier layer and the second was to etch into the polymer. The etch recipes for each step and the corresponding etch rates are given in Table 6.3. These etch processes were performed in a Plasma-Therm 790 Series RIE. Etch rates were determined by using ellipsometry to measure film thickness before and after etching blanket films. Etch times were then determined from measurements of the samples' polymer and imprint film thicknesses by ellipsometry.

Table 6.3 Etch recipes for photonic crystal pattern transfer into PMMA.

Etch Process	Gas Flow Rates (sccm)	Pressure (mT)	DC (V)	Etch Rate (nm/min)
<i>Breakthrough</i>	CHF ₃ = 15 O ₂ = 3	25	200	30
<i>Transfer</i> • <i>PMMA</i> • <i>w/coumarin 6</i>	O ₂ = 8	5	250	• 89 • 78

The thicknesses of the PMMA films required transfer etch times of 9 – 11.5 min. These long etch times resulted in undercutting from the relatively isotropic oxygen transfer etch. This undercutting appeared to exacerbate some of the defects seen in Figure 6.22 and damaged some outlying parts of the imprint fields, Figure 6.24. This result could have been improved by using thinner polymer films to reduce the etch time, and indicated that the available tooling limited the thickness of the structure that could be fabricated. This thickness limitation prohibited the vertical confinement necessary to probe the characteristics of the photonic crystal pattern. Fortunately, the defect-free fields remained so during the entire etch time, Figure 6.25. The diameter of the holes also increased during the etch process. Figure 6.26 shows a nominally 175 nm hole structure whose average diameter increased to 200 nm. After fabrication, the polymer photonic crystals had a radius to lattice constant ratio of $r/a = 0.34$ instead of the original value of 0.3. For the PMMA crystal structure, that corresponded to a gap for the frequencies $\omega a/2\pi c = 0.477 - 0.494$. For the defect-free 175 nm structure, $a = 292$ nm so the band gap would exist for the wavelengths from 591 nm – 612 nm. For the

PMMA/coumarin 6 composite, the gap would exist for $\omega a/2\pi c = 0.464 - 0.488$, or the wavelength range of 598 nm – 629 nm.

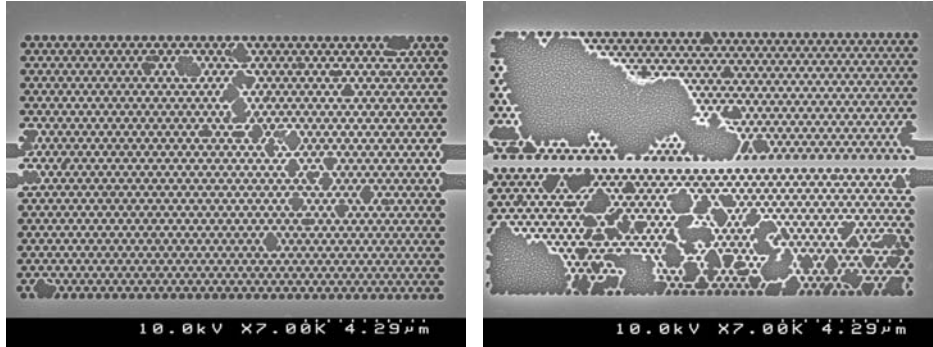


Figure 6.24 SEM micrographs of structures with undercut defects.

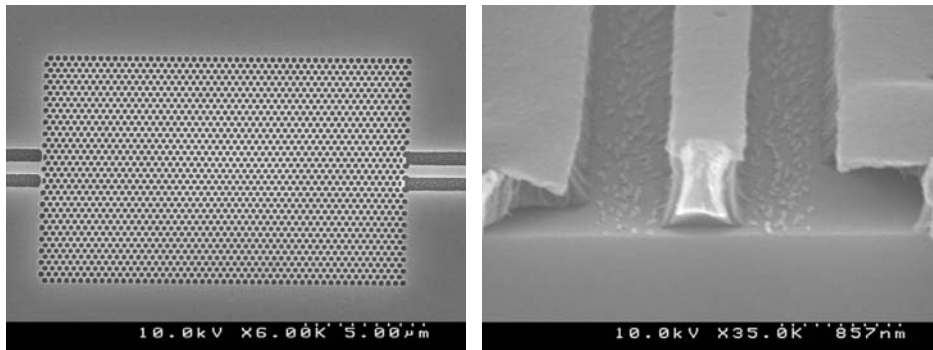


Figure 6.25 SEM micrographs of defect-free structure after etch and cross-section view of guide ridges confirming complete etch transfer into polymer film.

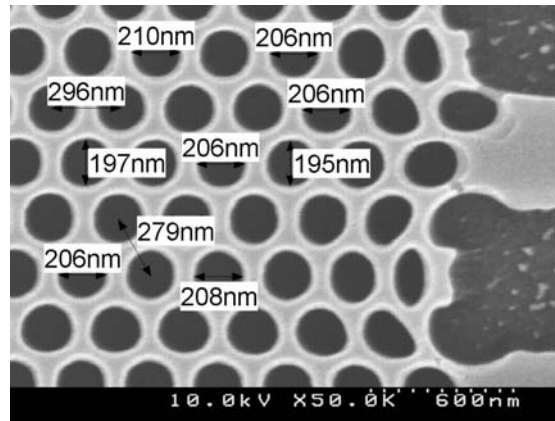


Figure 6.26 Micrograph showing feature measurements of 175 nm nominal features.

6.5 SUMMARY

The process steps needed to fabricate a two-dimensional photonic crystal by step and flash imprint lithography have been demonstrated. A photonic crystal pattern with a band gap in the visible region was designed and a template with the pattern was created using a negative tone e-beam process. This template fabrication procedure was included as part of a SEMATECH report on nanoimprint process development at the UT MRC. The template was then used to develop the SFIL patterning and etch processes to transfer the pattern into a polymer. Increases in the crystal's radial dimensions, primarily as a result of the etch process, shifted the band gap of the final structure away from the original design range. This shift could be compensated for by the addition of a high index additive to the polymer.

A demonstration of the photonic crystal requires refinement of the current process. The anisotropy of the transfer etch process needs to be improved to accommodate structure thicknesses of one micron or greater. Access to a more

sophisticated etch tool with better performance will likely be needed for sufficient anisotropy. Alternatively, an imprint process that incorporates a Teflon substrate could be developed. Further development of additives to raise the refractive index of the base polymer would lead to improvements in light confinement as well as a larger wavelength range of operation for the photonic crystal.

6.6 REFERENCES

1. Lopez, C. "Materials aspects of photonic crystals." *Advanced Materials* **2003**, *15* (20), 1679-1704.
2. Yablonovitch, E. "Inhibited spontaneous emission in solid-state physics and electronics." *Physical Review Letters* **1987**, *58* (20), 2059-62.
3. John, S. "Strong localization of photons in certain disordered dielectric superlattices." *Physical Review Letters* **1987**, *58* (23), 2486-9.
4. Yablonovitch, E.; Gmitter, T. J.; Leung, K. M. "Photonic band structure: the face-centered-cubic case employing nonspherical atoms." *Physical Review Letters* **1991**, *67* (17), 2295-8.
5. Yablonovitch, E.; Gmitter, T. J.; Meade, R. D.; Rappe, A. M.; Brommer, K. D.; Joannopoulos, J. D. "Donor and acceptor modes in photonic band structure." *Physical Review Letters* **1991**, *67* (24), 3380-3.
6. Yablonovitch, E. "Photonic band-gap structures." *Journal of the Optical Society of America B: Optical Physics* **1993**, *10* (2), 283-95.
7. Joannopoulos, J. D.; Meade, R. D.; Winn, J. N., *Photonic Crystals: Molding the Flow of Light*. Princeton University Press: Princeton, N.J., **1995**; p 137.

8. Villeneuve, P. R.; Abrams, D. S.; Fan, S.; Joannopoulos, J. D. "Single-mode waveguide microcavity for fast optical switching." *Optics Letters* **1996**, *21* (24), 2017-2019.
9. Villeneuve, P. R.; Fan, S.; Joannopoulos, J. D. "Microcavities in photonic crystals: mode symmetry, tunability, and coupling efficiency." *Physical Review B: Condensed Matter* **1996**, *54* (11), 7837-7842.
10. Fan, S.; Villeneuve, P. R.; Joannopoulos, J. D.; Schubert, E. F. "High extraction efficiency of spontaneous emission from slabs of photonic crystals." *Physical Review Letters* **1997**, *78* (17), 3294-3297.
11. Joannopoulos, J. D.; Villeneuve, P. R.; Fan, S. "Photonic crystals: putting a new twist on light." *Nature* **1997**, *386* (6621), 143-149.
12. Sakoda, K. "Optical transmittance of a two-dimensional triangular photonic lattice." *Physical Review B: Condensed Matter* **1995**, *51* (7), 4672-5.
13. Sakoda, K. "Symmetry, degeneracy, and uncoupled modes in two-dimensional photonic lattices." *Physical Review B: Condensed Matter* **1995**, *52* (11), 7982-6.
14. Sakoda, K. "Transmittance and Bragg reflectivity of two-dimensional photonic lattices." *Physical Review B: Condensed Matter* **1995**, *52* (12), 8992-9002.
15. Lin, H. B.; Tonucci, R. J.; Campillo, A. J. "Observation of two-dimensional photonic band behavior in the visible." *Applied Physics Letters* **1996**, *68* (21), 2927-2929.
16. Barra, A.; Cassagne, D.; Jouanin, C. "Existence of two-dimensional absolute photonic band gaps in the visible." *Applied Physics Letters* **1998**, *72* (6), 627-629.
17. Rosenberg, A.; Tonucci, R. J.; Bolden, E. A. "Photonic band-structure effects in the visible and near ultraviolet observed in solid-state dielectric arrays." *Applied Physics Letters* **1996**, *69* (18), 2638-2640.

18. Saravanamuttu, K.; Blanford, C. F.; Sharp, D. N.; Dedman, E. R.; Turberfield, A. J.; Denning, R. G. "Sol-Gel Organic-Inorganic Composites for 3-D Holographic Lithography of Photonic Crystals with Submicron Periodicity." *Chemistry of Materials* **2003**, *15* (12), 2301-2304.
19. Lin, S. Y.; Fleming, J. G.; Hetherington, D. L.; Smith, B. K.; Biswas, R.; Ho, K. M.; Sigalas, M. M.; Zubrzycki, W.; Kurtz, S. R.; Bur, J. "A three-dimensional photonic crystal operating at infrared wavelengths." *Nature (London)* **1998**, *394* (6690), 251-253.
20. Johnson, S. G.; Fan, S.; Villeneuve, P. R.; Joannopoulos, J. D.; Kolodziejski, L. A. "Guided modes in photonic crystal slabs." *Physical Review B: Condensed Matter and Materials Physics* **1999**, *60* (8), 5751-5758.
21. Imada, M.; Noda, S.; Chutinan, A.; Tokuda, T.; Murata, M.; Sasaki, G. "Coherent two-dimensional lasing action in surface-emitting laser with triangular-lattice photonic crystal structure." *Applied Physics Letters* **1999**, *75* (3), 316-318.
22. Smith, C. J. M.; Benisty, H.; Olivier, S.; Rattier, M.; Weisbuch, C.; Krauss, T. F.; De La Rue, R. M.; Houdre, R.; Oesterle, U. "Low-loss channel waveguides with two-dimensional photonic crystal boundaries." *Applied Physics Letters* **2000**, *77* (18), 2813-2815.
23. Moosburger, J.; Kamp, M.; Forchel, A.; Ferrini, R.; Leuenberger, D.; Houdre, R.; Anand, S.; Berggren, J. "Nanofabrication of high quality photonic crystals for integrated optics circuits." *Nanotechnology* **2002**, *13* (3), 341-345.
24. Sugimoto, Y.; Ikeda, N.; Carlsson, N.; Asakawa, K.; Kawai, N.; Inoue, K. "AlGaAs-based two-dimensional photonic crystal slab with defect waveguides for planar lightwave circuit applications." *IEEE Journal of Quantum Electronics* **2002**, *38* (7), 760-769.
25. Todaro, M. T.; Stomeo, T.; Vitale, V.; DeVittorio, M.; Passaseo, A.; Cingolani, R.; Romanato, F.; Businaro, L.; Di Fabrizio, E. "Nanofabrication of high refractive index contrast two-dimensional photonic crystal waveguides." *Microelectronic Engineering* **2003**, *67-68*, 670-675.

26. Jiang, Y.; Jiang, W.; Chen, X.; Gu, L.; Howley, B.; Chen, R. T. "Nano-photonic crystal waveguides for ultra-compact tunable true time delay lines." *Proceedings of SPIE-The International Society for Optical Engineering* **2005**, 5733 (Photonic Crystal Materials and Devices III), 166-175.
27. Stewart, M. D.; Johnson, S. C.; Sreenivasan, S. V.; Resnick, D. J.; Willson, C. G. "Nanofabrication with step and flash imprint lithography." *Journal of Microlithography, Microfabrication, and Microsystems* **2005**, 4 (1), 011002/1-011002/6.
28. Khusnatdinov, N.; Doyle, G.; Miller, M.; Stacey, N.; Watts, M.; Labrake, D. L. "Fabrication of nano and micro optical elements by step and flash imprint lithography." *Proceedings of SPIE - The International Society for Optical Engineering* **2006**, 6110 (Micromachining Technology for Micro-Optics and Nano-Optics IV), 61100.
29. Stewart, M. D.; Willson, C. G. "Imprint materials for nanoscale devices." *MRS Bulletin* **2005**, 30 (12), 947-952.
30. Fink, Y.; Urbas, A. M.; Bawendi, M. G.; Joannopoulos, J. D.; Thomas, E. L. "Block copolymers as photonic bandgap materials." *Journal of Lightwave Technology* **1999**, 17 (11), 1963-1969.
31. Kim, W.-S.; Yoon, K. B.; Bae, B.-S. "Nanopatterning of photonic crystals with a photocurable silica-titania organic-inorganic hybrid material by a UV-based nanoimprint technique." *Journal of Materials Chemistry* **2005**, 15 (42), 4535-4539.
32. Loncar, M.; Nedeljkovic, D.; Doll, T.; Vuckovic, J.; Scherer, A.; Pearsall, T. P. "Waveguiding in planar photonic crystals." *Applied Physics Letters* **2000**, 77 (13), 1937-1939.
33. Notomi, M.; Yamada, K.; Shinya, A.; Takahashi, J.; Takahashi, C.; Yokohama, I. "Extremely large group-velocity dispersion of line-defect waveguides in photonic crystal slabs." *Physical review letters* **2001**, 87 (25), 253902.
34. Zelsmann, M.; Picard, E.; Charvolin, T.; Hadji, E.; Heitzmann, M.; Dal'zotto, B.; Nier, M. E.; Seassal, C.; Rojo-Romeo, P.; Letartre, X. "Broadband optical

- characterization and modeling of photonic crystal waveguides for silicon optical interconnects." *Journal of Applied Physics* **2004**, 95 (3), 1606-1608.
35. Jiang, Y.; Jiang, W.; Gu, L.; Chen, X.; Chen, R. T. "80-micron interaction length silicon photonic crystal waveguide modulator." *Applied Physics Letters* **2005**, 87 (22), 221105-3.
 36. Meade, R. D.; Rappe, A. M.; Brommer, K. D.; Joannopoulos, J. D.; Alerhand, O. L. "Accurate theoretical analysis of photonic band-gap materials." *Physical Review B* **1993**, 48 (11), 8434.
 37. Johnson, S. G.; Joannopoulos, J. D. "Block-iterative frequency-domain methods for Maxwell's equations in a planewave basis." *Optics Express* **2001**, 8 (3), 173-190.
 38. Johnson, S. C. *Step and flash imprint lithography: Materials and process development*. PhD Dissertation, The University of Texas at Austin, Austin, TX, USA, **2005**.
 39. Vandenberghe, K. *Nanoimprint Lithography (NIL) Template Creation Process at the University of Texas - Microelectronics Research Center (UT-MRC) in Austin*; SEMATECH: 2007.
 40. Colburn, M.; Suez, I.; Choi, B. J.; Meissl, M.; Bailey, T.; Sreenivasan, S. V.; Ekerdt, J. G.; Willson, C. G. "Characterization and modeling of volumetric and mechanical properties for step and flash imprint lithography photopolymers." *Journal of Vacuum Science & Technology, B: Microelectronics and Nanometer Structures* **2001**, 19 (6), 2685-2689.

CHAPTER 7: CONCLUSIONS AND FUTURE WORK

7.1 PHOTORESIST COMPONENT EXTRACTION DURING IMMERSION

Immersion lithography emerged as a viable alternative to using smaller wavelength sources in lithographic processing only after several critical issues were investigated. One of these issues was whether intimate contact between water and photoresists during immersion would lead to a degradation of the imaging process and/or contamination. To address this, three different experimental techniques were used to observe the extraction of small molecule resist components by water.

The techniques used were liquid chromatography/mass spectroscopy (LCMS), scanning electrochemical microscopy (SECM) and liquid scintillation counting (LSC). The SECM method enabled the detection of photoacid generator in water during real-time immersion conditions and differentiated between PAG and photoacid formed during exposure. It provided qualitative evidence that during immersion some amount of PAG was extracted from the model 193 nm photoresists studied, but that amount was below the quantitative limit of the measurements. Both the LCMS and LSC measurements confirmed the presence of PAG in immersion water. Uncertainties associated with the LCMS measurements also prevented accurate quantification, but the results qualitatively agreed with the other two methods. The LSC approach enabled PAG, residual casting solvent and a base additive to be studied. Its detection limits, which could be improved by increasing analysis time, allowed quantification of both PAG and base extraction and determination of an upper limit for the casting solvents.

The PAG was seen to be extracted during the first few seconds of immersion in water. That amount did not increase with time or change with film thickness. A rinse before immersion prevented any additional extraction from taking place. These results indicated that the PAG was only extracted from the surface of the resist films, an observation that was consistent with studies of PAG distribution. No detectable amount of residual casting solvent was extracted from the films, a result that was also consistent with solvent distribution models that claim a depletion of solvent molecules at the surface. A base additive was also extracted in small amounts. That amount did not increase with immersion time, but was insensitive to a prerinse.

These results indicated that while some amount of the photoresist components were extracted by water during immersion, these amounts were small and occurred only during the first few seconds of immersion. PAG extraction could be avoided with a prerinse step, but if base extraction were to pose a problem a protective top coat would likely be needed. While these measurements helped address one of the initial critical issues with immersion, they could be applied to others. In this work, only model acrylic photoresists were studied. Several other platforms exist that could work with immersion, such as the styrene-based 248 nm resists, and their interactions with water should be characterized. Another area for future work is the study of component diffusion through photoresists. Currently, little is understood about how base additives diffuse through a resist film and it is difficult to quantify since the base is such a small percentage of the whole formulation. LSC provides a ready means to quantify these materials using well

established techniques such as the “Halt Development” experiment to determine component distribution and bilayer film experiments to measure diffusion.^{1,2}

7.2 HIGH INDEX MATERIALS FOR IMMERSION LITHOGRAPHY

Materials for second-generation immersion lithography were also investigated. To further improve resolution limits, fluids with higher refractive indices than water are needed. However, several constraints have been placed on the next generation fluids, including high transparency and physical properties essentially unchanged from water. Because of these constraints, composite solutions of water and high index additives were studied.

Ionic compounds were identified in early work as potential additives, so a systematic survey of their optical properties in aqueous solutions was conducted. In general it was found that the anion species had a significant effect on a solution’s index and absorbance and the cation had only a small influence. While essentially all of the additives resulted in higher index values, the increase in absorbance for most was too great even at very low concentrations. However, the survey did lead to the development of a series of additives with a methylsulfonate anion that had some of the highest index values and lowest absorption coefficients measured for these types of materials. This series even included microelectronics-friendly quaternary ammonium cations. Yet, the target values for the optical properties were not reached, with the indices still too low and absorption too high. Also, the viscosities and contact angles differed significantly from water. Despite missing the targets, these additives could still be useful. The restrictions

placed on the absorption coefficient, viscosity and contact angle were for engineering reasons rather than physical limitations. The fluid handling systems and working distances between the lens and wafer in immersion exposure tools could be redesigned for these fluids. More importantly, with an index value of $n = 1.56$, the fluid would no longer have the lowest index value in the relevant film stack. A new lens material would need to be identified with a greater index to warrant the use of a fluid with the target index. Any further increases would also require high index photoresists.

The ionic additive survey also revealed that an increase in the absorption coefficient always followed an increase in the refractive index. This is a result of the connection between the two properties as defined by the Kramers-Kronig relation. The theoretical nature of the refractive index and absorption coefficient was reviewed, and it was found that they could be described mathematically by models consistent with the Kramers-Kronig relation using physically meaningful parameters. One such model is the Lorentz model, which allows specification of the location, magnitude and width of absorption peaks. While this model and many others are typically used to fit experimental data, they could also be used to create dispersion curves representing an ideal structure with the desired n and k values for a particular wavelength. This was demonstrated, but required several assumptions regarding the general nature of the structure. These assumptions were necessary since exact specification of the optical properties requires knowledge of their behavior over the entire electromagnetic spectrum. The resulting model for a structure that would lead to the target immersion fluid

properties did not present a unique solution, but did serve as a guide to a new set of potential additives.

These additives, sulfonate salts of cyclic hydrocarbons, showed potential for achieving a high index from a theoretical point of view. However, they have a couple of practical limitations that must be overcome. The first is their limited solubility and the formation of micelles. Preparation of analogs with several sulfonate groups attached to the rings could improve both matters. Second, their absorption initially appeared to be much greater than that of water. It was not clear whether that was due to the compounds themselves or impurities. Improved purification is therefore necessary to determine if the salts tested are viable additive candidates or if structural alternations are needed to improve absorption behavior.

There is also ample future work for the modeling approach. The first concern is the inability of the Lorentz model to accurately represent the absorption behavior in the higher wavelength tail region of a peak. Another type of oscillator model should be chosen to represent the absorption, such as a Gaussian or Poisson function. Accurate representation of this tail region is important since an artificially high extinction coefficient at 193 nm could lead to an otherwise promising set of spectra being discarded.

Also, as stated above, an accurate description of n and k for any material requires knowledge of their dispersion throughout the entire spectrum. This can be overcome when a model is used in conjunction with experimental data to describe the behavior for a known over a limited wavelength range, such as in ellipsometry. For an *a priori* model intended to lead to a structure, several assumptions must be made to specify constraints

on the model parameters. The current assumptions were empirical in nature, so they led to reasonable spectra but did not represent physical limits. To refine the constraints, a better understanding of the potential breadth and magnitude of absorption peaks in the vacuum UV and below is needed. There is little experimental data available for this region, so a study should be undertaken to learn about the absorption behavior for a variety of structures. Ionization should also be included in that study, as it is common for the positions of ionization peaks to be studied and not their absolute magnitude.³ Additional constraints could also come from the inclusion of characteristics like oscillator strengths in the model calculations. Oscillator strength is the area under the intensity spectrum of an absorption peak for any electron transition. Quantum mechanics relates the sum of the oscillator strengths to the total number of electrons in the system.⁴

7.3 POLYMER-BASED PHOTONIC CRYSTALS FROM SFIL

The step and flash imprint lithography process is a next-generation lithographic technology with the versatility to pattern a large range of structures applicable to semiconductors, photonics and other areas. With the resolution of e-beam lithography combined with higher throughput, SFIL is particularly suited for the area of photonic crystals. To demonstrate this, a photonic crystal pattern was designed with a band gap in the visible region. The process steps required to print the structure with SFIL were then developed. These included a template fabrication procedure, SFIL patterning process and etch process to transfer the pattern into a polymer underlayer. The polymer was chosen for its transparency in the visible region and compatibility with high index, organic

additives. The etch process was found to alter the size of the features in the crystal structure relative to their spacing, which shifted the location of the band gap. This size change needs to be accounted for in designing actual devices, especially for systems that will have narrow band gaps that will be sensitive to even small changes. The use of an index increasing additive was found to shift the location of the band gap as well.

A demonstration of the photonic crystal itself will require several process improvements. These include the use of an etch tool with improved anisotropy over the tools available at the MRC, the use of a Teflon substrate and the further development of high index additives. These could include oxide nanoparticles whose surfaces were functionalized with a reactive ligand, semiconductor quantum dots whose optical properties are can be tailored to specific applications based on their size or nonlinear molecules whose properties can be modulated by external stimuli.⁵⁻⁷ Additives such as these could also allow for the design of active devices such as modulators in addition to passive devices like waveguides. However, they will require further developments themselves as most composites incorporating these additives currently can contain only nanomolar quantities rather than the large fractions needed for significant changes to the refractive index.

7.4 REFERENCES

1. Burns, S. D. *Understanding Fundamental Mechanisms of Photoresist Dissolution*. PhD Dissertation, The University of Texas at Austin, Austin, TX, USA, **2003**.

2. Stewart, M. D. *Catalyst diffusion in positive-tone chemically amplified photoresists*. PhD Dissertation, The University of Texas at Austin, Austin, TX, USA, **2003**.
3. Limao-Vieira, P.; Giuliani, A.; Delwiche, J.; Parafita, R.; Mota, R.; Dufлот, D.; Flament, J. P.; Drage, E.; Cahillane, P.; Mason, N. J.; Hoffmann, S. V.; Hubin-Franskin, M. J. "Acetic acid electronic state spectroscopy by high-resolution vacuum ultraviolet photo-absorption, electron impact, He(I) photoelectron spectroscopy and ab initio calculations." *Chemical Physics* **2006**, 324 (2-3), 339-349.
4. Orchin, M.; Jaffé, H. H., *Symmetry, orbitals, and spectra (S.O.S.)*. Wiley-Interscience: New York, **1971**; p 396.
5. Brus, L. "Chemical approaches to semiconductor nanocrystals." *Journal of Physics and Chemistry of Solids* **1998**, 59 (4), 459-465.
6. Burland, D. M.; Miller, R. D.; Walsh, C. A. "Second-order nonlinearity in poled-polymer systems." *Chemical Reviews (Washington, DC, United States)* **1994**, 94 (1), 31-75.
7. Caruso, F. "Nanoengineering of particle surfaces." *Advanced Materials (Weinheim, Germany)* **2001**, 13 (1), 11-22.

APPENDIX A: SYNTHESIS OF RADIOLABELED PHOTOACID GENERATOR AND BASE ADDITIVE

A.1 ¹⁴C-TRIPHENYLSULFONIUM PERFLUORO-1-BUTANESULFONATE^{1,2}

¹⁴C-Triphenylsulfonium perfluorobutanesulfonate (TPS nonaflate). ¹⁴C-labeled Diphenyl Sulfoxide: Break-seal ampules containing ¹⁴C labeled benzene (Sigma-Aldrich, Inc., 1.4mCi, SA of 10.3 mCi/mmol) were cooled in an ice bath. The ampules were ruptured and rinsed with 20 mL of benzene. The benzene was transferred to an oven dried 100 mL three neck round bottom flask under nitrogen. Thionyl chloride (0.6 mL, 8.2 mmol) was added and the flask was cooled to 0 °C before triflic acid (3.1 mL, 35.3 mmol) was added. The ice bath was removed after 1 hour and the reaction stirred for 24 hours at room temperature. The reaction was quenched by pouring the solution over ice and neutralizing with sodium bicarbonate. The neutralized solution was extracted with four 30 mL portions of methylene chloride. The combined organics were dried over magnesium sulfate. The solution was filtered to remove the magnesium sulfate and distilled to remove methylene chloride and benzene. The residue was dissolved in boiling hexanes and decanted away from the hexane insoluble yellow oil. The yellow oil was extracted with boiling hexanes once more. The combined hexanes solutions were cooled in an ice bath and diphenyl sulfoxide precipitated out as a white solid that was isolated by filtration and dried under vacuum. Yield: 1.32 g (80%). Mp: 69-72 °C. ¹H NMR (CDCl₃, ppm): δ 7.4 (m, 6H), δ 7.6 (m, 4H)

Triphenylsulfonium Bromide (¹⁴C-TPS bromide): A 875 mg (36 mmol) portion of powdered magnesium was suspended in 20 mL of dry diethyl ether in a oven-dried

500 mL three-neck flask equipped with a Teflon coated stir bar, reflux condenser, and dropping funnel. A positive pressure of dry nitrogen was maintained throughout the reaction. The dropping funnel was charged with 5.9 g (37.5 mmol) of bromobenzene and 10 mL of diethyl ether of which 1-2 mL were added immediately. An iodine crystal was added to initiate the reaction and the remaining bromobenzene solution was added drop wise at a rate to maintain reflux. The solution was allowed to stir overnight under a nitrogen atmosphere. The ether solvent was removed by heating in an 80 °C bath *in vacuo* with stirring for two hours, giving a semi-solid brown residue. Freshly distilled heptane, 50mL, was added to the flask was removed by heating in an 80 °C bath *in vacuo*. This was repeated three times. Dry heptane, 100 mL, and 50 mL of dry benzene were added to the flask and the reaction was heated to reflux. A 1.32 g (6.5 mmol) portion of diphenyl sulfoxide was dissolved in 30 mL freshly distilled benzene and added dropwise to the refluxing phenyl magnesium bromide mixture. After addition was complete, the mixture was maintained at reflux over night, followed by cooling to 0 °C with an ice bath. HBr, 80 mL of 25%, was added slowly to maintain a temperature below 20 °C, and allowed to stir overnight. The aqueous phase was collected, and the organic phase washed with two 30 mL portions of 5% HBr. The combined aqueous phases were extracted with four 30 mL portions of dichloromethane. The organics were dried over MgSO₄ and removed *in vacuo* to give a tan powdered product. Yield: 0.324 g (15%). Melting point = 284-286 °C. ¹H NMR (CDCl₃, ppm): δ 7.6 (m, 9H), δ 7.8 (m, 6H).

Triphenylsulfonium Perfluoro-1-butanesulfonate (¹⁴C-TPS nonaflate): In a 100 mL round bottom flask was placed 0.324 g (0.94 mmol) TPS bromide and 0.319 g (0.94

mmol) potassium perfluoro-1-butanesulfonate. To this mixture was added 10 mL deionized water and 10 mL of nitromethane. After stirring vigorously for one hour, the phases were separated, and the organic phase extracted 3x30 mL of deionized water followed by drying over MgSO₄. Removal of solvent *in vacuo* gave a viscous oil. After extracting the oil with ice cold diethyl ether several times a crystalline product was isolated. Filtration gives the desired product as a white solid. Yield: 0.23 g (43 %). MP = 88-89 °C. ¹H NMR (CDCl₃, ppm): δ 7.6 (m, 9H), δ 7.8 (m, 6H). ¹⁹F NMR (CDCl₃, reference = CFCl₃, ppm): δ -80.8 (3F, CF₃), -114.4 (2F, CF₃CF₂CF₂CF₂SO₃⁻), -121.1 (2F, CF₃CF₂CF₂CF₂SO₃⁻), -125.6 (2F, CF₃CF₂CF₂CF₂SO₃⁻). The SA was 8.60 ± 0.02 μCi/g.

A.2 ¹⁴C-TRIPENTYLAMINE

¹⁴C-Tripentylamine. Tosylation of ¹⁴C-labeled 1-Pentanol: A break-seal ampule containing ¹⁴C-labeled 1-pentanol (American Radiolabeled Chemicals, Inc., 1 mCi, SA of 5 mCi/mmol) was cooled in a dry ice-isopropyl alcohol bath. The ampule was ruptured and rinsed with 2.5 mL of 1-pentanol. The 1-pentanol (2.5 mL, 23 mmol) was distilled from calcium hydride directly into the oven dried 3 neck round bottom flask used for the tosylation reaction. Dichloromethane (20 mL) and pyridine (2.3 mL, 28 mmol) were added to the flask. The flask was cooled in an ice bath before tosyl chloride (4.83 g, 25.3 mmol) was added. The reaction was warmed to room temperature and stirred over night, then filtered through a celite plug to remove the pyridinium chloride that formed. The solution was then extracted with water (3 x 15 mL) and once with 20 mL of brine

solution. The organic layer was dried over MgSO₄ and removed in vacuo to give a clear oil. The oil was used for the next reaction without any further purification.

¹⁴C-Tripentylamine: The oil from the tosylation reaction was added to a 100 mL round bottom flask with dipentylamine (14.1 mL, 69 mmol), and K₂CO₃ (6.36 g, 46 mmol). The flask was heated and held at 100 °C overnight, then cooled and filtered through a celite plug to remove any solids. The plug was then rinsed with ethyl acetate. The organics were dried over MgSO₄ and the ethyl acetate removed in vacuo. The unreacted dipentylamine was removed by vacuum distillation at 37 °C @ 540 mtorr. The tripentylamine (2.4g, 46% yield) was isolated at 66-69 °C @ 540 mtorr. ¹HNMR (CDCl₃, ppm): δ 2.4 (t, 6H), δ 1.2-1.5 (m, 18H), δ 2.4 (t, 9H). The SA was 49.8 ± 0.1 μCi/g.

A.3 REFERENCES

1. Olah, G. A.; Marinez, E. R.; Prakash, G. K. S. "Trifluoromethanesulfonic Acid Catalyzed Preparation of Symmetrical Diaryl Sulfoxides from Arenes and Thionyl Chloride." *Synlett* **1999**, 1999 (09), 1397-1398.
2. Patterson, K. W. *Design, synthesis, and optimization of materials for 193 nm and 157 nm photoresists*. PhD Dissertation, The University of Texas at Austin, Austin, TX, USA, **2000**.

**APPENDIX B: CAUCHY COEFFICIENTS, MEAN SQUARED
ERROR AND 90% CONFIDENCE LIMITS FOR ELLIPSOMETRY
MEASUREMENTS**

HPLC Water

MSE=0.7858 90% Confidence Interval

A	1.3221	0.00066
B	0.00196	0.00014
C	8.75E-05	5.46E-06

0.1 mM NaCl

MSE=0.7324 90% CI

A	1.3232	0.00055
B	0.00248	0.00015
C	5.91E-05	7.19E-06

0.5 mM NaCl

MSE=1.416 90% CI

A	1.3229	0.00053
B	0.00259	0.00016
C	5.48E-05	7.84E-06

1 mM NaCl

MSE=1.662 90% CI

A	1.3216	0.00049
B	0.00264	0.00016
C	4.99E-05	8.00E-06

10 mM NaCl

MSE=1.278 90% CI

A	1.3237	0.00059
B	0.00247	0.00016
C	5.99E-05	7.56E-06

50 mM NaCl

MSE=1.874 90% CI

A	1.3225	0.00047
B	0.00261	0.00015
C	5.31E-05	7.84E-06

0.1 M NaCl

MSE=1.817 90% CI

A	1.323	0.00045
B	0.00266	0.00015
C	5.16E-05	7.67E-06

0.5 M NaCl

MSE=1.881 90% CI

A	1.3277	0.00044
B	0.00267	0.00015
C	5.86E-05	7.44E-06

1 M NaCl

MSE=1.428 90% CI

A	1.3338	0.00055
B	0.00257	0.00015
C	7.28E-05	7.25E-06

2 M LiBr			2 M NaBr		
MSE=0.3174		90% CI	MSE=0.8187		90% CI
A	1.3434	0.00067	A	1.3476	0.0007
B	0.00202	0.00016	B	0.00157	0.00018
C	0.00017	6.73E-06	C	0.0002	7.55E-06
2 M KBr			2 M RbBr		
MSE=1.152		90% CI	MSE=0.8209		90% CI
A	1.3475	0.00062	A	1.3517	0.00047
B	0.00172	0.00015	B	0.00199	0.00013
C	0.00019	6.53E-06	C	0.00018	6.24E-06
2 M CsBr			2 M NH₄Br		
MSE=0.878		90% CI	MSE=0.5875		90% CI
A	1.3526	0.00099	An.0	1.3528	0.00061
B	0.00234	0.00026	Bn.0	0.00181	0.00015
C	0.00016	1.12E-05	Cn.0	0.00019	6.41E-06
2 M TMA Br			2 M LiCl		
MSE=0.5107		90% CI	MSE=0.4059		90% CI
An.0	1.3616	0.00066	A	1.3359	0.00046
Bn.0	0.00192	0.00017	B	0.00246	0.00011
Cn.0	0.00019	7.44E-06	C	9.28E-05	4.86E-06
2 M NaCl			2 M KCl		
MSE=0.2547		90% CI	MSE=0.1629		90% CI
A	1.3418	0.00068	A	1.3437	0.00051
B	0.00218	0.00016	B	0.00166	0.00012
C	0.00012	6.55E-06	C	0.00013	4.83E-06
2 M RbCl			2 M CsCl		
MSE=0.4874		90% CI	MSE=0.7839		90% CI
A	1.3433	0.00042	A	1.3476	0.00032
B	0.00255	0.00011	B	0.00274	8.91E-05
C	9.41E-05	4.80E-06	C	8.57E-05	4.15E-06

2 M NH₄Cl

MSE=0.2989		90% CI
An.0	1.3428	0.0004
Bn.0	0.00257	9.79E-05
Cn.0	9.26E-05	4.17E-06

2 M TMA Cl

MSE=0.2537		90% CI
An.0	1.3534	0.00039
Bn.0	0.00248	0.0001
Cn.0	0.0001	4.43E-06

2 M Li Acetate

MSE=0.4712		90% CI
A	1.3412	0.00058
B	0.00231	0.00013
C	9.16E-05	5.47E-06

2 M Na Acetate

MSE=0.5263		90% CI
A	1.3418	0.0005
B	0.00226	0.00012
C	9.99E-05	4.93E-06

2 M K Acetate

MSE=0.4212		90% CI
A	1.3472	0.00064
B	0.00147	0.00015
C	0.00013	6.39E-06

2 M Rb Acetate

MSE=0.2495		90% CI
A	1.367	0.00047
B	0.00243	0.00012
C	0.00011	5.02E-06

2 M Cs Acetate

MSE=0.4902		90% CI
A	1.3746	0.00047
B	0.00226	0.00012
C	0.00011	5.08E-06

2 M NH₄ Acetate

MSE=0.4055		90% CI
An.0	1.3459	0.00042
Bn.0	0.0024	0.00011
Cn.0	9.48E-05	4.52E-06

2 M HCl

MSE=0.4676		90% CI
A	1.3382	0.00045
B	0.00277	0.00012
C	7.01E-05	5.60E-06

2 M HNO₃

MSE=1.562		90% CI
A	1.3365	0.00217
B	0.00274	0.00058
C	0.00011	2.61E-05

2 M H₂SO₄

MSE=0.4473		90% CI
A	1.3363	0.00087
B	0.00344	0.00023
C	3.79E-05	9.85E-06

2 M H₃PO₄

MSE=0.7233		90% CI
A	1.3454	0.00099
B	0.00289	0.00025
C	4.36E-05	1.09E-05

2 M Na₂SO₃			2 M NaHSO₃		
MSE=0.5673		90% CI	MSE=0.4174		90% CI
A	1.3667	0.00053	A	1.3501	0.00045
B	0.00281	0.00013	B	0.00237	0.00011
C	0.00011	5.70E-06	C	0.00011	4.85E-06
2 M NaHSO₄			2 M Na₂S₂O₃		
MSE=0.4034		90% CI	MSE=0.7213		90% CI
A	1.346	0.00038	A	1.3711	0.00067
B	0.00254	9.47E-05	B	0.00366	0.00017
C	7.07E-05	4.03E-06	C	8.39E-05	6.99E-06
2 M NaSCN			2M Na Perchlorate		
MSE=1.702		90% CI	MSE=0.6128		90% CI
A	1.3572	0.00108	An.0	1.3359	0.00036
B	0.00198	0.00027	Bn.0	0.00221	9.52E-05
C	0.0002	1.16E-05	Cn.0	8.15E-05	4.33E-06
2.35M TMA Acetate			2.55M MtEA Acetate		
MSE=0.9133		90% CI	MSE=1.547		90% CI
A	1.3646	0.00039	A	1.3948	0.00031
B	0.00274	0.0001	B	0.00297	0.0001
C	8.87E-05	4.80E-06	C	9.57E-05	5.19E-06
1.76M TPA Acetate			1.88M TBA Acetate		
MSE=1.586		90% CI	MSE=1.405		90% CI
A	1.3923	0.00034	A	1.4112	0.00036
B	0.00303	0.00011	B	0.00301	0.00011
C	8.62E-05	5.72E-06	C	9.87E-05	5.15E-06
2 M TMA Methyl Sulfate			1.36 M TMA Phosphate		
MSE=0.3518		90% CI	MSE=0.3678		90% CI
A	1.3508	0.00033	A	1.3709	0.00043
B	0.00262	8.86E-05	B	0.00288	0.00011
C	5.83E-05	4.04E-06	C	6.06E-05	4.89E-06

2.6 M TMA Succinate

MSE=0.5693		90% CI
A	1.3877	0.00033
B	0.00269	8.88E-05
C	0.0001	4.04E-06

50wt% TEA Cl

MSE=0.555		90% CI
A	1.4115	0.00035
B	0.00293	9.17E-05
C	0.00012	4.18E-06

55wt% TBA Bisulfate

MSE=0.8988		90% CI
A	1.4091	0.00031
B	0.00319	8.66E-05
C	6.56E-05	4.12E-06

2 M HO₃SCH₃

MSE=0.4789		90% CI
A	1.3397	0.00071
B	0.00272	0.00018
C	5.90E-05	8.07E-06

2 M Cs(O₃SCH₃)

MSE=0.7471		90% CI
A	1.351	0.00144
B	0.00328	0.00038
C	3.39E-05	1.73E-05

2 M Ba(O₃SCH₃)₂

MSE=0.3391		90% CI
A	1.3731	0.00065
B	0.00296	0.00017
C	5.68E-05	7.40E-06

2 M La(O₃SCH₃)₃

MSE=0.7287		90% CI
A	1.3953	0.00105
B	0.00296	0.00027
C	6.57E-05	1.20E-05

2.82 M La(O₃SCH₃)₃

MSE=2.4		90% CI
A	1.4387	0.00054
B	0.0037	2.07E-04
C	5.44E-05	1.12E-05

0.98 M Sodium cyclohexanesulfonate

MSE=0.8864		90% CI
A	1.3455	0.00136
B	0.00241	0.00033
C	8.31E-05	1.39E-05

5 wt% Sodium decalinsulfonate

MSE=1.111		90% CI
A	1.3313	0.00109
B	0.00206	0.00028
C	9.95E-05	1.19E-05

APPENDIX C: HIGH REFRACTIVE INDEX POLYMER STUDY

C.1 INTRODUCTION

High refractive index fluids enable larger numerical aperture lenses in exposure tools, which results in the angles of incidence on the photoresist films becoming increasingly oblique. At these oblique angles, the polarized nature of light reduces the process latitude. This loss can be partially mitigated by using a photoresist with a higher index of refraction. Preliminary studies on two different methods to increase the refractive index of the photoresists were performed using model polymer systems. First, polystyrene derivatives were used to illustrate the effect of adding and modifying pendant groups on the polymer backbone. Second, polynorbornene hexafluoroalcohol (PNBHFA) formulations were tested to study the effect of dissolution inhibitors on the index. A PNBHFA derivative, PNBHFA-SO₂ copolymer, was also used to examine polymer backbone modifications.

C.2 MATERIALS AND SAMPLE PREPARATION

Materials for high RI polymer survey experiments included polystyrene, polychlorostyrene and polyvinylbenzylchloride that were synthesized from monomers obtained from Sigma-Aldrich Co. The following synthetic procedure was used. Monomer, 5 g (48 mmol), was combined with 25 mg of benzoyl peroxide initiator in a flask with 20 mL of toluene. The flask was placed in a liquid nitrogen bath and evacuated. The freeze-thaw cycle was repeated three times to remove oxygen. Then the flask was

placed under nitrogen and the contents were stirred overnight at 70°C. The polymer was then precipitated in hexanes, then filtered, redissolved in dichloromethane and precipitated in hexane again. The product was then dried under vacuum overnight. The target molecular weight for all polymers was 30000.

Polyhydroxystyrene was obtained from Hoescht-Celanese Corp. (Summit, NJ) and used as received. PNBHFA was donated by AZ Electronic Materials (Sommerville, NJ) and used as received. Polynorbornene hexafluoroalcohol-sulfur dioxide copolymer (PNBHFA-SO₂) was synthesized by combining solutions of 2-(3,3,3-trifluoro-2-trifluoromethyl-2-hydroxypropyl) bicycle[2.2.1]hept-2-ene, 5 g, in 20 mL THF and 0.1 mL of 5-6 M t-butyl hydrogen peroxide in decane to 25 mL of condensed sulfur dioxide and carrying the polymerization out at -60°C for 6 hours. A solution of 150 mg of hydroquinone in 5 mL of THF was used to quench the reaction and then the solution was allowed to warm to room temperature to evolve SO₂. The polymer solution was combined with 75 mL of ethyl acetate and washed with 5% NaHCO₃ in water. The organic phase was then collected and washed with water (3x) and brine (2x), then dried over MgSO₄ and filtered. Ethyl acetate was evaporated, the polymer was dissolved in THF and then precipitated in hexane. The polymer was then filtered and dried under vacuum at 70°C overnight. Dissolution inhibitors (DIs), shown in Figure B.1, were added to PNBHFA. These DIs are di-*tert*-butyl carbonate of thiodiphenol (DI 1), di-*tert*-butyl carbonate of bis-(4-hydroxyphenol) sulfoxide (DI 2), di-*tert*-butyl carbonate of 4,4'-thiobisbenzenethiol (DI 3), methane sulfonic acid 4-(4-methanesulfonyloxyphenylsulfanyl)-phenylester (DI 4) and di-*tert*-butyl carbonate of bisphenol A (DI 5).

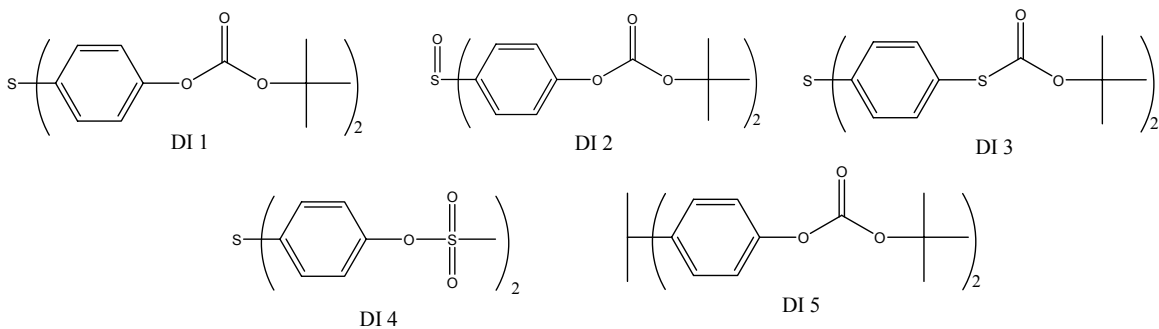


Figure C.1 Structures of dissolution inhibitors used in PNBHFA.

Polymer films were cast onto 2 in Si wafers by first preparing a 10 wt% solution in diglyme, from Sigma-Aldrich Co., for the polystyrene based polymers and PGMEA, also obtained from Sigma-Aldrich Co., for the PNBHFA based polymers. DI's were added to PNBHFA solutions at 5 wt% of the polymer. Films were cast at 2000 rpm for 30 s and then baked at 90°C for 90 s.

C.3 RESULTS

The refractive indices of the resists were determined from spectroscopic ellipsometric measurements made on a J.A. Woollam M-2000 variable angle spectroscopic ellipsometer. The ellipsometric parameters Ψ and Δ were fit to a Cauchy model by the Woollam WVASE32 software. Figure C.2 shows the data for the polystyrene derivatives and Figure C.3 shows those for the PNBHFA and PNBHFA-SO₂. Figure C.4 shows the results of added dissolution inhibitors to PNBHFA. From these

figures it can be seen that modest increases in the index of refraction of the base polymer were achieved by both backbone modification and addition of dissolution inhibitors.

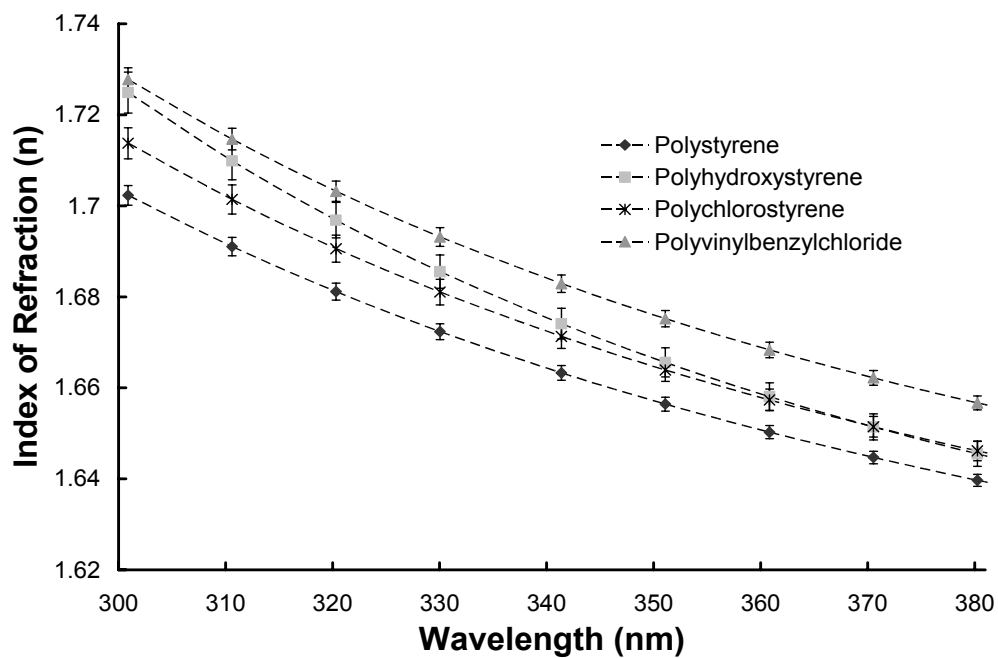


Figure C.2 Index of refraction vs. wavelength of polystyrene and derivatives.

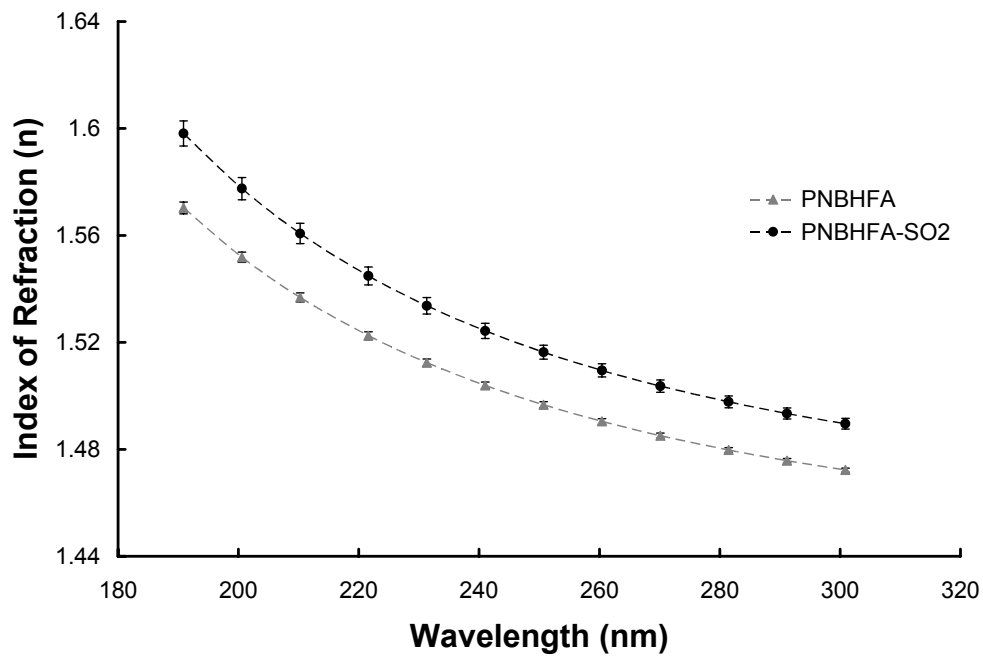


Figure C.3 Index of refraction vs. wavelength of PNBHFA and PNBHFA-SO₂.

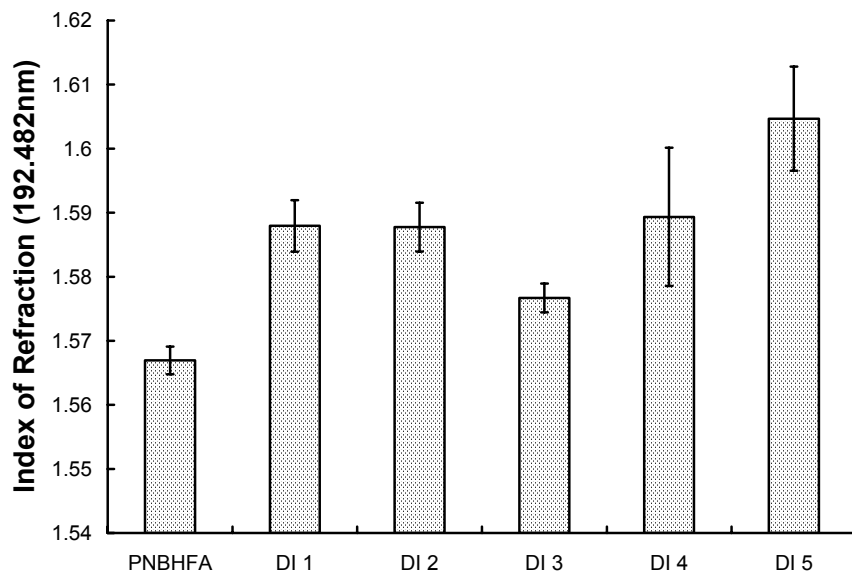


Figure C.4 Index of refraction PNBHFA with 5 wt% loading of dissolution inhibitors.

Bibliography

"IBM claims to make first processors with immersion lithography." *EE Times*, available at <<http://www.eetimes.com/showArticle.jhtml?articleID=54201799>> **2004**.

International Technology Roadmap for Semiconductors, available at, <<http://www.itrs.net/Links/2005ITRS/Home2005.htm>> **2006**.

Allen, R. D.; Wallraff, G. M.; Hinsberg, W. D.; Conley, W. E.; Kunz, R. R. "Designing high performance krypton monofluoride and argon monofluoride single-layer resists with methacrylate polymers." *Journal of Photopolymer Science and Technology* **1993**, 6 (4), 575-91.

Allen, R. D.; Wallraff, G. M.; Hofer, D. C.; Kunz, R. R. "Photoresists for 193-nm lithography." *IBM Journal of Research and Development* **1997**, 41 (1/2), 95-104.

Alpuche-Aviles, M. A.; Wipf, D. O. "Impedance Feedback Control for Scanning Electrochemical Microscopy." *Analytical Chemistry* **2001**, 73 (20), 4873-4881.

Azzam, R. M. A.; Bashara, N. M., *Ellipsometry and polarized light*. North-Holland Pub. Co.: Amsterdam, **1977**; p 529.

Baek, S.-Y.; Wei, A.; Cole, D. C.; Nellis, G.; Yeung, M.; Abdo, A.; Engelstad, R. "Simulation of the coupled thermal/optical effects for liquid immersion micro/nanolithography." *Proceedings of SPIE - The International Society for Optical Engineering* **2004**, 5377 (Pt. 1, Optical Microlithography XVII), 415-427.

Bard, A. J.; Mirkin, M. V., *Scanning Electrochemical Microscopy*. Marcel Dekker: New York, **2001**; p 650.

Bardeen, J.; Brattain, W. H. "The Transistor, A Semi-Conductor Triode." *Physical Review* **1948**, 74 (2), 230.

Barra, A.; Cassagne, D.; Jouanin, C. "Existence of two-dimensional absolute photonic band gaps in the visible." *Applied Physics Letters* **1998**, 72 (6), 627-629.

- Born, M.; Wolf, E., *Principles of optics : electromagnetic theory of propagation, interference and diffraction of light*. 7th expanded ed.; Cambridge University Press: Cambridge ; New York, **1999**; p 952.
- Böttcher, C. J. F., *Theory of electric polarization*. Elsevier Scientific Pub. Co.: Amsterdam, **1952**.
- Bourov, A.; Fan, Y.; Cropanese, F. C.; Lafferty, N. V.; Zavyalova, L.; Kang, H.; Smith, B. W. "Immersion microlithography at 193 nm with a Talbot prism interferometer." *Proceedings of SPIE - The International Society for Optical Engineering* **2004**, 5377 (Pt. 3, Optical Microlithography XVII), 1573-1578.
- Brodsky, C.; Byers, J.; Conley, W.; Hung, R.; Yamada, S.; Patterson, K.; Somervell, M.; Trinque, B.; Tran, H. V.; Cho, S.; Chiba, T.; Lin, S.-H.; Jamieson, A.; Johnson, H.; Vander Heyden, T.; Willson, C. G. "157 nm resist materials: Progress report." *Journal of Vacuum Science & Technology, B: Microelectronics and Nanometer Structures* **2000**, 18 (6), 3396-3401.
- Brueck, S. R. J.; Chen, X. "Spatial frequency analysis of optical lithography resolution enhancement techniques." *Journal of Vacuum Science & Technology, B: Microelectronics and Nanometer Structures* **1999**, 17 (3), 908-920.
- Brus, L. "Chemical approaches to semiconductor nanocrystals." *Journal of Physics and Chemistry of Solids* **1998**, 59 (4), 459-465.
- Budhlall, B.; Parris, G.; Zhang, P.; Gao, X.; Zarkov, Z.; Ross, B.; Kaplan, S.; Burnett, J. "High refractive index immersion fluids for 193 nm immersion lithography." *Proceedings of SPIE-The International Society for Optical Engineering* **2005**, 5754 (Pt. 2, Optical Microlithography XVIII), 622-629.
- Burland, D. M.; Miller, R. D.; Walsh, C. A. "Second-order nonlinearity in poled-polymer systems." *Chemical Reviews (Washington, DC, United States)* **1994**, 94 (1), 31-75.
- Burnett, J. H.; Kaplan, S. "Measurement of the refractive index and thermo-optic coefficient of water near 193 nm." *Proceedings of SPIE-The International Society for Optical Engineering* **2003**, 5040 (Pt. 3, Optical Microlithography XVI), 1742-1749.

- Burnett, J. H.; Kaplan, S. G. "Measurement of the refractive index and thermo-optic coefficient of water near 193 nm." *Journal of Microlithography, Microfabrication, and Microsystems* **2004**, 3 (1), 68-72.
- Burnett, J. H.; Kaplan, S. G.; Shirley, E. L.; Tompkins, P. J.; Webb, J. E. "High-index materials for 193 nm immersion lithography." *Proceedings of SPIE-The International Society for Optical Engineering* **2005**, 5754 (Pt. 2, Optical Microlithography XVIII), 611-621.
- Burns, R. L.; Punsalan, D.; Towidjaja, M. C.; Koros, W. J. "Strategies for purging the pellicle space for 157 nm lithography." *Journal of Vacuum Science & Technology B: Microelectronics and Nanometer Structures* **2002**, 20 (5), 1954-1960.
- Burns, S. D. *Understanding Fundamental Mechanisms of Photoresist Dissolution*. PhD Dissertation, The University of Texas at Austin, Austin, TX, USA, **2003**.
- Byers, J.; Patterson, K.; Cho, S.; McCallum, M.; Willson, C. G. "Recent advancements in cycloolefin based resists for ArF lithography." *Journal of Photopolymer Science and Technology* **1998**, 11 (3), 465-474.
- Calhoun, R. K.; Holler, F. J.; Geiger, R. F., Jr.; Nieman, T. A.; Caserta, K. J. "Wide-range bipolar pulse conductance instrument employing current and voltage models with sampled or integrated signal acquisition." *Analytica Chimica Acta* **1991**, 252 (1-2), 29-40.
- Caruso, F. "Nanoengineering of particle surfaces." *Advanced Materials (Weinheim, Germany)* **2001**, 13 (1), 11-22.
- Caserta, K. J.; Holler, F. J.; Crouch, S. R.; Enke, C. G. "Computer controlled bipolar pulse conductivity system for applications in chemical rate determinations." *Analytical Chemistry* **1978**, 50 (11), 1534-41.
- Chan, M.; Kunz, R. R.; Doran, S. P.; Rothschild, M. "Photolithography at 0.10 and 0.13 mm using ArF excimer laser lithography in combination with resolution enhancement techniques." *Journal of Vacuum Science & Technology, B: Microelectronics and Nanometer Structures* **1997**, 15 (6), 2404-2411.

- Chiao, R. Y.; Boyce, J. "Superluminality, paraelectricity, and Earnshaw's theorem in media with inverted populations." *Physical Review Letters* **1994**, 73 (25), 3383-6.
- Chipman, D. M. "Ionization potentials of water from valence bond and molecular orbital wave functions." *J. Am. Chem. Soc.* **1978**, 100 (9), 2650-2654.
- Chumanov, G.; Evanoff, D. D., Jr.; Luzinov, I.; Klep, V.; Zdryko, B.; Conley, W.; Zimmerman, P. "Nanocomposite liquids for 193 nm immersion lithography: a progress report." *Proceedings of SPIE-The International Society for Optical Engineering* **2005**, 5753 (Pt. 2, Advances in Resist Technology and Processing XXII), 847-850.
- Colburn, M.; Grot, A.; Amistoso, M. N.; Choi, B. J.; Bailey, T. C.; Ekerdt, J. G.; Sreenivasan, S. V.; Hollenhorst, J.; Willson, C. G. "Step and flash imprint lithography for sub-100-nm patterning." *Proceedings of SPIE-The International Society for Optical Engineering* **2000**, 3997 (Emerging Lithographic Technologies IV), 453-457.
- Colburn, M.; Johnson, S.; Stewart, M.; Damle, S.; Bailey, T. C.; Choi, B.; Wedlake, M.; Michaelson, T.; Sreenivasan, S. V.; Ekerdt, J.; Willson, C. G. "Step and flash imprint lithography: a new approach to high-resolution patterning." *Proceedings of SPIE-The International Society for Optical Engineering* **1999**, 3676 (Pt. 1, Emerging Lithographic Technologies III), 379-389.
- Colburn, M.; Suez, I.; Choi, B. J.; Meissl, M.; Bailey, T.; Sreenivasan, S. V.; Ekerdt, J. G.; Willson, C. G. "Characterization and modeling of volumetric and mechanical properties for step and flash imprint lithography photopolymers." *Journal of Vacuum Science & Technology, B: Microelectronics and Nanometer Structures* **2001**, 19 (6), 2685-2689.
- Conley, W.; Bendik, J. "Is ArF the final wavelength?" *Proceedings of SPIE-The International Society for Optical Engineering* **2004**, 5376 (Pt. 1, Advances in Resist Technology and Processing XXI), 16-20.
- Dammel, R., *Diazonaphthoquinone-based resists*. SPIE Optical Engineering Press: Bellingham, Wash., USA, **1993**; p 203.

- Dammel, R. R.; Houlihan, F. M.; Sakamuri, R.; Rentkiewicz, D.; Romano, A. "193 nm immersion lithography - Taking the plunge." *Journal of Photopolymer Science and Technology* **2004**, *17* (4), 587-602.
- Dewar, M. J. S.; Worley, S. D. "Photoelectron spectra of molecules. I. Ionization potentials of some organic molecules and their interpretation." *Journal of Chemical Physics* **1969**, *50* (2), 654-67.
- Edita, T.; Kenneth, A. G.; SangHun, L.; Hector, M.; Phillip, J. B.; Paul, E. D.; Alastair, A. M.; Jeffrey, B.; David, A. "At-wavelength interferometry for extreme ultraviolet lithography." *Journal of Vacuum Science & Technology B: Microelectronics and Nanometer Structures* **1997**, *15* (6), 2455-2461.
- Eisele, K. M.; Klausmann, E. "Effects of heavy metal contamination from corrosive gas and dopant handling equipment in silicon wafer processing." *Solid State Technology* **1984**, *27* (10), 177-80.
- Fan, S.; Villeneuve, P. R.; Joannopoulos, J. D.; Schubert, E. F. "High extraction efficiency of spontaneous emission from slabs of photonic crystals." *Physical Review Letters* **1997**, *78* (17), 3294-3297.
- Fan, Y.; Lafferty, N.; Bourov, A.; Zavyalova, L.; Smith Bruce, W. "Air bubble-induced light-scattering effect on image quality in 193 nm immersion lithography." *Applied optics* **2005**, *44* (19), 3904-11.
- Fan, Y.; Lafferty, N. V.; Bourov, A.; Zavyalova, L. V.; Smith, B. W. "Study of air-bubble-induced light scattering effect on image quality in 193-nm immersion lithography." *Proceedings of SPIE-The International Society for Optical Engineering* **2004**, 5377 (Pt. 1, Optical Microlithography XVII), 477-486.
- Fender, N.; Brock, P. J.; Chau, W.; Bangsaruntip, S.; Mahorowala, A. P.; Wallraff, G. M.; Hinsberg, W. D.; Larson, C. E.; Ito, H.; Breyta, G.; Burnham, K.; Truong, H.; Lawson, P.; Allen, R. D. "Characterization of new aromatic polymers for 157-nm photoresist applications." *Proceedings of SPIE-The International Society for Optical Engineering* **2001**, 4345 (Pt. 1, Advances in Resist Technology and Processing XVIII), 417-427.

- Ferlauto, A. S.; Ferreira, G. M.; Pearce, J. M.; Wronski, C. R.; Collins, R. W.; Deng, X.; Ganguly, G. "Analytical model for the optical functions of amorphous semiconductors from the near-infrared to ultraviolet: Applications in thin film photovoltaics." *Journal of Applied Physics* **2002**, 92 (5), 2424-2436.
- Fink, Y.; Urbas, A. M.; Bawendi, M. G.; Joannopoulos, J. D.; Thomas, E. L. "Block copolymers as photonic bandgap materials." *Journal of Lightwave Technology* **1999**, 17 (11), 1963-1969.
- Frechet, J. M. J.; Eichler, E.; Ito, H.; Willson, C. G. "Poly(p-tert-butoxycarbonyloxystyrene): a convenient precursor to p-hydroxystyrene resins." *Polymer* **1983**, 24 (8), 995-1000.
- Frechet, J. M. J.; Ito, H.; Willson, C. G. "RESINES POUR UV LOINTAIN METTANT EN OEUVRE UN MECANISME D'AMPLIFICATION CHIMIQUE (Sensitive Deep UV Resist Incorporation Chemical Amplification)." *Colloque Internationale sur la Microlithographie: Microcircuit Engineering 82* **1982**, 260.
- French, R. H.; Peng, S.; Wheland, R. C. "Use of highly purified hydrocarbons in vacuum ultraviolet applications." U.S. Patent No. 2005-141285 2005286031, 09/14/2005, **2005**.
- French, R. H.; Sewell, H.; Yang, M. K.; Peng, S.; McCafferty, D.; Qiu, W.; Wheland, R. C.; Lemon, M. F.; Markoya, L.; Crawford, M. K. "Imaging of 32-nm 1:1 lines and spaces using 193-nm immersion interference lithography with second-generation immersion fluids to achieve a numerical aperture of 1.5 and a k_1 of 0.25." *Journal of Microlithography, Microfabrication and Microsystems* **2005**, 4 (3), 031103.
- French, R. H.; Yang, M. K.; Lemon, M. F.; Synowicki, R. A.; Pribil, G. K.; Cooney, G. T.; Herzinger, C. M.; Green, S. E.; Burnett, J. H.; Kaplan, S. "Immersion fluid refractive indices using prism minimum deviation techniques." *Proceedings of SPIE - The International Society for Optical Engineering* **2004**, 5377 (Pt. 3, Optical Microlithography XVII), 1689-1694.
- Gardiner, A. B. *Measurement of Concentration Gradients in Photoresist Films and Study of the Influence of these Gradients on Photoresist Performance*. PhD Dissertation, The University of Texas at Austin, Austin, TX, USA, **1999**.

- Gardiner, A. B.; Burns, S.; Qin, A.; Willson, C. G. "Determination of residual casting solvent concentration gradients in resist films by a "halt development" technique." *Journal of Vacuum Science & Technology, B: Microelectronics and Nanometer Structures* **2001**, *19* (1), 136-141.
- Garrett, B. C.; Dixon, D. A.; Camaioni, D. M.; Chipman, D. M.; Johnson, M. A.; Jonah, C. D.; Kimmel, G. A.; Miller, J. H.; Rescigno, T. N.; Rossky, P. J.; Xantheas, S. S.; Colson, S. D.; Laufer, A. H.; Ray, D.; Barbara, P. F.; Bartels, D. M.; Becker, K. H.; Bowen, K. H., Jr.; Bradforth, S. E.; Carmichael, I.; Coe, J. V.; Corrales, L. R.; Cowin, J. P.; Dupuis, M.; Eisenthal, K. B.; Franz, J. A.; Gutowski, M. S.; Jordan, K. D.; Kay, B. D.; LaVerne, J. A.; Lymar, S. V.; Madey, T. E.; McCurdy, C. W.; Meisel, D.; Mukamel, S.; Nilsson, A. R.; Orlando, T. M.; Petrik, N. G.; Pimblott, S. M.; Rustad, J. R.; Schenter, G. K.; Singer, S. J.; Tokmakoff, A.; Wang, L.-S.; Wittig, C.; Zwier, T. S. "Role of water in electron-initiated processes and radical chemistry: issues and scientific advances." *Chemical Reviews (Washington, DC, United States)* **2005**, *105* (1), 355-389.
- Gates, B. D.; Xu, Q.; Stewart, M.; Ryan, D.; Willson, C. G.; Whitesides, G. M. "New approaches to nanofabrication: Molding, printing, and other techniques." *Chemical Reviews* **2005**, *105* (4), 1171-1196.
- Gehr, R. J.; Boyd, R. W. "Optical Properties of Nanostructured Optical Materials." *Chemistry of Materials* **1996**, *8* (8), 1807-1819.
- Gejo, J. L.; Kunjappu, J.; Turro, N. J.; Conley, W. "Outlook for Potential Third Generation Immersion Fluids" 3rd International Symposium on Immersion Lithography, **2006**; SEMATECH: 2006.
- Gittleman, J. I.; Abeles, B. "Comparison of the effective medium and the Maxwell-Garnett predictions for the dielectric constants of granular metals." *Physical Review B: Solid State* **1977**, *15* (6), 3273-5.
- Goodman, J. W., *Introduction to Fourier Optics*. McGraw-Hill: San Francisco, **1968**; p 287.
- Gruver, R. A.; Gaylord, R. H.; Bilyou, B. W.; Albaugh, K. B. "Relationship of wafer surface contamination to metallic contamination in process liquids." *Proceedings - Institute of Environmental Sciences* **1992**, *38th* (Vol. 1), 460-5.

- Gurevich, I. U. I. A.; Pleskov, I. U. V.; Rotenberg, Z. A., *Photoelectrochemistry*. Consultants Bureau: New York, **1980**; p 239.
- Hafeman, S.; Neureuther, A. R. "Simulation of imaging and stray light effects in immersion lithography." *Proceedings of SPIE - The International Society for Optical Engineering* **2003**, 5040 (Pt. 2, Optical Microlithography XVII), 700-712.
- Hawryluk, A. M.; Ceglio, N. M.; Markle, D. A. "EUV lithography." *Solid State Technology* **1997**, 40 (7), 151-159.
- Hawryluk, A. M.; Ceglio, N. M.; Markle, D. A. "EUV lithography." *Solid State Technology* **1997**, 40 (8), 75-78.
- Hawryluk, A. M.; Seppala, L. G. "Soft x-ray projection lithography using an x-ray reduction camera." *Journal of Vacuum Science & Technology B: Microelectronics and Nanometer Structures* **1988**, 6 (6), 2162-2166.
- Heller, W. "Remarks on refractive index mixture rules." *Journal of Physical Chemistry* **1965**, 69 (4), 1123-9.
- Hernandez, G. J. "Vacuum-ultraviolet absorption spectra of the cyclic ethers: trimethylene oxide, tetrahydrofuran, and tetrahydropyran." *Journal of Chemical Physics* **1963**, 38, 2233-42.
- Hernandez, G. J.; Duncan, A. B. F. "Vacuum ultraviolet absorption spectra of 1,4-dioxane and 1,3-dioxane." *Journal of Chemical Physics* **1962**, 36, 1504-8.
- Hill, M.; Hellmann, D.; Rother, M. "Quartz glass components and heavy-metal contamination." *Solid State Technology* **1994**, 37 (3), 49-50,52.
- Hinsberg, W.; Wallraff, G. M.; Larson, C. E.; Davis, B. W.; Deline, V.; Raoux, S.; Miller, D.; Houle, F. A.; Hoffnagle, J.; Sanchez, M. I.; Rettner, C.; Sundberg, L. K.; Medeiros, D. R.; Dammel, R. R.; Conley, W. E. "Liquid immersion lithography - Evaluation of resist issues." *Proceedings of SPIE-The International Society for Optical Engineering* **2004**, 5376 (Pt. 1, Advances in Resist Technology and Processing XXI), 21-33.

- Hinsberg, W. D.; MacDonald, S. A.; Clecak, N. J.; Snyder, C. D. "Airborne Contamination of a Chemically Amplified Resist. 2. Effect of Polymer Film Properties on Contamination Rate." *Chemistry of Materials* **1994**, *6* (4), 481-8.
- Hoffnagle, J. A.; Hinsberg, W. D.; Sanchez, M.; Houle, F. A. "Liquid immersion deep-ultraviolet interferometric lithography." *Journal of Vacuum Science & Technology, B: Microelectronics and Nanometer Structures* **1999**, *17* (6), 3306-3309.
- Horrocks, B. R.; Mirkin, M. V.; Pierce, D. T.; Bard, A. J.; Nagy, G.; Toth, K. "Scanning electrochemical microscopy. 19. Ion-selective potentiometric microscopy." *Analytical Chemistry* **1993**, *65* (9), 1213-24.
- Horrocks, B. R.; Schmidtke, D.; Heller, A.; Bard, A. J. "Scanning electrochemical microscopy. 24. Enzyme ultramicroelectrodes for the measurement of hydrogen peroxide at surfaces." *Analytical Chemistry* **1993**, *65* (24), 3605-14.
- Horrocks, D. L., *Applications of Liquid Scintillation Counting*. Academic Press: New York, **1974**; p 346.
- Horrocks, D. L. In *Liquid Scintillation: Science and Technology*, Noujaim, A. A.; Ediss, C.; Weibe, L. I., Eds. Academic Press: New York, **1976**; p 352.
- Howard, P. L., *Basic Liquid Scintillation Counting*. American Society of Clinical Pathologists: Chicago, **1976**; p 59.
- Hult, A.; MacDonald, S. A.; Willson, C. G. "Photoinitiated interfacial cationic polymerization." *Macromolecules* **1985**, *18* (10), 1804-9.
- Imada, M.; Noda, S.; Chutinan, A.; Tokuda, T.; Murata, M.; Sasaki, G. "Coherent two-dimensional lasing action in surface-emitting laser with triangular-lattice photonic crystal structure." *Applied Physics Letters* **1999**, *75* (3), 316-318.
- Ito, H.; Willson, C. G. "Chemical amplification in the design of dry developing resist materials." *Polymer Engineering & Science* **1983**, *23* (18), 1012-1018.

- Iwasa, S.; Maeda, K.; Nakano, K.; Ohfuji, T.; Hasegawa, E. "Design and characterization of alicyclic polymers with alkoxyethyl protecting groups for ArF chemically amplified resists." *Journal of Photopolymer Science and Technology* **1996**, *9* (3), 447-456.
- Jellison, G. E., Jr.; Modine, F. A. "Parameterization of the optical functions of amorphous materials in the interband region." *Applied Physics Letters* **1996**, *69* (3), 371-373.
- Jellison, G. E., Jr.; Modine, F. A. "Parameterization of the optical functions of amorphous materials in the interband region. [Erratum to document cited in CA125:207104]." *Applied Physics Letters* **1996**, *69* (14), 2137.
- Jiang, Y.; Jiang, W.; Chen, X.; Gu, L.; Howley, B.; Chen, R. T. "Nano-phonic crystal waveguides for ultra-compact tunable true time delay lines." *Proceedings of SPIE-The International Society for Optical Engineering* **2005**, 5733 (Photonic Crystal Materials and Devices III), 166-175.
- Jiang, Y.; Jiang, W.; Gu, L.; Chen, X.; Chen, R. T. "80-micron interaction length silicon photonic crystal waveguide modulator." *Applied Physics Letters* **2005**, *87* (22), 221105-3.
- Joannopoulos, J. D.; Meade, R. D.; Winn, J. N., *Photonic Crystals: Molding the Flow of Light*. Princeton University Press: Princeton, N.J., **1995**; p 137.
- Joannopoulos, J. D.; Villeneuve, P. R.; Fan, S. "Photonic crystals: putting a new twist on light." *Nature* **1997**, *386* (6621), 143-149.
- John, S. "Strong localization of photons in certain disordered dielectric superlattices." *Physical Review Letters* **1987**, *58* (23), 2486-9.
- Johnson, D. E.; Enke, C. G. "Bipolar pulse technique for fast conductance measurements." *Analytical Chemistry* **1970**, *42* (3), 329-35.
- Johnson, S.; Resnick, D. J.; Mancini, D.; Nordquist, K.; Dauksher, W. J.; Gehoski, K.; Baker, J. H.; Dues, L.; Hooper, A.; Bailey, T. C.; Sreenivasan, S. V.; Ekerdt, J. G.; Willson, C. G. "Fabrication of multi-tiered structures on step and flash imprint lithography templates." *Microelectronic Engineering* **2003**, 67-68, 221-228.

- Johnson, S. C. *Step and flash imprint lithography: Materials and process development*. PhD Dissertation, The University of Texas at Austin, Austin, TX, USA, **2005**.
- Johnson, S. G.; Fan, S.; Villeneuve, P. R.; Joannopoulos, J. D.; Kolodziejski, L. A. "Guided modes in photonic crystal slabs." *Physical Review B: Condensed Matter and Materials Physics* **1999**, *60* (8), 5751-5758.
- Johnson, S. G.; Joannopoulos, J. D. "Block-iterative frequency-domain methods for Maxwell's equations in a planewave basis." *Optics Express* **2001**, *8* (3), 173-190.
- Kawata, H.; Carter, J. M.; Yen, A.; Smith, H. I. "Optical projection lithography using lenses with numerical apertures greater than unity." *Microelectronic Engineering* **1989**, *9* (1-4), 31-36.
- Khusnatdinov, N.; Doyle, G.; Miller, M.; Stacey, N.; Watts, M.; Labrake, D. L. "Fabrication of nano and micro optical elements by step and flash imprint lithography." *Proceedings of SPIE - The International Society for Optical Engineering* **2006**, *6110* (Micromachining Technology for Micro-Optics and Nano-Optics IV), 61100.
- Kim, C. C.; Garland, J. W.; Abad, H.; Raccach, P. M. "Modeling the optical dielectric function of semiconductors: Extension of the critical-point parabolic-band approximation." *Physical Review B* **1992**, *45* (20), 11749.
- Kim, E. K.; Stewart, M. D.; Wu, K.; Palmieri, F. L.; Dickey, M. D.; Ekerdt, J. G.; Willson, C. G. "Vinyl ether formulations for step and flash imprint lithography." *Journal of Vacuum Science & Technology, B: Microelectronics and Nanometer Structures--Processing, Measurement, and Phenomena* **2005**, *23* (6), 2967-2971.
- Kim, W.-S.; Yoon, K. B.; Bae, B.-S. "Nanopatterning of photonic crystals with a photocurable silica-titania organic-inorganic hybrid material by a UV-based nanoimprint technique." *Journal of Materials Chemistry* **2005**, *15* (42), 4535-4539.
- King, F. W. "Efficient numerical approach to the evaluation of Kramers-Kronig transforms." *Journal of the Optical Society of America B: Optical Physics* **2002**, *19* (10), 2427-2436.

- Kramers, H. A. "La diffusion de la lumiere par les atomes." *Atti. Congr. Int. Fis.* **1927**, 2, 545-557.
- Kronig, R. d. L. "The theory of dispersion of x-rays." *Journal of the Optical Society of America* **1926**, 12, 547-57.
- Kunz, R. R.; Allen, R. D.; Hinsberg, W. D.; Wallraff, G. M. "Acid-catalyzed single-layer resists for argon fluoride lithography." *Proceedings of SPIE-The International Society for Optical Engineering* **1993**, 1925 (Advances in Resist Technology and Processing X), 167-75.
- Lee, K.; Kunjappu, J.; Jockusch, S.; Turro, N. J.; Widerschpan, T.; Zhou, J.; Smith, B. W.; Zimmerman, P.; Conley, W. "Amplification of the index of refraction of aqueous immersion fluids by ionic surfactants." *Proceedings of SPIE-The International Society for Optical Engineering* **2005**, 5753 (Pt. 1, Advances in Resist Technology and Processing XXII), 537-553.
- Lenhart, J. L.; Jones, R. L.; Lin, E. K.; Soles, C. L.; Wu, W.-l.; Fischer, D. A.; Sambasivan, S.; Goldfarb, D. L.; Angelopoulos, M. "Probing surface and bulk chemistry in resist films using near edge x-ray absorption fine structure." *Journal of Vacuum Science & Technology, B: Microelectronics and Nanometer Structures* **2002**, 20 (6), 2920-2926.
- LeSuer, R. J.; Fan, F.-R. F.; Bard, A. J. "Scanning Electrochemical Microscopy, 52. Bipolar Conductance Technique at Ultramicroelectrodes for Resistance Measurements." *Analytical Chemistry* **2004**, 76 (23), 6894-6901.
- LeSuer, R. J.; Fan, F.-R. F.; Bard, A. J.; Taylor, J. C.; Tsiartas, P.; Willson, G.; Conley, W. E.; Feit, G.; Kunz, R. R. "Using scanning electrochemical microscopy to probe chemistry at the solid-liquid interface in chemically amplified immersion lithography." *Proceedings of SPIE-The International Society for Optical Engineering* **2004**, 5376 (Pt. 1, Advances in Resist Technology and Processing XXI), 115-125.
- Limao-Vieira, P.; Giuliani, A.; Delwiche, J.; Parafita, R.; Mota, R.; Dufлот, D.; Flament, J. P.; Drage, E.; Cahillane, P.; Mason, N. J.; Hoffmann, S. V.; Hubin-Franskin, M. J. "Acetic acid electronic state spectroscopy by high-resolution vacuum ultraviolet photo-absorption, electron impact, He(I) photoelectron spectroscopy and ab initio calculations." *Chemical Physics* **2006**, 324 (2-3), 339-349.

- Lin, B. J. "The future of subhalf-micrometer optical lithography." *Microelectronic Engineering* **1987**, 6 (1-4), 31-51.
- Lin, B. J. "The k_3 coefficient in nonparaxial λ/NA scaling equations for resolution, depth of focus, and immersion lithography." *Journal of Microlithography, Microfabrication, and Microsystems* **2002**, 1 (1), 7-12.
- Lin, B. J. "Depth of focus in multilayered media - a long-neglected phenomenon aroused by immersion lithography." *Journal of Microlithography, Microfabrication, and Microsystems* **2004**, 3 (1), 21-27.
- Lin, H. B.; Tonucci, R. J.; Campillo, A. J. "Observation of two-dimensional photonic band behavior in the visible." *Applied Physics Letters* **1996**, 68 (21), 2927-2929.
- Lin, S. Y.; Fleming, J. G.; Hetherington, D. L.; Smith, B. K.; Biswas, R.; Ho, K. M.; Sigalas, M. M.; Zubrzycki, W.; Kurtz, S. R.; Bur, J. "A three-dimensional photonic crystal operating at infrared wavelengths." *Nature (London)* **1998**, 394 (6690), 251-253.
- Lind, J. E., Jr.; Zwolenik, J. J.; Fuoss, R. M. "Calibration of conductance cells at 25 Deg with aqueous solutions of potassium chloride." *Journal of the American Chemical Society* **1959**, 81, 1557-9.
- Loncar, M.; Nedeljkovic, D.; Doll, T.; Vuckovic, J.; Scherer, A.; Pearsall, T. P. "Waveguiding in planar photonic crystals." *Applied Physics Letters* **2000**, 77 (13), 1937-1939.
- Lopez, C. "Materials aspects of photonic crystals." *Advanced Materials* **2003**, 15 (20), 1679-1704.
- Lopez-Gejo, J.; Kunjappu, J. T.; Turro, N. J.; Conley, W. "Amplification of the index of refraction of aqueous immersion fluids with crown ethers: A progress report." *Proceedings of SPIE-The International Society for Optical Engineering* **2006**, 6153 (Pt. 1, Advances in Resist Technology and Processing XXIII), 61530.
- Lorentz, H. A., *The theory of electrons and its applications to the phenomena of light and radiant heat*. 2nd ed.; Dover Publications: New York, **1952**; p 343.

- Lucarini, V., *Kramers-Kronig relations in optical materials research*. Springer: Berlin, **2005**; p 160.
- Mack, C. A., *Inside PROLITH : a comprehensive guide to optical lithography simulation*. FINLE Technologies: Austin, **1997**.
- Mack, C. A. *Modeling solvent effects in optical lithography*. PhD Dissertation, The University of Texas at Austin, Austin, TX, USA, **1998**.
- Mack, C. A. "Off-axis illumination." *Microlithography World* **2003**, 12 (3), 14-16.
- Mack, C. A.; Byers, J. D. "Exploring the capabilities of immersion lithography through simulation." *Proceedings of SPIE-The International Society for Optical Engineering* **2004**, 5377 (Pt. 1, Optical Microlithography XVII), 428-441.
- Mauzeroll, J.; Buda, M.; Bard, A. J.; Prieto, F.; Rueda, M. "Detection of Tl(I) Transport through a Gramicidin-Dioleoylphosphatidylcholine Monolayer Using the Substrate Generation-Tip Collection Mode of Scanning Electrochemical Microscopy." *Langmuir* **2002**, 18 (24), 9453-9461.
- Maxwell-Garnett, J. C. "Colours in Metal Glasses and in Metallic Films." *Philosophical Transactions of the Royal Society of London. Series A, Containing Papers of a Mathematical or Physical Character* **1904**, 203, 385-420.
- Maxwell-Garnett, J. C. "Colours in Metal Glasses, in Metallic Films, and in Metallic Solutions. II." *Philosophical Transactions of the Royal Society of London. Series A, Containing Papers of a Mathematical or Physical Character* **1906**, 205, 237-288.
- McKinney, P. S.; Rosenthal, S. "Electrochemical reduction of the triphenyl-sulfonium ion." *Journal of Electroanalytical Chemistry and Interfacial Electrochemistry* **1968**, 16 (2), 261-70.
- Meade, R. D.; Rappe, A. M.; Brommer, K. D.; Joannopoulos, J. D.; Alerhand, O. L. "Accurate theoretical analysis of photonic band-gap materials." *Physical Review B* **1993**, 48 (11), 8434.

- Milton, G. W.; Eyre, D. J.; Mantese, J. V. "Finite Frequency Range Kramers Kronig Relations: Bounds on the Dispersion." *Physical Review Letters* **1997**, *79* (16), 3062-3065.
- Miyamatsu, T.; Wang, Y.; Shima, M.; Kusumoto, S.; Chiba, T.; Nakagawa, H.; Hieda, K.; Shimokawa, T. "Material design for immersion lithography with high refractive index fluid (HIF)." *Proceedings of SPIE-The International Society for Optical Engineering* **2005**, *5753* (Pt. 1, Advances in Resist Technology and Processing XXII), 10-19.
- Moore, G. E. "Cramming more components onto integrated circuits." *Electronics* **1965**, *38* (8).
- Moosburger, J.; Kamp, M.; Forchel, A.; Ferrini, R.; Leuenberger, D.; Houdre, R.; Anand, S.; Berggren, J. "Nanofabrication of high quality photonic crystals for integrated optics circuits." *Nanotechnology* **2002**, *13* (3), 341-345.
- Moreau, W. M., *Semiconductor lithography : principles, practices, and materials*. Plenum Press: New York, **1988**; p 931.
- Morrison, J. D.; Nicholson, A. J. C. "Ionization efficiency. II. The ionization potentials of some organic molecules." *Journal of Chemical Physics* **1952**, *20*, 1021-3.
- Mueller, K. E. *Diffusion in polymers using quartz crystal microbalance techniques*. PhD Dissertation, The University of Texas at Austin, Austin, TX, USA, **1998**.
- Mueller, K. E.; Koros, W. J.; Mack, C. A.; Willson, C. G. "Diffusivity measurements in polymers, part IV: acid diffusion in chemically amplified resists." *Proceedings of SPIE-The International Society for Optical Engineering* **1997**, *3049* (Advances in Resist Technology and Processing XIV), 706-711.
- Mugnai, D.; Mochi, I. "Superluminal X-wave propagation: energy localization and velocity." *Physical Review E: Statistical, Nonlinear, and Soft Matter Physics* **2006**, *73* (1-2), 016606/1-016606/5.
- Mulkens, J.; Streefkerk, B.; Hoogendorp, M.; Moerman, R.; Leenders, M.; de Jong, F.; Stavenga, M.; Boom, H. "Immersion lithography exposure systems: today's

- capabilities and tomorrow's expectations." *Proceedings of SPIE-The International Society for Optical Engineering* **2005**, 5754 (Pt. 2, Optical Microlithography XVIII), 710-724.
- Nakano, H.; Hata, H.; Takahashi, K.; Arakawa, M.; Chibana, T.; Honda, T.; Chiba, K.; Mori, S. "Development of ArF immersion exposure tool." *Proceedings of SPIE - The International Society for Optical Engineering* **2005**, 5754 (Pt. 2, Optical Microlithography XVIII), 693-700.
- Nellis, G.; Wei, A. "Preliminary analysis of laser-pulse-induced pressure variation for immersion lithography." *Journal of Microlithography, Microfabrication and Microsystems* **2004**, 3 (1), 84-86.
- Notomi, M.; Yamada, K.; Shinya, A.; Takahashi, J.; Takahashi, C.; Yokohama, I. "Extremely large group-velocity dispersion of line-defect waveguides in photonic crystal slabs." *Physical Review Letters* **2001**, 87 (25), 253902.
- Nozaki, K.; Watanabe, K.; Yano, E.; Kotachi, A.; Takechi, S.; Hanyu, I. "A novel polymer for a 193-nm resist." *Journal of Photopolymer Science and Technology* **1996**, 9 (3), 509-522.
- Nussenzveig, H. M., *Causality and Dispersion Relations*. Academic Press: New York, **1972**.
- Olah, G. A.; Marinez, E. R.; Prakash, G. K. S. "Trifluoromethanesulfonic Acid Catalyzed Preparation of Symmetrical Diaryl Sulfoxides from Arenes and Thionyl Chloride." *Synlett* **1999**, 1999 (09), 1397-1398.
- Orchin, M.; Jaffé, H. H., *Symmetry, orbitals, and spectra (S.O.S.)*. Wiley-Interscience: New York, **1971**; p 396.
- O'Toole, L.; Brint, P.; Kosmidis, C.; Boulakis, G.; Tsekeris, P. "Vacuum-ultraviolet absorption spectra of propanone, butanone and the cyclic ketones $C_nH_{2n-2}O$ ($n = 4, 5, 6, 7$)." *Journal of the Chemical Society, Faraday Transactions* **1991**, 87 (20), 3343-51.

- Owa, S.; Nagasaka, H. "Immersion lithography; its potential performance and issues." *Proceedings of SPIE-The International Society for Optical Engineering* **2003**, 5040 (Pt. 2, Optical Microlithography XVI), 724-733.
- Owa, S.; Nagasaka, H.; Ishii, Y.; Shiraishi, K.; Hirukawa, S. "Full-field exposure tools for immersion lithography." *Proceedings of SPIE - The International Society for Optical Engineering* **2005**, 5754 (Pt. 2, Optical Microlithography XVIII), 655-668.
- Owen, G.; Pease, R. F. W.; Markle, D. A.; Grenville, A.; Hsieh, R. L.; von Bunau, R.; Maluf, N. I. "1/8 μ m optical lithography." *Journal of Vacuum Science & Technology, B: Microelectronics and Nanometer Structures* **1992**, 10 (6), 3032-3036.
- Palmieri, F.; Stewart, M. D.; Wetzel, J.; Hao, J.; Nishimura, Y.; Jen, K.; Flannery, C.; Li, B.; Chao, H.-L.; Young, S.; Kim, W. C.; Ho, P. S.; Willson, C. G. "Multi-level step and flash imprint lithography for direct patterning of dielectrics" **2006**; International Society for Optical Engineering, Bellingham WA, WA 98227-0010, United States: San Jose, CA, United States, 2006; p 61510.
- Parsons, B. F.; Chandler, D. W. "On the Dissociation of van der Waals Clusters of X₂-Cyclohexane (X = O, Cl) Following Charge-Transfer Excitation in the Ultraviolet." *J. Phys. Chem. A* **2003**, 107 (49), 10544-10553.
- Patterson, K. W. *Design, synthesis, and optimization of materials for 193 nm and 157 nm photoresists*. PhD Dissertation, The University of Texas at Austin, Austin, TX, USA, **2000**.
- Patterson, K.; Okoroanyanwu, U.; Shimokawa, T.; Cho, S.; Byers, J.; Willson, C. G. "Improving performance of 193 nm photoresists based on alicyclic polymers." *Proceedings of SPIE-The International Society for Optical Engineering* **1998**, 3333 (Pt. 1, Advances in Resist Technology and Processing XV), 425-437.
- Peiponen, K. E.; Vartiainen, E. M. "Kramers-Kronig relations in optical data inversion." *Physical Review B* **1991**, 44 (15), 8301.
- Peng, S.; French, R. H.; Qiu, W.; Wheland, R. C.; Yang, M.; Lemon, M. F.; Crawford, M. K. "Second generation fluids for 193 nm immersion lithography." *Proceedings*

- of SPIE-The International Society for Optical Engineering **2005**, 5754 (Pt. 1, Optical Microlithography XVIII), 427-434.
- Pickett, L. W.; Hoeflich, N. J.; Liu, T.-C. "Vacuum ultraviolet absorption spectra of cyclic compounds. II. Tetrahydrofuran, tetrahydropyran, 1,4-dioxan, and furan." *Journal of the American Chemical Society* **1951**, 73, 4865-9.
- Pickett, L. W.; Muntz, M.; McPherson, E. M. "Vacuum ultraviolet absorption spectra of cyclic compounds. I. Cyclohexane, cyclohexene, cyclopentane, cyclopentene, and benzene." *Journal of the American Chemical Society* **1951**, 73, 4862-5.
- Querry, M. R.; Wieliczka, D. M.; Segelstein, D. J. "Water (H₂O)." In *Handbook of optical constants of solids*, Palik, E. D., Ed. Academic Press: Boston, **1991**; Vol. 2, p 1096 p.
- Rabinowitch, E. "Electron-transfer spectra and their photochemical effects." *Reviews of Modern Physics* **1942**, 14, 112-31.
- Rai-Choudhury, P., *Handbook of microlithography, micromachining, and microfabrication*. SPIE Optical Engineering Press; Institution of Electrical Engineers: Bellingham, Wash., USA; London, UK, **1997**.
- Raub, A. K.; Brueck, S. R. J. "Deep-UV immersion interferometric lithography." *Proceedings of SPIE-The International Society for Optical Engineering* **2003**, 5040 (Pt. 2, Optical Microlithography XVI), 667-678.
- Raymonda, J. W. "Rydberg States in Cyclic Alkanes." *The Journal of Chemical Physics* **1972**, 56 (8), 3912-3920.
- Reichmanis, E.; Thompson, L. F. "Polymer materials for microlithography." *Chemical Reviews (Washington, DC, United States)* **1989**, 89 (6), 1273-89.
- Rosenberg, A.; Tonucci, R. J.; Bolden, E. A. "Photonic band-structure effects in the visible and near ultraviolet observed in solid-state dielectric arrays." *Applied Physics Letters* **1996**, 69 (18), 2638-2640.

- Rubingh, R.; Moers, M.; Suddendorf, M.; Vanoppen, P.; Kisteman, A.; Thier, M.; Blahnik, V.; Piper, E. "Lithographic performance of a dual stage, 0.93NA ArF step and scan system." *Proceedings of SPIE - The International Society for Optical Engineering* **2005**, 5754 (Pt. 2, Optical Microlithography XVIII), 681-692.
- Sakoda, K. "Optical transmittance of a two-dimensional triangular photonic lattice." *Physical Review B: Condensed Matter* **1995**, 51 (7), 4672-5.
- Sakoda, K. "Symmetry, degeneracy, and uncoupled modes in two-dimensional photonic lattices." *Physical Review B: Condensed Matter* **1995**, 52 (11), 7982-6.
- Sakoda, K. "Transmittance and Bragg reflectivity of two-dimensional photonic lattices." *Physical Review B: Condensed Matter* **1995**, 52 (12), 8992-9002.
- Saravanamuttu, K.; Blanford, C. F.; Sharp, D. N.; Dedman, E. R.; Turberfield, A. J.; Denning, R. G. "Sol-Gel Organic-Inorganic Composites for 3-D Holographic Lithography of Photonic Crystals with Submicron Periodicity." *Chemistry of Materials* **2003**, 15 (12), 2301-2304.
- Schmid, G. M.; Stewart, M. D.; Wetzel, J.; Palmieri, F.; Hao, J.; Nishimura, Y.; Jen, K.; Kim, E. K.; Resnick, D. J.; Liddle, J. A.; Willson, C. G. "Implementation of an imprint damascene process for interconnect fabrication." *Journal of Vacuum Science and Technology B: Microelectronics and Nanometer Structures* **2006**, 24 (3), 1283-1291.
- Sekine, Y.; Kawashima, M.; Yamazoe, K.; Honda, T.; Ohkubo, A.; Kishikawa, Y.; Iwasaki, Y.; Suzuki, A. "Analysis of imaging properties for hyper-NA ArF immersion lithography." *Proceedings of SPIE-The International Society for Optical Engineering* **2005**, 5754 (Pt. 2, Optical Microlithography XVIII), 701-709.
- Selzer, Y.; Mandler, D. "Scanning Electrochemical Microscopy. Theory of the Feedback Mode for Hemispherical Ultramicroelectrodes: Steady-State and Transient Behavior." *Analytical Chemistry* **2000**, 72 (11), 2383-2390.
- Sewell, H.; McCafferty, D.; Markoya, L.; Hendrickx, E.; Hermans, J.; Ronse, K. "32nm node technology development using interference immersion lithography."

- Proceedings of SPIE-The International Society for Optical Engineering* **2005**, 5753 (Pt. 1, Advances in Resist Technology and Processing XXII), 491-501.
- Shibuya, M. "Resolution enhancement techniques for optical lithography and optical imaging theory." *Optical Review* **1997**, 4 (1B), 151-160.
- Shida, N.; Ushirogouchi, T.; Asakawa, K.; Nakase, M. "Novel ArF excimer laser resists based on menthyl methacrylate terpolymer." *Journal of Photopolymer Science and Technology* **1996**, 9 (3), 457-464.
- Shockley, W. "The theory of *p-n* junction in semiconductors and *p-n* junction transistors." *Bell Systems Technical Journal* **1949**, 28, 435.
- Sild, S.; Karelson, M. "A General QSPR Treatment for Dielectric Constants of Organic Compounds." *J. Chem. Inf. Model.* **2002**, 42 (2), 360-367.
- Skoog, D. A.; West, D. M., *Fundamentals of analytical chemistry*. 3rd ed.; Holt, Rinehart, and Winston: New York, **1976**; p 804.
- Smith, B. W.; Bourov, A.; Fan, Y.; Zavyalova, L. V.; Lafferty, N. V.; Cropanese, F. C. "Approaching the numerical aperture of water - Immersion lithography at 193 nm." *Proceedings of SPIE-The International Society for Optical Engineering* **2004**, 5377 (Pt. 1, Optical Microlithography XVII), 273-284.
- Smith, B. W.; Fan, Y.; Slocum, M.; Zavyalova, L. "25 nm immersion lithography at 193 nm wavelength." *Proceedings of SPIE-The International Society for Optical Engineering* **2005**, 5754 (Pt. 1, Optical Microlithography XVIII), 141-147.
- Smith, B. W.; Kang, H.; Bourov, A.; Cropanese, F.; Fan, Y. "Water immersion optical lithography for the 45nm node." *Proceedings of SPIE-The International Society for Optical Engineering* **2003**, 5040 (Pt. 2, Optical Microlithography XVI), 679-689.
- Smith, B. W.; Zavyalova, L.; Estroff, A. "Benefiting from polarization - Effects on high-NA imaging." *Proceedings of SPIE - The International Society for Optical Engineering* **2004**, 5377 (Pt. 1, Optical Microlithography XVII), 68-79.

Smith, C. J. M.; Benisty, H.; Olivier, S.; Rattier, M.; Weisbuch, C.; Krauss, T. F.; De La Rue, R. M.; Houdre, R.; Oesterle, U. "Low-loss channel waveguides with two-dimensional photonic crystal boundaries." *Applied Physics Letters* **2000**, *77* (18), 2813-2815.

Stein, G.; Treinin, A. "Absorption spectra of anions in solution. III. Ionic effects." *Transactions of the Faraday Society* **1960**, *56*, 1393-403.

Stewart, M. D. *Catalyst diffusion in positive-tone chemically amplified photoresists*. PhD Dissertation, The University of Texas at Austin, Austin, TX, USA, **2003**.

Stewart, M. D.; Johnson, S. C.; Sreenivasan, S. V.; Resnick, D. J.; Willson, C. G. "Nanofabrication with step and flash imprint lithography." *Journal of Microlithography, Microfabrication, and Microsystems* **2005**, *4* (1), 011002/1-011002/6.

Stewart, M. D.; Patterson, K.; Somervell, M. H.; Willson, C. G. "Organic imaging materials: a view of the future." *Journal of Physical Organic Chemistry* **2000**, *13* (12), 767-774.

Stewart, M. D.; Wetzel, J. T.; Schmid, G. M.; Palmieri, F.; Thompson, E.; Kim, E. K.; Wang, D.; Sotodeh, K.; Jen, K.; Johnson, S. C.; Hao, J.; Dickey, M. D.; Nishimura, Y.; Laine, R. M.; Resnick, D. J.; Willson, C. G. "Direct imprinting of dielectric materials for dual damascene processing." *Proceedings of SPIE-The International Society for Optical Engineering* **2005**, *5751* (Pt. 1, Emerging Lithographic Technologies IX), 210-218.

Stewart, M. D.; Willson, C. G. "Imprint materials for nanoscale devices." *MRS Bulletin* **2005**, *30* (12), 947-952.

Stokes, S.; Pickett, L. W. "Absorption of bicycloheptane and bicycloheptene in the vacuum ultraviolet." *Journal of Chemical Physics* **1955**, *23*, 258-60.

Streetman, B. G.; Banerjee, S., *Solid state electronic devices*. 5th ed.; Prentice Hall: Upper Saddle River, N.J., **2000**; p 558.

- Stroud, D. "Generalized effective-medium approach to the conductivity of an inhomogeneous material." *Physical Review B* **1975**, *12* (8), 3368.
- Styrkas, D.; Doran, S. J.; Gilchrist, V.; Keddie, J. L.; Lu, J. R.; Murphy, E.; Sackin, R.; Su, T.-J.; Tzitzinou, A. "Application of ellipsometry to polymers at interfaces and in thin films." In *Polymer Surfaces and Interfaces III*, Richards, R. W.; Peace, S. K., Eds. Wiley-Interscience: New York, **1999**; pp 1-42.
- Sugimoto, Y.; Ikeda, N.; Carlsson, N.; Asakawa, K.; Kawai, N.; Inoue, K. "AlGaAs-based two-dimensional photonic crystal slab with defect waveguides for planar lightwave circuit applications." *IEEE Journal of Quantum Electronics* **2002**, *38* (7), 760-769.
- Switkes, M.; Bloomstein, T. M.; Kunz, R. R.; Rothschild, M.; Ruberti, J. W.; Shedd, T. A.; Yeung, M. S. "Scattering in liquid immersion lithography." *Proceedings of SPIE-The International Society for Optical Engineering* **2004**, 5377 (Pt. 1, Optical Microlithography XVII), 469-476.
- Switkes, M.; Kunz, R. R.; Rothschild, M.; Sinta, R. F.; Yeung, M.; Baek, S. Y. "Extending optics to 50 nm and beyond with immersion lithography." *Journal of Vacuum Science & Technology, B: Microelectronics and Nanometer Structures--Processing, Measurement, and Phenomena* **2003**, *21* (6), 2794-2799.
- Switkes, M.; Kunz, R. R.; Sinta, R. F.; Rothschild, M.; Gallagher-Wetmore, P. M.; Krukonis, V. J.; Williams, K. "Immersion liquids for lithography in the deep ultraviolet." *Proceedings of SPIE-The International Society for Optical Engineering* **2003**, 5040 (Pt. 2, Optical Microlithography XVI), 690-699.
- Switkes, M.; Rothschild, M. "Immersion lithography at 157 nm." *Journal of Vacuum Science & Technology, B: Microelectronics and Nanometer Structures* **2001**, *19* (6), 2353-2356.
- Switkes, M.; Rothschild, M. "Resolution enhancement of 157-nm lithography by liquid immersion." *Proceedings of SPIE-The International Society for Optical Engineering* **2002**, 4691 (Pt. 1, Optical Microlithography XV), 459-465.
- Switkes, M.; Rothschild, M.; Shedd, T. A.; Burnett, H. B.; Yeung, M. S. "Bubbles in immersion lithography." *Journal of Vacuum Science & Technology, B:*

- Microelectronics and Nanometer Structures--Processing, Measurement, and Phenomena* **2005**, 23 (6), 2409-2412.
- Synowicki, R. A.; Pribil, G. K.; Cooney, G.; Herzinger, C. M.; Green, S. E.; French, R. H.; Yang, M. K.; Burnett, J. H.; Kaplan, S. "Fluid refractive index measurements using rough surface and prism minimum deviation techniques." *Journal of Vacuum Science and Technology B: Microelectronics and Nanometer Structures* **2004**, 22 (6), 3450-3453.
- Sze, S. M., *Modern semiconductor device physics*. Wiley: New York, **1998**; p 556.
- Takanashi, A.; Harada, T.; Akeyama, M.; Kondo, Y.; Kurosaki, T.; Kuniyoshi, S.; Hosaka, S.; Kawamura, Y. "Pattern forming apparatus." U.S. Patent No. 4,480,910, **1984**.
- Tauc, J.; Grigorovici, R.; Vancu, A. "Optical Properties and Electronic Structure of Amorphous Germanium." *physica status solidi (b)* **1966**, 15 (2), 627-637.
- Taylor, J. C.; Chambers, C. R.; Deschner, R.; LeSuer, R. J.; Conley, W. E.; Burns, S. D.; Willson, C. G. "Implications of immersion lithography on 193 nm photoresists." *Proceedings of SPIE-The International Society for Optical Engineering* **2004**, 5376 (Pt. 1, Advances in Resist Technology and Processing XXI), 34-43.
- Taylor, J. C.; Hostetler, T.; Kornilovich, P.; Kramer, K. "Photonic crystals from step and flash imprint lithography." *Proceedings of SPIE-The International Society for Optical Engineering* **2006**, 6151 (Pt. 1, Emerging Lithographic Technologies X), 61510L/1-61510L/8.
- Thompson, L. F.; Willson, C. G.; Bowden, M. J., *Introduction to microlithography*. 2nd ed.; American Chemical Society: Washington, DC, **1994**; p 527.
- Thompson, L. F.; Willson, C. G.; Fréchet, J. M. J., *Materials for microlithography : radiation-sensitive polymers*. American Chemical Society: Washington, D.C., **1984**; p 494.
- Todaro, M. T.; Stomeo, T.; Vitale, V.; DeVittorio, M.; Passaseo, A.; Cingolani, R.; Romanato, F.; Businaro, L.; Di Fabrizio, E. "Nanofabrication of high refractive

- index contrast two-dimensional photonic crystal waveguides." *Microelectronic Engineering* **2003**, 67-68, 670-675.
- Toll, J. S. "Causality and the Dispersion Relation: Logical Foundations." *Physical Review* **1956**, 104 (6), 1760.
- Tompkins, H. G.; McGahan, W. A., *Spectroscopic Ellipsometry and Reflectometry: A User's Guide*. Wiley: New York, **1999**; p 228.
- Truskett, V. N.; Watts, M. P. C. "Trends in imprint lithography for biological applications." *Trends in Biotechnology* **2006**, 24 (7), 312-317.
- Urbach, F. "The long-wave-length edge of photographic sensitivity and of the electronic absorption of solids." *Physical Review* **1953**, 92, 1324.
- Vandenberghe, K. *Nanoimprint Lithography (NIL) Template Creation Process at the University of Texas - Microelectronics Research Center (UT-MRC) in Austin*; SEMATECH: 2007.
- Villeneuve, P. R.; Abrams, D. S.; Fan, S.; Joannopoulos, J. D. "Single-mode waveguide microcavity for fast optical switching." *Optics Letters* **1996**, 21 (24), 2017-2019.
- Villeneuve, P. R.; Fan, S.; Joannopoulos, J. D. "Microcavities in photonic crystals: mode symmetry, tunability, and coupling efficiency." *Physical Review B: Condensed Matter* **1996**, 54 (11), 7837-7842.
- Vogt, B. D.; Soles, C. L.; Prabhu, V. M.; Jones, R. L.; Wu, W.-L.; Lin, E. K.; Goldfarb, D. L.; Angelopoulos, M. "Measurements of water distribution in thin lithographic films." *Proceedings of SPIE-The International Society for Optical Engineering* **2004**, 5376 (Pt. 1, Advances in Resist Technology and Processing XXI), 56-62.
- Wallraff, G. M.; Hinsberg, W. D. "Lithographic Imaging Techniques for the Formation of Nanoscopic Features." *Chemical Reviews (Washington, D. C.)* **1999**, 99 (7), 1801-1821.

- Wang, L.-G.; Liu, N.-H.; Lin, Q.; Zhu, S.-Y. "Superluminal propagation of light pulses: a result of interference." *Physical Review E: Statistical, Nonlinear, and Soft Matter Physics* **2003**, 68 (6-2), 066606/1-066606/10.
- Wei, A.; Abdo, A.; Nellis, G.; Engelstad, R.; Chang, J.; Lovell, E.; Beckman, W. "Simulating fluid flow characteristics during the scanning process for immersion lithography." *Journal of Vacuum Science & Technology, B: Microelectronics and Nanometer Structures--Processing, Measurement, and Phenomena* **2003**, 21 (6), 2788-2793.
- Wei, A.; El-Morsi, M.; Nellis, G.; Abdo, A.; Engelstad, R. "Predicting air entrainment due to topography during the filling and scanning process for immersion lithography." *Journal of Vacuum Science & Technology, B: Microelectronics and Nanometer Structures--Processing, Measurement, and Phenomena* **2004**, 22 (6), 3444-3449.
- Wei, A.; Nellis, G.; Abdo, A.; Engelstad, R.; Chen, C.-F.; Switkes, M.; Rothschild, M. "Preliminary microfluidic simulation for immersion lithography." *Proceedings of SPIE-The International Society for Optical Engineering* **2003**, 5040 (Pt. 2, Optical Microlithography XVI), 713-723.
- Wei, A. C.; Nellis, G. F.; Abdo, A. Y.; Engelstad, R. L.; Chen, C.-f.; Switkes, M.; Rothschild, M. "Microfluidic simulations for immersion lithography." *Journal of Microlithography, Microfabrication, and Microsystems* **2004**, 3 (1), 28-34.
- Whittaker, A. K.; Blakey, I.; Liu, H.; Hill, D. J. T.; George, G. A.; Conley, W.; Zimmerman, P. "High-RI resist polymers for 193 nm immersion lithography." *Proceedings of SPIE-The International Society for Optical Engineering* **2005**, 5753 (Pt. 2, Advances in Resist Technology and Processing XXII), 827-835.
- Wooten, F., *Optical Properties of Solids*. Academic Press: New York, **1972**; p 260.
- Yablonovitch, E. "Inhibited spontaneous emission in solid-state physics and electronics." *Physical Review Letters* **1987**, 58 (20), 2059-62.
- Yablonovitch, E. "Photonic band-gap structures." *Journal of the Optical Society of America B: Optical Physics* **1993**, 10 (2), 283-95.

- Yablonovitch, E.; Gmitter, T. J.; Leung, K. M. "Photonic band structure: the face-centered-cubic case employing nonspherical atoms." *Physical Review Letters* **1991**, *67* (17), 2295-8.
- Yablonovitch, E.; Gmitter, T. J.; Meade, R. D.; Rappe, A. M.; Brommer, K. D.; Joannopoulos, J. D. "Donor and acceptor modes in photonic band structure." *Physical Review Letters* **1991**, *67* (24), 3380-3.
- Yamachika, M.; Patterson, K.; Cho, S.; Rager, T.; Yamada, S.; Byers, J.; Paniez, P. J.; Mortini, B.; Gally, S.; Sassoulas, P. O.; Willson, C. G. "Improvement of post-exposure delay stability in alicyclic ArF excimer photoresists." *Journal of Photopolymer Science and Technology* **1999**, *12* (4), 553-560.
- Zelmann, M.; Picard, E.; Charvolin, T.; Hadji, E.; Heitzmann, M.; Dal'zotto, B.; Nier, M. E.; Seassal, C.; Rojo-Romeo, P.; Letartre, X. "Broadband optical characterization and modeling of photonic crystal waveguides for silicon optical interconnects." *Journal of Applied Physics* **2004**, *95* (3), 1606-1608.
- Zhang, P.; Budhlall, B. M.; Parris, G. E.; Barber, L. C. "Immersion lithography fluids." U.S. Patent No. 2005-30132 2005173682, 01/07/2005, **2005**.
- Zhou, J.; Fan, Y.; Bourov, A.; Lafferty, N.; Cropanese, F.; Zavyalova, L.; Estroff, A.; Smith, B. W. "Immersion lithography fluids for high NA 193 nm lithography." *Proceedings of SPIE-The International Society for Optical Engineering* **2005**, 5754 (Pt. 2, Optical Microlithography XVIII), 630-637.
- Zhou, J.; Fan, Y.; Bourov, A.; Smith Bruce, W. "Inorganic immersion fluids for ultrahigh numerical aperture 193 nm lithography." *Applied optics* **2006**, *45* (13), 3077-82.

Vita

James Christopher Taylor was born in Charleston, WV on July 10, 1980, the son of Janet Ellen Taylor and James William Taylor, Jr. After graduating as valedictorian at Capital High School, Charleston, WV, in 1998, he enrolled at West Virginia University, Morgantown, WV. He received the degree of Bachelor of Science in Chemical Engineering with a minor in Physics in 2002. In September 2002 he entered the Graduate School of The University of Texas at Austin to pursue a Doctorate of Philosophy in Chemical Engineering.

Permanent Address: 1946 Bobcat Ave, SW, Albany, OR 97321

This dissertation was typed by the author.